Diagnostic Load Tests of Two Prestressed Concrete Bridges

by

Photis Panayioti Matsis, B.S.C.E.

Thesis

Presented to the Faculty of the Graduate School of

The University of Texas at Austin

in Partial Fulfillment

of the Requirements

for the Degree of

Master of Science in Engineering

The University of Texas at Austin

August, 1999

Diagnostic Load Tests of Two Prestressed Concrete Bridges

Approved by
Supervising Committee:

Supervisor: Sharon L. Wood

Michael E. Kreger

Dedication

This work is dedicated with love to my family and friends, and especially to my parents and to my brother. Their love and support were essential in completing this research. I also dedicate this thesis to my late friend, Takis, who left us so suddenly nearly one year ago.

Acknowledgements

I would like to thank Prof. Sharon L. Wood for her continuous guidance and patience throughout this research, and for her understanding and support until the completion of this thesis. I would also like to thank Prof. Michael E. Kreger for being my second reader.

I would like to offer many thanks to the Texas Department of Transportation for providing the funding and support necessary to make this research project possible and especially to Keith Ramsey for his continual assistance throughout this project.

Many thanks to my colleagues and members of the research team: David Jáuregui, Norm Grady, David McIlrath, Blanca Velázquez, Karl Pennings, Charles Bowen, Dilip Maniar and Scott Barney, for their assistance and support that made it possible to conduct the three load tests. Thank you all for being such good friends and for sharing so much of your knowledge with me. I offer special thanks to my dear friend Christiana Antoniou for her continual support and friendship during this research.

Finally, I would like to thank my parents for their love, patience and moral support. Their guidance and their teachings have been invaluable lessons to me throughout the entirety of my education.

July 29, 1999

Abstract

Diagnostic Load Tests of Two Prestressed Concrete Bridges

Photis Panayioti Matsis, M.S.E.

The University of Texas at Austin, 1999

Supervisor: Sharon L. Wood

Many of the state's bridges are designed for loads that are lower than the current design loads set by the American Association of State Highway and Transportation Officials (AASHTO). The economic impact of load posting, closing, or replacing bridges across the entire state has led the Texas Department of Transportation to sponsor a series of research projects to investigate the actual performance of different types of bridges. Diagnostic load tests have been used in the past to demonstrate that the actual performance of most bridges is better than assumed by simplifying design procedures also used in the load rating. This thesis addresses the possibility of load testing prestressed concrete I-beam bridges to measure their response and evaluate their actual behavior based on the measurements. Differences between the expected behavior and the measured response are examined. An assessment of the rating of the structures based on the findings of the diagnostic load tests is also made.

Table of Contents

List of Tables

List of Figures

Chapter 1. INTRODUCTION

The Texas Department of Transportation (TxDOT) has been concerned with the increasing traffic of heavy vehicles on bridges across Texas. Many of the state's bridges are designed for loads that are lower than the current design loads set by the American Association of State Highway and Transportation Officials (AASHTO). If the available live-load moment capacity of a bridge is less than the maximum moments induced on the structure by typical vehicles, then the bridge must be posted to limit the weight of vehicles permitted to cross it. The cost of inspections to assess the condition of these bridges and the altering of trucking routes across the state can have significant economic impacts on both the trucking industry and the state.

The actual performance of most bridges is better than assumed by simplifying design procedures that are also used for load rating. The economic impact of load posting, closing, or replacing bridges across the entire state has led TxDOT to sponsor a series of research projects to investigate the actual performance of these structures. The research focuses on ways of measuring and evaluating the response of different types of bridges in an attempt to represent and take advantage of the actual behavior of the structure during the load-rating procedures. This would offer the means of rating the bridges in a more favorable way than the initial rating.

The main objective of this thesis is to present and evaluate the measured responses of two prestressed concrete bridges during load testing. Two typical prestressed concrete bridges of similar structural details and design were selected for the research. The discussion of the bridges and test procedures is followed by a presentation and evaluation of the measured responses and rating of each bridge.

1.1 NONDESTRUCTIVE LOAD TESTING FOR LOAD RATING

During a nondestructive load test, a bridge is subjected to loads that are lower than the elastic limit of the structure. The measured field response of the bridge under the known loads is evaluated by comparing it with results obtained analytically [8]. The information that is gathered during a nondestructive load test may be used to determine a more realistic analytical model for the structure. The increased stiffness or rotational restraint at the ends can be used to revise the rating for the bridge. In some cases, closing or posting of the structure can be avoided.

A great number of bridges have been tested to evaluate their behavior by observing their measured response under predetermined live loads caused by trucks traveling along the spans. Two types of nondestructive testing methods are used to evaluate the response of the bridges: proof and diagnostic load tests. Proof load tests are used to establish the ability of the bridge to carry the full dead load and an additional live load. The bridge is loaded incrementally to a load that

approaches the elastic limit of the structure. The loading is stopped when either a target load is reached or when inelastic response is initiated [8].

Diagnostic load tests are performed with loading vehicles that weigh less than the expected live-load capacity of the bridges. The purpose of these types of tests is to examine the response of the structure to known loads both in terms of individual components and in terms of the system as a whole.

The information that is gathered during a diagnostic load test can help the researchers obtain a better understanding of the behavior of the bridge. Some of the most important issues that are examined during a test include assessing the condition of the bridge, investigating the degree of composite action and the participation of secondary elements, and establishing the differences between actual and assumed material properties. One of the most important issues that are investigated is the effective stiffness of these structures and the distribution of the loads among the various bridge elements.

The load rating is done with a certain code-defined truck configuration, and the rating applies only for the specific truck. The current legal design vehicle is the HS-20 vehicle [2]. The ten-cubic yard dump trucks that are used in the diagnostic load tests described in this thesis are not legal rating vehicles, but the measured response of the bridges can provide valuable insight into their behavior.

Load rating is usually performed based on procedures outlined in the Manual for Condition Evaluation of Bridges (AASHTO Manual) [3]. They are based on simplified calculations that are used in the standard design of bridges.

Standard load rating procedures have an inherent conservatism because of their simplicity and applicability to almost all types of bridge systems.

The procedures outlined in the Manual for Condition Evaluation of Bridges define two different levels for load rating. The inventory rating level relates to the customary design level of service load performance of the structure. It reflects the safe live load that the bridge can resist for an indefinite period of time. The operating rating level describes the maximum permissible live load that can be supported by the bridge [3].

1.2 OBJECTIVES AND SCOPE OF THIS RESEARCH

The use of prestressed concrete bridges in the state's highways is extensive because of the high strength and good serviceability characteristics of these medium-span bridges. Currently, there are nearly 6400 prestressed concrete I-beam bridges in Texas. As part of a comprehensive project sponsored by the Texas Department of Transportation to evaluate a number of different types of bridges, diagnostic load tests were conducted on two prestressed concrete bridges and the results are described in this thesis. Both of these bridges were designed based on HS-20 loading. The load rating for these two bridges is presented in the BRINSAP [9] database of the Texas Department of Transportation. The rating for both structures is at HS-20 for inventory level and HS-27 for operating level rating. These ratings are the maximum ratings that are given in the TxDOT database for any bridge.

One of the most important observations during the load testing of different concrete and steel bridges is the reserve capacity of the structures. The two prestressed concrete bridges investigated in this thesis are similar in structural details and they are typical of this type of highway bridge. This thesis addresses the possibility of load testing prestressed concrete bridges to measure their response and evaluate their actual behavior based on the measurements. The implementation of a procedure for diagnostic load tests that would adequately capture the response of prestressed concrete bridges is addressed. Differences between the expected behavior and the measured response are examined. An assessment of the rating of the structures based on the findings of the diagnostic load tests is also made.

The structural characteristics of the bridges are presented in Chapter 2. The implementation and testing procedures for the diagnostic load tests are discussed in Chapter 3. The measured data are presented in Chapter 4. Chapter 5 presents an evaluation of the test results. The results obtained from the load rating of the two bridges based on current codes are presented in Chapter 6. Conclusions and recommendations about the diagnostic load tests in relation to the measured responses are presented in Chapter 7. Appendix A contains representative plots of the measured data. Appendix B presents the neutral axis calculations for the composite sections. Finally, Appendices C and D summarize various parameters used in the load rating calculations for the two bridges.

Chapter 2. DESCRIPTION OF THE TWO PRESTRESSED CONCRETE BRIDGES

This section describes the two prestressed concrete bridges that are studied in this thesis. The bridges have many similar features, including length and member size. The primary differences include age, slab details, and angle of skew. Throughout this report, the first bridge is identified as the "Slaughter Creek Bridge" and the second is identified as the "Nolanville Bridge."

2.1 SLAUGHTER CREEK BRIDGE

The first bridge is located south of Austin, Texas, on the northbound access road of Interstate Highway 35 over Slaughter Creek. It was selected to be studied under the load rating project because of its proximity to the University of Texas and relatively easy access to the prestressed concrete girders. The bridge was constructed in 1991 and is in excellent condition. The estimated traffic flow across the bridge is approximately 34,550 vehicles per day [9].

The Slaughter Creek Bridge is 310-ft. long, and consists of three spans of lengths 100, 110, and 100 feet, respectively. The prestressed concrete girders were simply-supported at both ends of each span. A cast-in-place slab provides some degree of continuity between spans for live loads. There is no continuity at the abutment end. The south-most span was selected for this study. Figure 2.1 shows a side view of this first span in the direction of traffic.

Figure 2.1 Side View of the Instrumented Span at the Slaughter Creek Bridge

Figure 2.2 shows a plan view of the span and Fig. 2.3 shows its cross section. Five, Type IV, precast, prestressed concrete girders span longitudinally between skewed supports at an 8-ft spacing. The angle of skew is 15 degrees as shown in Fig. 2.2. Three in. of cast in-place concrete over 4.5-in. precast concrete panels form the 7.5-in. thick slab on top of the girders. Type T502 traffic rails span longitudinally along the east and west edges of the roadway. The overall width of the bridge is 38 feet and the clear roadway is 36 feet.

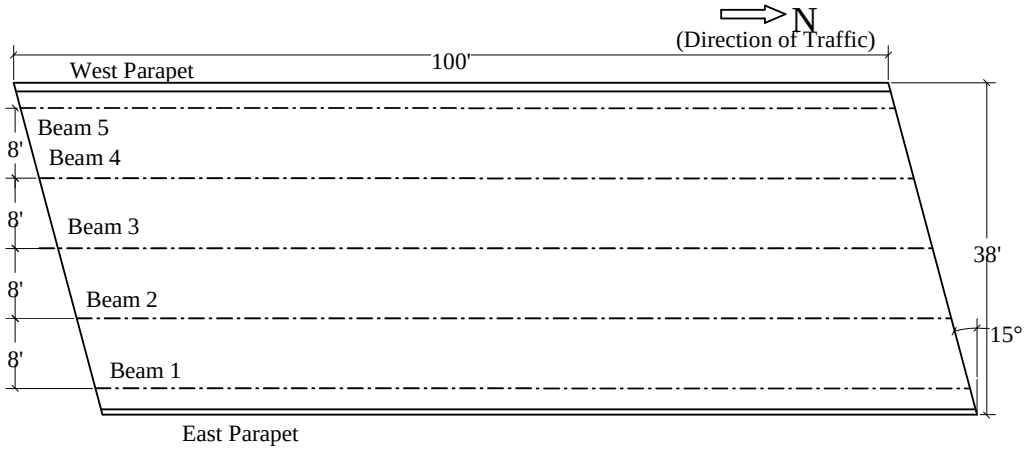

Figure 2.2 Plan View of the Instrumented Span - Slaughter Creek Bridge

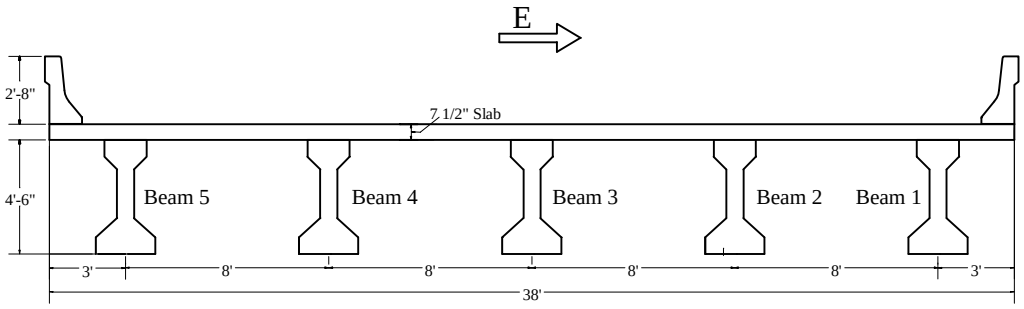

Figure 2.3 Cross Section of the Instrumented Span - Slaughter Creek Bridge

Figure 2.4 shows the cross section of a typical Type IV, precast, prestressed concrete girder. The cross section of the Type T502 parapet rail is shown in Fig. 2.5. The specified concrete compressive strength for the rails is 3600 psi and they are considered to contribute to the bending stiffness of the exterior composite sections.

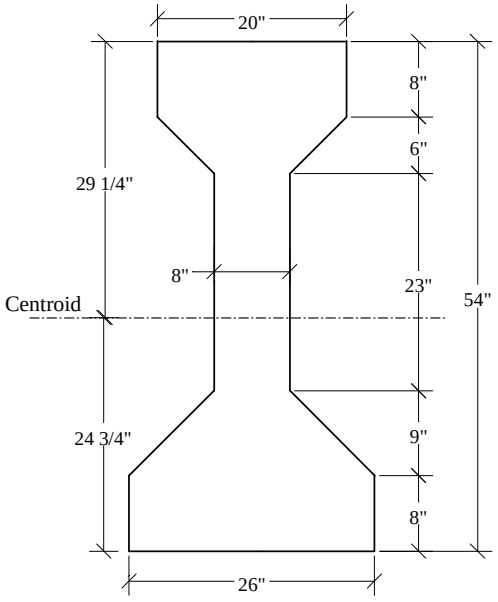

Figure 2.4 Cross Section of a Typical Type IV, Precast, Prestressed Concrete Girder

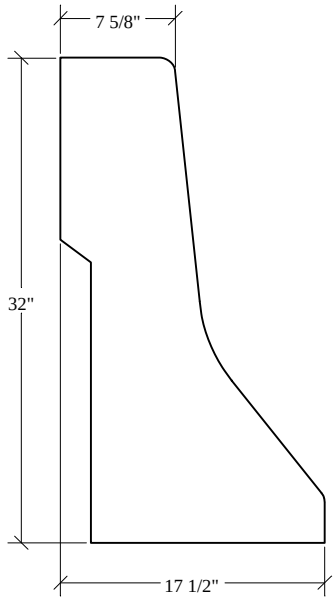

Figure 2.5 Cross Section of a Typical Type T502 Parapet Rail

The specified 28-day concrete compressive strength for the interior girders is 5000 psi and 7700 psi for the exterior girders. All of the precast girders have ½-in. diameter, seven-wire strands initially prestressed to 75% of 270 ksi. The strands are nominally spaced at 2 in. on center. Figure 2.6 shows a typical elevation of half of the span of an interior girder and its cross section at the mid-span and at the supports. The drawings include the girder centroids and the strand patterns in each case. Six of the 36 strands used in the interior girders are depressed. The eccentricity of the strands is 13.08 in. at the ends and 20.75 in. at the mid-span of the beams. Figure 2.7 includes similar information about the exterior girders. These had 58 straight strands at an eccentricity of 10.41 in.

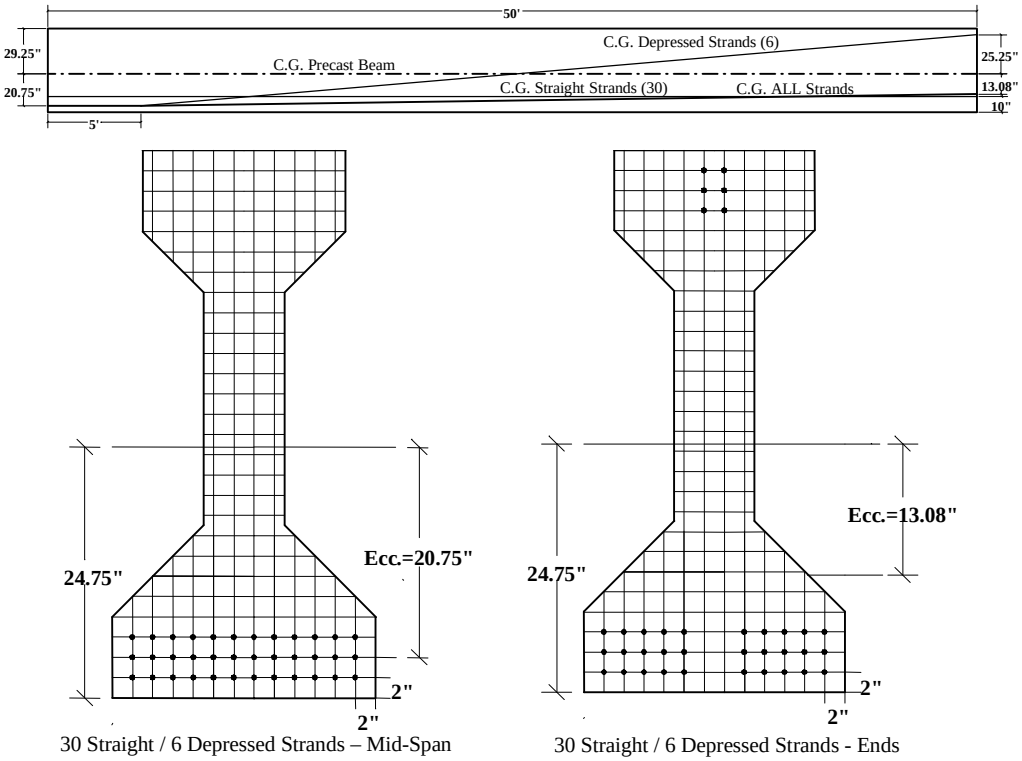

30 Straight / 6 Depressed Strands – Mid-Span

30 Straight / 6 Depressed Strands - Ends

Figure 2.6 Elevation and Cross Section Views of the Interior Girders, Mid-Span and End Sections, Slaughter Creek Bridge

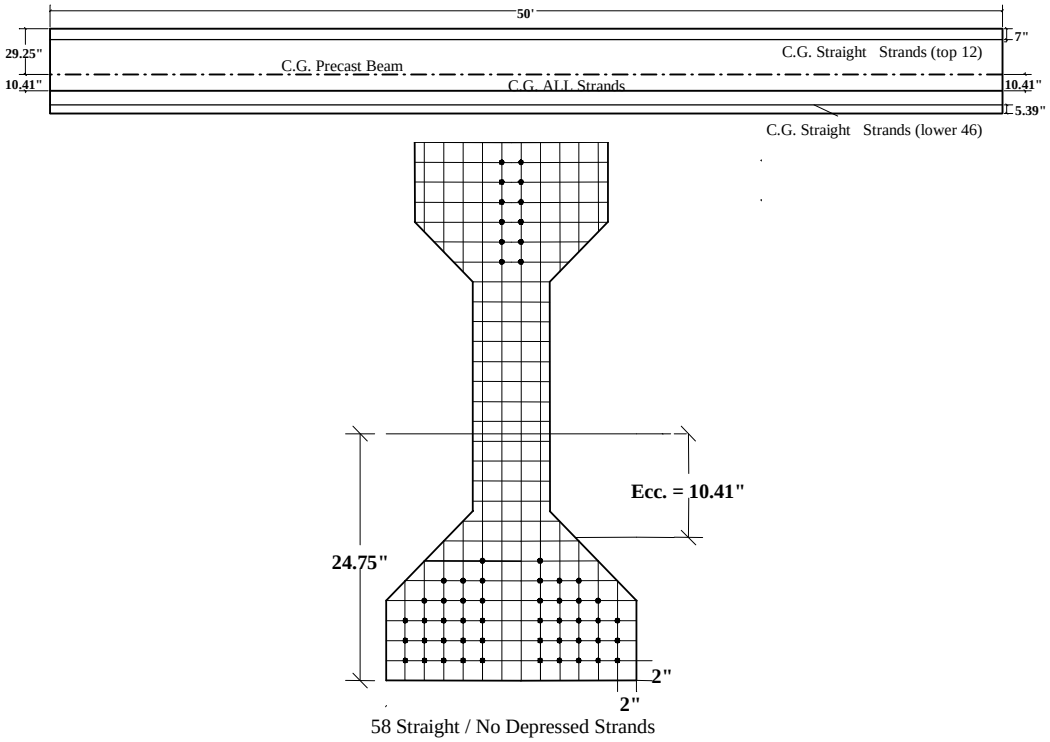

Figure 2.7 Elevation and Cross Section Views of the Exterior Girders, Slaughter Creek Bridge

Casting the 3-inch slab on top of the 4.5-in. precast panels forms interior and exterior composite sections. The connectors cast in the precast girders are #3 reinforcing bars spaced at 1-ft, and they are expected to facilitate composite action between the precast girders and the cast-in-place slab. The interior and exterior girders are defined as shown in Fig. 2.8 and 2.9 respectively. Note that a 20-in. wide layer of concrete is cast between the precast Type IV girders and the slab. Its thickness varies along the span. The thickness is estimated to be ½ in. at mid-span, ¾ in. at the two-thirds span, and 1 in. at the five-sixths span.

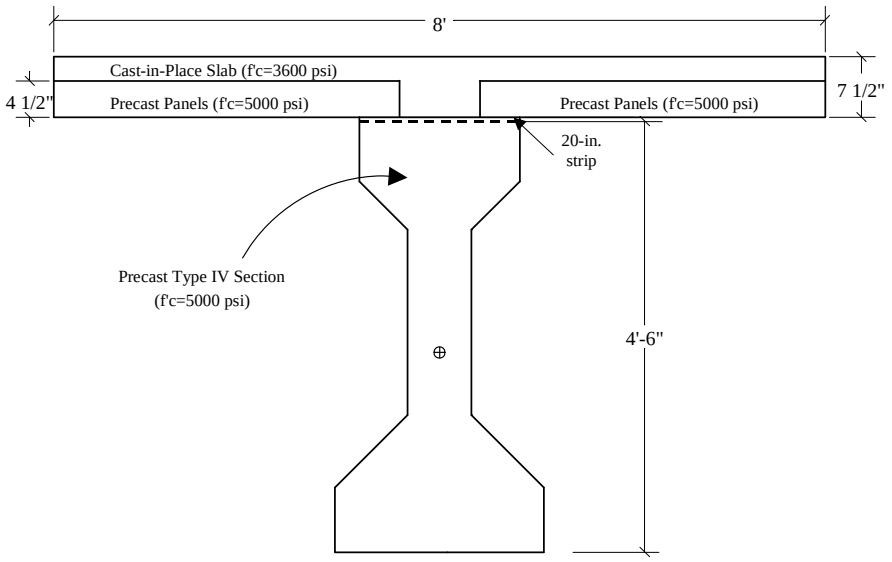

Figure 2.8 Composite Section for Interior Girder - Slaughter Creek Bridge

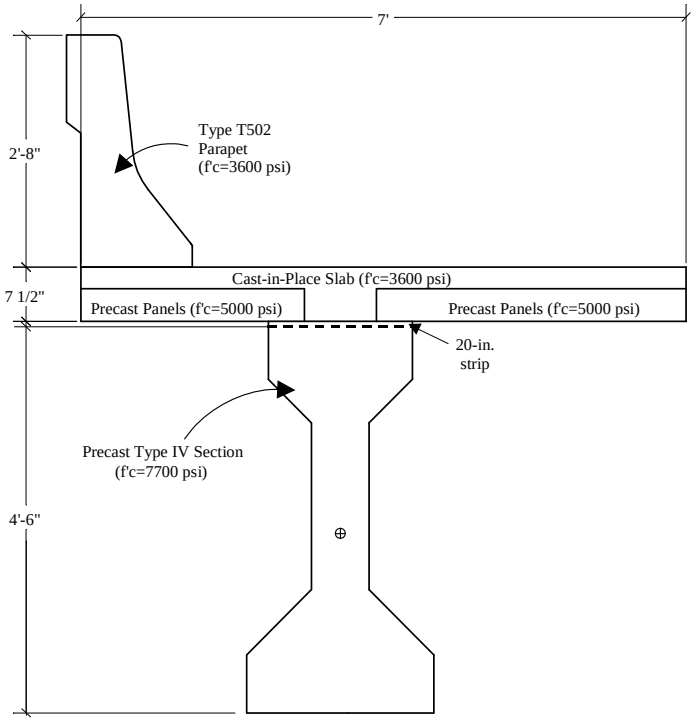

Figure 2.9 Composite Section for Exterior Girder - Slaughter Creek Bridge

2.2 OLD NOLANVILLE ROAD BRIDGE

The second bridge is located in Nolanville, Texas, on eastbound Texas Highway 190. This bridge was studied in conjunction with researchers from New Mexico State University and Bridge Diagnostics, Inc.. The Nolanville prestressed concrete bridge was one of five bridges tested during a one-week period in September 1998. The bridge was selected primarily because of its proximity to Fort Hood. It also has nearly the same dimensions as the Slaughter Creek Bridge, and therefore, provided the opportunity to evaluate the measured response of similar precast, prestressed concrete girder bridges. The bridge was constructed in 1977 and is in excellent condition. Eastbound traffic on highway 190 crosses the bridge and the estimated traffic flow is approximately 15,390 vehicles per day. Figure 2.10 shows an elevation view of the instrumented span of the structure.

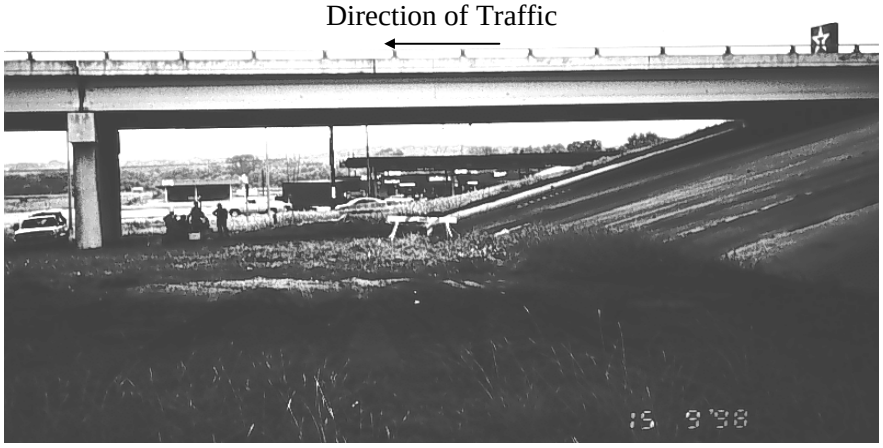

Figure 2.10 Side View of the Instrumented Span at the Nolanville Bridge

The Nolanville Bridge is 306 ft. long, and consists of three, 102-ft. long, simply-supported spans. The first span in the direction of traffic was selected for

this study. Figure 2.11 shows a plan view of the bridge and Fig. 2.12 shows its cross section. Five, Type IV, precast, prestressed concrete girders span longitudinally between the supports at a 9.5-ft spacing. Unlike the Slaughter Creek Bridge, the Nolanville Bridge has no skew, but it has diaphragms that are located at quarter-points and at the ends of the spans. Modified Type T4 aluminum traffic rails also span longitudinally along the north and south edges of the roadway. The overall width of the bridge is 43'-8" and the clear roadway is 42 feet. There were no precast panels used in this case, and the width of the cast-in-place slab was 8.25-in. Cracks indicate that unintended continuity is present at the abutment end, but there is no indication of continuity between adjacent spans.

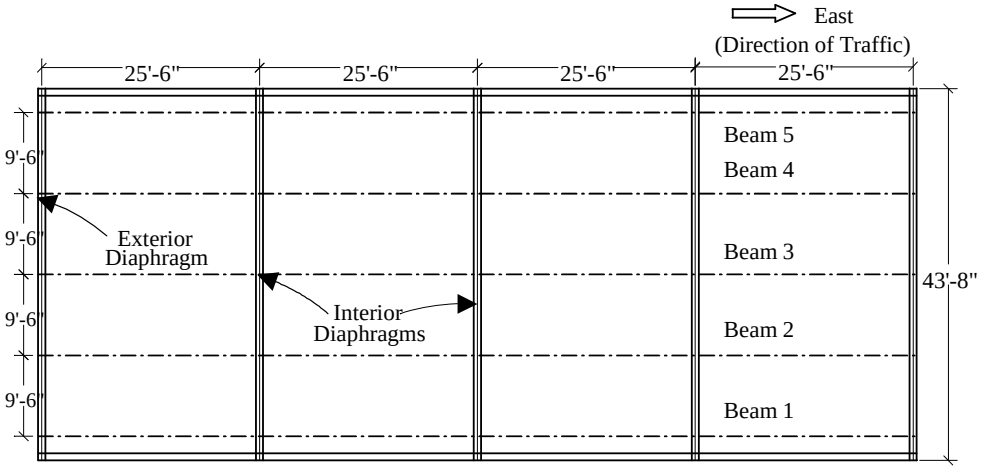

Figure 2.11 Plan View of the Instrumented Span at the Nolanville Bridge

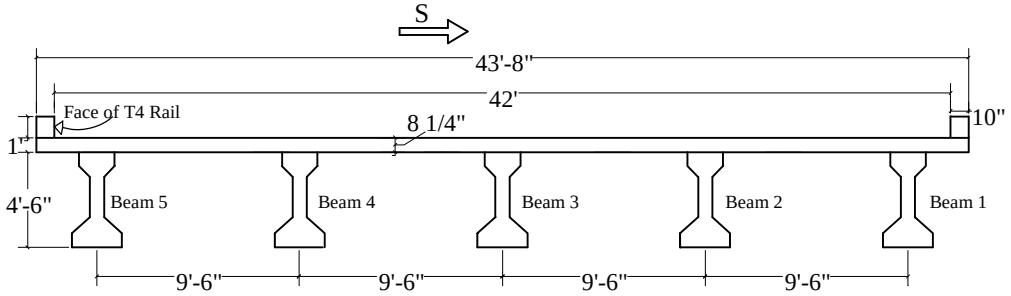

Figure 2.12 Cross Section of the Instrumented Span at the Nolanville Bridge

The specified 28-day concrete compressive strength for the precast girders is 6200 psi. All girders were cast with ½-in. diameter, seven-wire strands initially prestressed to 70% of 270 ksi. The strands are nominally spaced on a 2-in. grid as shown in Fig. 2.13. The figure also includes half of an elevation view of the beams. Ten of the 48 strands are depressed, yielding an eccentricity of 10.92 in. at the ends and 19.67 in. at the mid-span of the girders. The figure represents all five girders at the Nolanville Bridge.

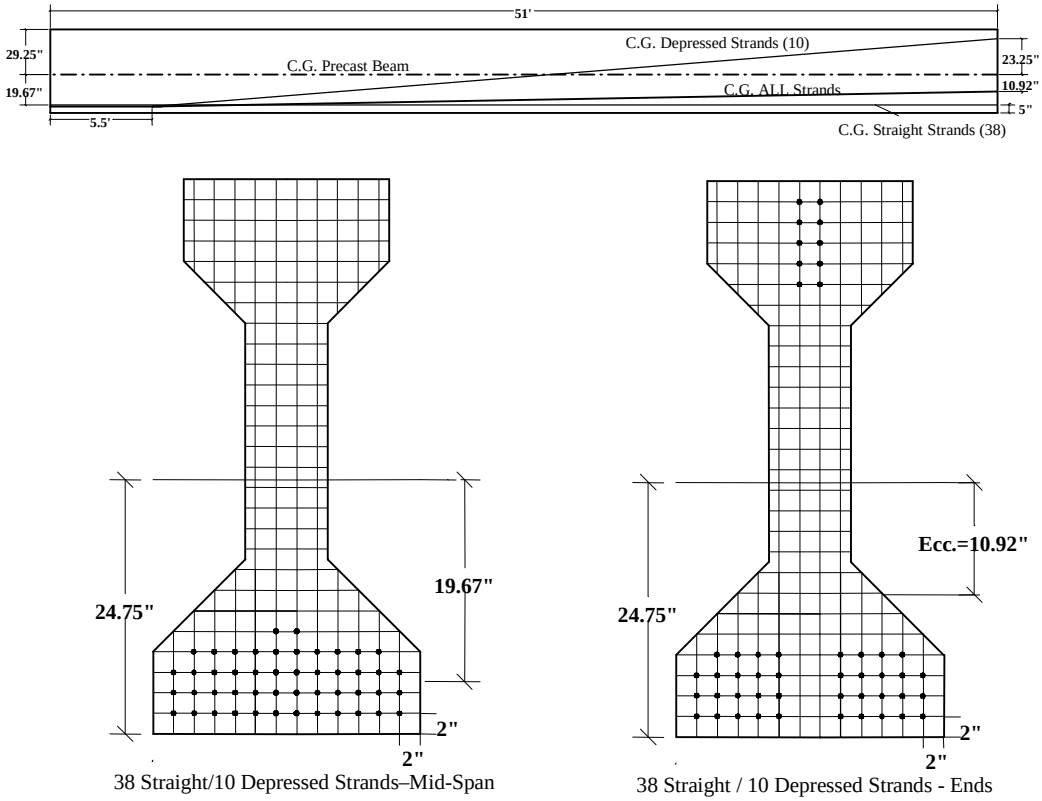

Figure 2.13 Elevation and Cross Section Views of the Girders, Mid-Span and End Sections, Nolanville Bridge

Similar to the Slaughter Creek Bridge, casting the 8.25-in. slab forms composite sections for the interior and exterior girders. These are defined in Fig. 2.14 and Fig. 2.15, respectively. The thickness of the 20-in. layer of concrete varies from ½-in. at the mid-span section to ¾-in. at the three-quarter span. Finally, 6-in. thick diaphragms are cast at the quarter points of the span spanning between the girders. The interior diaphragms are 31 in. deep and the end diaphragms are 22 in. deep. These are shown in Fig. 2.16 and Fig. 2.17 respectively. Note that the interior diaphragms frame into the web and part of the bottom flange of the Type-IV girders, and the end diaphragms frame into the top flanges of the girders.

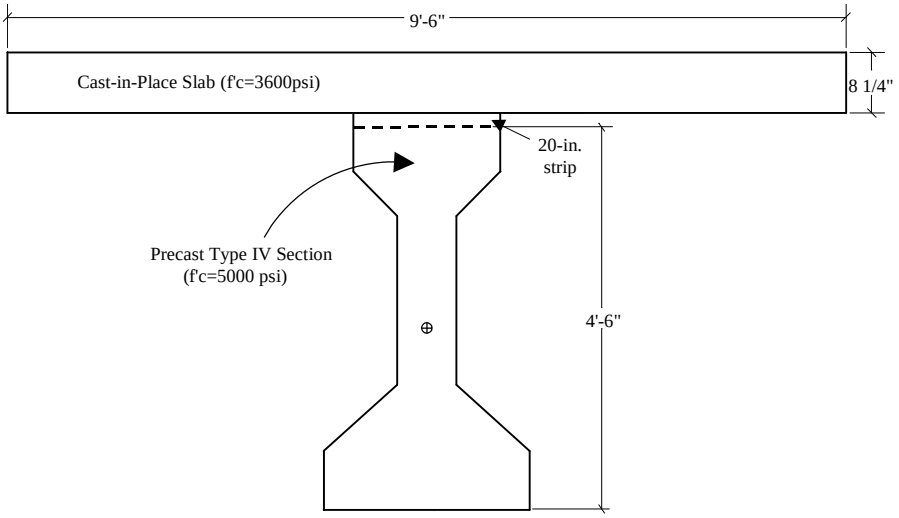

Figure 2.14 Composite Section for Interior Girder - Nolanville Bridge

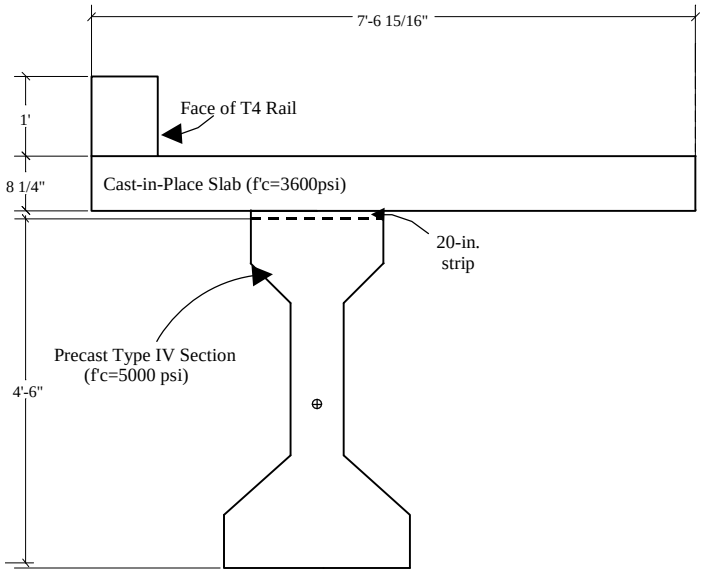

Figure 2.15 Composite Section for Exterior Girder - Nolanville Bridge

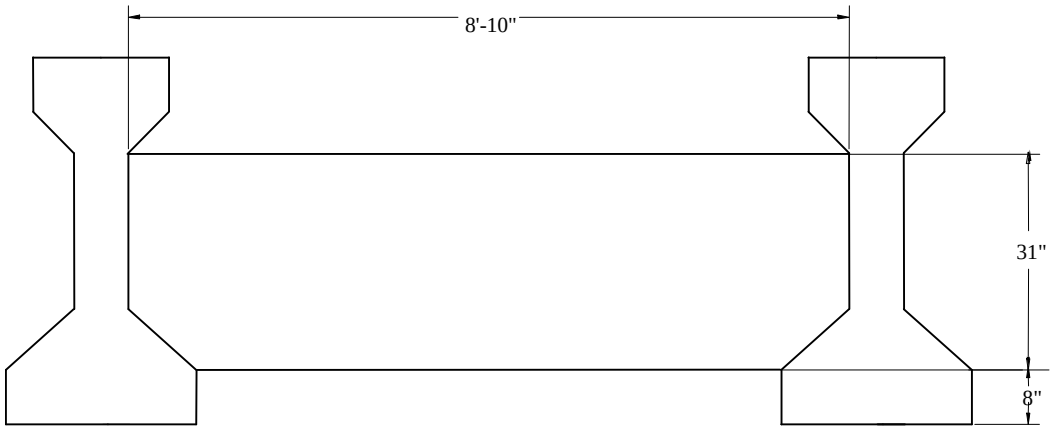

Figure 2.16 Interior Diaphragm Spanning Between Girders – Nolanville Bridge

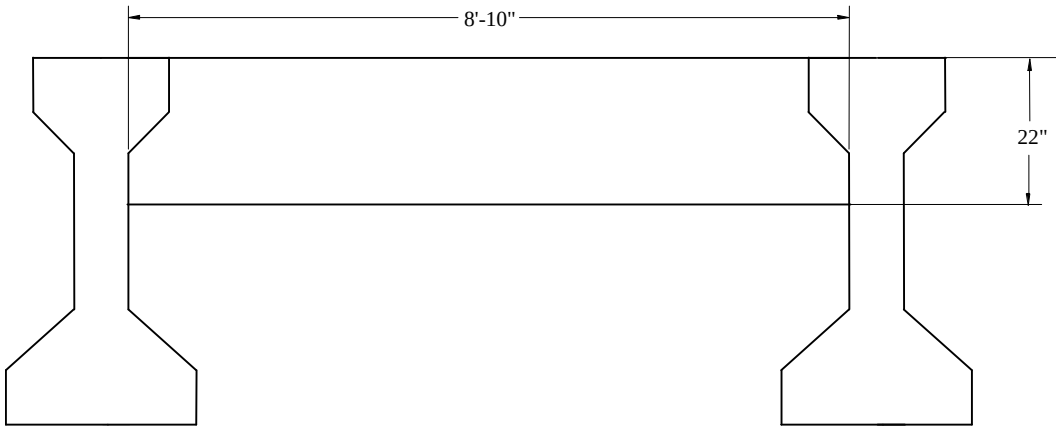

Figure 2.17 End Diaphragm Spanning Between Girders – Nolanville Bridge

2.3 COMPARISON OF THE CHARACTERISTICS OF THE TWO BRIDGES

As noted, the two bridges are similar in many ways. The primary differences are the skew of the Slaughter Creek Bridge and the use of concrete diaphragms in the Nolanville Bridge. In addition, the Slaughter Creek Bridge had concrete parapets at the edges of the roadway and the Nolanville Bridge had aluminum rails. Important characteristics of the two bridges are compared in Table 2.1. Characteristics of the girders are compared in Table 2.2.

Table 2.1 Summary of Details for the Two Prestressed Concrete Bridges

Bridge Detail	Slaughter Creek Bridge	Nolanville Bridge
Number of Spans	3	3
Length of Instrumented Span	100'	102'
Total Width of Bridge	38'	43'-8"
Width of Roadway	36'	42'
Angle of Skew	15º	0º
Number of Precast Type IV Girders	5	5
f'c	5000 psi - interior 7700 psi - exterior	6200 psi
Precast Girder Spacing	8'	9'-6"
Precast Panel Thickness	4.5"	-
f'c	5000 psi - interior	-
Cast-in-Place Slab Thickness	3"	8.25"
f'c	3600 psi	3600 psi
Parapet Rail Type	T502	Modified T4
Material	Precast Concrete	Aluminum
f'c	3600 psi	-
Number of Diaphragms Per Span	0	5

Table 2.2 Summary of Girder Details

Girder Detail	Slaughter Creek Bridge	Nolanville Bridge
Initial Prestress in Strands	202.5 ksi	189 ksi
Number of 0.5-in.Strands - Interior	36	48
Number of Depressed Strands	6	10
Eccentricity at Ends of Span	13.08 in.	10.92 in.
Eccentricity at Mid-Span	20.75 in.	19.67 in.
Number of 0.5-in.Strands - Exterior	58	48
Number of Depressed Strands	0	10
Eccentricity at Ends of Span	10.41 in.	10.92 in.
Eccentricity at Mid-Span	10.41 in.	19.67 in.

Chapter 3. INSTRUMENTATION AND PROCEDURES FOR THE TWO DIAGNOSTIC LOAD TESTS

This chapter describes the three diagnostic load tests that were conducted on the two prestressed concrete girder bridges. The Slaughter Creek Bridge was tested in October 1997 and February 1998, and the Nolanville Bridge was tested in September 1998. These tests are identified as Test Series 1, 2, and 3, respectively, throughout this thesis. The data collected from each of these tests are presented in Chapter 4 and evaluated in Chapter 5.

3.1 OVERVIEW OF DIAGNOSTIC LOAD TESTS

During each diagnostic load test, vehicles of known weight and dimensions were driven across the instrumented span of the bridge. The primary testing parameters included the type of vehicle, the number of vehicles on the bridge simultaneously, and the transverse location of the vehicles.

The instrumentation attached to the bridge was selected to allow the researchers to determine the moment induced in each prestressed concrete girder and assess the performance of the bridge based on these values. The magnitude of the total moment induced during the load test provided an indication of the degree of rotational restraint at the ends of the girders, while the individual girder moments were used to determine the distribution factors.

3.2 INSTRUMENTATION AND DATA ACQUISITION SYSTEM

3.2.1 Strain Gages

Strains were measured on the surface of the concrete using 120-Ohm electrical resistance strain gages. These strain gages are 60-mm long and are manufactured with two, 3-ft long wires. Researchers added a third wire to provide temperature compensation for the gages before attaching them to the bridge.

A wire strain gage, such as the concrete strain gages, is essentially an electrical resistor that operates in a quarter-bridge circuit as the variable resistance. During a load test, strain is induced in the bridge at the location where the strain gage has been placed. This causes the length and resistance of the gage to change. Using the calibrated data acquisition system, the changes in strain are recorded in terms of variations in the voltage output of the electrical resistor based on a 5-volt excitation. Strain is obtained by relating the change in voltage output to the change in the gage's length relative to its initial length.

3.2.2 Data Acquisition System

The data are measured in terms of a voltage output using a calibrated data acquisition system. A Campbell Scientific CR9000 data-acquisition system was used for recording the data during all of the Test Series described in this thesis. The data-acquisition hardware and the software written to collect the data are described in the dissertation by Jáuregui [6].

Figure 3.1 shows the various parts of this system. Eleven junction boxes and a total of 55 completion boxes can be used. Each completion box is

connected to a strain gage to complete the quarter-bridge circuit. Each junction box, conveniently labeled A through K, supports 5 completion boxes. The junction boxes are directly connected to the CR9000. Also necessary is a 12-volt D.C. battery whose voltage is reduced to 5 volts inside the CR9000 to become the excitation for the system. The system is not complete without a computer that has the software platform to operate the CR9000 application program.

The main reason for testing the Slaughter Creek Bridge twice was the need to check some of the hardware changes and software developments that had been implemented in the data acquisition system. The main difference was a reduced level of noise in the data. Data were collected at a frequency of 100Hz during Test Series 1 and 10Hz during Test Series 2.

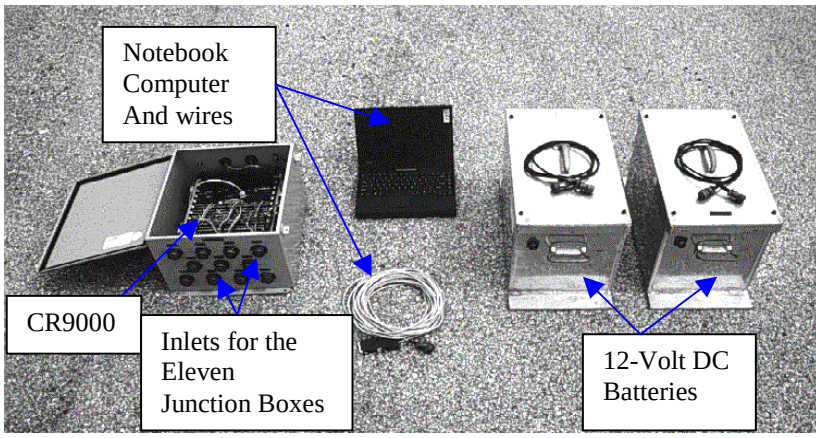

Figure 3.1 Campbell Scientific CR9000 Data-Acquisition System, Batteries and Notebook Computer Used in Each Test Series

Figure 3.2 shows a photograph of the cables used to connect the instrumentation in preparation for a field test. In order to support the junction

boxes, completion boxes and wires close to the gage, “H-hangers” have been used between the prestressed concrete girders. Using a configuration involving the junction boxes as an intermediate step from the CR9000 to the gages offers the advantage of reduced congestion of all the cables in the field. This is very important, because depending on the bridge layout, some of the gages may be more than 50 feet from the data-acquisition system. A total of fifty-five cables of this length would make it very difficult for the research team to work beneath the bridge.

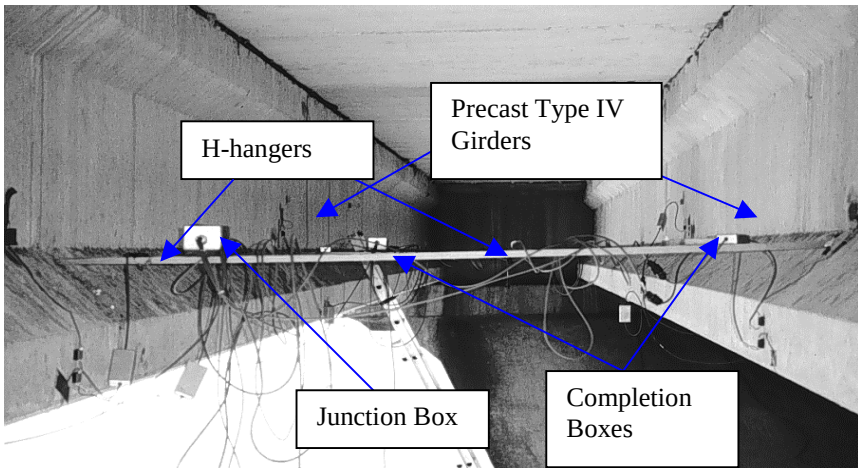

Figure 3.2 H-hangers Used to Support the Junction and Completion Boxes Connected to the Strain Gages

3.3 LOADING VEHICLES

The vehicles used during the diagnostic load tests were ten-cubic-yard dump trucks provided by the Texas Department of Transportation. During Test Series 3 in Nolanville, the U.S. Army provided a Heavy Equipment Transportation System (HETS) as an additional loading vehicle. Throughout this thesis, D1 and D2 denote the two dump trucks used in Test Series 1, and D3 refers to the dump truck used in Test Series 2. D4 and HETS refer to the two vehicles used in Test Series 3.

3.3.1 Dump Trucks

A photograph of a typical ten-cubic-yard truck during a run is shown in Fig. 3.3. Figure 3.4 shows the dimensions of truck D1, and Fig. 3.5 represents trucks D2, D3 and D4, which had identical dimensions.

Figure 3.3 Photograph of a Ten Cubic-Yard Dump Truck Used for the Diagnostic Load Tests

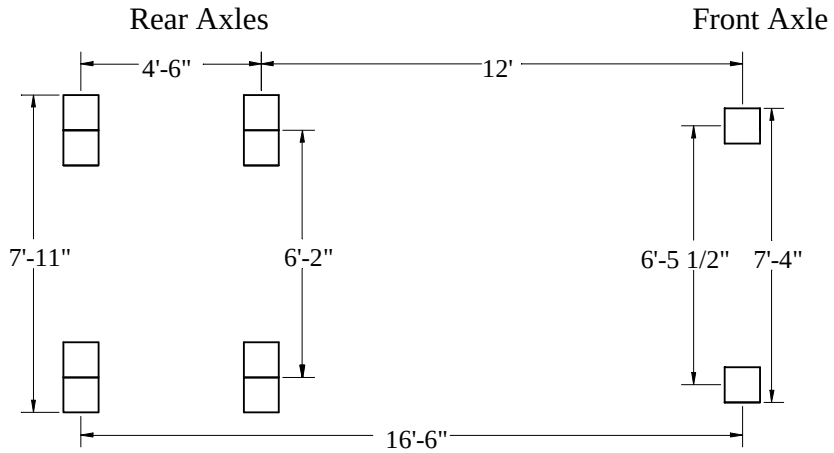

Figure 3.4 Dimensions and Axle Loads for Dump Truck D1

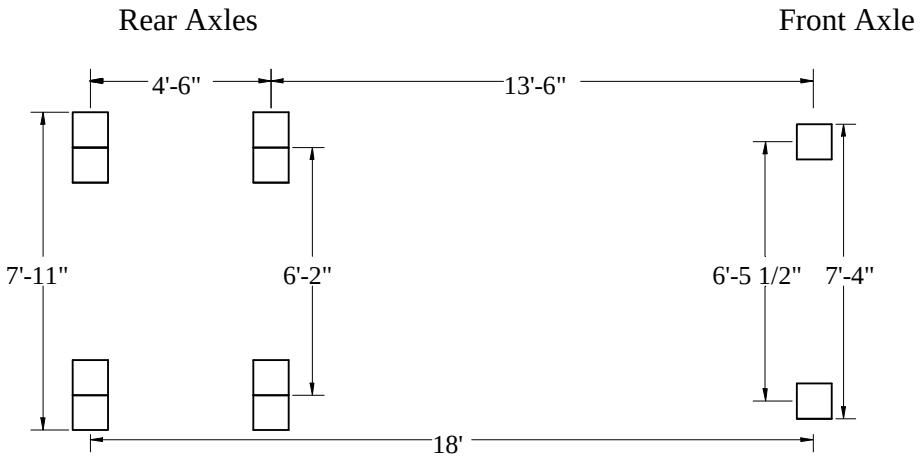

Figure 3.5 Dimensions and Axle Loads for Dump Trucks D2, D3 and D4

Before each test, the trucks were weighed at a weigh station, and the loads were reported for each axle group. Table 3.1 shows the loads for dump trucks D1 through D4.

Table 3.1 Axle Loads for the Dump Trucks

Truck I.D.	Front Axle Load (kips)	Tandem Load/Axle (kips)	Total Weight (kips)
D1	11.8	14.3	40.4
D2	11.6	15.4	42.4
D3	10.2	14.8	39.7
D4	10.1	18.2	46.5

3.3.2 Heavy Equipment Transportation System (HETS)

Figure 3.6 is a photograph of the 225-kip HETS truck. A layout showing the dimensions of this vehicle is shown in Fig. 3.7.

Figure 3.6 Photograph of the HETS Vehicle, Test Series 3, Nolanville Bridge

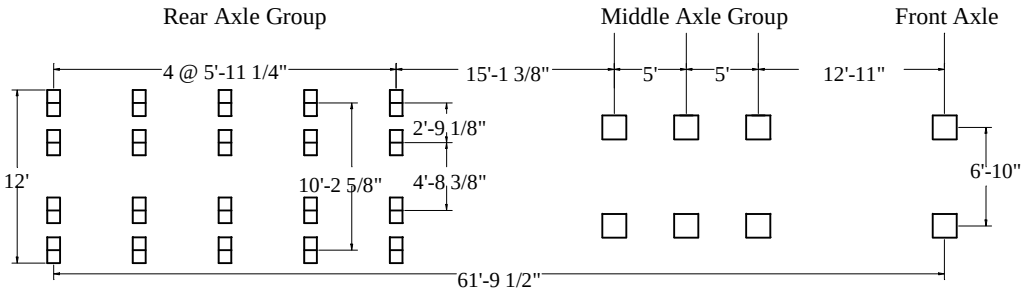

Figure 3.7 Dimensions and Axle Loads for the HETS Truck

Table 3.2 lists the axle loads starting from the front axle group and moving to the back of the vehicle.

Table 3.2 Axle Loads for the HETS

Axle Position	Axle Loads (kip/axle)
Front	21.9
Middle	19.7
	19.2
	18.6
Rear	23.9
	28.9
	27.9
	28.1
	27.0

3.4 LOCATION OF INSTRUMENTS FOR TEST SERIES 1 AND 2

Concrete strain gages were used to monitor the response of the bridges under the live loads applied by the loading vehicles. This section presents the locations where strain gages were placed on the Slaughter Creek Bridge for Test Series 1 and 2.

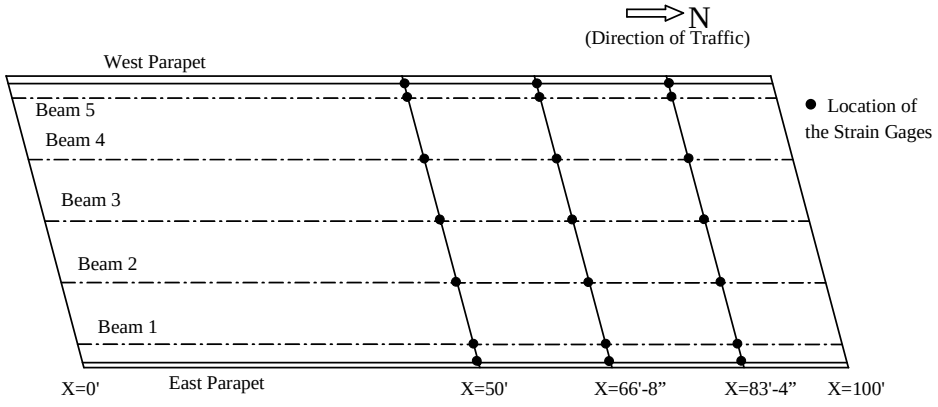

Figure 3.8 Instrumentation Layout Used in Test Series 1 and 2, Slaughter Creek Bridge

A total of 36 strain gages were placed on the Slaughter Creek Bridge at the locations shown in Fig. 3.8. Note that the dots in the figure may indicate more than one gage. Three sections, each corresponding to a third-point of the second half of the span, were selected to instrument. Their longitudinal positions, measured from the abutment end, were 50’ (mid-span), 66’-8” (two-thirds span) and 83’-4” (five-sixths span).

3.4.1 Strain Gages on the Girders

There were 30 strain gages mounted on the precast girders at the three longitudinal positions. Two gages were mounted on the cross section of each girder: one at the extreme tension (bottom) fiber for measuring maximum strains, and one 20 in. above the bottom surface. The second gage is necessary for locating the neutral axis and calculating the induced moments in the composite sections. Figure 3.9 shows the cross section of a Type IV girder illustrating the locations of both of these gages. Figure 3.10 shows a photograph of a gage mounted at the extreme bottom fiber of a precast girder.

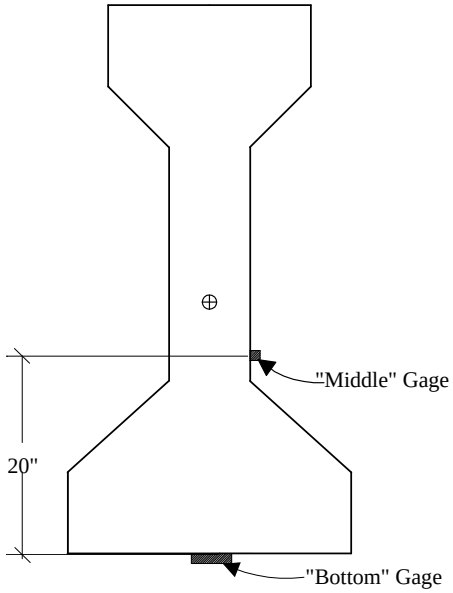

Figure 3.9 Cross Section of the Type IV Girder with the Two Strain-Gage Locations

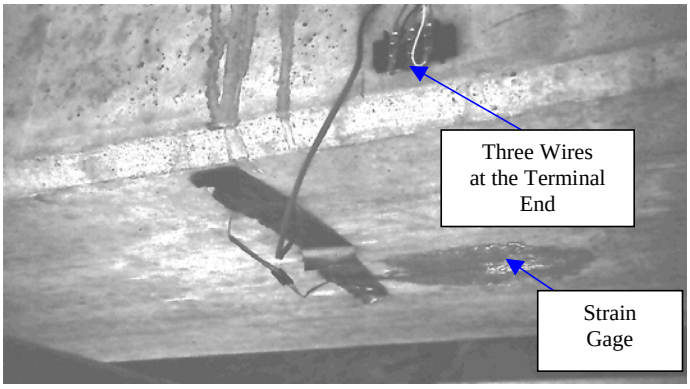

Figure 3.10 Wire Concrete Gage Placed at the Extreme Bottom Fiber of the Precast Section

3.4.2 Strain Gages on the Parapets

Six gages were placed at the top of the type T502 parapet rails on both sides of the roadway. The intent was to examine the straight-line theory and

verify that the parapets are part of the composite sections resisting bending. Figure 3.11 shows the location of these gages on the sections.

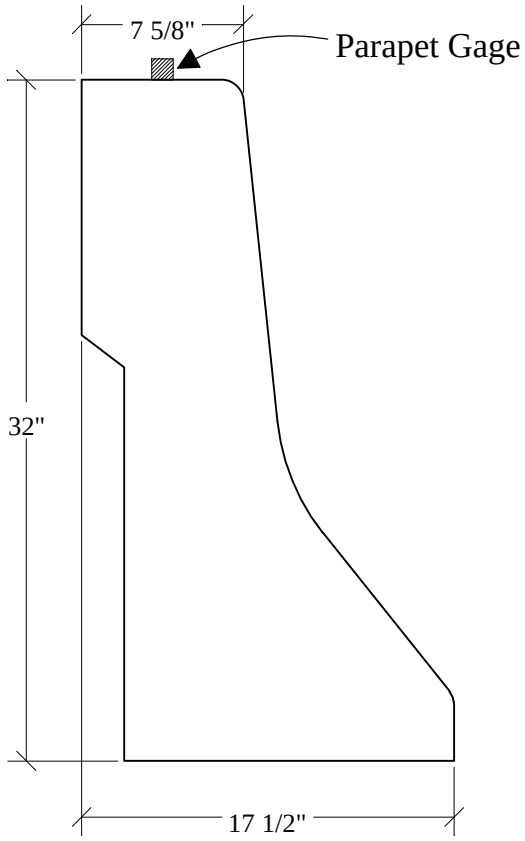

Figure 3.11 Cross Section of Type T502 Parapet with Strain Gage Location

3.5 LOCATION OF INSTRUMENTS FOR TEST SERIES 3

The similarity of the Nolanville Bridge to the Slaughter Creek Bridge allowed the implementation of a similar instrumentation layout for Test Series 3. A total of 26 wire strain gages were placed in two longitudinal sections: at the mid-span (51 ft) and three-quarter span (76.5 ft) sections measured from the

abutment end. Figure 3.12 shows the longitudinal gage locations in a plan view of the Nolanville Bridge.

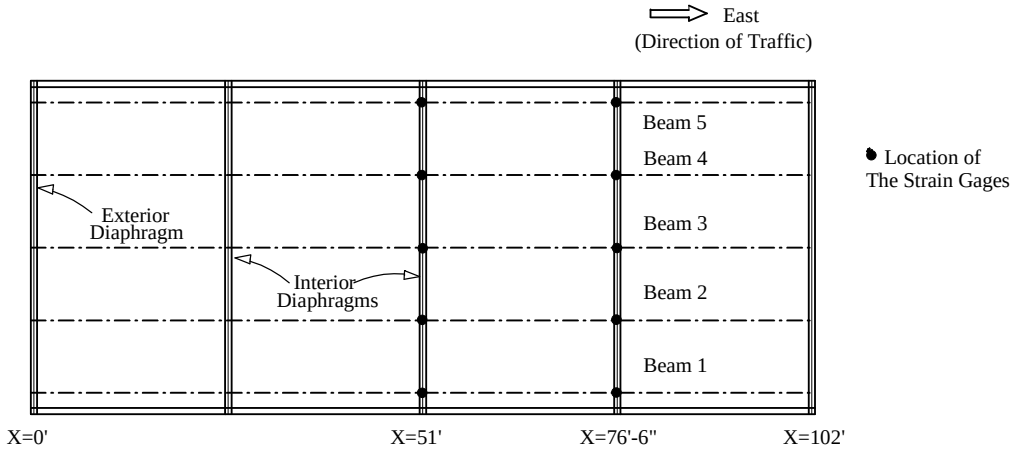

Figure 3.12 Instrumentation Layout Used in Test Series 3, Nolanville Bridge

3.5.1 Strain Gages on the Girders

There were a total of twenty-two gages on the girder cross sections at the two longitudinal locations. Two gages were mounted on the cross section of each girder at the same locations as in Test Series 1 and 2. In addition, two of the girders (B3 and B4) were also instrumented at 3 in. below the slab-girder intersection but only at the mid-span section. Figure 3.13 shows all three of these gage locations over the depth of the precast member.

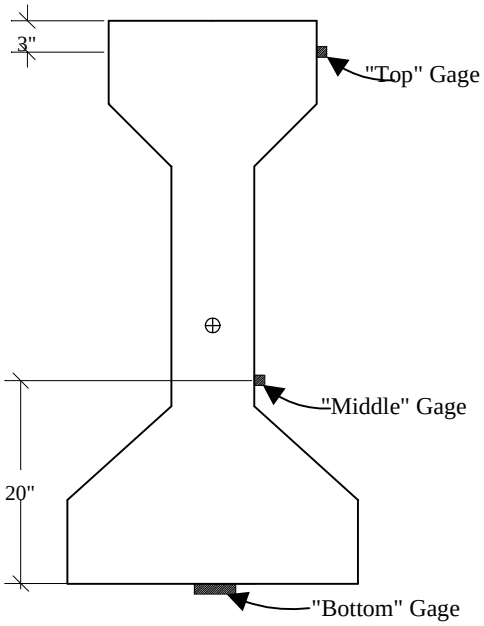

Figure 3.13 Cross Section of the Type IV Girder with the Three Strain-Gage Locations

The modified type T4 aluminum rails were not instrumented in this case. After examining the construction details, it was decided that they did not increase the bending stiffness of the exterior girders appreciably.

3.5.2 Strain Gages on the Diaphragms

During the Test Series at the Nolanville Bridge, four gages were also attached to the mid-span diaphragm. Two gages were placed between girders 2 and 3, and two were placed between girders 3 and 4. One of the gages was located 1 in. from the top edge of the diaphragm and the other was located 1 in. from the bottom edge of the diaphragm. Figure 3.14 shows the locations of the two gages on the surface of the concrete at the interior diaphragm.

This was done to observe the levels of bending of these members as they prevent the out-of-plane rotations of the precast girders. The measurements taken at these locations are discussed in Section 4.3.2.

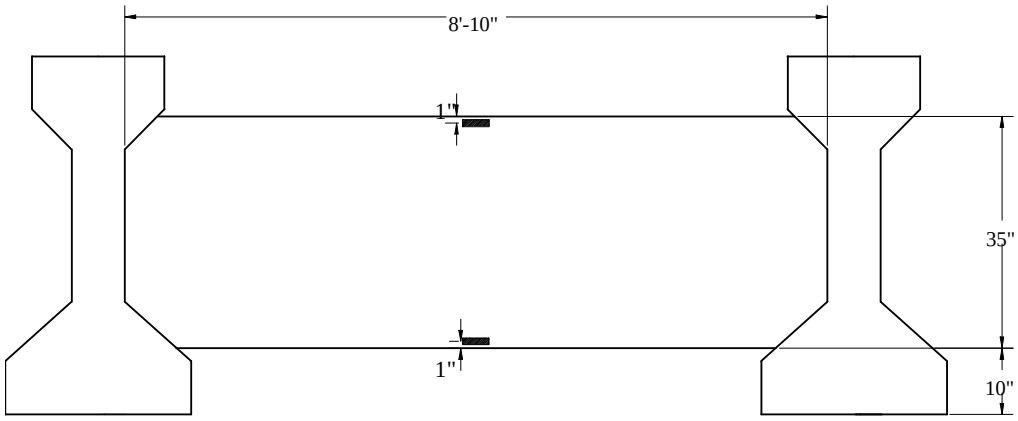

Figure 3.14 Strain Gages Attached to the Surface of the Interior Diaphragms

3.6 SUMMARY OF THE GAGE LOCATIONS FOR THE THREE TEST SERIES

Table 3.3 summarizes the instrumentation layouts used in the three Test Series studied.

Table 3.3 Summary of the Locations of the Strain Gages

Test Series	Distance from End in Direction of Traffic (ft)	Number of Strain gages		
		Prestressed Girders	Parapet Rails	Diaphragms
1	50	10	2	-
	66.7	10	2	-
	83.3	10	2	-
2	50	10	2	-
	66.7	10	2	-
	83.3	10	2	-
3	51'	12	0	4
	76.5'	10	0	0

3.7 TRANSVERSE TRUCK PATHS

The objective of each diagnostic load test is to study the distribution of loads among the girders. For this reason, the trucks were run longitudinally along the instrumented spans and at various transverse paths across the width of the bridge. The wheel lines were positioned on the deck to induce maximum live-load moment in the girders. This is necessary in order to proceed with the load-rating calculations.

Four transverse paths were run during Test Series 1 and 2 and three paths were run during Test Series 3. In each case, P1 represents the path closest to the right edge in the direction of traffic. P3 in TS3 and P4 in TS1 and TS2 refer to the path closest to the left edge. Figures 3.14 through 3.16 show plan and cross section views of the Slaughter Creek Bridge indicating the paths run by vehicles D1 through D3 during Test Series 1 and 2. Figures 3.17 through 3.20 follow with similar information for Test Series 3 at the Nolanville Bridge for vehicles D4 and the HETS. Note that in Test Series 1, there were 6 runs where both vehicles (D1 and D2) moved simultaneously along the span. These are called “combined truck” runs, and are defined in Fig. 3.16.

The broken lines represent the locations of the front left tires of the loading vehicles except for paths P1 and P2 in Test Series 3, where they represent the location of the front-right tires. The arrows in the cross section views indicate the wheels of the rear axles as the trucks move in the direction of traffic. The centerlines of the precast, Type IV, girders are shown in the plan view.

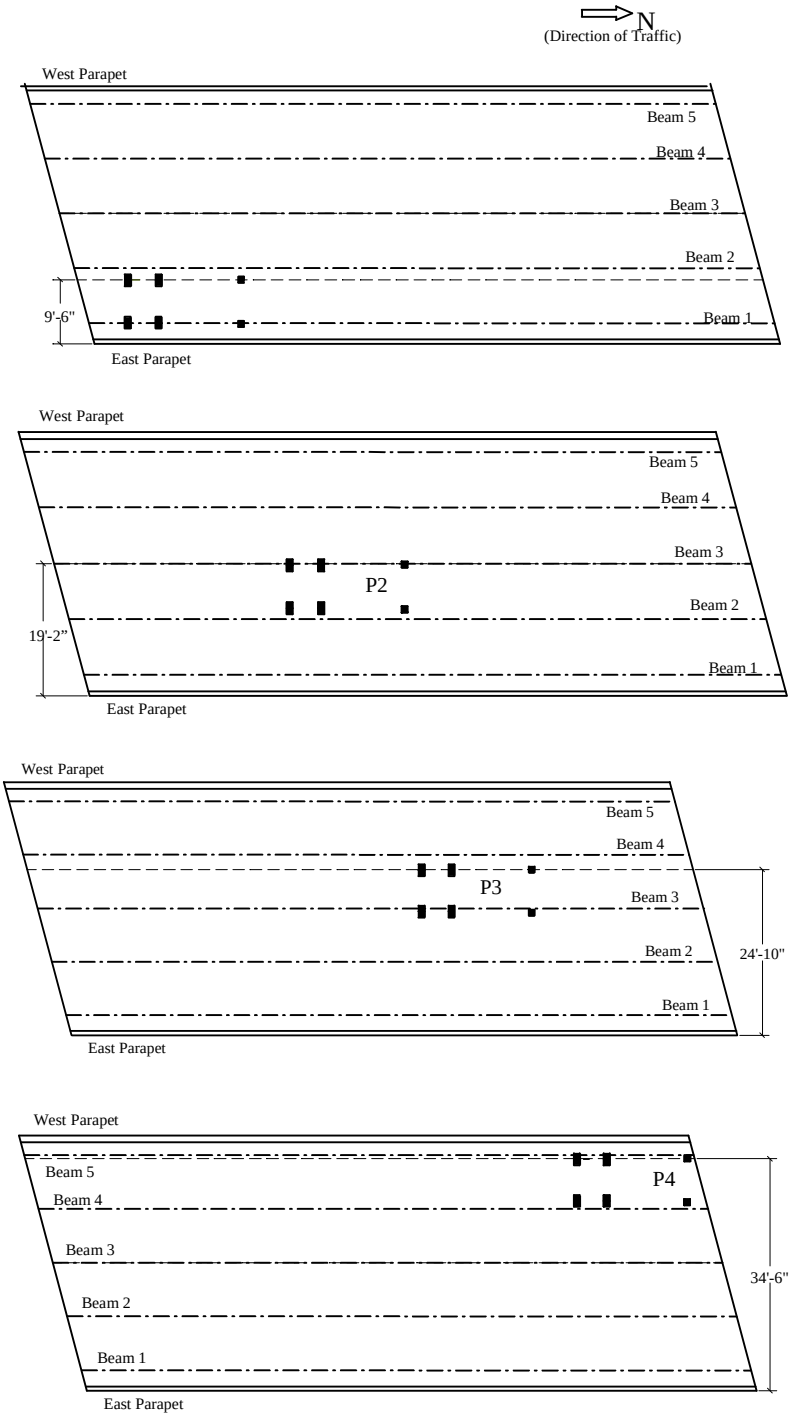

Figure 3.15 Truck Paths P1 through P4, Test Series 1&2, Plan View

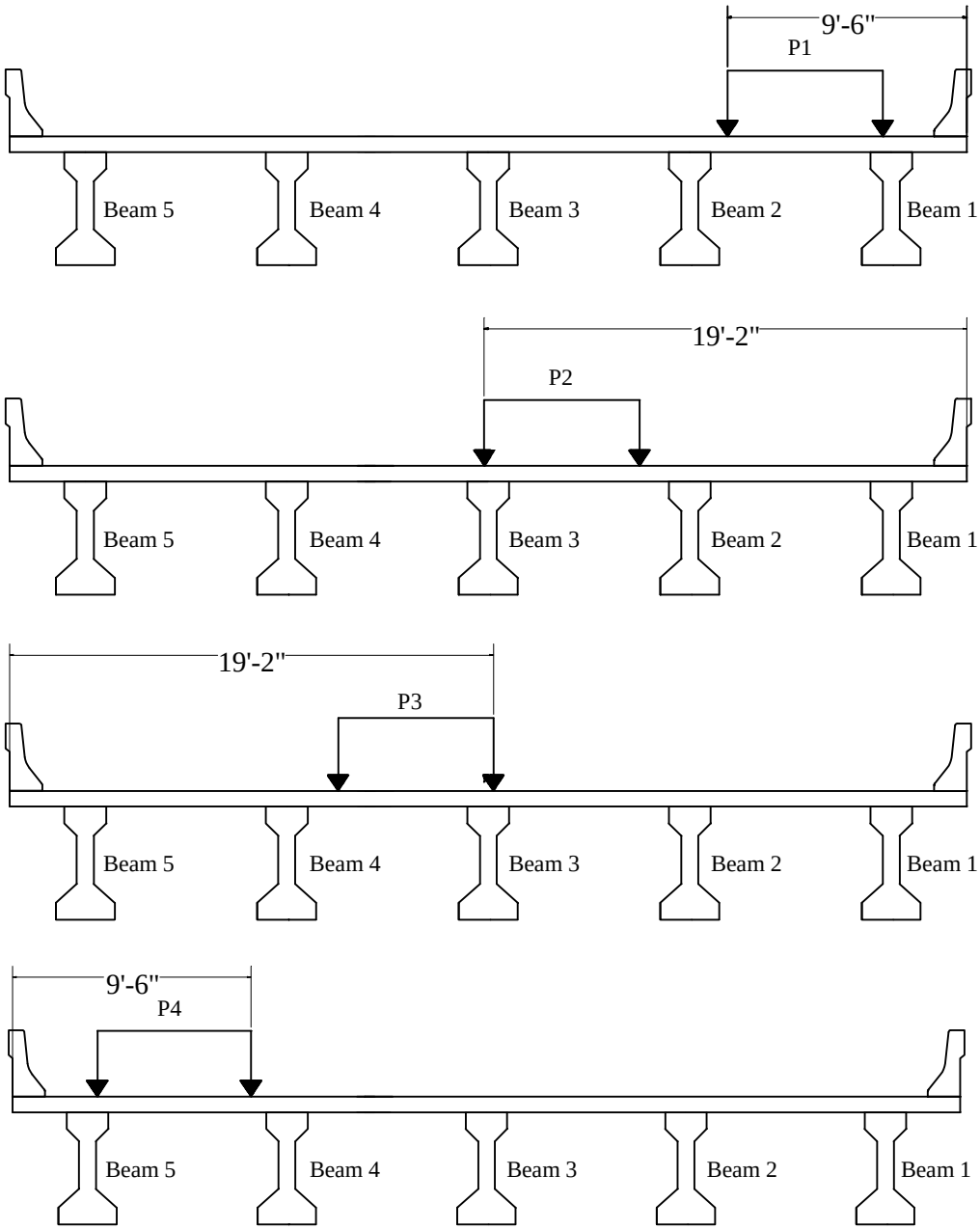

Figure 3.16 Truck Paths P1 through P4, Test Series 1&2, Cross Section View

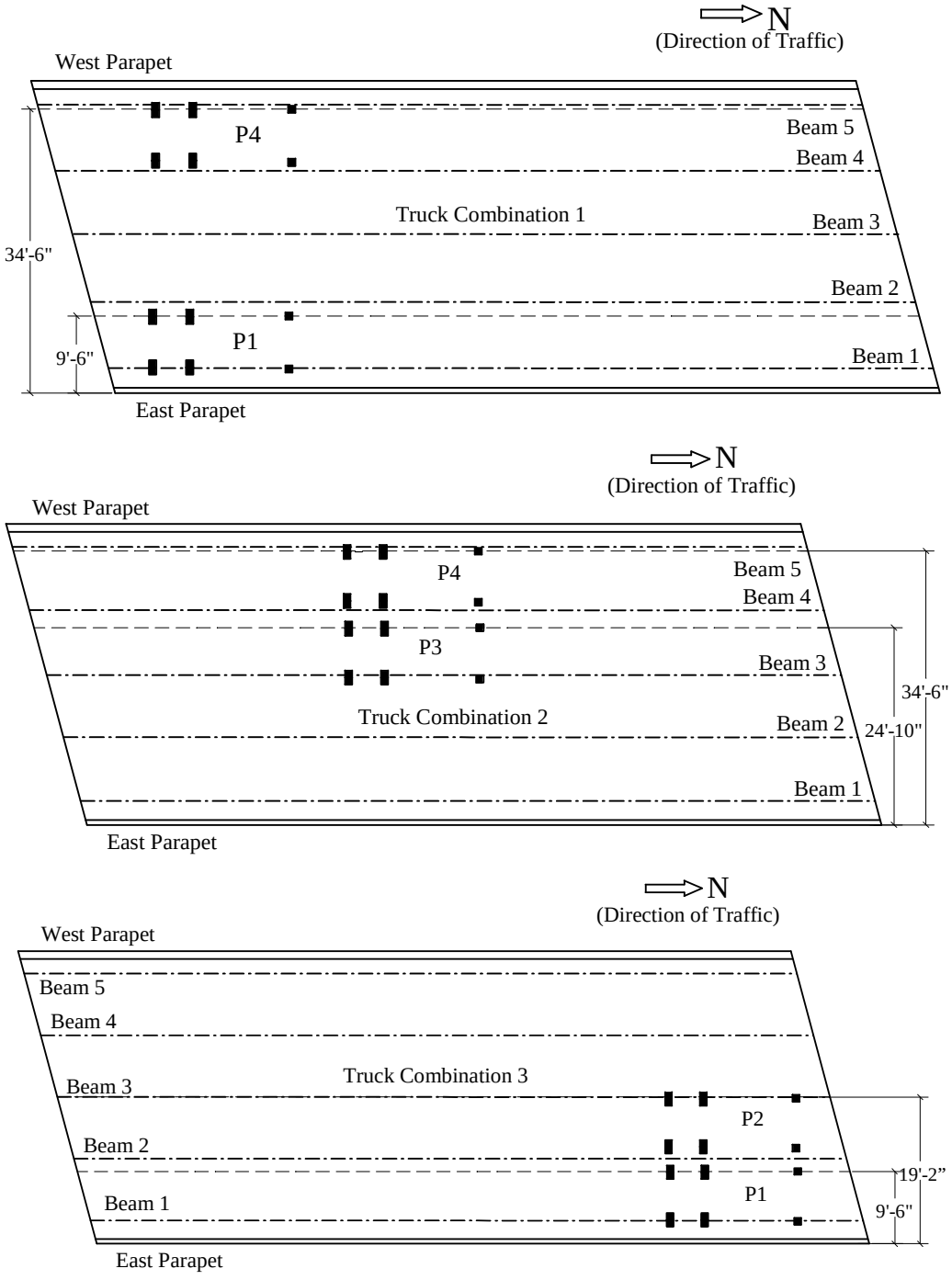

Figure 3.17 Combined Truck Paths during Test Series 1, Plan View

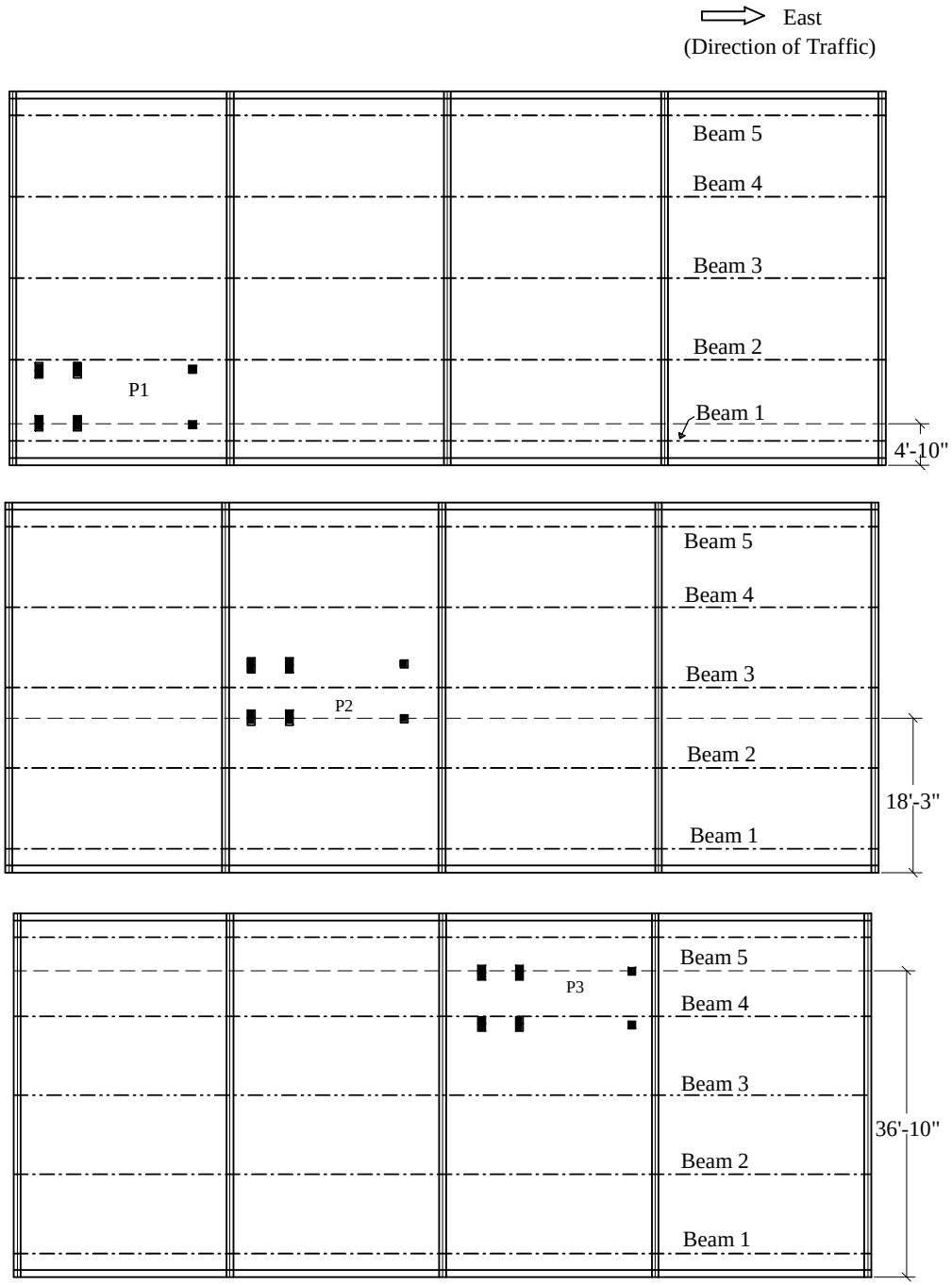

Figure 3.18 Truck Paths P1 through P3, Test Series 3, Plan View

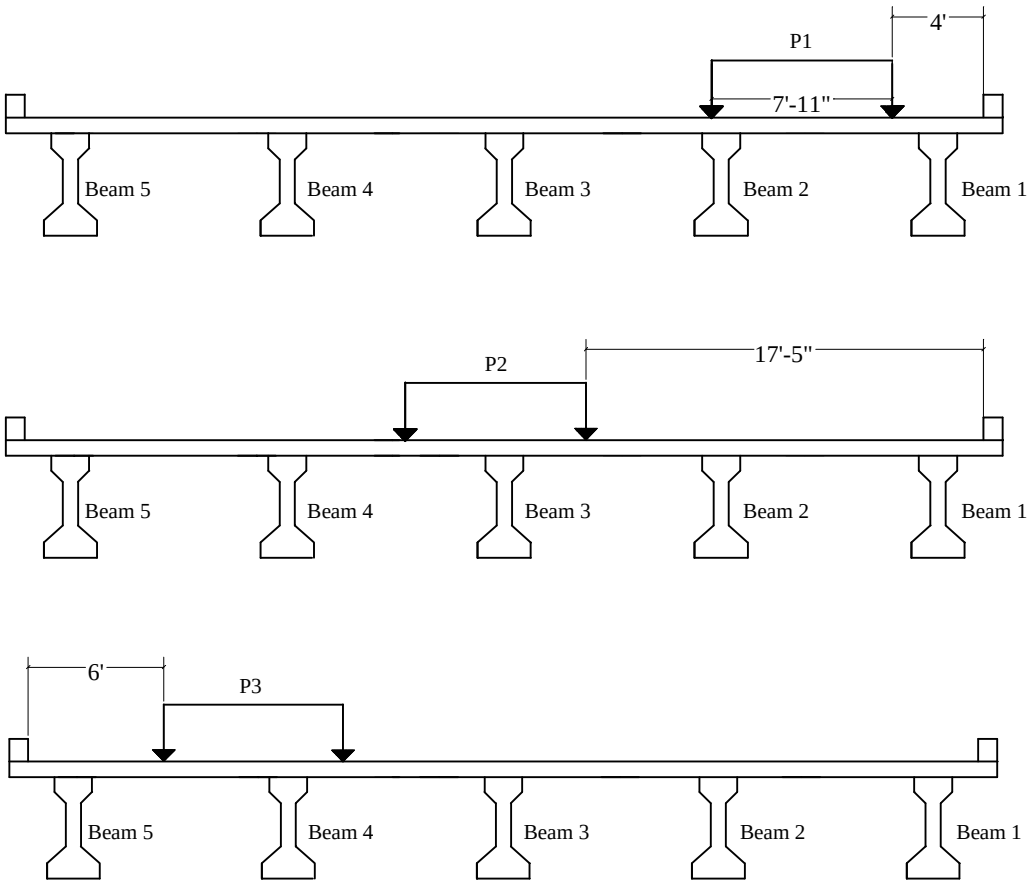

Figure 3.19 Truck Paths P1 through P3, Test Series 3, Cross Section View

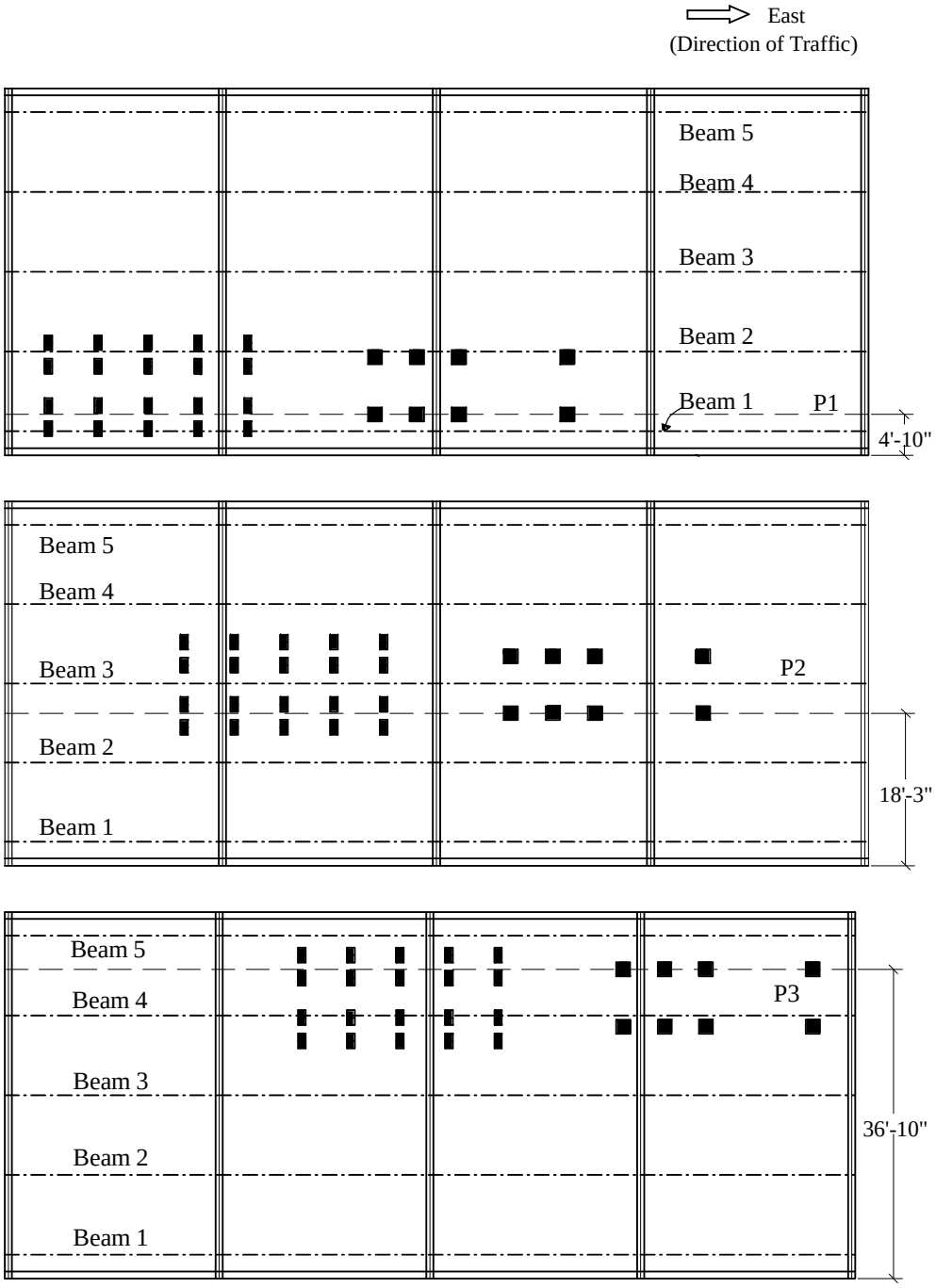

Figure 3.20 HETS Paths P1 through P3, Test Series 3, Plan View

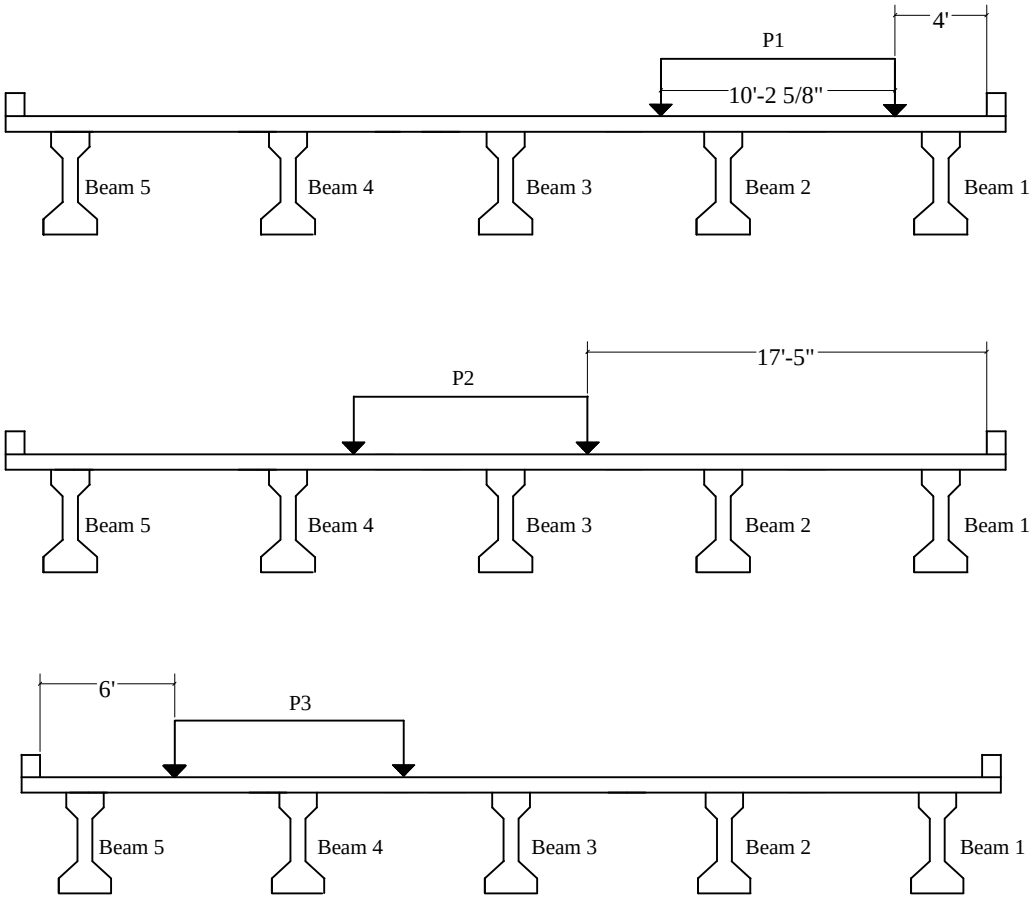

Figure 3.21 HETS Paths P1 through P3, Test Series 3, Cross Section View

There were eight single truck and six combination truck runs in the first Test Series, eight single truck runs in the second and eleven single truck runs in the third Test Series for a total of 33 runs. Table 3.4 presents a summary of all the runs, including the vehicles and their paths.

Table 3.4 Summary of the Vehicle Runs during all Three Test Series

Test Series	Run	Bridge I.D.	Vehicle I.D.	Vehicle Path(s)
TS1	1	Slaughter	D2	P4
	2	Creek	D1	P4
	3		D2	P3
	4		D1	P3
	5		D2	P2
	6		D1	P2
	7		D2	P1
	8		D1	P1
	9		COMBO 1	D1-P4 / D2-P1
	10		COMBO 1	D1-P4 / D2-P1
	11		COMBO 2	D2-P4 / D1-P3
	12		COMBO 2	D2-P4 / D1-P3
	13		COMBO 3	D1-P2 / D2-P1
	14		COMBO 3	D2-P2 / D1-P1
TS2	15	Slaughter	D3	P4
	16	Creek	D3	P4
	17		D3	P3
	18		D3	P3
	19		D3	P2
	20		D3	P2
	21		D3	P1
	22		D3	P1
TS3	23	Nolanville	HETS	P1
	24		HETS	P3
	25		HETS	P2
	26		HETS	P2
	27		HETS	P2
	28		D4	P3
	29		D4	P3
	30		D4	P2
	31		D4	P2
	32		D4	P1
	33		D4	P1

Chapter 4. MEASURED RESPONSES OF THE TWO BRIDGES

This chapter presents the data that were measured during the three diagnostic load tests of the Slaughter Creek and Nolanville prestressed concrete bridges. The measured strains obtained during each Test Series are discussed. Within a given test, each run was duplicated in order to examine the reproducibility of the data. Representative strain histories from one pass of each vehicle path are plotted in Appendix A.

4.1 GENERAL DISCUSSION REGARDING THE MEASURED DATA

The data recorded by the data acquisition system are initially in terms of variations in the voltage. The corresponding live-load strains are directly related to these voltage outputs. The strain is related to the output voltage, the applied excitation voltage, and the gage factor:

$$\mu\varepsilon = \frac{4(E_{out})}{(GF)(E_{in})} * 10^6 \qquad (4.1)$$

where

$\mu\varepsilon$ = Microstrain

E_{out} = Output voltage (mvolts)

E_{in} = Input excitation (approximately 5000 mvolts for all tests)

GF = Gage factor (approximately 2.09 for the wire strain gages used in this investigation).

4.1.1 Notation Used

The following notation is used throughout the discussion regarding the locations of the instruments. The strain gages attached to the girders are identified as "B#H-X" where "B#" identifies the girder (Beam 1 through Beam 5). The letter "H" indicates the depth of the gage on the cross section ("B" refers to the gage attached to the bottom fiber, "M" refers to the gage attached to the web, and "T" refers to the gage attached to the top flange of the girder). For simplicity, the gage at the bottom fiber is called a "bottom" gage, and the web gage is called a "middle" gage. Finally, the index "X" denotes the longitudinal distance from the abutment end of the span. The instrumented sections are located 50', 66', and 83' from the abutment for the Slaughter Creek Bridge, and 51' and 76.5' from the abutment for the Nolanville Bridge.

Similarly, the gages attached to the top of the parapets are identified as "PT#-X" where "PT#" identifies the parapet rail (Parapet 1 is next to Beam 1, and Parapet 2 is next to Beam 5). The index "X" indicates the longitudinal distance from the abutment.

The notation used for the diaphragm gages is "D##H." The index "D##" identifies the two girders adjacent to the gage and "H" identifies the gage location on the diaphragm. A "T" refers to the gage close the top edge of the diaphragm and a "B" refers to the gage close to the bottom edge of the diaphragm.

4.1.2 Measured Data

Figure 4.1 is an example of the strain readings obtained at the exterior girder B5 at the Slaughter Creek Bridge during Test Series 2. The data were obtained during Run 16 when vehicle D3 traveled along path P4. The vertical axis indicates the level of the induced live-load strains in units of microstrain, with positive values indicating tension and negative values indicating compression. The horizontal axis represents the location of the centroid of the rear axles of the vehicle in feet from the abutment. The two plots are for the bottom and middle gages at mid-span and for the bottom gages at the mid-span and two-thirds span respectively.

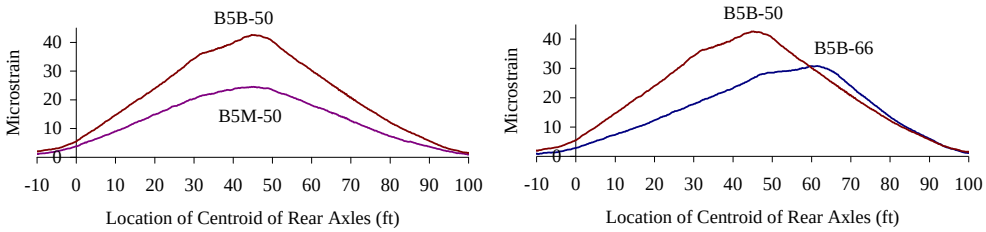

Figure 4.1 Example of Strain Data, Run 16

The information depicted in Fig. 4.1 is important for a number of reasons. If a preliminary run is conducted before the actual test begins, then it can be identified that the gages are working and an early assessment of the noise level in the data can be made. For these tests, the noise was typically in the range of ±2 microstrain.

The peaks in the response are identified at the points where the axles of the vehicle are directly above the gage locations. The maximum measured strain for the bottom gage at mid-span during the runs involving one loading vehicle was 43 microstrain. Also, the strain values induced at the extreme bottom fiber at mid-span are greater than the corresponding strains at mid-depth of the section, and the maximum mid-span strains are greater than the maximum strains induced at two-thirds of the span. Finally, the absence of significant strain reversals suggests a low level of continuity at the supports.

4.1.3 Problems Associated with the Measured Data

As with most field tests, problems with the measured data may occur. An improperly attached gage may record readings that are inconsistent or with high levels of drift. Hardware problems with the wired connections or other parts of the system can result in zero readings or readings with high levels of noise. Table 4.1 identifies the gages that were present in each Test Series and indicates those that recorded reliable and unreliable data.

One problem that has been observed during other diagnostic load tests is the effect of temperature gradients on the performance of the gages. As mentioned in Chapter 3, temperature compensation is achieved with the addition of the third wire on the gages before they are attached to the surfaces of the concrete members. When tests take a few hours to complete, any variations in ambient temperature can affect the epoxy material that is used to attach each gage to the bridge. In order to eliminate any temperature effects, the data were set to

zero before each run at the time of the tests. The values by which the data were adjusted to set the initial zero were not more than 1 or 2 microstrain.

This issue was investigated by a previous researcher that performed similar diagnostic field tests on a pan-girder bridge in Buda, Texas [10]. During those test runs, the data were set to zero only at the beginning of the first run. Plots of the readings recorded by specific gages at selected time intervals are presented in that thesis to show the variation of strain with time due to changes in ambient temperature.

Table 4.1 Summary of the Measured Data

Test Series	Section I.D.	Gage Location	Beam 1	Beam 2	Beam 3	Beam 4	Beam 5	Parapet 1	Parapet 2	Diaph. 23	Diaph. 34
TS1	Mid-Span	Top	-	-	-	-	-	R	R	-	-
	(50')	Middle	R	R	R	R	R	-	-	-	-
		Bottom	R	R	R	R	R	-	-	-	-
	2/3-Span	Top	-	-	-	-	-	R	R	-	-
	(66.7')	Middle	R	R	R	R	R	-	-	-	-
		Bottom	R	R	R	R	R	-	-	-	-
	5/6-Span	Top	-	-	-	-	-	R	R	-	-
	(83.3')	Middle	U	R	R	R	R	-	-	-	-
		Bottom	R	R	R	R	R	-	-	-	-
TS2	Mid-Span	Top	-	-	-	-	-	R	R	-	-
	(50')	Middle	R	R	R	R	R	-	-	-	-
		Bottom	R	R	R	R	R	-	-	-	-
	2/3-Span	Top	-	-	-	-	-	R	R	-	-
	(66.7')	Middle	R	R	R	R	R	-	-	-	-
		Bottom	R	R	R	R	R	-	-	-	-
	5/6-Span	Top	-	-	-	-	-	R	R	-	-
	(83.3')	Middle	R	R	R	R	R	-	-	-	-
		Bottom	R	R	R	R	R	-	-	-	-
TS3	Mid-Span	Top	-	-	R	R	-	-	-	R	U
	(51')	Middle	U	R	R	R	R	-	-	-	-
		Bottom	U	U	R	R	R	-	-	R	R
	3/4-Span	Top	-	-	-	-	-	-	-	-	-
	(76.5')	Middle	R	U	R	R	R	-	-	-	-
		Bottom	R	R	R	R	R	-	-	-	-

R=Reliable Data, U=Unreliable Data, - = Section not Instrumented

4.1.4 Overcoming the Problems Associated with the Measured Data

Some of the different types of problems discussed above may be overcome by adjusting against the drift and by averaging the values to minimize the noise. Adjusting against the drift was achieved by subtracting the initial value of strain from the recorded histories. This resulted in zero strains at the beginning and end of each run, and corrected the entire strain history. Overall, the levels of drift were small enough that they did not cause any significant problems in the data. Figure 4.2 shows this adjustment for one gage.

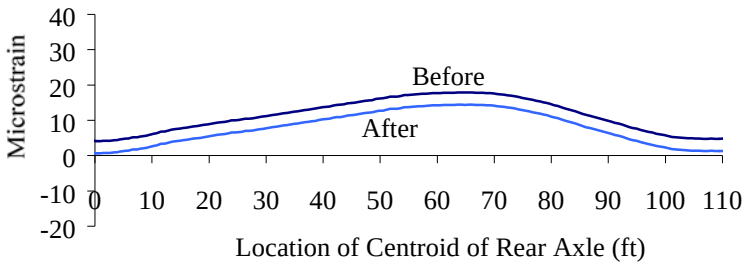

Figure 4.2 Example of Adjusting the Strains Against Drift

Noise was an issue for some of the channels. Subsequent investigations have linked the noise to loose soldered connections in some of the completion boxes. However, in order to reduce the noise in the recorded strains, an averaging technique was used. The number of data points averaged was selected according to the frequency at which the data were collected. A moving five-point average was used in Test Series 2 and 3 where the data were collected at 10 Hz, and up to 30 points were used in Test Series 1 where the data were collected at 100 Hz. Figure 4.3 shows the outcome of averaging the strains.

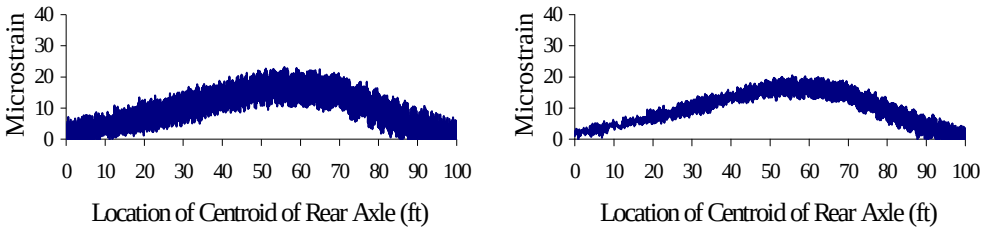

Figure 4.3 Example of Using a Moving Seven-Point Average to Reduce the Noise in Measured Strain Data

4.2 STRAIN READINGS FROM TEST SERIES 1 AND 2 - SLAUGHTER CREEK PRESTRESSED CONCRETE BRIDGE

This section presents the data obtained during the two tests conducted at the Slaughter Creek Bridge. The two Test Series had identical instrumentation layouts and transverse paths of the loading vehicles. The gages that were present during Test Series 1 were checked before the second Test Series. The six parapet gages and one gage attached to the web of girder 1 were replaced prior to Test Series 2.

The strains are presented in terms of the maximum values obtained at the various sections for all the runs. The data are separated into four groups: three referring to the girder strains at each of the three sections and one discussing the results obtained at the parapets.

4.2.1 Strains Measured at Girder Sections Located at Mid-Span

Ten gages were attached to the surface of the prestressed concrete girders at mid-span. Five were attached to the bottom surface of the sections and five

were attached to the web, 20 in. above the bottom surface (Fig. 3.9). The maximum strains measured at the bottom surface of the girders are summarized in Table 4.2 and the strains measured at the webs are summarized in Table 4.3.

The maximum strain measured at mid-span was 43 microstrain and was recorded at the bottom fiber of the exterior girder (Beam 5) for Run 1 when vehicle D2 traveled along the path closest to the edge and the girder (P4). For the cases of two trucks, the maximum strain was 54 microstrain, and was recorded at the same girder for Run 11 when the two vehicles traveled along paths P4 and P3 respectively. It is important to note that the gages at the exterior girders recorded negligible strains when the vehicle moved along the path closest to the opposite side of the roadway. This is expressed by the very small values reported in Tables 4.1 and 4.2. Any record within 1-2 microstrain represents the noise level rather than the induced strains.

Table 4.2 Maximum Strains Measured at Mid-Span on the Bottom Surface of the Prestressed Concrete Girders, Test Series 1 and 2

Run #	Loading Vehicle	Vehicle Path	Maximum Strain, microstrain				
			BEAM 1 B1B-50	BEAM 2 B2B-50	BEAM 3 B3B-50	BEAM 4 B4B-50	BEAM 5 B5B-50
1	D2	P4	1	4	13	28	43
2	D1	P4	0	4	12	28	37
4	D1	P3	4	14	32	26	12
5	D2	P2	12	26	33	17	5
6	D1	P2	12	25	32	16	6
7	D2	P1	43	33	14	7	1
8	D1	P1	42	30	13	3	3
9	D1&D2	P4/P1	38	36	25	32	41
10	D1&D2	P4/P1	38	35	25	33	39
11	D1&D2	P4/P3	5	19	43	52	54
12	D1&D2	P4/P3	6	20	45	53	53
13	D1&D2	P2/P1	52	52	44	21	7
14	D1&D2	P1/P2	49	51	46	23	7
15	D3	P4	0	3	10	26	41
16	D3	P4	1	4	10	27	43
17	D3	P3	5	14	31	23	11
18	D3	P3	5	13	30	23	11
19	D3	P2	12	24	32	17	8
20	D3	P2	11	23	32	17	7
21	D3	P1	38	29	12	4	0
22	D3	P1	38	29	12	5	1

*No reliable data were obtained from Run 3

Table 4.3 Maximum Strains Measured at Mid-Span on the Surface of the Webs of the Prestressed Concrete Girders, Test Series 1 and 2

Run #	Loading Vehicle	Vehicle Path	Maximum Strain, microstrain				
			BEAM 1 B1M-50	BEAM 2 B2M-50	BEAM 3 B3M-50	BEAM 4 B4M-50	BEAM 5 B5M-50
1	D2	P4	0	2	6	18	25
2	D1	P4	0	1	6	17	20
4	D1	P3	2	9	17	14	6
5	D2	P2	6	13	17	10	2
6	D1	P2	7	13	16	9	2
7	D2	P1	23	16	6	3	0
8	D1	P1	24	15	5	4	1
9	D1&D2	P4/P1	22	17	12	20	22
10	D1&D2	P4/P1	21	18	11	20	21
11	D1&D2	P4/P3	2	10	21	30	29
12	D1&D2	P4/P3	2	10	22	31	29
13	D1&D2	P2/P1	29	28	20	11	2
14	D1&D2	P1/P2	26	27	22	11	3
15	D3	P4	0	2	5	16	23
16	D3	P4	1	2	5	17	25
17	D3	P3	2	8	15	12	5
18	D3	P3	2	8	15	12	5
19	D3	P2	6	14	16	9	3
20	D3	P2	5	13	16	9	3
21	D3	P1	21	14	5	2	0
22	D3	P1	21	15	5	2	1

*No reliable data were obtained from Run 3

A set of strain data recorded by the ten mid-span gages during Run 16 is presented in Fig. 4.4. Figure 3.14 illustrates the path of the loading vehicle. These plots are representative of the strain histories recorded at mid-span during the entire set of runs at the Slaughter Creek Bridge. As expected, the maximum strain values for this run vary from highest at girder 5 to practically zero at

girder 1. The trend is the same in all plots, with local peaks forming when the rear axles are directly over the gages. In this run, these peaks are more pronounced at girders 5 and 4 than the rest, because the vehicle is located between the girders. The plots are smoother in girder 3 and the strains induced in the remaining two girders are very small. Also significant is the absence of strain reversal between interior supports. The strains decrease to zero when the rear axles leave the instrumented span.

Figure 4.5 shows the profiles of the maximum strains recorded at the bottom surface of the five girders at mid-span for paths P1 through P4 for vehicles D1 and D2. The horizontal axis represents the distance across the width of the bridge looking North in the direction of traffic. As expected, the values corresponding to each girder are very close to one another. Some small differences are expected because vehicles D1 and D2 are not identical.

Figure 4.6 shows the profiles of the maximum strains recorded at the bottom surface of the five girders at mid-span for Runs 9 through 14 involving vehicles D1 and D2 moving simultaneously along the indicated paths. Figure 3.17 illustrates the locations of the vehicles during these runs. The strain profiles are similar for identical vehicle passes.

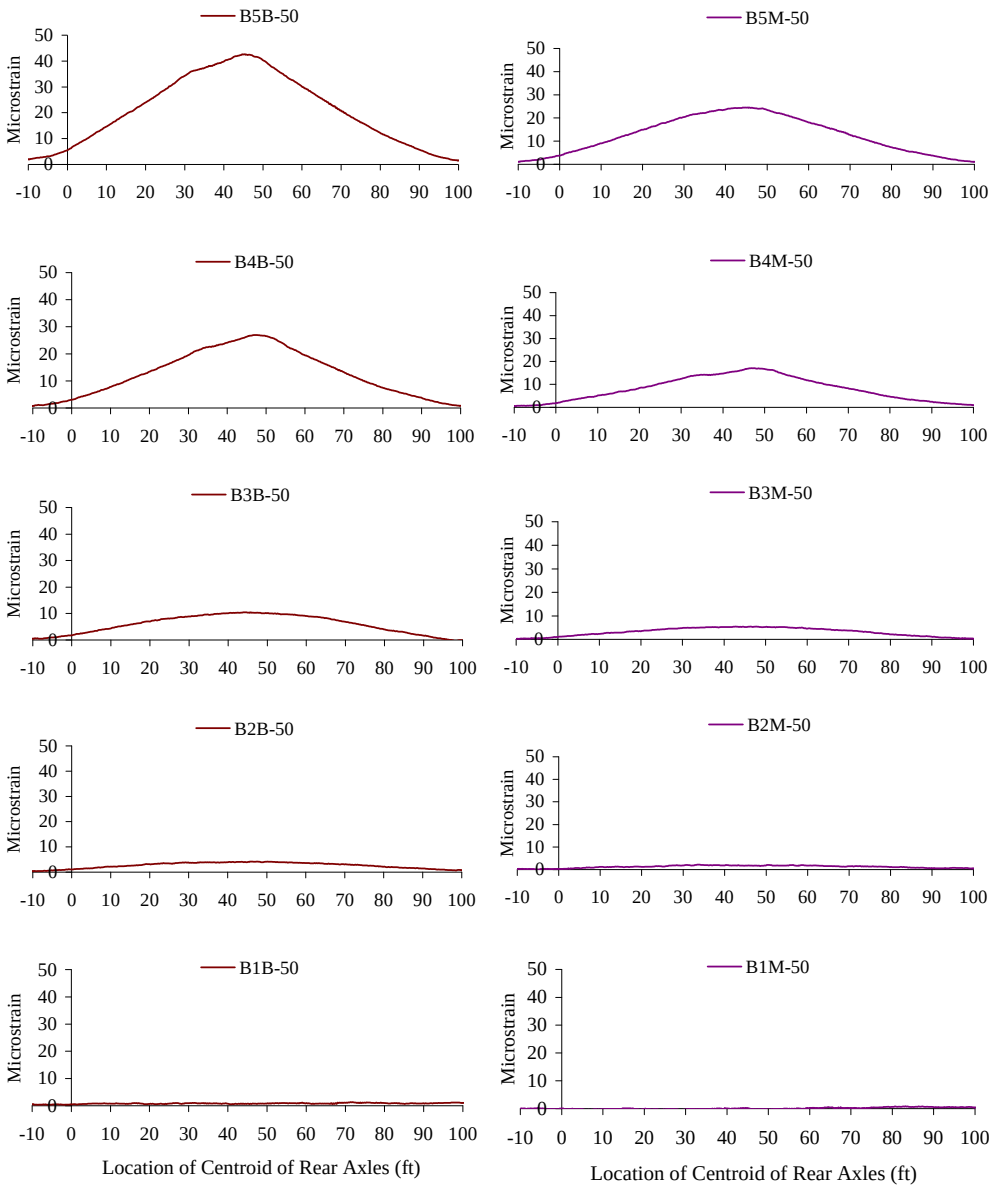

Figure 4.4 Strain Histories for the Gages at Mid-Span, Run 16

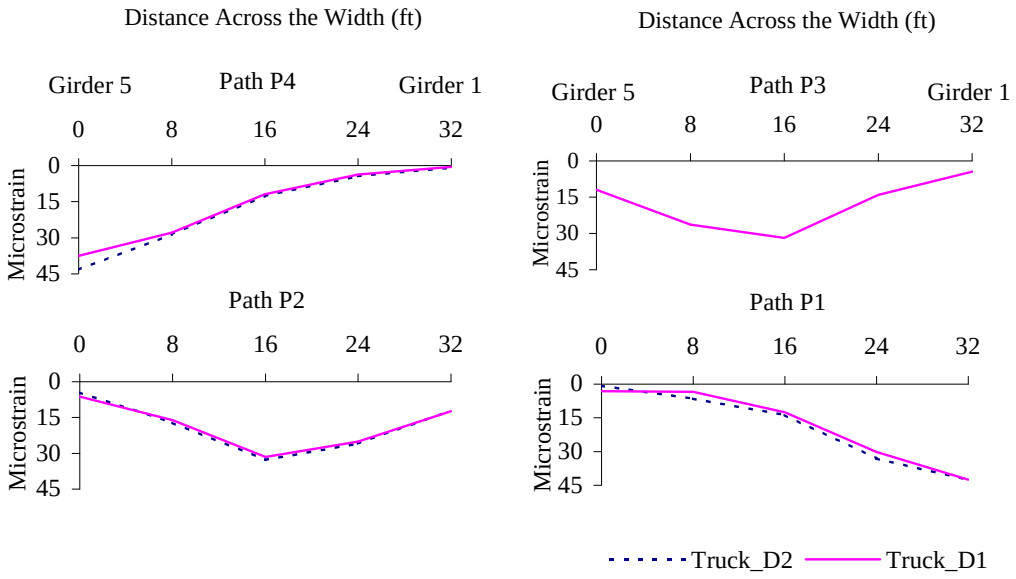

Figure 4.5 Maximum Strain Profiles for Gages at Mid-Span, Runs 1-8

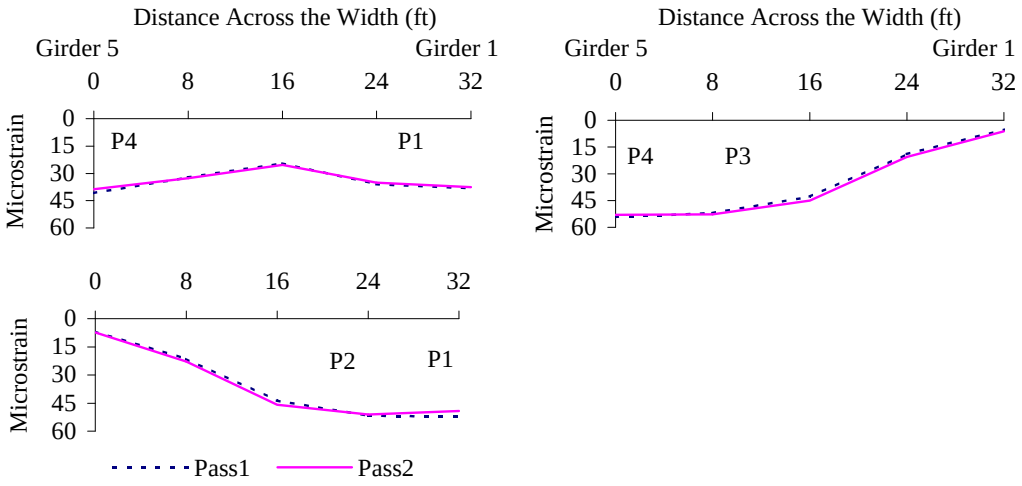

Figure 4.6 Maximum Strain Profiles for Gages at Mid-Span, Runs 9-14

4.2.2 Strains Measured at Girder Sections Located at Two-Thirds Span

A section located 66.7 feet from the abutment was instrumented similarly to the mid-span section. Ten gages were attached to the surface of the concrete at the same two locations over the depth of the Type IV precast sections. The maximum strains measured by the bottom gages are shown in Table 4.4 and those measured by the middle gages are shown in Table 4.5.

Table 4.4 Maximum Strains Measured at 66.7-ft. on the Bottom Surface of the Prestressed Concrete Girders, Test Series 1 and 2

Run #	Loading Vehicle	Vehicle Path	Maximum Strain, microstrain				
			BEAM 1 B1B-66	BEAM 2 B2B-66	BEAM 3 B3B-66	BEAM 4 B4B-66	BEAM 5 B5B-66
1	D2	P4	0	4	11	24	32
2	D1	P4	0	4	12	25	28
4	D1	P3	3	19	30	29	9
5	D2	P2	7	22	30	15	5
6	D1	P2	8	25	28	14	4
7	D2	P1	29	32	13	4	0
8	D1	P1	28	31	10	6	1
9	D1&D2	P4/P1	27	35	22	28	30
10	D1&D2	P4/P1	26	34	23	28	29
11	D1&D2	P4/P3	3	15	37	46	39
12	D1&D2	P4/P3	3	17	37	46	37
13	D1&D2	P2/P1	34	53	41	21	5
14	D1&D2	P1/P2	31	49	41	20	5
15	D3	P4	1	3	10	21	30
16	D3	P4	1	3	9	21	31
17	D3	P3	4	13	28	19	8
18	D3	P3	3	13	28	19	9
19	D3	P2	7	21	28	13	4
20	D3	P2	6	20	28	13	5
21	D3	P1	27	28	11	4	1
22	D3	P1	26	28	11	4	0

*No reliable data were obtained from Run 3

Table 4.5 Maximum Strains Measured at 66.7-ft. on the Surface of the Web of the Prestressed Concrete Girders, Test Series 1 and 2

Run #	Loading Vehicle	Vehicle Path	Maximum Strain, microstrain				
			BEAM 1 B1M-66	BEAM 2 B2M-66	BEAM 3 B3M-66	BEAM 4 B4M-66	BEAM 5 B5M-66
1	D2	P4	1	2	6	14	18
2	D1	P4	1	2	6	14	17
4	D1	P3	3	8	15	12	5
5	D2	P2	4	12	15	9	3
6	D1	P2	4	14	15	8	2
7	D2	P1	17	15	5	2	0
8	D1	P1	15	13	4	1	-1
9	D1&D2	P4/P1	14	16	10	16	18
10	D1&D2	P4/P1	14	17	11	15	16
11	D1&D2	P4/P3	1	9	20	25	21
12	D1&D2	P4/P3	1	9	19	25	20
13	D1&D2	P2/P1	20	27	20	10	4
14	D1&D2	P1/P2	16	24	20	10	1
15	D3	P4	1	2	5	13	17
16	D3	P4	1	2	5	13	18
17	D3	P3	1	7	15	11	4
18	D3	P3	1	7	14	11	4
19	D3	P2	4	12	15	7	1
20	D3	P2	3	11	15	8	2
21	D3	P1	14	13	5	2	0
22	D3	P1	14	14	4	2	1

*No reliable data were obtained from Run 3

A set of strain data recorded by these ten gages is shown in Fig. 4.7. The plots are based on the same run (Run 16) that was used to develop the histories presented for the mid-span gages in Fig. 4.4. As expected, the readings recorded at this section are smaller than those at mid-span.

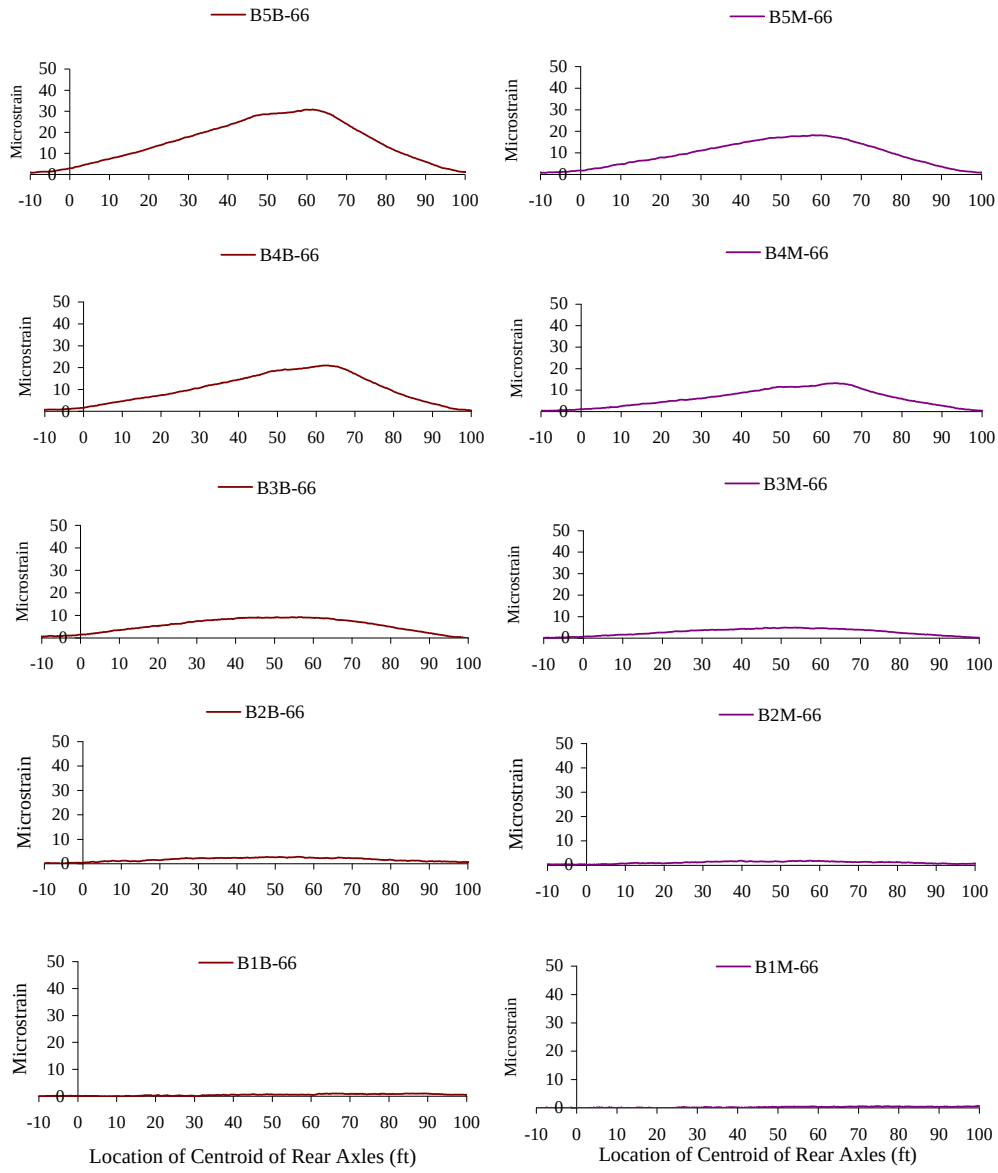

Figure 4.7 Strain Histories for the Gages at 66.7 ft, Run 16

These plots are representative of the strain histories recorded at the two-thirds section during the entire set of runs at the Slaughter Creek Bridge. As in

the case of the mid-span gages, the maximum strain values vary from highest at girder 5 to practically zero at girder 1 with the strains decreasing to zero when the rear axles leave the instrumented span. The lack of symmetry in the curves is due to the fact that the local peaks occur when the rear axles of the loading vehicle are directly over the gages. This is different from what was shown in Fig. 4.4 where the curves were nearly symmetric about the mid-span of the bridge.

Figure 4.8 shows the profiles of the maximum strains recorded at the bottom surface of the five girders at the 66.7-foot section for paths P1 through P4 for vehicles D1 and D2. The horizontal axis represents the distance across the width of the bridge looking in the direction of traffic. As expected, the values corresponding to each girder are very close to one another because the two loading vehicles are very similar in dimensions and axle loads.

Figure 4.9 shows the profiles of the maximum strains recorded at the bottom surface of the five girders at the 66.7-ft section for the set of Runs 9 through 14 involving vehicles D1 and D2 moving simultaneously along the span. The plots show both passes of the vehicles and the paths are identified in each case. Similar profiles are obtained for identical vehicle passes adding favorably to the repeatability of the measured data.

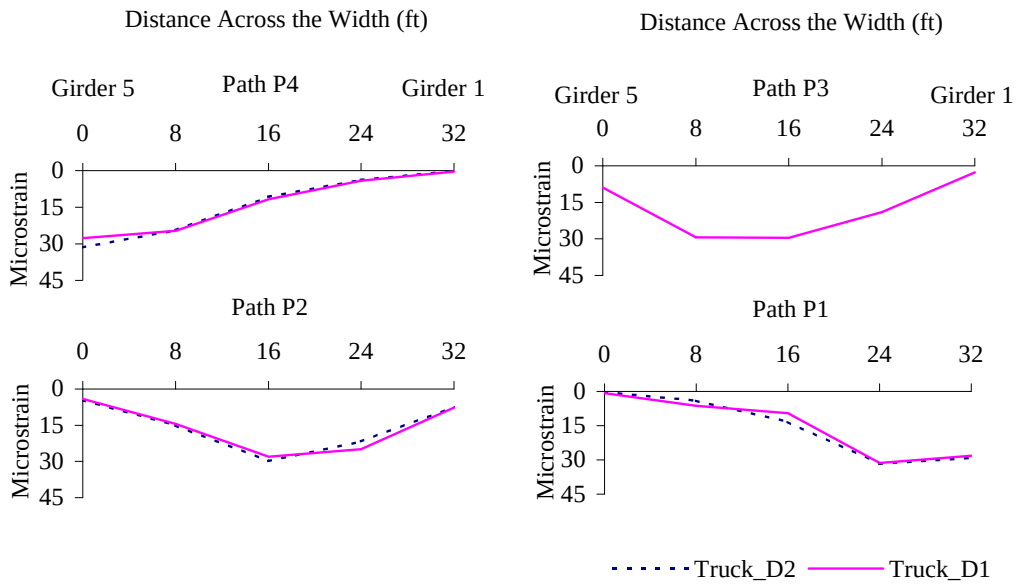

Figure 4.8 Maximum Strain Profiles for Gages at 66.7 ft, Runs 1-8

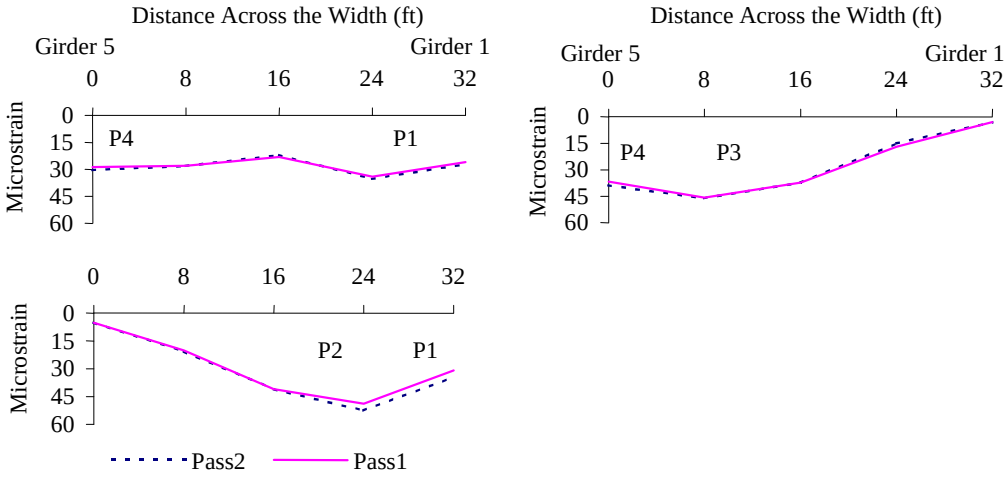

Figure 4.9 Maximum Strain Profiles for Gages at 66.7 ft, Runs 9-14

4.2.3 Strains Measured at Girder Sections Located at Five-Sixths Span

Ten gages were attached to the surface of the concrete at a section located 83.3 feet from the abutment end. This section corresponded to five sixths of the span. The maximum strains measured at the bottom fibers are shown in Table 4.6 and those measured at the webs are shown in Table 4.7.

Table 4.6 Maximum Strains Measured at 83.3-ft. on the Bottom Surface of the Precast Girders, Test Series 1, Microstrain

Run #	Loading Vehicle	Vehicle Path	Maximum Strain, microstrain				
			BEAM 1 B1B-83	BEAM 2 B2B-83	BEAM 3 B3B-83	BEAM 4 B4B-83	BEAM 5 B5B-83
1	D2	P4	0	2	4	15	19
2	D1	P4	0	2	4	14	17
4	D1	P3	2	12	17	18	3
5	D2	P2	5	12	18	11	2
6	D1	P2	4	16	17	12	1
7	D2	P1	17	19	9	5	1
8	D1	P1	16	18	7	3	0
9	D1&D2	P4/P1	14	22	12	18	19
10	D1&D2	P4/P1	15	20	12	17	17
11	D1&D2	P4/P3	2	8	19	28	21
12	D1&D2	P4/P3	2	8	19	29	20
13	D1&D2	P2/P1	22	30	25	14	2
14	D1&D2	P1/P2	19	27	25	13	1
15	D3	P4	1	2	3	14	18
16	D3	P4	1	2	3	14	18
17	D3	P3	2	7	16	14	5
18	D3	P3	3	7	16	14	3
19	D3	P2	4	11	17	9	1
20	D3	P2	4	11	18	10	2
21	D3	P1	16	16	8	2	1
22	D3	P1	15	17	7	3	0

*No reliable data were obtained from Run 3

Table 4.7 Maximum Strains Measured at 83.3-ft. on the Surface of the Webs of the Prestressed Concrete Girders, Test Series 1 and 2

Run #	Loading Vehicle	Vehicle Path	Maximum Strain, microstrain				
			BEAM 1 B1M-83	BEAM 2 B2M-83	BEAM 3 B3M-83	BEAM 4 B4M-83	BEAM 5 B5M-83
1	D2	P4	-	2	3	8	10
2	D1	P4	-	3	4	10	8
4	D1	P3	-	7	15	14	2
5	D2	P2	-	7	11	5	1
6	D1	P2	-	6	11	6	1
7	D2	P1	-	9	4	1	0
8	D1	P1	-	8	6	4	0
9	D1&D2	P4/P1	-	8	8	8	9
10	D1&D2	P4/P1	-	9	7	9	9
11	D1&D2	P4/P3	-	4	11	15	10
12	D1&D2	P4/P3	-	5	13	16	10
13	D1&D2	P2/P1	-	16	14	9	0
14	D1&D2	P1/P2	-	13	14	6	0
15	D3	P4	0	1	2	7	9
16	D3	P4	1	1	2	8	10
17	D3	P3	1	4	10	11	2
18	D3	P3	1	4	10	7	2
19	D3	P2	3	6	10	4	1
20	D3	P2	2	6	11	4	1
21	D3	P1	9	7	4	1	0
22	D3	P1	9	7	4	1	0

*No reliable data were obtained from Run 3

The strains measured at this section are smaller than the corresponding strains measured at the mid-span and two-thirds sections. This was expected, because the gages are near the interior support and the induced live load strains are low for this type of bridge and truckload configurations. The influence that any inherent error in the system or improper attachment of a gage at the field may

have on these readings would be higher. Figure 4.10 shows a set of strain-response histories measured at this section during the same run as that used to present the measured data at the other two sections (Fig. 4.4 and 4.7).

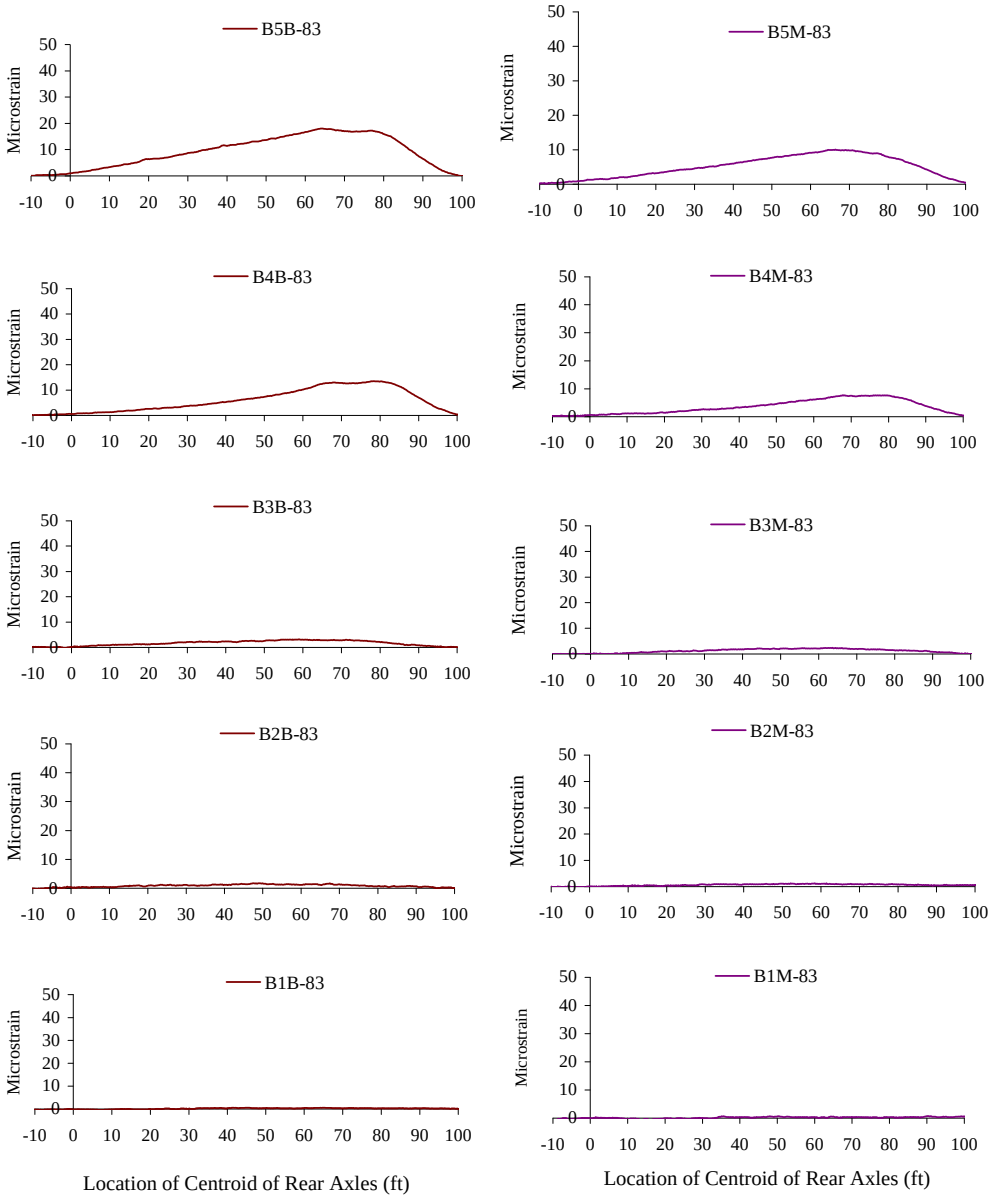

Figure 4.10 Strain Histories for the Gages at 83.3 ft, Run 16

The plots represent the strain histories recorded at the five-sixths section at the Slaughter Creek Bridge. The strains are lower than the strains measured at the mid-span and two-thirds sections, but the trends in the plots are consistent with the observations made in those cases. The local peaks occur when the rear axles of the loading vehicle are directly over the gages located at five-sixths of the span.

Figure 4.11 shows the profiles of the maximum strains recorded at the bottom surface of the girders at the 83.3-ft section. The plots represent paths P1 through P4 for the loading vehicles D1 and D2. The trends are similar to those depicted by Fig. 4.5 and 4.8, with the two trucks inducing nearly identical peak strains when moving along the same path.

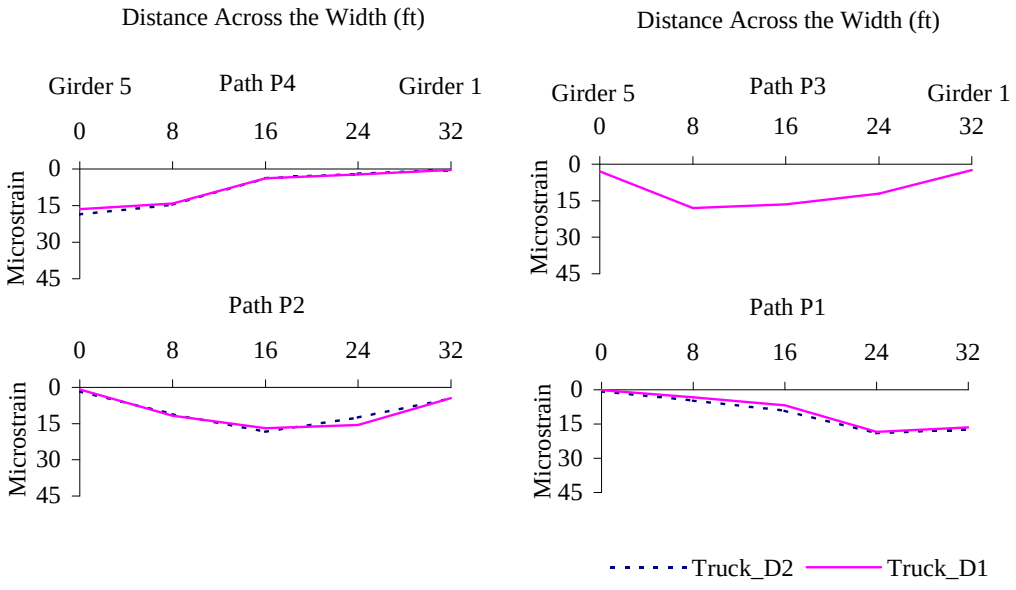

Figure 4.11 Maximum Strain Profiles for Gages at 83.3 ft, Runs 1-8

Figure 4.12 shows the profiles of the maximum strains recorded at the bottom surface of the five girders at the 83.3-ft section for Runs 9 through 14, where vehicles D1 and D2 were moving side by side along the indicated paths. The two passes along the paths that are indicated in each case induce nearly identical maximum strains at the bottom surface of the five girders.

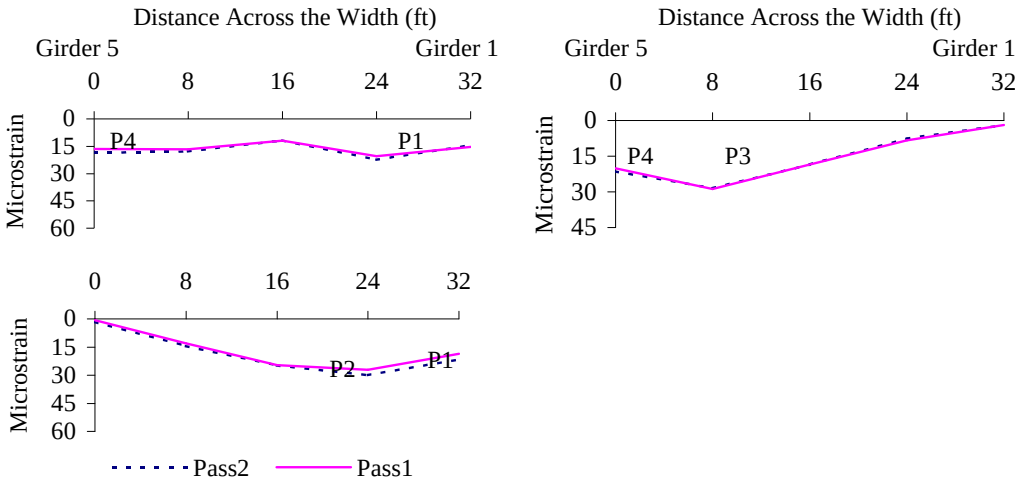

Figure 4.12 Maximum Strain Profiles for Gages at 83.3 ft, Runs 1-8

4.2.4 Strains Measured at the Parapet Rails for the Three Sections

The data recorded at the top of the parapet rails at both edges of the roadway are presented in this section. Based on the structural details of this bridge, it was decided to examine the degree that the type T502 parapets participated in resisting bending. The gages were primarily placed in order to see if any appreciable strains were induced from the induced live loads. There were two gages at each instrumented section for a total of six gages.

Table 4.8 presents the maximum strains recorded by the parapet gages at the three sections for each run. Strains at the level of ±2 microstrain were measured when the vehicles moved along the interior paths, P2 and P3. These values were essentially zero and they were not considered reliable. When the trucks moved along the exterior paths, the gages located on the parapet closest to the load in each case measured appreciable strains. This information was useful in that the parapets contributed to the bending stiffness of the exterior sections as expected prior to the test.

The maximum strains recorded by the gages located at the 66.7-ft section were greater than the strains measured at mid-span and at the five-sixths span. After an on-site observation, it was verified that the presence of cuts in the parapet at the mid-span section could be the most probable cause of the very small readings at that section. Strains at the five-sixths span were also higher than the corresponding values at mid-span.

Figure 4.13 shows the recorded strain histories for all six gages located at the two parapet rails. The strain plots correspond to Run 16 used earlier in this section to present the girder gages. They are representative of the response corresponding to the loading vehicle moving along one of the exterior paths, and they depict the trends of the maximum values presented in Table 4.8. The strain histories reach a maximum when the vehicle is located over each section.

Table 4.8 Maximum Compressive Strains Measured on the Top Surface of the Parapet Rails, Test Series 1 and 2

Run #	Loading Vehicle	Vehicle Path	Maximum Strain, microstrain					
			PARAPET 1 (East)			PARAPET 2 (West)		
			PT1-50	PT1-66	PT1-83	PT2-50	PT2-66	PT2-83
1	D2	P4	-2	-1	-3	-1	-25	-11
2	D1	P4	-3	-1	-1	-1	-23	-6
4	D1	P3	-3	-10	-8	-3	-10	-9
5	D2	P2	-3	-9	-5	-2	-6	-3
6	D1	P2	-2	-11	-5	-2	-6	-6
7	D2	P1	-1	-27	-9	-2	-1	-2
8	D1	P1	-3	-27	-9	-2	-3	-3
9**	D1&D2	P4/P1	0	0	0	-1	-24	-2
10	D1&D2	P4/P1	-1	-25	-7	0	-21	-8
11	D1&D2	P4/P3	-1	-4	-3	1	-33	-13
12	D1&D2	P4/P3	-4	-4	-3	0	-32	-10
13	D1&D2	P2/P1	-1	-37	-14	-3	-7	-5
14	D1&D2	P1/P2	-1	-32	-11	0	-4	-3
15	D3	P4	-1	0	-2	-3	-21	-12
16	D3	P4	-2	-3	-2	-2	-22	-8
17	D3	P3	0	-3	-2	0	-6	-2
18	D3	P3	0	-2	-1	1	-7	-1
19	D3	P2	0	-6	-1	-2	-3	-2
20	D3	P2	-1	-7	-3	-2	-5	-5
21	D3	P1	-2	-25	-8	-3	-1	-5
22	D3	P1	3	-26	-6	-3	-2	-3

**Unreliable data with the gages on Parapet 1 during Run 9

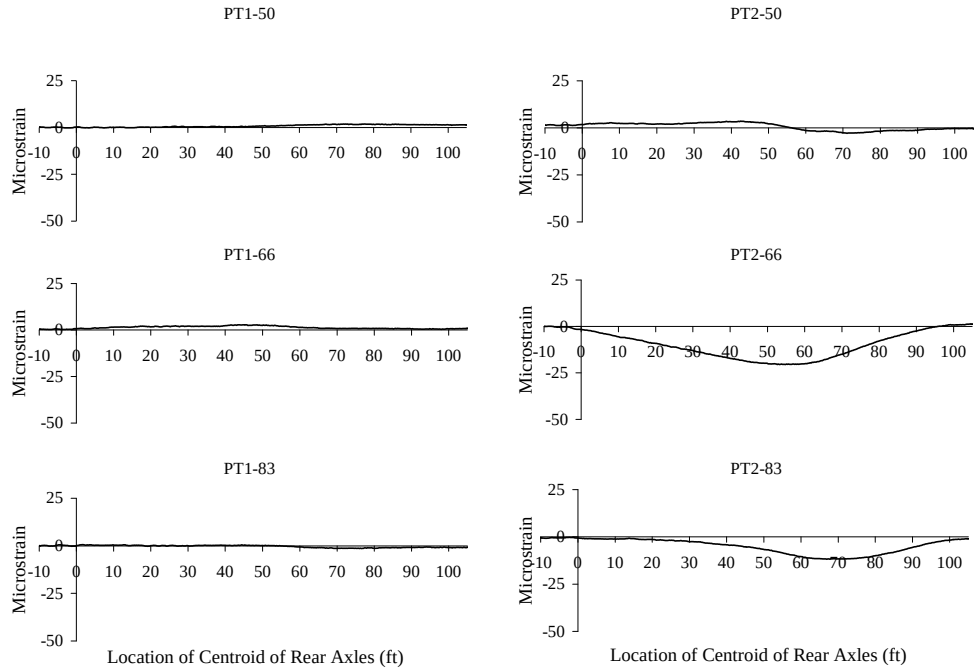

Figure 4.13 Strain Histories for Gages at the Top of the Parapets, Run 16

4.3 STRAIN READINGS FROM TEST SERIES 3 - NOLANVILLE PRESTRESSED CONCRETE BRIDGE

The data obtained during the Test Series conducted at the Nolanville Bridge on September, 1998 are presented in this section. The presentation is similar in format to that of the two tests conducted at the Slaughter Creek Bridge. The data are presented in terms of the maximum strain values obtained at the various sections for all the runs.

Twenty-six strain gages were mounted for this Test Series at the mid-span and the three-quarter span sections. After examining the details of this bridge, the rails were not instrumented as no significant contribution to bending was expected. Two vehicles were used in this test: a ten-cubic yard truck (D4), similar to those used when testing the Slaughter Creek Bridge, and one Heavy Equipment Transportation System (HETS) provided by the U.S. Army. The strain data are presented separately for each instrumented section and the sets of data corresponding to each loading vehicle are differentiated. Figures 3.5 and 3.6 show sketches of the two vehicles and Table 3.1 and Table 3.2 show the axle loads for D4 and for the HETS respectively.

4.3.1 Strains Measured at Girder Sections Located at Mid-Span

Twelve gages were attached to the surface of the Type IV, prestressed concrete girders at mid-span. Five gages were attached to the bottom surface of the sections and 5 gages were attached to the web, 20 in. above the bottom. In the cases of girders 3 and 4, an additional strain gage was placed near the top of the precast sections, 3 in. below the slab-girder intersection. Figure 3.13 shows

the three gage locations on the girders. The transverse paths of the vehicles are shown in Fig. 3.18 through 3.21 for vehicles D4 and the HETS.

Table 4.9 shows the maximum strains measured at the bottom surface of the girders and Table 4.10 summarizes the maximum strains measured from the gages located at the webs. Table 4.11 shows the maximum compressive strains recorded by the gages located at the top flanges of girders 3 and 4. The maximum tensile strain induced when the dump truck was on the bridge was 33 microstrain, and the maximum tensile strain induced by the HETS was 106 microstrain. Note that compressive strains were recorded in Beam 5 during Runs 23, 32 and 33 along path P1. The strains indicate a relatively small negative bending of the exterior girder when the load is concentrated on the other side of the structure.

Table 4.9 Maximum Strains Measured at Mid-Span on the Bottom Surface of the Prestressed Concrete Girders, Test Series 3

Run #	Loading Vehicle	Vehicle Path	Maximum Strain, microstrain				
			BEAM 1 B1B-51	BEAM 2 B2B-51	BEAM 3 B3B-51	BEAM 4 B4B-51	BEAM 5 B5B-51
23	HETS	P1	-	-	49	24	-12
24	HETS	P3	-	-	74	79	102
25	HETS	P2	-	-	98	53	31
26	HETS	P2	-	-	98	50	28
27	HETS	P2	-	-	99	53	31
28	D4	P3	-	-	21	30	33
29	D4	P3	-	-	22	30	32
30	D4	P2	-	-	31	14	7
31	D4	P2	-	-	32	14	7
32	D4	P1	-	-	14	8	-5
33	D4	P1	-	-	15	10	-4

Table 4.10 Maximum Strains Measured at Mid-Span on the Surface of the Webs of the Prestressed Concrete Girders, Test Series 3

Run #	Loading Vehicle	Vehicle Path	Maximum Strain, microstrain				
			BEAM 1 B1M-51	BEAM 2 B2M-51	BEAM 3 B3M-51	BEAM 4 B4M-51	BEAM 5 B5M-51
23	HETS	P1	-	51	25	5	-4
24	HETS	P3	-	12	32	51	53
25	HETS	P2	-	29	51	40	12
26	HETS	P2	-	30	51	38	10
27	HETS	P2	-	28	51	40	12
28	D4	P3	-	3	9	16	14
29	D4	P3	-	4	9	17	14
30	D4	P2	-	9	16	10	3
31	D4	P2	-	8	16	10	3
32	D4	P1	-	16	7	3	-3
33	D4	P1	-	16	8	4	-2

Table 4.11 Maximum Compressive Strains Measured at Mid-Span on the Top Flange of the Prestressed Concrete Girders, Test Series 3, Microstrain

Run #	Loading Vehicle	Vehicle Path	Compressive Strain, με	
			BEAM 3 B3T-51	BEAM 4 B4T-51
23	HETS	P1	-17	-10
24	HETS	P3	-17	-24
25	HETS	P2	-17	-11
26	HETS	P2	-17	-11
27	HETS	P2	-17	-11
28	D4	P3	-5	-8
29	D4	P3	-5	-8
30	D4	P2	-6	-3
31	D4	P2	-6	-3
32	D4	P1	-5	-2
33	D4	P1	-4	-3

A set of strain data recorded by the mid-span gages during Run 28 is presented in Fig. 4.14. This group of plots is representative of the set of runs

with the ten-cubic yard truck. The maximum strain values vary from highest at the girders closest to the load to lowest at the girders farthest from the load. The local peaks form when the rear axles are directly over the mid-span gages. The bottom gages are in tension and the top gages in compression for the entire duration of the run, indicating no strain reversal between supports. The strains decrease to zero when the rear axles are off the instrumented span.

Figure 4.15 shows the histories recorded at mid-span for Run 24 with the HETS vehicle. The trends in the response are similar and the induced strains are nearly three times greater in this case. The horizontal axes represent the location of the front axle. The maximum strains were recorded when the front axle was 90 feet from the abutment end.

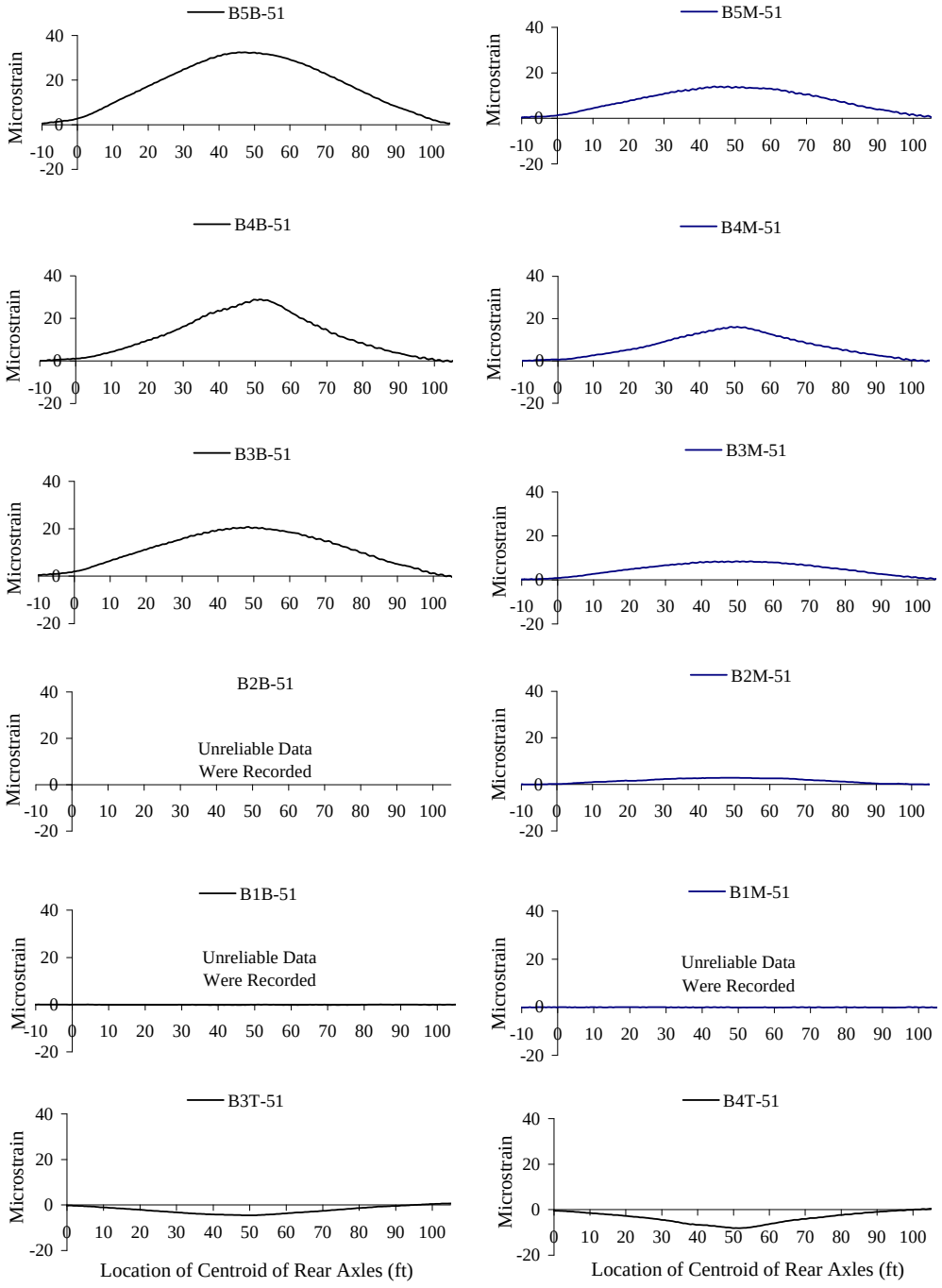

Figure 4.14 Strain Histories for Gages Located at the Surface of the Girders at Mid-Span Section, D4, Run 28

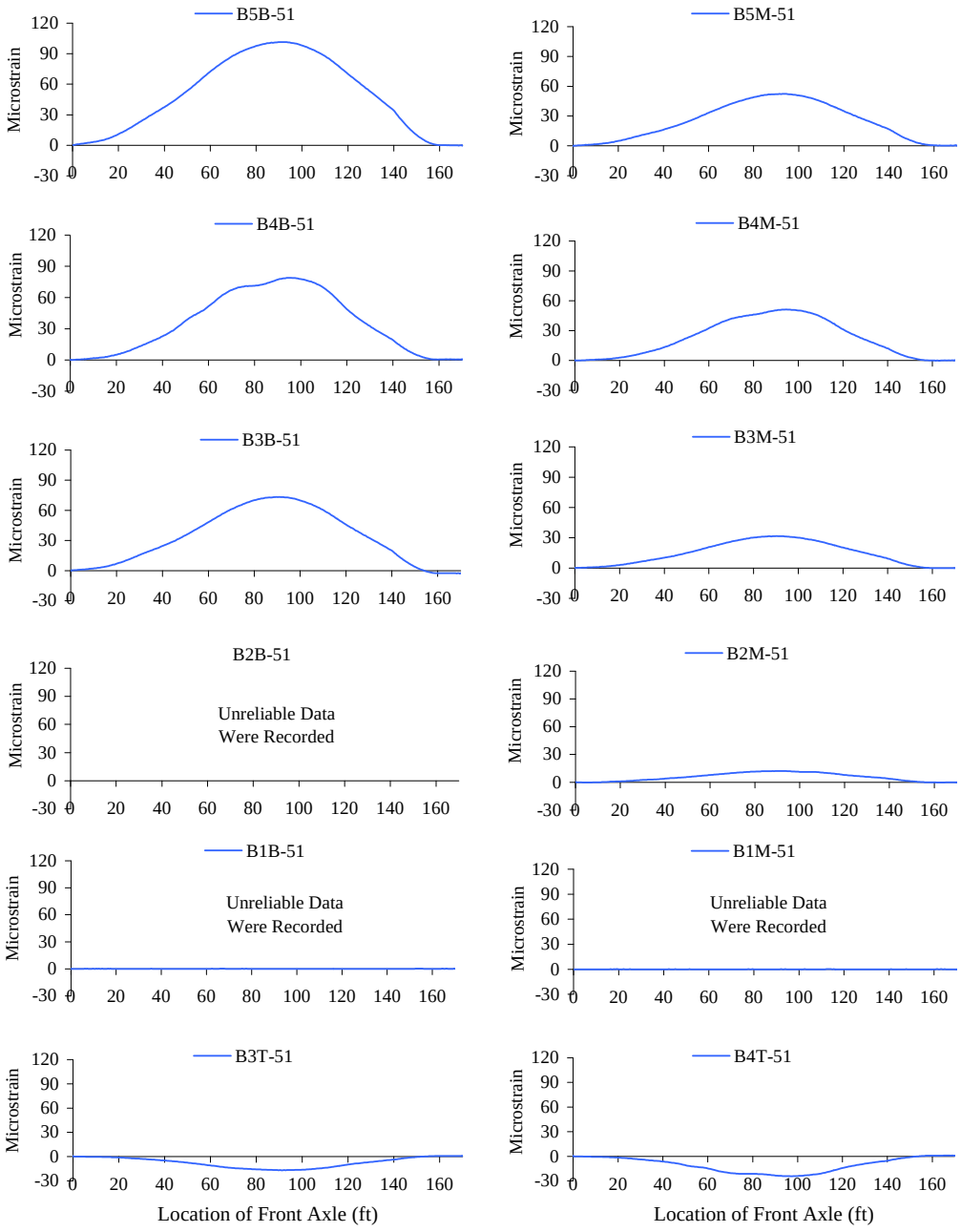

Figure 4.15 Strain Histories for Gages Located at the Surface of the Girders at Mid-span Section, HETS, Run 24

4.3.2 Strains Measured at the Interior Diaphragm at Mid-Span

Four gages were attached to the mid-span diaphragm as discussed in Section 3.5.2. The purpose was to obtain measurements in order to capture the behavior of the interior diaphragm under the truckloads. Figure 4.16 shows the strain histories obtained from Run 28 with vehicle D4 and Fig. 4.17 shows the corresponding histories obtained during Run 24 with the HETS vehicle.

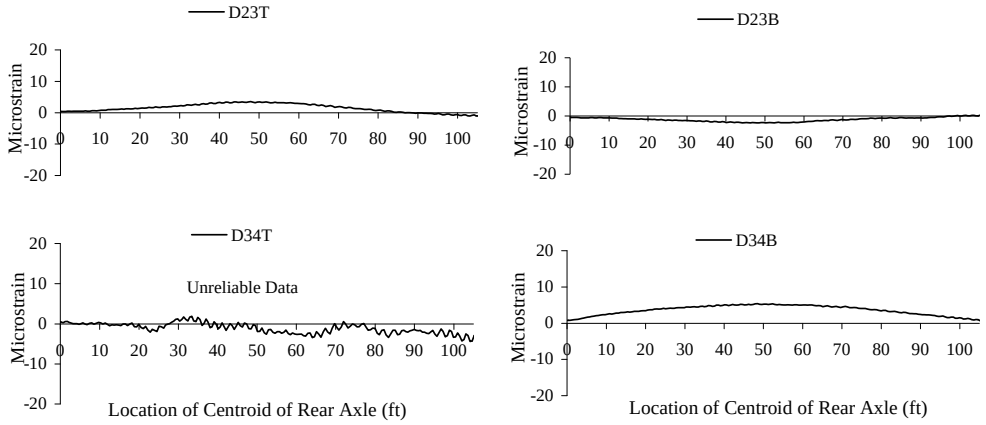

Figure 4.16 Strain Histories for Diaphragm Gages at Mid-Span, Run 28

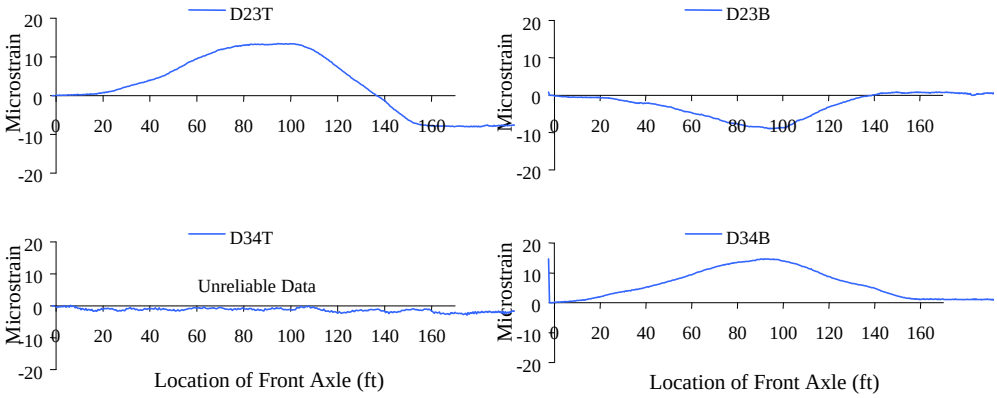

Figure 4.17 Strain Histories for Diaphragm Gages at Mid-Span, Run 24

The measured responses indicate that the diaphragms provide restraint against out-of-plane motions of the precast girders. As the load moves along path P3, the part of the diaphragm between girders 3 and 4 is under positive bending, as indicated by the tension in the bottom gage. The bottom flanges of the girders pull on the diaphragm, as they tend to deflect in the outward direction under the applied loads. The opposite is true about the adjacent portion of the diaphragm that frames into girders 2 and 3. The bottom part of the diaphragm is compressed when the bottom flanges of the girders tend to move inward during the run. The two sets of plots show similar trends for both vehicles moving along the exterior path (P3).

The maximum strains measured by the diaphragm gages are summarized in Table 4.12 and Table 4.13. Based on the discussion above, positive or negative bending can be expected in the diaphragms depending on the vehicle location relative to the gages. The presentation is in terms of the maximum tensile and compressive strains recorded during Runs 23 through 33. The maximum strain induced by truck D4 was 12 microstrain, and that induced by the HETS was 40 microstrain. These values are 30% of the maximum strain induced in a single girder at the extreme tension fiber. The maximum effects were recorded when the vehicles were moving along the interior path P2, mainly because the wheel loads were closer to the gages.

Table 4.12 Maximum Compressive Strains Measured at Mid-Span on the Surface of the Interior Diaphragm, Test Series 3, Microstrain

Run #	Loading Vehicle	Vehicle Path	Compressive Strain			
			Diaphragm D23		Diaphragm D34	
			D23T	D23B	D34T*	D34B
23	HETS	P1	-4	0	-	-18
24	HETS	P3	-8	-9	-	0
25	HETS	P2	-8	0	-	0
26	HETS	P2	-7	0	-	0
27	HETS	P2	-7	0	-	0
28	D4	P3	-1	-2	-	0
29	D4	P3	0	-2	-	0
30	D4	P2	-7	0	-	0
31	D4	P2	-7	0	-	0
32	D4	P1	-2	0	-	-5
33	D4	P1	-1	0	-	-4

*Unreliable Data were recorded by D34T

Table 4.13 Maximum Tensile Strains Measured at Mid-Span on the Surface of the Interior Diaphragm, Test Series 3, Microstrain

Run #	Loading Vehicle	Vehicle Path	Tensile Strain			
			Diaphragm D23		Diaphragm D34	
			D23T	D23B	D34T*	D34B
23	HETS	P1	2	3	-	3
24	HETS	P3	13	1	-	15
25	HETS	P2	7	40	-	39
26	HETS	P2	9	40	-	38
27	HETS	P2	9	39	-	39
28	D4	P3	4	0	-	5
29	D4	P3	4	1	-	6
30	D4	P2	0	11	-	11
31	D4	P2	0	11	-	11
32	D4	P1	2	1	-	1
33	D4	P1	1	1	-	1

*Unreliable Data were recorded by D34T

4.3.3 Strains Measured at Girder Sections Located at Three-Quarter Span

A section located 76.5 ft from the abutment was instrumented similarly to the mid-span section. Ten gages were attached to the surface of the Type IV, prestressed concrete girders. Five gages were attached to the bottom surface of the sections and five were attached to the web, 20 in. above the bottom surface.

The maximum strains that were measured by the bottom and middle gages are summarized in Table 4.14 and Table 4.15 respectively. The maximum strain induced when the dump truck was on the bridge was 33 microstrain, and the maximum strain induced by the HETS was 106 microstrain. In general, the magnitudes of the strains measured at this section are lower than the corresponding values recorded at mid-span.

Small negative bending was induced in exterior girders 1 and 5 when the vehicles moved along the paths adjacent to the aluminum rails. Compressive strains were recorded by the bottom and middle gages in girder 1 during Runs 24, 28 and 29, and in girder 5 during Runs 23, 32 and 33. The effect was more pronounced with the HETS.

Table 4.14 Maximum Strains Measured at 76.5-ft. on the Bottom Surface of the Prestressed Concrete Girders, Test Series 3

Run #	Loading Vehicle	Vehicle Path	Maximum Strain, microstrain				
			BEAM 1 B1B-76.5	BEAM 2 B2B-76.5	BEAM 3 B3B-76.5	BEAM 4 B4B-76.5	BEAM 5 B5B-76.5
23	HETS	P1	101	73	28	21	-11
24	HETS	P3	-8	21	46	79	106
25	HETS	P2	19	40	64	43	28
26	HETS	P2	21	42	63	40	26
27	HETS	P2	20	41	64	43	27
28	D4	P3	-2	6	14	29	31
29	D4	P3	-2	7	15	30	30
30	D4	P2	7	13	24	10	8
31	D4	P2	6	14	27	10	8
32	D4	P1	32	28	11	6	-3
33	D4	P1	33	27	9	6	-3

Table 4.15 Maximum Strains Measured at 76.5-ft. on the Surface of the Web of the Prestressed Concrete Girders, Test Series 3

Run #	Loading Vehicle	Vehicle Path	Maximum Strain, microstrain				
			BEAM 1 B1M-76.5	BEAM 2 B2M-76.5	BEAM 3 B3M-76.5	BEAM 4 B4M-76.5	BEAM 5 B5M-76.5
23	HETS	P1	48	-	14	10	-4
24	HETS	P3	-3	-	21	43	42
25	HETS	P2	7	-	34	23	10
26	HETS	P2	8	-	33	22	9
27	HETS	P2	8	-	34	24	10
28	D4	P3	-1	-	6	15	13
29	D4	P3	-1	-	6	15	13
30	D4	P2	3	-	12	5	3
31	D4	P2	3	-	13	6	3
32	D4	P1	15	-	4	3	-1
33	D4	P1	15	-	5	2	-1

A set of strain data recorded by the three-quarter span gages during Run 28 is presented in Fig. 4.18. This group of plots is representative of the set of

runs with truck D4. Figure 4.19 is a plot of the histories recorded at the three-quarter span for Run 24 with the HETS vehicle. The response is similar to the response measured at mid-span.

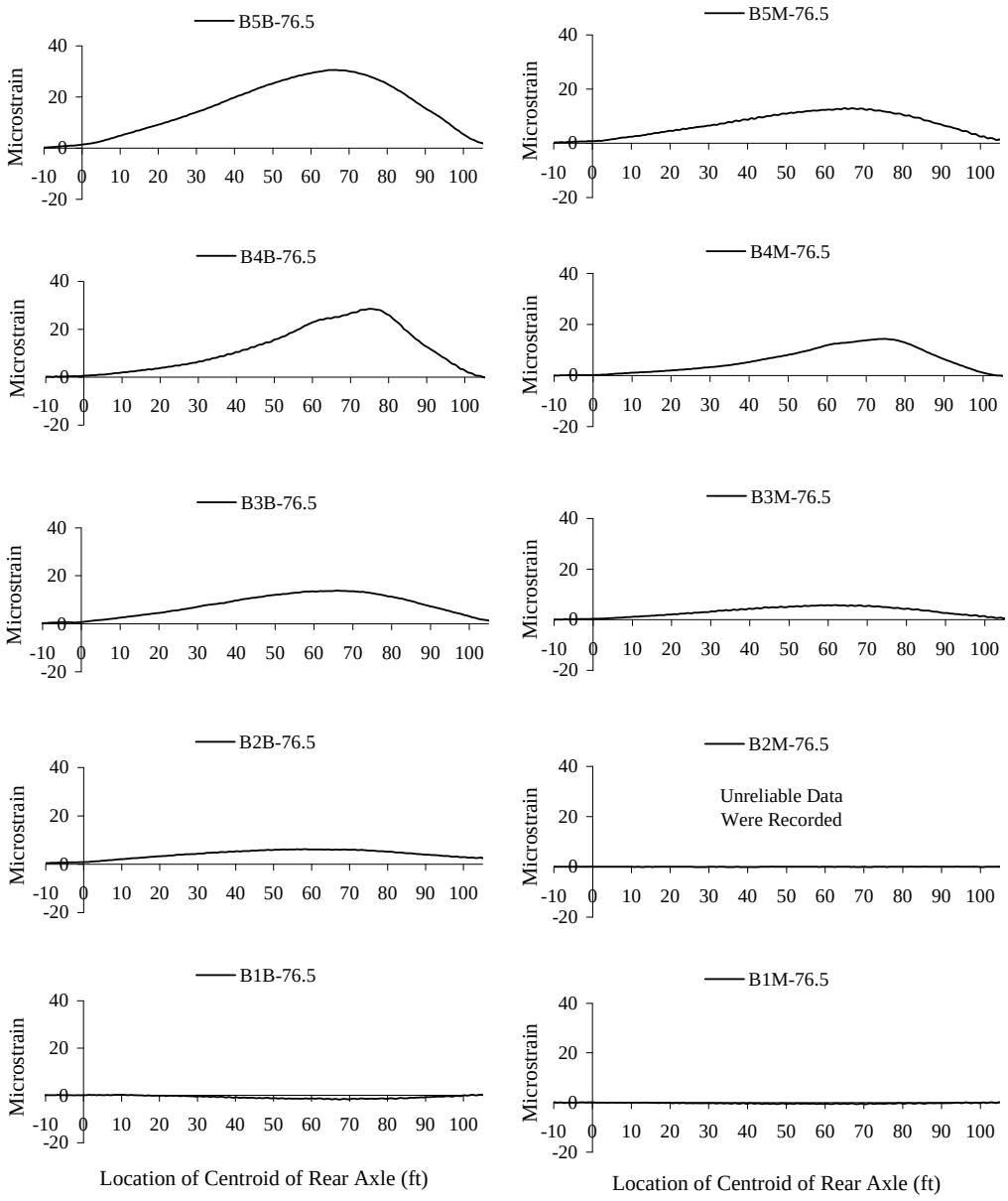

Figure 4.18 Strain Histories for Gages Located at the Surface of the Girders at Three-Quarter Span, D4, Run 28

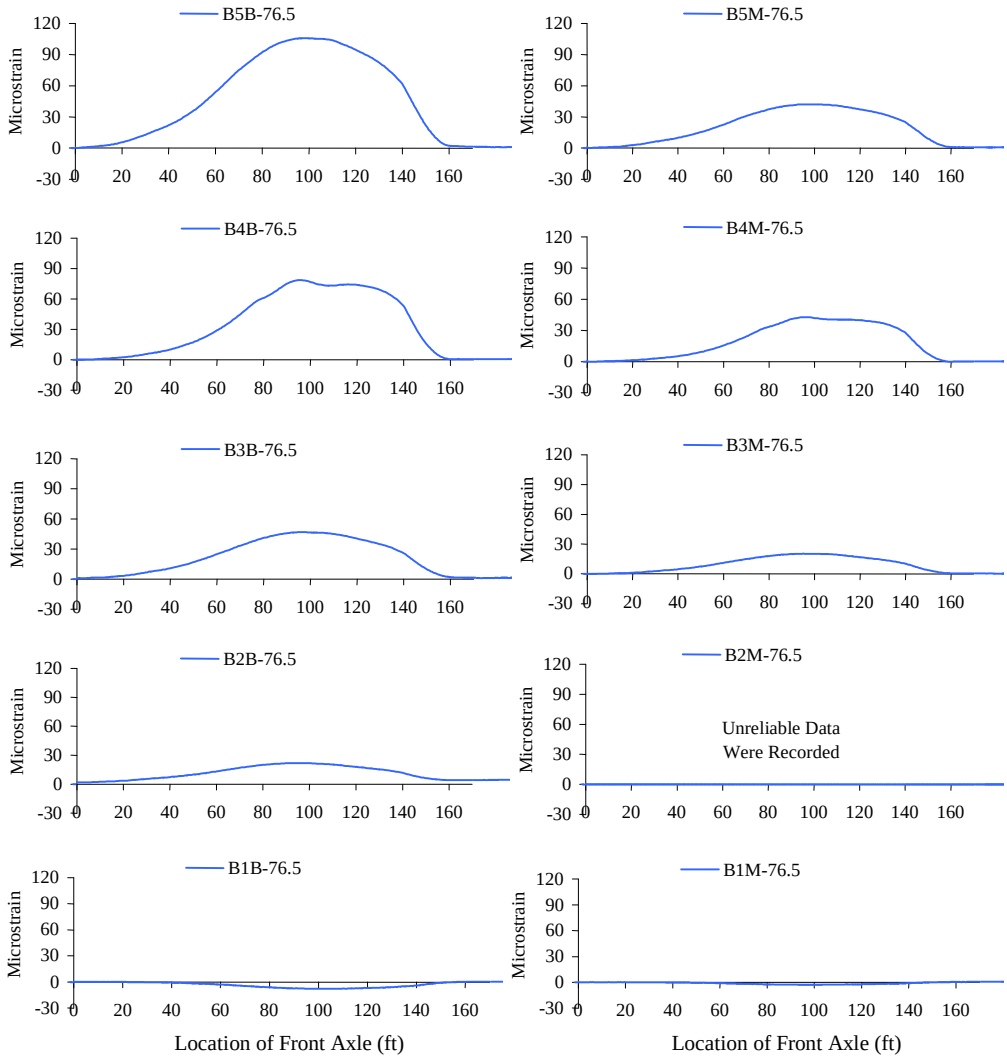

Figure 4.19 Strain Histories for Gages Located at the Surface of the Girders at Three-Quarter Span, HETS, Run 24

4.4 SUMMARY OF THE MEASURED RESPONSES OF THE TWO BRIDGES

The measured responses for the three diagnostic load tests on the two prestressed concrete bridges were presented. The recorded data were shown in the form of the strains measured at selected longitudinal sections: mid-span, two-thirds span, and five-sixths span for the Slaughter Creek Bridge and mid-span and three-quarter span for the Nolanville Bridge. The data showed that the maximum recorded girder strains for the 40-kip trucks, ranged between 33 and 38 microstrain and the maximum strain measured with the HETS truck at the Nolanville Bridge was 106 microstrain.

Chapter 5 presents an evaluation of the experimental data with emphasis on the neutral axis depths in the sections, the induced live load moments and their distribution. The load rating of the structures is discussed in Chapter 6.

Chapter 5. EVALUATION OF THE MEASURED RESPONSES OF THE TWO PRESTRESSED CONCRETE BRDIGES

This chapter evaluates the responses of the two prestressed concrete bridges during the diagnostic load tests. First, a discussion regarding the measured and calculated neutral axis depths is presented. A discussion of live-load moments calculated from the measured strains follows. The results are compared with moments obtained from various line-girder analyses. The chapter ends with a discussion of the moment distribution factors. The load ratings for the longitudinal members of the two bridges are discussed in Chapter 6.

5.1 ESTABLISHING THE SECTION AND MATERIAL PROPERTIES

5.1.1 Neutral Axis Depths

The location of the neutral axis provides useful information about the behavior of the individual girders during the tests and provides a means of comparing the observed and calculated responses. Two gages, separated by 20 in. vertically were attached to the prestressed girders at the same longitudinal position (Fig. 3.9 and 3.13). This made it possible to estimate the neutral axis depths from the measured strains during each run by assuming a linear variation of strain within the girder.

It is expected that the transverse reinforcement in the precast girders would facilitate composite action between the girders and the cast-in-place slab. Therefore, the cross sections were analyzed assuming uncracked properties and

composite action. The calculated neutral axis depths were then compared with those inferred from the measured data.

Figure 5.1 shows a sketch of the assumed distribution of live-load strains that are induced over the depth of the composite section.

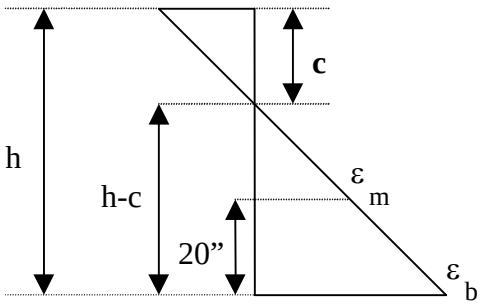

Figure 5.1 Linear Strain Distribution for Evaluating the Neutral Axis Depth

The term h refers to the total depth of the composite section from the bottom surface of the precast girder to the top of the slab. The neutral axis depth is denoted by c and it is measured from the top of the slab so that the results are consistent between interior and exterior sections. The bottom and middle strains are taken from the readings of the two gages and they are identified as ε_b and ε_m respectively. Equation 5.1 can be derived by similar triangles in order to express the neutral axis depth.

$$\frac{h-c}{20} = \frac{\varepsilon_b}{\varepsilon_b - \varepsilon_m} \Rightarrow c = \frac{(h-20)\varepsilon_b - h\varepsilon_m}{\varepsilon_b - \varepsilon_m} \qquad (5.1)$$

Figure 5.2 shows typical plots of the inferred neutral axis depth in girder 4 at the Nolanville Bridge as it varies with the longitudinal location of the vehicle. The chart on the left corresponds to Run 29 of truck D4 and the chart on the right corresponds to Run 24 of the HETS vehicle. The two lines on each chart represent the neutral axis depths that are calculated at the mid-span and three-quarter span sections of the girder. The calculations of the neutral axis depths from the measured strain data were performed within the ranges where the levels of strain at the bottom of the cross sections were higher than 10 to 15 microstrain.

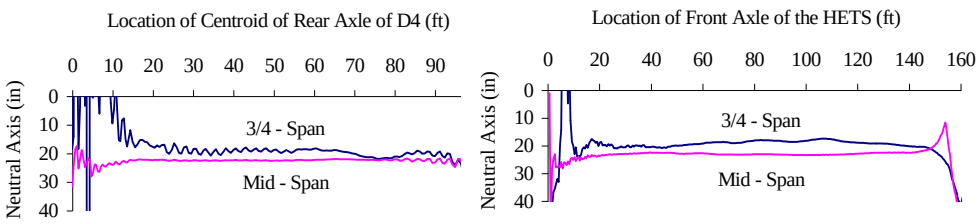

Figure 5.2 Variation of Neutral Axis Depth with Longitudinal Location of the Loading Vehicles

In order to evaluate the experimental measurements of the neutral axis depths, a calculation based on gross cross section properties was performed. The different values of the moduli of elasticity of the concrete in the precast girders, the precast panels and the cast-in-place slab as well as the modulus of the 0.5-in. strands in the girders were considered in the definition of a transformed composite section. Representative spreadsheets that were developed for

calculating the neutral axis depths are shown in Appendix B for the interior and exterior sections of both bridges at the mid-span section.

Table 5.1 is constructed based on the calculations of Appendix B to show the neutral axis depths calculated at the different longitudinal positions. Changes in the eccentricity of the strands and in the thickness of the 20-in. wide layer of concrete at each section, are the only factors responsible for the small variation of the values of the neutral axis depths with longitudinal location. The resulting values were very close to each other and subsequent analyses have been based only on the mid-span values of the neutral axis depths in defining the moments of inertia and section moduli for the composite sections.

Table 5.1 Calculated Neutral Axis Depths at the Different Sections for Each Bridge, in.

	Slaughter Creek Bridge			Nolanville Bridge	
Beam	50'	66.7'	83.3'	51'	76.5'
1	19.9	20.1	20.3	25.6	25.8
2	22.7	22.8	23.1	22.6	22.8
3	22.7	22.8	23.1	22.6	22.8
4	22.7	22.8	23.1	22.6	22.8
5	19.9	20.1	20.3	25.6	25.8
Strip thickness (in)	0.5	0.7	1	0.5	0.75
Total Depth (in)	62	62.2	62.5	62.75	63

Table 5.2 presents the neutral axis depths that were inferred from the measured strains at the mid-span section. The table also includes the corresponding calculated values for the composite and the non-composite

sections. Note that the parapets were considered in the calculations of the neutral axis depths of the exterior girders at the Slaughter Creek Bridge. However, the traffic rails in the Nolanville Bridge were neglected based on the details of the bridge and the relatively deep neutral axis depths measured for the exterior girders.

Table 5.2 Comparison of Measured and Calculated Neutral Axis Depths at the Mid-Span Section

Bridge I.D.	Neutral Axis Depths	Beam 1	Beam 2	Beam 3	Beam 4	Beam 5
Slaughter	Measured (in)	18.9	20.2	20.7	18.7	19.6
Creek	Calculated, Composite Section (in)	19.9	22.7	22.7	22.7	19.9
Bridge	Calculated, Girder alone (in)	37.3	37.3	37.3	37.3	37.3
TS1, TS2	Difference (% of Depth=62")**	2	4	3	6	1
Nolanville	Measured (in)	29.3	-	22.6	20.4	29.7
Bridge	Calculated, Composite Section (in)	25.6	22.6*	22.6	22.6	25.6
TS3	Calculated, Girder alone (in)	38.0	38.0	38.0	38.0	38.0
	Difference (% of Depth=62.75")**	6	-	0	3	7

*Calculated value is based on the readings at the three-quarter span section

** (Measured Neutral Axis - Calculated Neutral Axis for Composite Sections)/(Depth of Composite Section)

The calculated values are based on the properties of the materials listed in Table 5.3. The differences between the calculated values and those based on the measured strains are included in the table as percentages of the depths of the composite sections. These differences are within a few percent, with the maximum difference occurring at the exterior sections of the Nolanville Bridge. In that case, the neutral axis depths were deeper than expected based on gross cross-sectional properties by approximately 15%. Cracking of the cast-in-place

slab at the exterior section would result in lower effective slab participation in bending.

5.1.2 Moduli of Elasticity for the Concrete Materials

Another issue related to the moment calculations was the values for the moduli of elasticity for the precast and cast-in-place concrete materials. The actual values for these variables were not known. As a starting point, the design compressive strengths of the materials, as indicated on the structural plans, were used to calculate the moduli of elasticity using Eq. 5.2 from Section 8.7.1 of the 1996 AASHTO Standard Specifications [2].

$$E_c = 57{,}000\sqrt{f'_c} \tag{5.2}$$

where

f'_c = Concrete compressive strength, psi

E_c = Modulus of elasticity for concrete, psi

Later in the analysis, it was deemed more appropriate to increase the modulus of elasticity by approximately 5% to account for the differences between the actual concrete strength and the specified 28-day compressive strength. Table 5.3 shows the values of the modulus of elasticity calculated based on the design compressive strengths of the concrete and the values used to calculate the live-load moments. Note that a lower value of the modulus of elasticity was used

in the calculations for the exterior section at the Nolanville Bridge. This reflected the possibility that the slab at the exterior section was cracked.

Table 5.3 Values of the Moduli of Elasticity Used in the Analyses, ksi

Bridge I.D.		Location on the Bridge			
		Exterior Girder	Interior Girder	Cast-in-place Slab	Precast Slab Panels
Slaughter Creek Bridge	Design	5000	4000	3500	4000
	Assumed**	5500	4600	3900	4600
Nolanville Bridge	Design	4500	4500	3400	-
	Assumed**	5000	5000	3900/3400*	-

*Lower value is for the exterior section, where the slab is assumed cracked

*Modulus of elasticity used to calculate live-load moments from measured strains

5.1.3 Moments of Inertia for the Composite Sections

One issue that was addressed before calculating the moments was defining the moments of inertia and section moduli for the composite sections. As discussed in Section 5.1.1, the variation of the neutral axis depth with the longitudinal location of the section was not significant. The values used for the calculations of the moments are shown in Table 5.4, and they are based on the geometry of the mid-span section.

Table 5.4 Calculated Properties for the Composite Sections Used in the Moment Calculations

Bridge I.D.	Girder	Longitudinal Section (ft)	Neutral Axis Depth (in.)	20-in. Strip Thickness (in.)	Cbottom (h-c) (in.)	Total Depth (h) (in.)	Moment of Inertia (in^4)	Section Modulus (in^3)
Slaughter Creek	Exterior	50	19.9	0.50	42.1	62.0	821000	19500
		66.7	20.1	0.70	42.1	62.2	827000	19600
		83.3	20.3	1.00	42.2	62.5	835000	19800
	Interior	50	22.7	0.50	39.3	62.0	664000	16900
		66.7	22.8	0.70	39.4	62.2	673000	17100
		83.3	23.1	1.00	39.4	62.5	685000	17400
Nolanville	Exterior	51	25.6	0.50	37.2	62.8	636000	17100
		76.5	25.8	0.75	37.2	63.0	650000	17500
	Interior	51	22.6	0.50	40.1	62.8	722000	18000
		76.5	22.8	0.75	40.2	63.0	738000	18400

As discussed earlier, the neutral axis depths measured for the exterior girders at the Nolanville Bridge were deeper than expected from theory and gross cross section properties. In that case, the problem was bound by varying the modulus of elasticity of the slab participating in bending with the exterior girder from 3900 ksi to 3400 ksi in calculating the properties of the composite section. The results are presented in Table 5.5. The variation of the calculated section moduli is not large. The values corresponding to the lower modulus of elasticity for the slab were used in calculating the live-load moments.

Table 5.5 Variation in the Section Properties Calculated for the Exterior Composite Section at the Nolanville Bridge

E_{slab} (ksi)	Longitudinal Section (ft)	Neutral Axis Depth (in)	Moment of Inertia (in^4)	Section Modulus (in^3)
3900	51	24.5	668000	17500
3900	76.5	24.9	683000	18000
3400	51	25.6	636000	17100
3400	76.5	26.0	650000	17600

5.2 CALCULATING LIVE-LOAD MOMENTS FROM THE MEASURED STRAINS

5.2.1 Calculations of the Cracking Stresses

The next step was to investigate the levels of live-load stresses that would result in a tensile concrete stress at the extreme tension fiber equal to the allowable service-load tensile stress after the prestress losses. Table 5.6 summarizes the results of the calculations for the interior and exterior girders of each bridge. The table includes the material and section properties used in the stress calculations at the mid-span section and they are based on the structural plans. Equation 5.3 is based on Section 9.15.2.2 of the 1996 AASHTO Standard Specifications for Highway Bridges [2]. The expression used for the calculations of the moduli of elasticity for the sections is discussed next in Section 5.2.2.

Table 5.6 Live-Load Stresses and Strains Required at Mid-Span to Reach the Allowable Service-Load Tensile Stresses

Bridge I.D.	Girder	Concrete Compressive Strength (f'_c) (psi)	Calculated Neutral Axis Depth (in)	Moment of Inertia (in^4)*	Effective Prestress (f_{pe})** (ksi)	Modulus of Elasticity (E) (ksi)	Allowable Tensile Stresses (ksi)	Required Live-Load Stresses (ksi)**	Required Live-Load Strains (με)
Slaughter Creek	Interior	6500	22.7	664000	2.80	4600	0.48	0.84	183
	Exterior	9200	19.9	821000	2.90	5500	0.58	1.23	225
Nolanville	Interior	7700	22.6	722000	3.10	5000	0.53	0.76	152
	Exterior	7700	25.6	636000	3.00	5000	0.53	1.09	218

*Corresponding to composite section

**Refer to Appendix C for the detailed calculations for the f_{pe} and additional live-load stresses

**$f_{required}=f_{allow}+f_{pe}-f_{dead}$

$$f_{allowable} = 6\sqrt{f'_c} \tag{5.3}$$

where

$f_{allowable}$ = Allowable tensile stresses at service loads, psi

f'_c = Compressive strength of the concrete, psi

f_{pe} = Effective prestress after losses, ksi (Appendix C)

f_{dead} = Dead load stresses, ksi (Appendix C)

The lowest calculated value of live load strain required to reach the allowable stresses at the extreme tension fiber of the concrete after losses is 183με for the interior girder at the Slaughter Creek Bridge and 152με for the interior girder at the Nolanville Bridge. The measured data with the ten-cubic yard dump trucks never exceeded a level of 45με and those with the HETS vehicle during the Test Series 3 were kept below 110με. It is concluded that the beams did not crack due to the stresses induced during the diagnostic load tests. Based on these calculations and the fact that the measured neutral axis depths were close to the calculated values based on gross cross-sectional properties, it is concluded that the beams had not been cracked during their service life. Therefore, the elastic material properties are used in subsequent calculations.

5.2.2 Calculation of the Live-Load Moments

The total live-load moments that were induced by the loading vehicles were calculated using principles of elastic analysis. Equation 5.4 was used to relate the strains measured at the bottom surface of the girders to the corresponding moments in the girders. The latter were summed up over all five girders across each of the instrumented sections to obtain the total moment induced in the structure. Equation 5.5 shows this calculation.

$$Mi = (\frac{1}{12}10^{-6})\frac{E_i I_i}{h - c_i}\varepsilon_i \quad (5.4)$$

$$M_{total} = \sum_{i=1}^{5} Mi \quad (5.5)$$

where

M_i = Individual moment in girder i, k-ft

M_{total} = Total Moment induced in the structure, k-ft

E_i = Modulus of elasticity for girder i, ksi

I_i = Moment of inertia of the composite section, in^4 (Table 5.2)

h = Total depth of the composite section, in. (Fig. 5.1)

c_i = Composite neutral axis depth from top of the slab, in. (Fig. 5.1)

ε_i = Measured strain at the extreme bottom fiber, με

During Test Series 3 at the Nolanville Bridge, unreliable data were recorded at beams 2 and 3 at mid-span. The calculations of the moments for beam 2 were performed using the readings by the middle gage at mid-span and the neutral axis depth that was inferred by the readings at the three-quarter span. The moment at beam 1 was determined by assuming that the ratios of the moments calculated at the other girders to the moment for beam 1 at the three-quarter span would also apply at the mid-span section.

The set of plots in Fig. 5.3 represents typical individual girder moment histories. Figure 5.4 shows the total moment histories for each section. The

moments are calculated for Run 19 and plotted against the longitudinal position of the centroid of the rear axles of the trucks. The moments peak when the rear axles are located above the gages, and the induced mid-span moments are higher than those recorded at the other sections. These trends were also observed during the presentation of the measured strain data in Chapter 4.

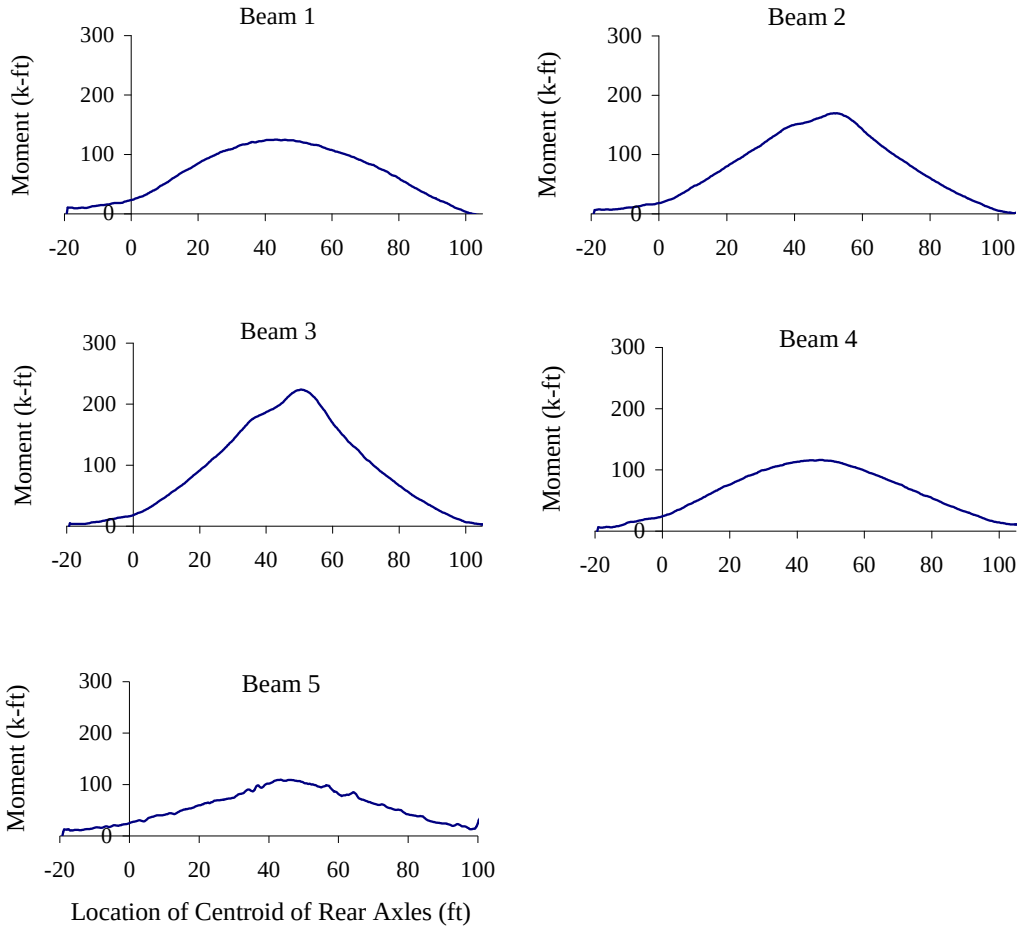

Figure 5.3 Typical Individual Girder Moment Histories at Mid-Span Section, Run 19

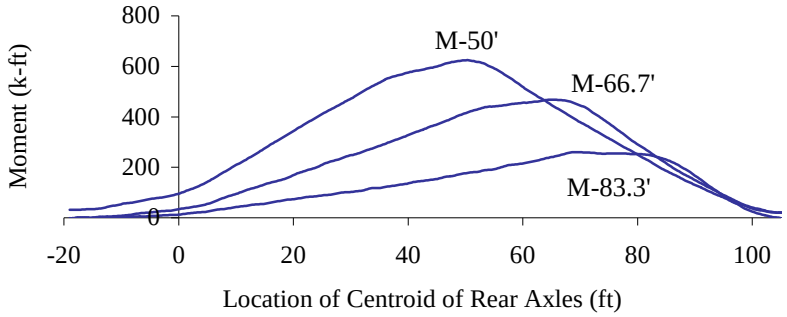

Figure 5.4 Total Measured Live-Load Moments at Each Section, Run 19

The maximum live-load girder and total moments induced during each run are presented in Tables 5.7 through 5.9. The maximum mid-span moment measured in a single girder at the Slaughter Creek Bridge was 387 k-ft for runs with a single dump truck and 485 k-ft for runs with two dump trucks. Maximum moments for the Nolanville Bridge were 292 k-ft for the standard dump truck and 1016 k-ft for the HETS.

The maximum moments occurred in exterior girders when the vehicle was moving close to the edge of the bridge. This observation was more pronounced in the case of the exterior girder at the Slaughter Creek Bridge. The presence of the parapet, the higher number of strands (58) and the higher compressive strength of the concrete material (7700 psi) compared with the interior section (36 strands and 5000 psi concrete) are the factors raising the bending stiffness of the exterior section. Also, the lack of diaphragms or other secondary elements in the bridge that would enhance the distribution of the load in the transverse direction results in higher moments calculated at this section.

Table 5.7 Maximum Girder Moments at the Slaughter Creek Bridge, k-ft

Run	BEAM 1			BEAM 2			BEAM 3			BEAM 4			BEAM 5		
#	50'	66.7'	83.3'	50'	66.7'	83.3'	50'	66.7'	83.3'	50'	66.7'	83.3'	50'	66.7'	83.3'
1	6	1	1	26	17	4	79	59	20	173	146	91	387	280	160
2	3	2	2	21	18	7	75	71	24	169	152	84	335	268	142
4	36	21	17	112	95	54	199	177	101	185	161	94	106	78	20
5	104	64	36	159	133	70	205	188	116	105	82	66	40	40	12
6	105	65	35	153	143	87	197	175	106	91	76	65	53	34	4
7	373	254	145	204	189	111	87	82	57	36	18	24	5	2	3
8	369	245	137	184	192	112	77	59	42	19	36	18	10	-1	-5
9	336	239	120	220	216	135	155	138	74	194	166	104	365	270	158
10	329	229	131	218	213	128	159	145	76	201	171	102	345	256	142
11	46	26	15	118	93	47	271	238	120	321	286	180	485	347	184
12	53	26	16	126	106	50	283	237	119	323	281	180	474	327	173
13	460	301	180	320	311	176	275	252	155	125	111	74	61	44	10
14	432	274	158	319	307	173	290	262	159	140	122	82	64	46	13
15	2	3	1	20	19	8	66	61	20	162	131	88	366	265	156
16	11	9	5	30	18	10	66	59	20	167	139	86	382	275	155
17	46	32	19	90	80	43	195	179	106	140	117	87	100	73	45
18	41	27	23	83	80	41	190	176	94	144	121	87	100	77	28
19	108	65	35	151	130	72	199	177	110	105	78	55	67	39	28
20	110	56	36	142	128	71	198	181	114	103	80	60	63	41	26
21	335	237	135	179	178	100	77	69	50	26	22	15	-3	3	-7
22	333	231	131	183	179	105	78	69	47	31	24	16	9	3	1

Table 5.8 Maximum Girder Moments at the Nolanville Bridge, k-ft

Run	BEAM 1		BEAM 2		BEAM 3		BEAM 4		BEAM 5	
#	51'	76.5'	51'	76.5'	51'	76.5'	51'	76.5'	51'	76.5'
23	1016	691	803	575	378	227	175	155	-90	-85
24	-85	-59	194	168	561	372	641	587	870	811
25	272	148	450	318	745	498	376	319	231	214
26	301	162	471	335	743	510	358	297	210	195
27	301	153	444	328	757	503	378	321	228	209
28	-16	-13	38	48	158	108	210	213	243	234
29	-16	-13	63	50	164	113	213	218	239	228
30	79	48	124	133	235	221	102	73	51	58
31	83	47	120	106	235	204	100	72	55	59
32	292	243	251	212	103	68	52	42	-34	-23
33	282	246	239	210	103	61	49	37	-25	-22

Table 5.9 Maximum Total Moments Induced in the Two Bridges during the Three Diagnostic Load Tests, k-ft

Test Series	Bridge I.D.	Run	Total Moment (k-ft)		
		#	50'	66.7'	83.3'
TS1	Slaughter	1	671	503	276
	Creek	2	603	511	259
		4	638	532	286
		5	613	507	300
		6	599	493	297
		7	705	545	340
		8	659	533	314
		9	1270	1029	591
		10	1252	1014	579
		11	1241	990	546
		12	1259	977	538
		13	1241	1019	595
		14	1245	1011	585
TS2	Slaughter	15	616	479	273
	Creek	16	656	500	276
		17	571	481	300
		18	558	481	273
		19	630	489	300
		20	616	486	307
		21	620	509	307
		22	634	506	300
			51'	76.5'	
TS3	Nolanville	23	2462	1733	
		24	2351	1997	
		25	2074	1497	
		26	2083	1499	
		27	2108	1514	
		28	665	616	
		29	695	622	
		30	591	533	
		31	593	488	
		32	732	588	
		33	698	576	

5.2.3 Evaluating Superposition in the Calculated Live-Load Moments

The live-load moments measured during Test Series 1 can be used to determine if superposition may be used to combine the moments obtained when a single truck is on the bridge to obtain the moments induced by multiple vehicles. Table 5.10 compares the moments induced during the runs involving the combination of the two trucks with those obtained by adding the values of the moments induced by the corresponding single-truck runs. In general, the sum of moments induced by single-truck runs tends to be higher than the corresponding value of the moment induced by two trucks by less than 5%. The agreement is good, and superposition appears to be valid for the loads that were applied to the bridge during the diagnostic load tests. This small difference in moments is probably due to minor variations in the paths of the trucks and difficulties associated with driving the two trucks across the bridge at exactly the same speed.

Table 5.10 Superposition of Total Live-Load Moments Measured during Test Series 1, k-ft

Run	Combination Truck Runs			Single Truck Runs			% Difference		
#	50'	66.7'	83.3'	50'	66.7'	83.3'	50'	66.7'	83.3'
9	1270	1029	591	1308	1056	599	-3	-3	-1
10	1252	1014	579	1308	1056	599	-4	-4	-3
11	1241	990	546	1309	1035	562	-5	-5	-3
12	1259	977	538	1309	1035	562	-4	-6	-4
13	1241	1019	595	1304	1038	637	-5	-2	-7
14	1245	1011	585	1272	1040	614	-2	-3	-5

*(Moment from combination truck runs - Sum of moments from single runs) / (Moment from combination truck runs)

5.3 CALCULATING LIVE-LOAD MOMENTS USING A LINE-GIRDER ANALYSIS

In order to evaluate the response of each bridge, it is necessary to compare the measured live-load moments with the calculated results based on statics. A series of line-girder analyses was performed to evaluate moments in the bridge at various vehicle positions. This method would result in calculating the maximum total moment expected during the diagnostic load tests.

5.3.1 Initial Approach

The bridge structures were initially idealized as simply-supported beams and the loading vehicles as series of concentrated loads moving in the longitudinal direction. The maximum moment induced by a series of point loads at a specific point along the length of a beam is caused when one of the loads is located at that point [4]. The location of the vehicles was varied across the span of the girder.

Figure 5.5 shows a typical sketch of a single girder representing the Slaughter Creek Bridge with the second axle of truck D3 located over the mid-span section. This configuration resulted in a maximum moment at mid-span. The plot represents the moment history calculated at mid-span with the specified vehicle moving along the "x" direction. Note that the span length that would be effective in bending is less than the lengths of the precast girders because of the finite width of the elastomeric bearings located at each end. The effective span lengths were reduced from 100 ft to 98.8 ft for the Slaughter Creek Bridge and from 102 ft to 100.8 ft for the Nolanville Bridge.

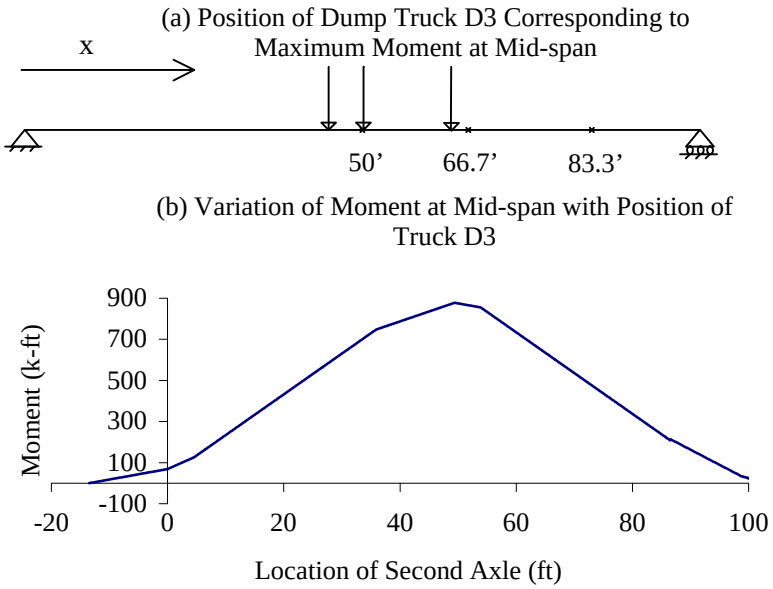

Figure 5.5 Mid-Span Moment History with Vehicle D3 Based on Line-Girder Analysis of Slaughter Creek Bridge

Similar analyses were performed for both bridges and for all loading configurations. The values of maximum moments obtained at each instrumented section during all runs are listed in Table 5.11. The maximum moments measured during the experiments are expressed as moments and as percentages of the total line-girder moments in each case.

The measured moments are 15 to 35 percent lower than maximum moments calculated from the line-girder analysis. Note that gross cross-section properties and composite sections were used to convert the measured strains into moments. Therefore, the reported measured moments represent a logical upper bound of the actual moments induced in the bridge. While it is possible that the

modulus of elasticity of the concrete is larger than the value that was assumed in Table 5.3, it is unlikely that the variation of material properties alone could account for these large differences.

Table 5.11 Comparison of Simple Beam Line-Girder Moments with the Maximum Measured Moments, k-ft

Test Series	Bridge I.D.	Run #	Total Measured Moment (k-ft)			Calculated Maximum Moment (k-ft)			Percent of Calculated Moment (%)		
			50'	66.7'	83.3'	50'	66.7'	83.3'	50'	66.7'	83.3'
TS1	Slaughter Creek	1	671	503	276	934	803	501	72	63	55
		2	603	511	259	894	770	486	67	66	53
		4	638	532	286	894	770	486	71	69	59
		5	613	507	300	934	803	501	66	63	60
		6	599	493	297	894	770	486	67	64	61
		7	705	545	340	934	803	501	75	68	68
		8	659	533	314	894	770	486	74	69	65
		9	1270	1029	591	1812	1560	967	70	66	61
		10	1252	1014	579	1812	1560	967	69	65	60
		11	1241	990	546	1812	1560	967	68	63	56
		12	1259	977	538	1812	1560	967	69	63	56
		13	1241	1019	595	1812	1560	967	68	65	62
		14	1245	1011	585	1812	1560	967	69	65	60
TS2	Slaughter Creek	15	616	479	273	878	757	467	70	63	58
		16	656	500	276	878	757	467	75	66	59
		17	571	481	300	878	757	467	65	64	64
		18	558	481	273	878	757	467	64	64	58
		19	630	489	300	878	757	467	72	65	64
		20	616	486	307	878	757	467	70	64	66
		21	620	509	307	878	757	467	71	67	66
		22	634	506	300	878	757	467	72	67	64
			51'	76.5'		51'	76.5'		51'	76.5'	
TS3	Nolanville	23	2462	1733		3630	2582		68	67	
		24	2351	1997		3630	2582		65	77	
		25	2074	1497		3630	2582		57	58	
		26	2083	1499		3630	2582		57	58	
		27	2108	1514		3630	2582		58	59	
		28	665	616		1061	755		63	82	
		29	695	622		1061	755		65	82	
		30	591	533		1061	755		56	71	
		31	593	488		1061	755		56	65	
		32	732	588		1061	755		69	78	
		33	698	576		1061	755		66	76	

*Ends of girders are assumed to be simply-supported

5.3.2 Factors Affecting the Moment Calculations

This section discusses possible error sources that would affect the observed differences between the maximum moments calculated based on the line-girder analyses and the maximum moments calculated from the strain data. Some of these sources are related to the experimental procedures and others to the analytical approaches and assumptions.

One possibility lies in the fact that any errors in the set up, wiring or initial balancing of the data-acquisition system could cause an inherent error in the data. This error is expected to be on the order of a few microstrain. The level of the maximum measured strains for all runs with the ten cubic yard dump trucks is on the order of 45 microstrain. Any inherent error in the system could lower the maximum measured strains, and subsequently the resulting moments, by about five percent. This is more important at the instrumented sections away from mid-span, because the measured strains were lower at those locations, and the effect that a fixed error would have on these measurements would be even greater.

Improper orientation of the strain gages in the field is another factor that can influence the measured data. Despite the great caution that is taken at the time of installation, some of the gages may not be exactly straight and well aligned with the longitudinal directions of the girders. This would result in lower measurements than the actual bending strains. However, since the data are repeatable, the gage orientation is not expected to greatly affect the results.

Other reasons relate to assumptions that were made for the exact properties and amounts of the materials. The modulus of elasticity for the concrete materials and the presence of asphalt and regular reinforcement can affect the bending stiffness of the sections and therefore the calculated moments. The information on these parameters is not well defined and any assumptions that were made could affect the final values of total and girder moments.

The second set of reasons relates to the assumptions made during the analytical approach used to calculate the line-girder total moments. Idealizing a bridge structure as a two dimensional beam, and representing the wheels as concentrated loads acting as single points without any finite longitudinal and transverse dimensions would result in modeling a more severe loading configuration than the actual. Also, any errors in the distribution of the weights among the axles would result in either higher or lower measurements.

The possibility of secondary effects due to induced axial compression at the bases of the girders was considered. The slenderness ratio (L/r) of the composite sections is calculated to be approximately 60. This means that even if the girders were ideally restrained against translation at both ends, the level of axial load that would be introduced at the bottom of the girders for this type of loading would be very low. The bearings at the Slaughter Creek Bridge are 15 in. in diameter and those at the Nolanville Bridge are 22 in. in length. Some shearing force would be responsible for negative moments developing at the locations of the bearings but they would not significantly reduce the total moments induced in the sections. Finally, the very high length-to-depth ratio

(18) and very low axial-to-bending stiffness ratio (7%) of the composite sections also preclude appreciable secondary effects.

5.3.3 Moments Developed at the Ends – Experimental Approach

Even if the beams are designed to act as simply-supported members, careful on-site investigation and information obtained from the structural plans of the two bridges, suggested that some negative moment could result at the ends of the girders. Figure 5.6 shows the two ends of the span at the Slaughter Creek Bridge and Fig. 5.7 shows the corresponding ends for the Nolanville Bridge.

A distinct crack at the interior end and an opening at the abutment end of the Slaughter Creek Bridge can be seen in Fig. 5.6. The reverse is shown in Fig. 5.7 at the Nolanville Bridge, with the crack forming at the abutment end and the opening at the interior end. During the discussions that follow, the cracked ends will be called “restrained” and the others “free.” The continuous slab at the interior end and the framing of the slab and end-diaphragms at the abutment end could be responsible for the development of some negative moment at the restrained ends in the Slaughter Creek and Nolanville Bridges respectively.

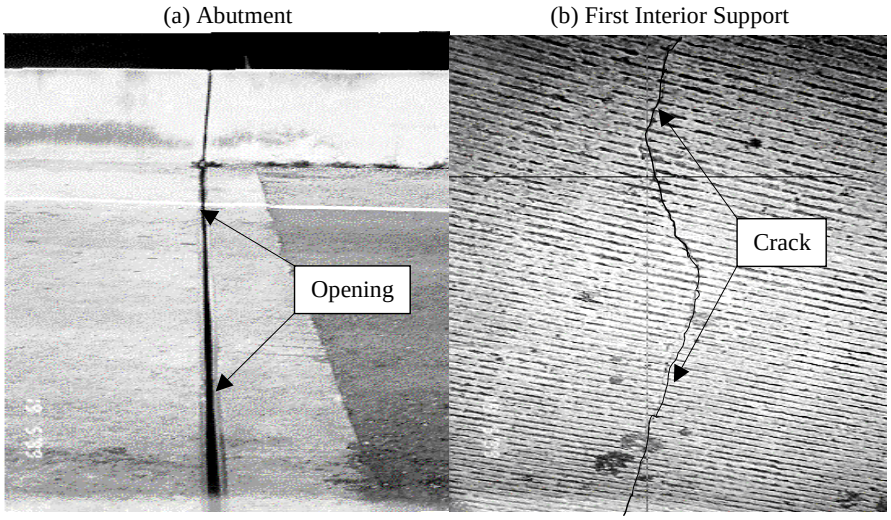

Figure 5.6 Photographs of the Ends of the First Span of the Slaughter Creek Bridge

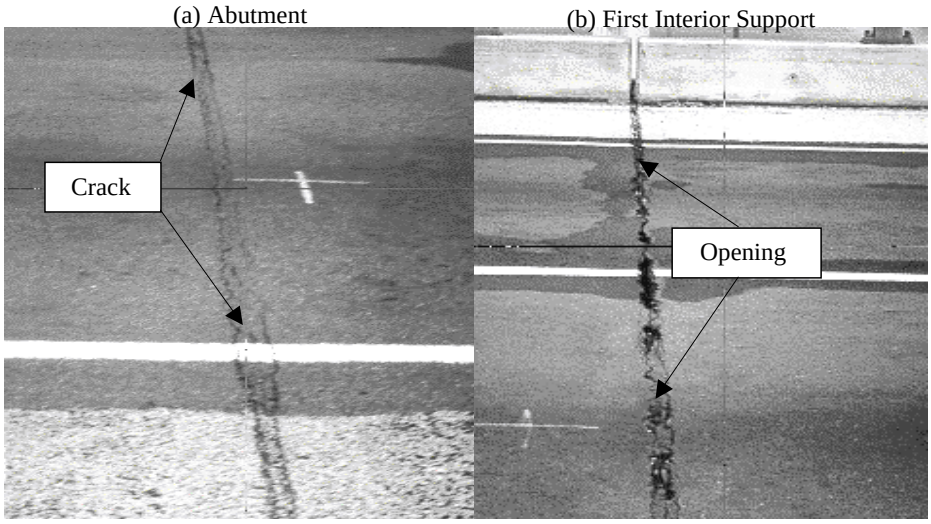

Figure 5.7 Photographs of the Ends of the First Span of the Nolanville Bridge

Consider the truck located at a certain longitudinal position on the span. The live-load shear force from the front axle of the vehicle to the first interior end of the beam is constant. The same is true for the live-load shear force from the

last axle of the vehicle to the abutment end, because there is no point load within the specified segments of the beam. The variation of the moment in the specified constant-shear region is linear. By selecting the range of truck locations for each structure in a way that the instrumented sections are included in the constant-shear region, the total moments calculated at these sections would lie on a straight line. The value of the moment at the restrained end can be found by continuing the line that joins the two points until it intersects the restrained end of the beam. The configurations shown in Fig. 5.8 and 5.9 illustrate the resulting shear force and moment diagrams for a location of the truck within the specified range for each bridge.

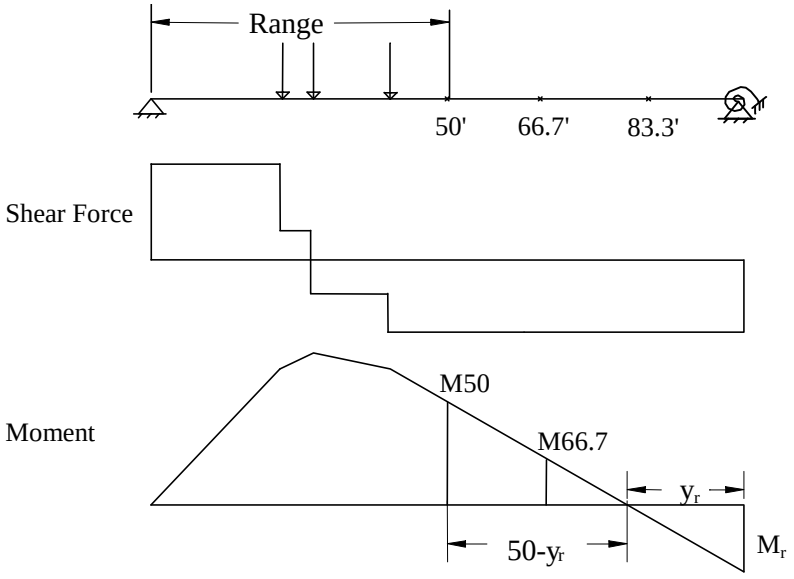

Figure 5.8 Configuration Used to Estimate the Moments at the Restrained End of the Slaughter Creek Bridge

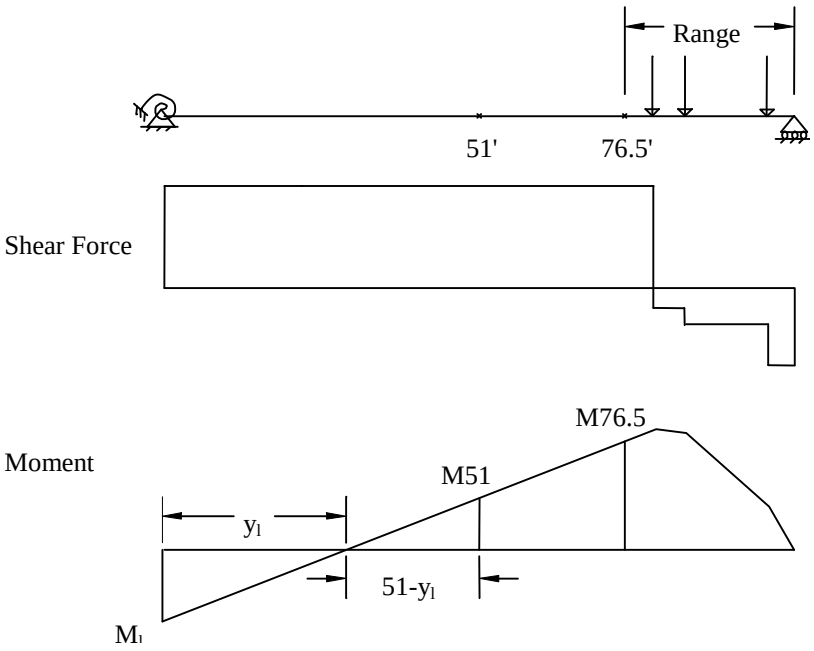

Figure 5.9 Configuration Used to Estimate the Moments at the Restrained End of the Nolanville Bridge

For the Slaughter Creek Bridge, the range was defined from the beginning of the span until the mid-span section. For the Nolanville Bridge, the range was taken from the three-quarter span until the end of the span. The moment at the restrained end was evaluated by using the moments measured at two sections: the mid-span and two-thirds span for the Slaughter Creek Bridge, and the mid-span and three-quarter span for the Nolanville Bridge. Using statics and similar triangles, Eqs. 5.6 through 5.9 can be developed in order to quantify the end moment.

For Slaughter Creek Bridge, and based on Fig. 5.8, the expressions for the distance y_r in feet and the moment M_r in k-ft are:

$$y_r = \frac{50M_{66.7'} - 33.3M_{50'}}{M_{66.7'} - M_{50'}} \tag{5.6}$$

$$M_r = \frac{y_r}{50 - y_r} M_{50'} \tag{5.7}$$

For the Nolanville Bridge, the subscripts change and the corresponding expressions now become:

$$y_l = \frac{76.5M_{51'} - 51M_{76.5'}}{M_{51'} - M_{76.5'}} \tag{5.8}$$

$$M_l = \frac{y_l}{51 - y_l} M_{51'} \tag{5.9}$$

The results from the dump truck runs for each bridge are summarized in Table 5.12. The maximum moment measured at mid-span is also included in the table. The end restraints are presented as moment magnitudes and as percentages of the maximum moments. The values are generally uniform with any inconsistencies resulting from the manipulation that is involved in calculating the girder moments, their sums, and the end moments based on the preceding equations. For the given ranges of the loading vehicles, when the magnitudes of the mid-span moments were closer than expected to the corresponding moments at the two-thirds or three-quarter span, Eqs. 5.6 through 5.9 yielded relatively very small values for the negative moments. This was the case for five runs, as shown in Table 5.12. Figure 5.10 shows a typical plot of the variation of the calculated moment at the end for Run 20 within the specified range for the

Slaughter Creek Bridge. The calculated moment histories for the two sections used in the calculations are also included in the figure.

It is important to note that the actual levels of peak end moments are expected to be about 15-20% higher than those reported in Table 5.11 especially in the case of the Slaughter Creek Bridge. This is because the maximum mid-span moment occurs when the truck is beyond the specified range that results in constant shear forces in the members. The effect is less obvious in the Nolanville Bridge, because the analysis was performed for ranges closer to the mid-span.

The results show that the degree of end restraint that can be expected in each case is appreciable and on the order of 30-35% of the total measured moment for the Slaughter Creek Bridge and 65% for the Nolanville Bridge. These end moments are responsible for lowering the measured moments much more than the factors that were discussed earlier in this section.

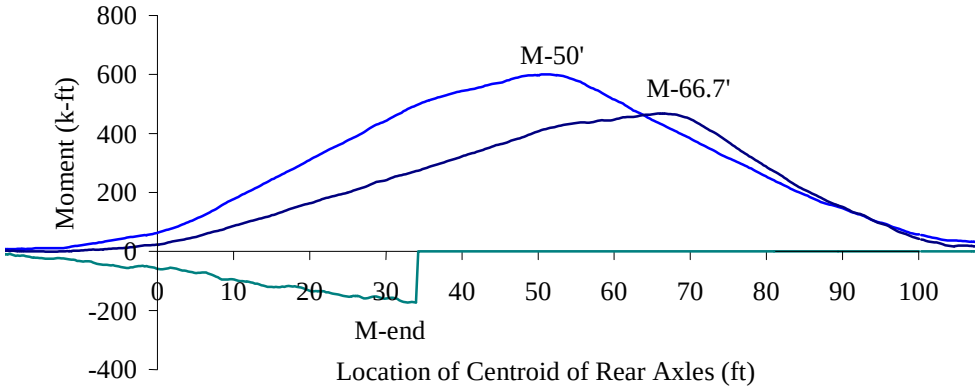

Figure 5.10 Typical History of the Moment Induced at the Restrained End and Total Moments at Two Sections for the Slaughter Creek Bridge

Table 5.12 End Moments Indicated by the Maximum Measured Moments within the Specified Ranges, k-ft

Test Series	Bridge I.D.	Run #	Mmax (k-ft)	Mend (k-ft)	|Mend|/Mmax (%)
TS1	Slaughter Creek	1	671	-140	21
		2	603	-44	7
		4	638	-153	24
		5	613	-175	29
		6	599	-147	25
		7	705	-182	26
		8	659	-72	11
		9	1270	-218	17
		10	1252	-213	17
		11	1241	-232	19
		12	1259	-253	20
		13	1241	-253	20
		14	1245	-218	18
TS2	Slaughter Creek	15	616	-114	19
		16	656	-170	26
		17	571	-65	11
		18	558	-63	11
		19	630	-218	35
		20	616	-173	28
		21	620	-87	14
		22	634	-150	24
TS3	Nolanville	28	665	-432	65
		29	695	-414	60
		30	591	-505	85
		31	593	-496	84
		32	732	-393	54
		33	698	-405	58

5.3.4 Moments Developed at the Ends – Line-Girder Approach

Having established the existence of end restraint and the expected level of end moments from the measured data, it was important to investigate the phenomenon analytically. The objective was to quantify the effect that end restraint had on the maximum positive moments and be able to better model the behavior of the structures.

Line-girder analyses of all the cases were performed with the beams modeled as propped-cantilevers. This would establish the maximum possible end restraint and bound the problem. The actual levels of end restraint could then be evaluated as a percent of the fixed case. Figures 5.11 and 5.12 show the models used for each bridge and the resulting histories of the moments at the fixed ends.

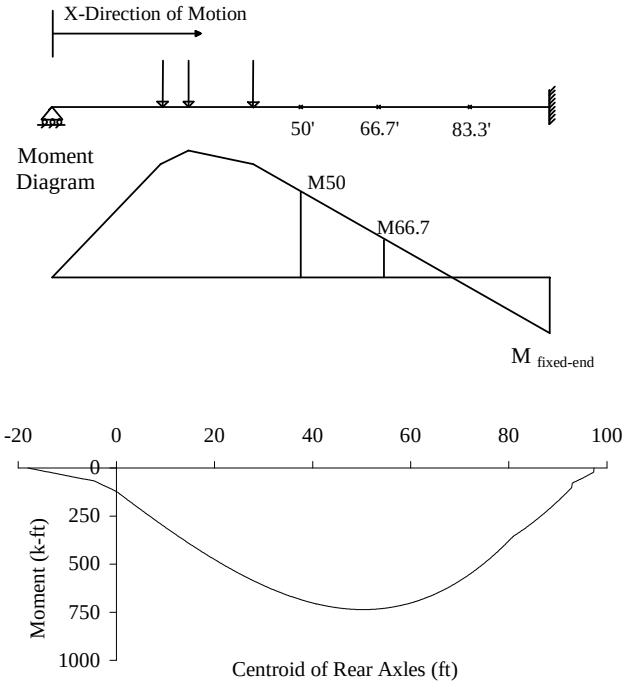

Figure 5.11 Line Girder Mid-span Moment History at the Fixed End for the Propped-Cantilever Beam Model at the Slaughter Creek Bridge

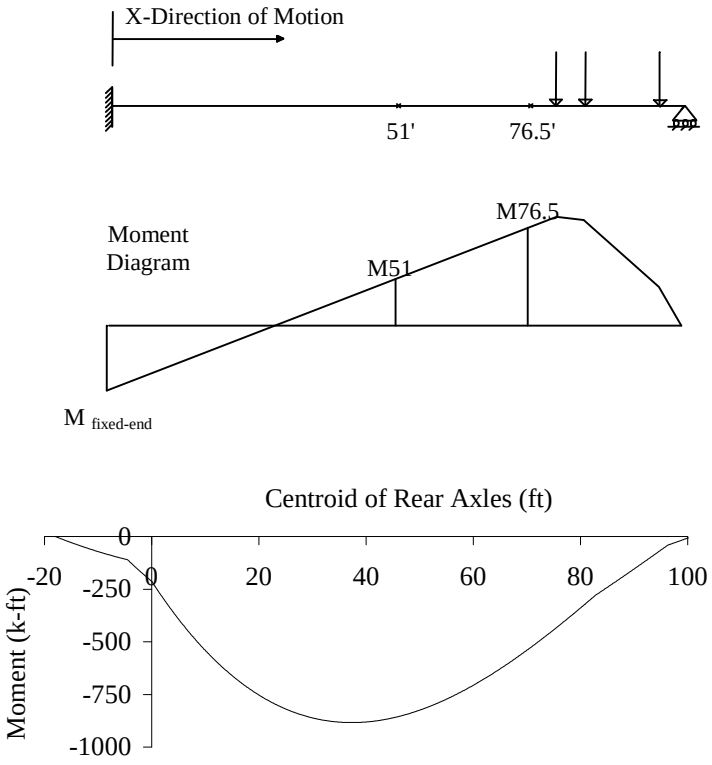

Figure 5.12 Line Girder Mid-span Moment History at the Fixed End for the Propped-Cantilever Beam Model at the Nolanville Bridge

Table 5.13 presents the maximum values calculated at each of the instrumented sections using the propped-cantilever models. The positive moments measured during the diagnostic load tests exceeded the calculated positive moments in the propped cantilever beams. The ratios of the maximum measured moments to the calculated moments range up to 180% for Slaughter Creek and up to 125% for the Nolanville Bridge. The lower percentages indicate that more fixity would be expected in the case of the Nolanville Bridge. Note

that the calculated moment histories for the 83.3-ft section at the Slaughter Creek Bridge are negative, and the moment ratios would not be valid for those values.

Table 5.13 Comparison of Propped-Cantilever Line-Girder Moments with the Maximum Measured Moments, k-ft

Test Series	Bridge I.D.	Run #	Total Moment (k-ft)			Calculated Maximum Moment (k-ft)			Percent of Calculated Moment (%)		
			50'	66.7'	83.3'	50'	66.7'	83.3'	50'	66.7'	83.3'**
TS1	Slaughter Creek	1	671	503	276	523	300	-286	128	167	-
		2	603	511	259	546	313	-299	110	163	-
		4	638	532	286	546	313	-299	117	170	-
		5	613	507	300	523	300	-286	117	169	-
		6	599	493	297	546	313	-299	110	158	-
		7	705	545	340	523	300	-286	135	181	-
		8	659	533	314	546	313	-299	121	170	-
		9	1270	1029	591	1061	609	-579	120	169	-
		10	1252	1014	579	1061	609	-579	118	166	-
		11	1241	990	546	1061	609	-579	117	162	-
		12	1259	977	538	1061	609	-579	119	160	-
		13	1241	1019	595	1061	609	-579	117	167	-
		14	1245	1011	585	1061	609	-579	117	166	-
TS2	Slaughter Creek	15	616	479	273	515	296	-280	120	162	-
		16	656	500	276	515	296	-280	127	169	-
		17	571	481	300	515	296	-280	111	162	-
		18	558	481	273	515	296	-280	108	162	-
		19	630	489	300	515	296	-280	122	165	-
		20	616	486	307	515	296	-280	120	164	-
		21	620	509	307	515	296	-280	120	172	-
		22	634	506	300	515	296	-280	123	171	-
			51'	76.5'		51'	76.5'		51'	76.5'	
TS3	Nolanville	23	2462	1733		1990	1802		124	96	
		24	2351	1997		1990	1802		118	111	
		25	2074	1497		1990	1802		104	83	
		26	2083	1499		1990	1802		105	83	
		27	2108	1514		1990	1802		106	84	
		28	665	616		634	625		105	99	
		29	695	622		634	625		110	100	
		30	591	533		634	625		93	85	
		31	593	488		634	625		94	78	
		32	732	588		634	625		116	94	
		33	698	576		634	625		110	92	

*Restrained ends of girders are modeled as fixed ends

**-Invalid Ratios

These analyses provided the maximum expected levels of end restraint. The moment developed at the fixed end of a propped-cantilever beam due to a unit rotation at the pinned end is equal to 3EI/L, with L corresponding to the span length for each girder and the other terms as defined in Eq. 5.4. This is shown in Fig. 5.13.

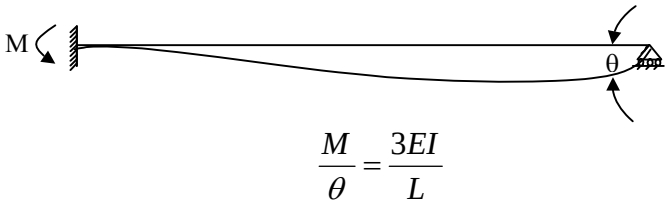

Figure 5.13 Fixed-End Moment due to Rotation at Pinned End, Propped-Cantilever Beam

Based on these findings and because of the need to adjust the analytical model to reflect the trends observed in the measured response of the bridges, the restrained ends in each bridge were modeled as rotational springs. The partial restraint would yield results between the solutions obtained assuming simply-supported beams and the solutions based on propped-cantilever beams. Also, it would be possible to quantify the end restraint analytically by relating end restraint to the maximum value corresponding to the fixed end case.

5.3.5 Moments Developed at the Ends – Rotational Springs

Because of the error in the calculated moments and the additional steps involved in obtaining the end moments of Table 5.12, the measured data

(Eqs. 5.6-5.9) did not justify the use of these values from Table 5.11 directly, but only as an indication of the expected level of restraint. The ends of the beams were modeled as rotational springs with stiffness k_s, as expressed by Eqs. 5.10 and 5.11. The resulting moments at the corresponding ends were assumed to be in the form of Eq. 5.12. This formulation offers a good means of representing the variation in the end moments with the longitudinal truck positions. The resulting plots have a similar shape to those based on the propped-cantilever cases of Fig. 5.11 and 5.12. The objective was to reach solutions that would vary with the spring constants until the best agreement with the measured data could be reached.

Based on the notation explained following Eq. 5.13, the expression for the spring constant at the Slaughter Creek Bridge is

$$k_{sb} = b\frac{EI}{L} \tag{5.10}$$

and the corresponding expression for the Nolanville Bridge is

$$k_{sa} = a\frac{EI}{L} \tag{5.11}$$

The expression for the end moment is of the form

$$M_{end} = k_s \theta_{end} \tag{5.12}$$

The springs were modeled at the restrained ends of simply-supported beams based on the sketches shown in Fig. 5.14 and 5.15 for the Slaughter Creek

and Nolanville Bridge respectively. The angle of rotation at each end was expressed using Eq. 5.13 with the index n in the summation representing the number of point loads on the span. The variation in the angles was modeled as the series of concentrated loads moved along the span. Combining Eqs. 5.10 through 5.12 eliminates the "EI" terms, and the resulting moments developed at the springs were obtained based on the dimensions of the girder.

$$(EI)\theta_{end} = \frac{1}{6L}\sum_{i=1}^{n} P_i a_i (L - a_i)(2L - a_i) \qquad (5.13)$$

where

θ_{end} = Angle of rotation at the restrained end of the girder, rad

L = Span length of girder, ft

P_i = Point load representing the load for one axle, kips

a_i = Distance of point load P_i from restrained end, ft

Superposition was used in order to correct the values of the moments calculated at each instrumented section. Figures 5.14 and 5.15 show each girder model with the springs at the restrained ends. The first moment diagram is the resulting live load moment due to the series of concentrated loads and the following diagram is due to the induced moment in the spring. Adding the two diagrams reduces the value of the moment and corrects it for end restraint.

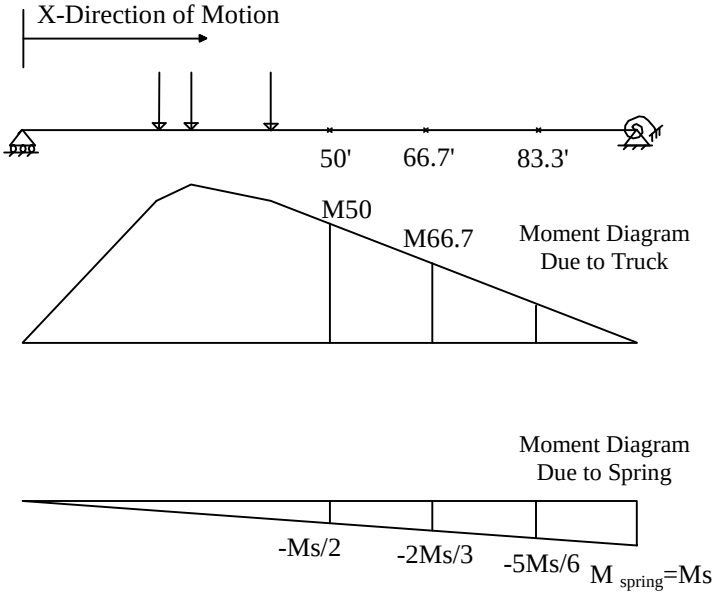

Figure 5.14 Line-Girder Model with Rotational Spring at the Restrained End, Slaughter Creek Bridge

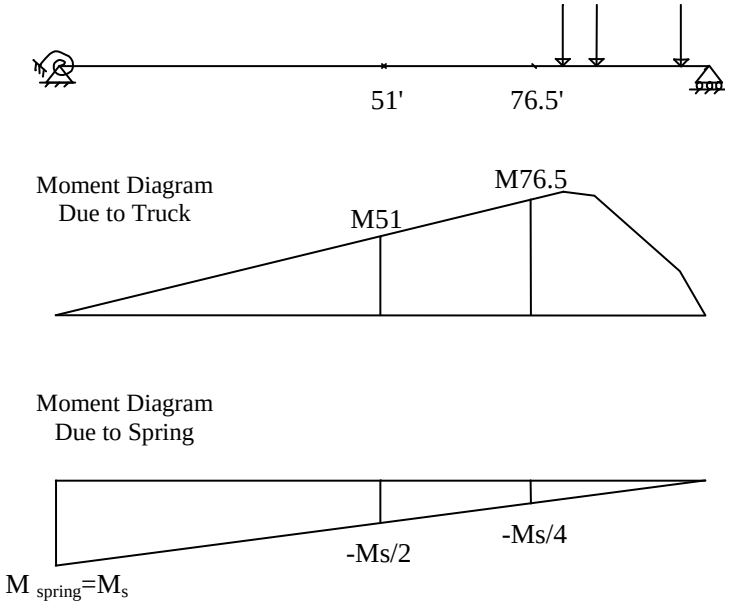

Figure 5.15 Line-Girder Model with Rotational Spring at the Restrained End, Nolanville Bridge

The magnitudes of the diagrams change with the longitudinal positions of the vehicles. From Fig. 5.14, the reduction of the mid-span moment at the Slaughter Creek Bridge is half of what is induced at the restrained end. The sections away from mid-span are reduced by two-thirds and five-sixths of the end moment respectively. In the case of the Nolanville Bridge, the mid-span moment is reduced by one half of the induced live-load moment at the end, but that at the three-quarter span is reduced only by a fourth, as shown in Fig. 5.15. This was very useful in explaining why the measured mid-span strains and moments were closer than expected to those at the three-quarter span section.

The maximum effects occur at different longitudinal positions of the trucks for each section. A continuous calculation was set up in order to model the reduced moments for each case. A set of plots showing typical line-girder moments for the instrumented sections and restrained ends of each bridge are shown in Fig. 5.16 and 5.17. Figure 5.16 corresponds to vehicle D3 moving along the Slaughter Creek Bridge and Fig. 5.17 is a similar figure for vehicle D4 at the Nolanville Bridge. Each chart shows four plots for each section. The maximum curves for the plots of total moment correspond to the histories of maximum moments calculated assuming the ends of the beams to be simply-supported. The minimum values correspond to the propped-cantilever beam models. In Fig. 5.16, the two intermediate plots correspond to the calculated moment history using b=1.8 and to a typical plot of the moment history that was measured during Run 19. Similarly, Fig. 5.17 includes a plot corresponding to

a=2.25 and a typical measured moment history (Run 28) for the Nolanville Bridge. The measured end moments are plotted for the valid ranges.

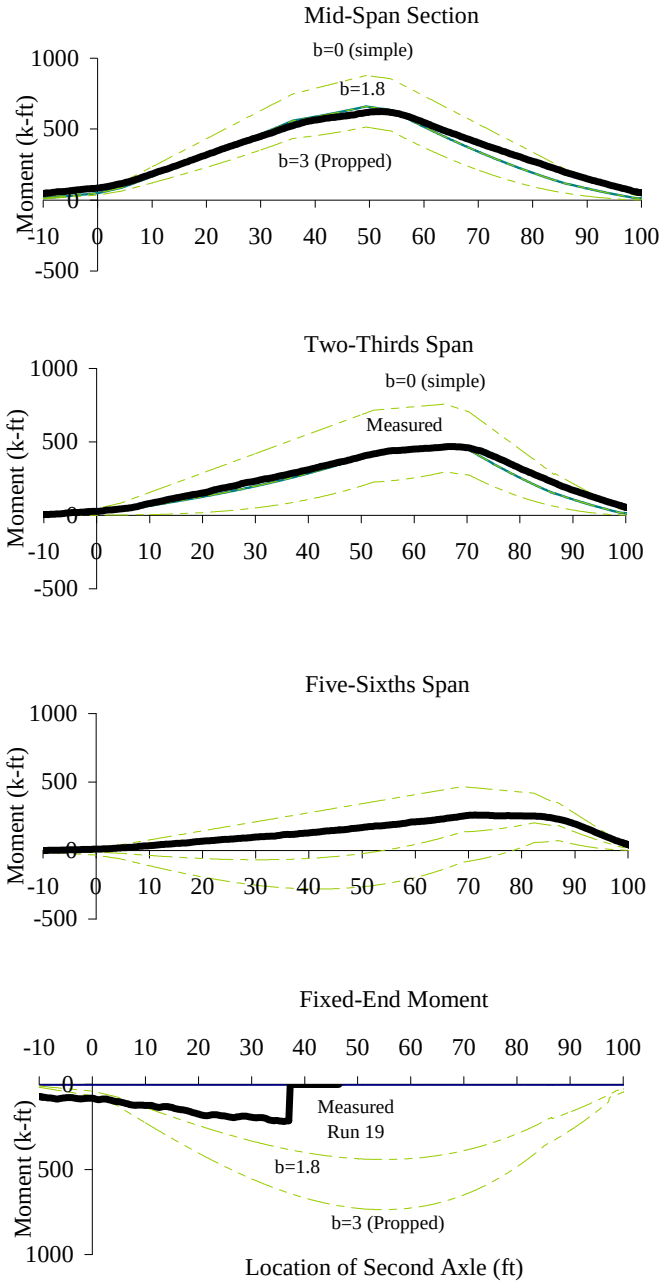

Figure 5.16 Variations of the Line-Girder Moments with Increasing End Restraint, Truck D3, Slaughter Creek Bridge

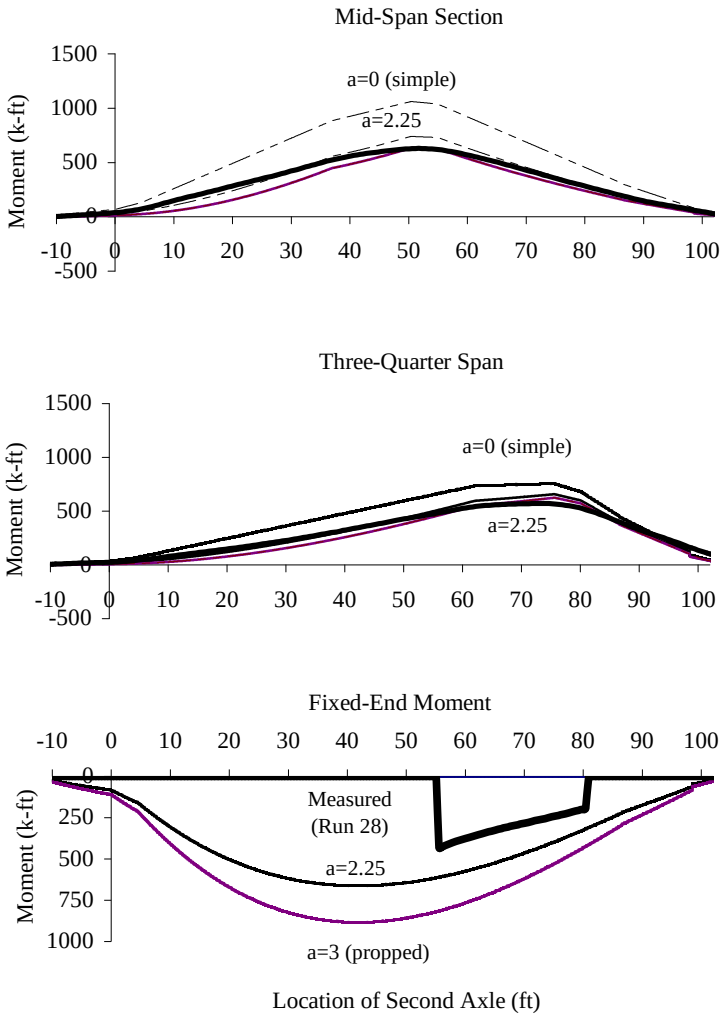

Figure 5.17 Variations of the Line-Girder Moments with Increasing End Restraint, Truck D4, Nolanville Bridge

Table 5.14 presents the maximum calculated values for the moments at the restrained ends of each bridge.

Table 5.14 Maximum Magnitudes of the End Moments Obtained from Line-Girder Analyses with Variable End Restraint

Bridge I.D.	Test Series	Loading Vehicle	Runs (#)	Simply Supported	Calculated Maximum End Moments* (k-ft)						Propped Cantilever
				b=0	b=1.0	b=1.2	b=1.4	b=1.6	b=1.8	b=2.0	b=3
Slaughter	1	D2	1,5,7	0	250	300	350	400	450	500	751
Creek	1	D1	2,4,6,8	0	262	314	367	419	471	524	786
	1	D1&D2	15 to 22	0	245	294	344	393	442	491	736
	2	D3	9 to 14	0	507	609	710	812	913	1015	1522
Nolanville				a=0	a=1	a=1.50	a=1.75	a=2.0	a=2.25	a=2.50	a=3
	3	D4	23-27	0	295	441	515	589	663	737	884
	3	HETS	28-33	0	1169	1754	2046	2338	2631	2923	3507

*Restrained ends of girders are modeled as rotational springs

The percentages of the maximum measured moments to the line girder values for all runs are also shown in Tables 5.15 through 5.17 for various values of the constants. Table 5.15 compares the corresponding mid-span values, Table 5.16 compares the two-thirds or three-quarter span values for each bridge, and Table 5.17 compares the values for the five-sixths span of the Slaughter Creek Bridge. The spring constants that would best approach the measured behavior in each case were obtained from these tables by selecting them so that the measured results would be approximately equal to 95% of the calculated values. This allowed for the uncertainties in the assumptions and methodologies that are involved in the calculations of the analytical and experimental moments, as discussed in Section 5.3.2. The best agreement was achieved with the constant b being approximately equal to 1.8 for the Slaughter Creek Bridge, and the constant a being approximately equal to 2.25 for the Nolanville Bridge. The

relative magnitude of the constants was expected based on the level of end moments as indicated in Table 5.12 from the measured data.

Table 5.15 Comparison of Maximum Measured Moments at Mid-Span Sections to Analytical Line-Girder Moments of Variable End Restraint, %

Test Series	Run #	Measured Moment (k-ft)	Simply Supported	Measured/Calculated (%)						Propped Cantilever
			b=0	b=1.0	b=1.2	b=1.4	b=1.6	b=1.8	b=2.0	b=3
TS1	1	671	72	83	86	89	92	96	99	123
	2	603	67	78	81	84	87	90	93	115
	4	638	71	83	86	89	92	95	99	122
	5	613	66	76	79	81	84	87	91	112
	6	599	67	78	80	83	86	89	93	115
	7	705	75	88	91	94	97	101	104	129
	8	659	74	86	88	91	95	98	102	126
	9	1270	70	81	84	87	90	93	97	120
	10	1252	69	80	83	86	89	92	95	118
	11	1241	68	79	82	85	88	91	95	117
	12	1259	69	81	83	86	89	92	96	119
	13	1241	68	79	82	85	88	91	95	117
	14	1245	69	80	82	85	88	91	95	117
TS2	15	616	70	81	84	87	90	93	97	120
	16	656	75	87	90	93	96	99	103	127
	17	571	65	75	78	81	83	86	90	111
	18	558	64	74	76	79	82	85	88	108
	19	630	72	83	86	89	92	95	99	122
	20	616	70	81	84	87	90	93	97	120
	21	620	71	82	85	87	91	94	97	120
	22	634	72	84	87	89	93	96	100	123
Average Percentage			70	81	84	86	90	93	96	119
			a=0	a=1	a=1.5	a=1.75	a=2.0	a=2.25	a=2.50	a=3
TS3	23	2462	68	80	88	92	97	103	109	124
	24	2351	65	76	84	88	93	98	104	118
	25	2074	57	67	74	78	82	86	92	104
	26	2083	57	68	74	78	82	87	92	105
	27	2108	58	68	75	79	83	88	93	106
	28	665	63	72	78	82	86	90	94	105
	29	695	65	76	82	86	90	94	99	110
	30	591	56	64	70	73	76	80	84	93
	31	593	56	65	70	73	76	80	84	94
	32	732	69	80	86	90	94	99	104	116
	33	698	66	76	82	86	90	94	99	110
Average Percentage			62	72	78	82	86	91	96	108

Table 5.16 Comparison of Maximum Measured Moments at 66.7 and 76.5-ft Sections to Analytical Line-Girder Moments of Variable End Restraint, %

Test Series	Run #	Measured Moment (k-ft)	Simply Supported	Measured/Calculated (%)						Propped Cantilever
			b=0	b=1.0	b=1.2	b=1.4	b=1.6	b=1.8	b=2.0	b=3
TS1	1	503	63	79	83	88	93	99	106	161
	2	511	66	83	88	93	98	105	112	170
	4	532	69	87	91	97	102	109	116	177
	5	507	63	79	84	88	94	100	106	162
	6	493	64	80	85	89	95	101	108	164
	7	545	68	85	90	95	101	107	114	174
	8	533	69	87	92	97	103	109	117	177
	9	1029	66	83	87	92	98	104	111	169
	10	1014	65	82	86	91	96	102	109	166
	11	990	63	80	84	89	94	100	107	162
	12	977	63	79	83	88	93	99	106	160
	13	1019	65	82	86	91	97	103	110	167
	14	1011	65	81	86	91	96	102	109	166
TS2	15	479	63	79	84	88	94	100	106	162
	16	500	66	83	87	92	98	104	111	169
	17	481	64	80	84	89	94	100	107	162
	18	481	64	80	84	89	94	100	107	162
	19	489	65	81	85	90	96	102	109	165
	20	486	64	81	85	90	95	101	108	164
	21	509	67	84	89	94	100	106	113	172
	22	506	67	84	88	93	99	105	112	171
Average Percentage			65	82	86	91	97	103	110	167
			a=0	a=1	a=1.5	a=1.75	a=2.0	a=2.25	a=2.50	a=3
TS3	23	1733	67	75	80	83	85	88	91	96
	24	1997	77	87	92	95	98	102	105	111
	25	1497	58	65	69	71	74	76	79	83
	26	1499	58	65	69	71	74	76	79	83
	27	1514	59	66	70	72	75	77	80	84
	28	616	82	87	89	91	92	94	95	99
	29	622	82	87	90	92	93	95	96	100
	30	533	71	75	77	78	80	81	82	85
	31	488	65	69	71	72	73	74	75	78
	32	588	78	83	85	87	88	89	91	94
	33	576	76	81	83	85	86	88	89	92
Average Percentage			70	76	80	81	83	85	88	91

Table 5.17 Comparison of Maximum Measured Moments at 83.3-ft Section to Analytical Line-Girder Moments of Variable End Restraint, %

Test Series	Run #	Measured Moment (k-ft)	Simply Supported	Measured/Calculated (%)						Propped Cantilever
			b=0	b=1.0	b=1.2	b=1.4	b=1.6	b=1.8	b=2.0	b=3
TS1	1	276	55	88	96	105	116	130	147	-
	2	259	53	85	93	102	113	126	143	-
	4	286	59	94	103	113	125	139	158	-
	5	300	60	96	104	114	126	141	160	-
	6	297	61	98	107	117	129	145	165	-
	7	340	68	108	118	129	143	160	182	-
	8	314	65	104	113	124	137	153	174	-
	9	591	61	97	105	115	127	142	162	-
	10	579	60	95	103	113	125	139	158	-
	11	546	56	89	97	106	118	132	149	-
	12	538	56	88	96	105	116	130	147	-
	13	595	62	97	106	116	128	143	163	-
	14	585	60	96	104	114	126	141	160	-
TS2	15	273	58	91	99	109	120	135	153	-
	16	276	59	92	100	110	122	136	155	-
	17	300	64	100	109	120	132	148	168	-
	18	273	58	91	99	109	120	135	153	-
	19	300	64	100	109	120	132	148	168	-
	20	307	66	103	112	122	135	152	172	-
	21	307	66	103	112	122	135	152	172	-
	22	300	64	100	109	120	132	148	168	-
Average Percentage			61	96	104	114	127	142	161	

Overall, the sums and the relative magnitudes of the calculated moments at the instrumented sections were closer to the measured moments than what was found initially by assuming the ends of the line-girder to be simply-supported. In the case of the Nolanville Bridge, the results also showed that the three-quarter span moment was decreased at a much slower rate than the moment at the mid-span section. This provided an explanation to how the two sets of measurements were in some runs closer than what had been expected.

Another observation was that the level of the maximum measured moments during the runs of the vehicles along the exterior paths was higher than

the resulting maximum moments corresponding to the vehicles moving along the interior paths. A possible explanation of this could be that the end moments developed at the springs of the girders are proportional to how much each end rotates. Quantitatively, the expected level of the rotational restraint is lower in the cases of the outside runs where most of the load is carried by one or two girders and the participation of the whole bridge system is less efficient than in the cases of the inside runs. This is more pronounced in the response of the Nolanville Bridge where the exterior runs induce larger strains in the more flexible exterior girders, and the presence of diaphragms allows a more efficient distribution of the loads throughout the structure.

In conclusion, line-girder models with rotational springs at the restrained ends were used to calculate the moment histories for the various sections analytically. Increasing the spring constants increased the end moments in each case and reduced the total moments calculated at each section assuming the ends to be simply-supported. This information from the results of the diagnostic load tests are used in Chapter 6 to calculate a more realistic maximum live-load moment induced on the bridges by the code-based rating vehicle.

5.4 CALCULATING THE DISTRIBUTION FACTORS FOR MOMENTS

The purpose of this section is to present the measured distribution factors for the live-load moments in the girders as fractions of the total moment induced in the bridge during each run. These factors are compared with the distribution factors calculated for each structure based on current codes that are used for the load rating of bridge structures.

5.4.1 Distribution Factors Calculated from the Experimental Moments

The distribution factors for the live-load moments that were induced in the individual girders during each of the runs of the three diagnostic load tests can be calculated using Eq. 5.14.

$$DF_i = \frac{M_i}{M_{total}} \tag{5.14}$$

where

DF_i = Moment Distribution factor for girder i,

M_i = Live-load moment induced in girder i

M_{total} = Total live-load moment induced in the bridge

Tables 5.18 and 5.19 show the calculated moment distribution factors for the two bridges based on the maximum measured moments for each girder shown in Table 5.7 and Table 5.8 for the Slaughter Creek and Nolanville Bridges respectively. The total live-load moments that were induced in the bridge during each of the 33 runs have been presented in Table 5.9.

Table 5.18 Calculated Distribution Factors based on the Measured Moments, Slaughter Creek Bridge

Run	BEAM 1			BEAM 2			BEAM 3			BEAM 4			BEAM 5		
#	50'	66.7'	83.3'	50'	66.7'	83.3'	50'	66.7'	83.3'	50'	66.7'	83.3'	50'	66.7'	83.3'
1	0.01	0.00	0.00	0.04	0.03	0.01	0.12	0.12	0.07	0.26	0.29	0.33	0.58	0.56	0.58
2	0.00	0.00	0.01	0.03	0.04	0.03	0.12	0.14	0.09	0.28	0.30	0.32	0.56	0.52	0.55
4	0.06	0.04	0.06	0.18	0.18	0.19	0.31	0.33	0.35	0.29	0.30	0.33	0.17	0.15	0.07
5	0.17	0.13	0.12	0.26	0.26	0.23	0.33	0.37	0.39	0.17	0.16	0.22	0.07	0.08	0.04
6	0.18	0.13	0.12	0.26	0.29	0.29	0.33	0.35	0.36	0.15	0.15	0.22	0.09	0.07	0.01
7	0.53	0.47	0.43	0.29	0.35	0.33	0.12	0.15	0.17	0.05	0.03	0.07	0.01	0.00	0.01
8	0.56	0.46	0.44	0.28	0.36	0.36	0.12	0.11	0.13	0.03	0.07	0.06	0.02	0.00	-0.02
9	0.26	0.23	0.20	0.17	0.21	0.23	0.12	0.13	0.13	0.15	0.16	0.18	0.29	0.26	0.27
10	0.26	0.23	0.23	0.17	0.21	0.22	0.13	0.14	0.13	0.16	0.17	0.18	0.28	0.25	0.25
11	0.04	0.03	0.03	0.10	0.09	0.09	0.22	0.24	0.22	0.26	0.29	0.33	0.39	0.35	0.34
12	0.04	0.03	0.03	0.10	0.11	0.09	0.22	0.24	0.22	0.26	0.29	0.33	0.38	0.33	0.32
13	0.37	0.30	0.30	0.26	0.31	0.30	0.22	0.25	0.26	0.10	0.11	0.12	0.05	0.04	0.02
14	0.35	0.27	0.27	0.26	0.30	0.30	0.23	0.26	0.27	0.11	0.12	0.14	0.05	0.05	0.02
15	0.00	0.01	0.00	0.03	0.04	0.03	0.11	0.13	0.07	0.26	0.27	0.32	0.59	0.55	0.57
16	0.02	0.02	0.02	0.05	0.04	0.04	0.10	0.12	0.07	0.25	0.28	0.31	0.58	0.55	0.56
17	0.08	0.07	0.06	0.16	0.17	0.14	0.34	0.37	0.35	0.25	0.24	0.29	0.18	0.15	0.15
18	0.07	0.06	0.08	0.15	0.17	0.15	0.34	0.37	0.34	0.26	0.25	0.32	0.18	0.16	0.10
19	0.17	0.13	0.12	0.24	0.27	0.24	0.32	0.36	0.37	0.17	0.16	0.18	0.11	0.08	0.09
20	0.18	0.12	0.12	0.23	0.26	0.23	0.32	0.37	0.37	0.17	0.16	0.20	0.10	0.08	0.08
21	0.54	0.47	0.44	0.29	0.35	0.33	0.12	0.14	0.16	0.04	0.04	0.05	0.00	0.01	-0.02
22	0.53	0.46	0.44	0.29	0.35	0.35	0.12	0.14	0.16	0.05	0.05	0.05	0.01	0.01	0.00

Table 5.19 Calculated Distribution Factors based on the Measured Moments, Nolanville Bridge

Run	BEAM 1		BEAM 2		BEAM 3		BEAM 4		BEAM 5	
	51'	76.5'	51'	76.5'	51'	76.5'	51'	76.5'	51'	76.5'
23	0.41	0.40	0.33	0.33	0.15	0.13	0.07	0.09	-0.04	-0.05
24	-0.04	-0.03	0.08	0.08	0.24	0.19	0.27	0.29	0.37	0.41
25	0.13	0.10	0.22	0.21	0.36	0.33	0.18	0.21	0.11	0.14
26	0.14	0.11	0.23	0.22	0.36	0.34	0.17	0.20	0.10	0.13
27	0.14	0.10	0.21	0.22	0.36	0.33	0.18	0.21	0.11	0.14
28	-0.02	-0.02	0.06	0.08	0.24	0.18	0.32	0.35	0.37	0.38
29	-0.02	-0.02	0.09	0.08	0.24	0.18	0.31	0.35	0.34	0.37
30	0.13	0.09	0.21	0.25	0.40	0.41	0.17	0.14	0.09	0.11
31	0.14	0.10	0.20	0.22	0.40	0.42	0.17	0.15	0.09	0.12
32	0.40	0.41	0.34	0.36	0.14	0.12	0.07	0.07	-0.05	-0.04
33	0.40	0.43	0.34	0.36	0.15	0.11	0.07	0.06	-0.04	-0.04

The maximum values of the distribution factors were approximately 60% for the Slaughter Creek Bridge and 41% for the Nolanville Bridge. In both cases,

the maximum distribution factors occurred in the exterior girders for truck paths adjacent to the parapet.

The values corresponding to the three ten-cubic yard dump trucks (D1-D3) at the Slaughter Creek Bridge are nearly identical for each of the four transverse paths. During Runs 9 through 14, trucks D1 and D2 moved along the bridge simultaneously as shown in Fig. 3.16. The maximum distribution factor measured during those runs was 39% for Run 11 when one of the loading vehicles was adjacent to the parapet (P4) and the other vehicle was in the first interior path next to it (P3). Similar observations can be made for Run 13, where the maximum distribution factor was 37% and the two vehicles moved along paths P1 and P2. Note that these are percentages of a higher moment than the moments induced by the corresponding single runs. Referring to runs 1 and 4, the maximum distribution factors for beam 5 were 58% and 17% respectively. The average of the sum of these two is 37.5%, which is very close to the 39% obtained for Run 11.

Finally, the distribution factors that are calculated based on the measured live-load moments obtained during the third test series at the Nolanville Bridge are very similar for the ten-cubic yard truck D4 and the HETS. The maximum distribution factor calculated during the third test series was 41%, and it occurred when the loading vehicle was adjacent to the edge of the bridge, similar to the findings from the first two diagnostic tests at the Slaughter Creek Bridge.

Table 5.20 shows the maximum distribution factors that were recorded during the runs for each of the five loading vehicles used in the three Test Series.

Information about the path of the vehicle and the beam for which the maximum distribution factor was recorded is also included.

Table 5.20 Maximum Distribution Factors Calculated Based on the Mid-Span Moments Recorded during the Three Diagnostic Load Tests

Test Series	Loading Vehicle	Run #	Beam #	Transverse Path	Maximum Distribution Factors
1	D1	2,8	5,1	P4, P1	0.56
1	D2	1	5	P4	0.58
2	D3	15	5	P4	0.59
3	D4	32 and 33	1	P1	0.40
3	HETS	23	1	P1	0.41

5.4.2 Distribution Factors Calculated Based on Applicable Codes

Although the load-rating for the longitudinal members of the two bridges is discussed in Chapter 6 and Appendix C, this section presents the applicable code-based moment distribution factors for each bridge. These factors are calculated based on the "1996 AASHTO Standard Specifications for Highway Bridges" [2] and the "1998 AASHTO LRFD Bridge Design Specifications" [1]. Throughout this thesis, the first code is called "1996 Specifications" and the second code is called "1998 LRFD."

The moment distribution factors are calculated based on two different expressions presented in the two codes. The equations that follow are taken from the two codes directly, and the results of the calculations are summarized in Table 5.21. Note that there is an important difference in the definitions of the distribution factors in the two codes. The 1996 Specifications define these

factors as the fraction of the total moment induced by one line of wheels (both front and rear). The 1998 LRFD defines the distribution factors as fractions of the total moment induced by the entire set of axle loads.

The first expression is taken from Table 3.23.1 of Section 3.23.2.2 of the 1996 Specifications. The live load bending moment for a prestressed concrete girder is equal to the fraction of the total live moment due to one line of wheels given by Eqs. 5.15a and 5.15b.

$$Fraction = \frac{S}{7.0} \qquad (5.15a)$$

if the bridge is designed for one traffic lane, and

$$Fraction = \frac{S}{5.5} \qquad (5.15b)$$

if the bridge is designed for two or more traffic lanes,

where

S = Centerline spacing of the girders, ft

The second way by which the moment distribution factors have been calculated is given in Table 4.6.2.2.2b-1 of the 1998 LRFD. Equations 5.16a and 5.16b present the expressions for the distribution factors for precast concrete beams with one design lane loaded and two design lanes loaded, respectively.

$$g_m = 0.06 + (\frac{S}{14})^{0.4}(\frac{S}{L})^{0.3}(\frac{K_g}{12Lt_s^3})^{0.1} \quad (5.16a)$$

$$g_m = 0.075 + (\frac{S}{9.5})^{0.6}(\frac{S}{L})^{0.2}(\frac{K_g}{12Lt_s^3})^{0.1} \quad (5.16b)$$

in which

$$K_g = n(I + Ae_g^2) \quad (5.16c)$$

and

$$n = \frac{E_B}{E_D} \quad (5.16d)$$

where

g_m = Distribution factor for the moment

L = Span of beam, ft

t_s = Depth of the concrete slab, in

K_g = Longitudinal stiffness parameter, in^4

I = Moment of inertia of the noncomposite beam, in^4

A = Area of the noncomposite beam, in^2

e_g = Distance between centers of gravity of beam and deck, in

E_B = Modulus of elasticity for the beam material, ksi

E_D = Modulus of elasticity for the deck material, ksi

Table 5.21 summarizes the values for the distribution factors obtained for the interior members using the two methods. Note that the results represent fractions of the total moment induced by all the axles and not just a single line of

wheels. The first column represents the results of the first method, where the distribution factors are only a function of the spacing of the precast sections and the type of construction used in the structures. The calculations in the second method involve more section and member parameters that would influence the load distribution in the bridges. The last column shows the results that were calculated from the moments that were induced during the diagnostic load tests on the two bridges.

Table 5.21 Distribution Factors Calculated from Code-Based Expressions Used in the Load Rating of Bridges

Bridge I.D.	Girder Spacing (ft)	Number of Traffic Lanes	1996 AASHTO Specifications [3.23.2.2]	1998 AASHTO LRFD [4.6.2.2.2b]	Maximum* Measured From Diagnostic Tests
Slaughter Creek	8	One	0.57	0.47	0.59
		Two	0.73	0.68	0.78**
Nolanville Bridge	9.5	One	0.68	0.52	0.41
		Two	0.86	0.74	-

* Maximum occurred at the exterior girders

** Twice as high as the 0.39 obtained for the combination truck runs (refer to Table 5.18)

The maximum experimental distribution factors are a function of the transverse location of the loading vehicle in each case. In the case of the Slaughter Creek Bridge, paths P1 and P4 were approximately 2 ft from the edge of the parapet with one wheel line moving over beams 1 and 5 respectively. This resulted in high values for the distribution factors (60%) in the exterior girders. However, when a line of wheels was placed over beam 3 for paths P2 and P3, the maximum measured distribution factor for the interior girder was below 40%.

In the case of the Nolanville Bridge, the maximum distribution factors were lower than the values obtained at the Slaughter Creek Bridge and the values calculated based on the code equations (Eqs. 5.15-5.17). The measured distribution factors were approximately 40-43% for all three transverse truck paths. This was expected because the loading was the same for the three truck paths, with the wheel lines centered over the girders. This was a less severe loading configuration than that caused by placing a line of wheels directly over the girders. The presence of diaphragms in the structure was also responsible for distributing the load more efficiently and lowering the maximum values of the experimental distribution factors. A discussion of the distribution factors used in the load-rating calculations is presented in Chapter 6.

5.5 SUMMARY

This chapter provided an evaluation of the responses of two prestressed concrete bridges during diagnostic load testing. The neutral axis depths were calculated from the measured strains, and they were found to range between 20 and 23" from the top of the slab. The measured values corresponded to those calculated assuming fully composite action and uncracked sections.

The maximum moments were found to be between 15 and 35% lower than what was calculated from line-girder analyses of simply-supported beams. Possible error sources relating to the experimental and analytical procedures and assumptions were first discussed. Based on on-site details, the measured data were then investigated and an appreciable level of end moments was indicated. The theoretical models were changed to that of propped cantilever beams in an

attempt to bound the problem. Finally, the restrained ends were modeled as rotational springs with stiffness proportional to EI/L of the beams. The constants of proportionality that improved the results to approximately 95% of the theory were approximately 1.8 for the Slaughter Creek Bridge and 2.25 for the Nolanville Bridge.

The distribution factors calculated from the measured data were presented. The maximum values were 60% and 40% for the Slaughter Creek and Nolanville Bridges respectively. These occurred at exterior girders when the loading vehicles were traveling along the paths adjacent to the edges of each bridge. The stiffer exterior members attracted relatively more moment than the corresponding interior girders for similar loading with one line of wheels traveling over the girders. This higher stiffness resulted in lower stresses.

The distribution factors that are based on the "1996 AASHTO Standard Specifications for Highway Bridges" [2] and the "1998 AASHTO LRFD Bridge Design Specifications" [1] were presented. These values are used for the load rating of bridges. In the case of the Slaughter Creek Bridge, the calculated factors were lower than the maximum factors resulting from the truck paths where one line of wheels moved over the exterior girders, and higher than the values resulting from the truck paths along the central part of the bridge. In the case of the Nolanville Bridge, the wheel lines were centered over the girders and this resulted in a less severe loading configuration. The experimental distribution factors were lower than the factors calculated from the code equations and much lower than the distribution factors corresponding to the Slaughter Creek Bridge.

Chapter 6. LOAD RATING PROCEDURES FOR THE TWO PRESTRESSED CONCRETE BRDIGES

This chapter presents the results of the load rating of the Slaughter Creek and Nolanville prestressed concrete bridges. A discussion of the AASHTO load-rating procedures is given first. All terms and expressions used in this chapter are given in Appendices C and D. These two appendices also describe the steps involved in calculating the parameters used in the rating equation for the interior and exterior girders of each bridge. The values obtained for the two bridges are summarized in this chapter and the results from the load rating are presented. Finally, the chapter ends with a discussion of two ways by which the initial rating can be revised to reflect the information obtained from the diagnostic load tests conducted on the bridges.

6.1 NOTATION

Throughout this chapter, many references are made to codes and other documents. In order to avoid repeating lengthy names every time, Table 6.1 presents a summary of the notation that will be used throughout Chapter 6 and Appendices C and D when referring to each document. The reference number is used in all the tables where equations or terms are defined to indicate their source.

Table 6.1 Notation for the References Used in Chapter 6 and Appendices C and D

Full Name of the Reference	Reference Number	Notation
1996 AASHTO Standard Specifications for Highway Bridges	[2]	Standard Specifications
AASHTO 1994 Manual for Condition Evaluation of Bridges (1995-1996 Interim Revisions)	[3]	1994 Manual
1999 Pre-Final Draft Manual for Condition Evaluation and Load and Resistance Factor Rating of Highway Bridges	[7]	1999 Manual
1993 Manual for Bridge Rating through Load Testing (Final Draft)	[8]	1993 Manual

6.2 THE RATING EQUATION

There are two load levels at which the rating is performed: inventory and operating levels. The inventory rating level relates to the customary design level of service-load performance of the structure, and the operating rating describes the maximum permissible live load that may cross the structure [3]. The results are presented for both levels of load rating.

The general form of the rating equation is expressed by Eq. 6.1. For this thesis, the term "effect" refers to the bending moment in the members. Consequently, the terms in the numerator and denominator have units of moment.

$$RF = \frac{C - A_1 D}{A_2 L(1+I)} \tag{6.1}$$

where

RF = Rating factor for the live-load carrying capacity

C = Capacity of the member

D = Dead-load effect on the member

L = Live-load effect on the member from the rating vehicle
$= (DF_{max}) * (M_T)$

M_T = Maximum total moment induced in the bridge by the rating vehicle

DF_{max} = Maximum fraction of total moment expected in a single member

I = Impact factor used with the live-load effect

A_1 = Dead load factor

A_2 = Live load factor

The AASHTO rating vehicle is the HS-20 vehicle that is described in Appendix D. The rating of the bridge member is expressed in tons. This is obtained by multiplying the calculated rating factor by the weight of the nominal truck used in determining the live load moment. This is expressed by Eq. 6.2.

$$RT = (RF)W \tag{6.2}$$

where

RT = Rating of the bridge member, tons

W = Weight of nominal rating vehicle = 20 tons for the HS-20

The main concept expressed by Eq. 6.1 is that the rating factor for a member is equal to the ratio of the available moment capacity of the member to the moment induced in the member by the live loads. It expresses the safe level

of loading. For this reason, the numerator includes a reduction in capacity due to the dead loads acting on the member. A value greater than one for the resulting rating factor indicates that the calculated available moment capacity of the member is expected to be greater than the moment induced by the loading vehicle. The rating of the bridge is therefore equal to the smallest rating factor of all members.

The dead-load factors are used to account for variations in the material properties and dimensions. The live-load factors account for uncertainties in the expected loads and load combinations and for their effects on the structure and the individual member. These load factors also recognize that overweight vehicles regularly cross highway bridges.

In addition to the strength requirements expressed by Eq. 6.1, load ratings are also based on stresses in the concrete and prestressing steel. Four additional expressions for the inventory level rating and one additional expression for the operating rating level are used to perform these checks based on the Load Factor method. These expressions are presented in the 1996 interim revisions of the 1994 Manual for Condition Evaluation of Bridges [3] and they are based on stress computations. The expressions are given below including the type of allowable stress check that they represent.

Allowable tensile stress in the concrete – bottom fiber:

$$RF^{inv} = \frac{(6\sqrt{f'_c} - f_{db} + f_{pb})}{f_{lb}} \text{ (Concrete tension)} \qquad (6.3)$$

Allowable compressive stress in the concrete - top fiber:

$$RF^{inv} = \frac{(0.6 f'_c - f_{dt} - f_{pt})}{f_{lt}} \text{ (Concrete compression)} \qquad (6.4)$$

$$RF^{inv} = \frac{(0.4 f'_c - 0.5(f_{dt} + f_{pt})}{f_{lt}} \text{ (Concrete compression)} \qquad (6.5)$$

Allowable tensile stress in prestressing steel:

$$RF^{inv} = \frac{(0.8 f_y - f^*_d - f^*_p)}{f^*_l} \text{ (Prestressing steel tension)} \qquad (6.6)$$

$$RF^{oper} = \frac{(0.9 f_y - f^*_d - f^*_p)}{f^*_l} \text{ (Prestressing steel tension)} \qquad (6.7)$$

where

RF^{inv} = Rating factor at inventory level

RF^{oper} = Rating factor at operating level

f'_c = Compressive strength of the concrete, psi

$6\sqrt{f'_c}$ = Allowable tensile stress for the concrete, psi

f_{db} = Unfactored dead-load tensile stress in the concrete along the bottom fiber, psi

f_{pb} = Unfactored compressive stress in the concrete along the bottom fiber due to prestress force after all losses, psi

f_{lb} = Unfactored live-load tensile stress in the concrete along the bottom fiber including impact, psi

f_{dt} = Unfactored live-load compressive stress in concrete along top fiber of girder, psi

f_{pt} = Unfactored compressive stress in the concrete along top fiber of girder due to prestress force after all losses, psi

=Average compression – tensile bending stress due to eccentricity

f_{lt} = Unfactored live-load compressive stress in concrete along top fiber of girder including impact, psi

f_y = Prestressing steel yield stress, psi

f^*_d = Unfactored average dead-load tensile stress in the strands, psi

f^*_p = Unfactored tensile stress in the strands due to prestress force after all losses, psi

f^*_l = Unfactored average live-load tensile stress in the strands including impact, psi

6.3 OVERVIEW OF THE LOAD RATING CALCULATIONS

Many terms must be calculated before applying Eq. 6.1 to determine the rating factor for each girder. For the purpose of this thesis, a general spreadsheet was developed in order to automate the load rating calculations for the interior and exterior girders of the two prestressed concrete bridges. The detailed steps of the spreadsheet are presented in the form of tables in Appendices C and D. Appendix C presents the input information about the characteristics of the bridge and the section and material properties. It also discusses the dead load and capacity calculations for the section, including the ductility checks. Appendix D presents the calculations of the live-load moments and distribution factors. The applicable load factors A_1 and A_2 for the inventory and operating level ratings are also included in the appendix, along with the results obtained for the rating factors.

6.4 RESULTS OF THE INITIAL RATING CALCULATIONS

Table 6.2 summarizes the values of the terms used in the load-factor rating expressions for each of the four girders at the mid-span section. The parameters that were used in the calculations are defined in Tables C.1 through C.5, D.1 and D.2.

Table 6.2 Summary of Main Values Used in the Load Rating of Each Girder

Symbol	Units	Slaughter Creek Bridge		Nolanville Bridge	
		Interior Girder	Exterior Girder	Interior Girder	Exterior Girder
$C=M_n$	k-ft	6810	8440	8970	8640
A_1	-	1.30	1.30	1.30	1.30
D	k-ft	1990	1960	2400	2180
A_2-inv	-	2.17	2.17	2.17	2.17
A_2-oper	-	1.30	1.30	1.30	1.30
DF_{max}	-	0.727	0.727	0.864	0.864
M_T	k-ft	1500	1500	1530	1530
I	-	0.223	0.223	0.221	0.221
$M_T(1+I)$	k-ft	1830	1830	1880	1880
$0.001(6)f'_c$	ksi	0.484	0.575	0.526	0.526
$0.6f'_c$	ksi	3.90	5.52	4.62	4.62
f_{db}	ksi	2.24	2.15	2.71	2.44
f_{pb}	ksi	2.79	3.04	3.15	3.12
f_{lb}	ksi	0.946	0.806	1.09	1.09
f_v	ksi	243	243	243	243
f_d*	ksi	11.5	4.7	12.1	10.9
f_p*	ksi	157	152	137	135
f_l*	ksi	5.18	2.72	5.31	5.24
f_{dt}	ksi	2.61	2.47	3.18	2.85
f_{pt}^{**}	ksi	-0.915	0.134	-0.943	-0.934
f_{lt}	ksi	0.545	0.382	0.612	0.746

** The negative sign in stress f_{pt} implies tension

The calculated rating factors based on the Load Factor method are presented in Table 6.3, and the rating of the members in tons, based on an HS-20 vehicle, is given in Table 6.4. The only rating factor less than 1.0 is that calculated for the interior girder at the Nolanville Bridge based on allowable tensile stresses for the concrete at the bottom fiber and it is equal to 0.90. For inventory level rating, the calculated rating factors based on the strength of the girders, range from 1.46 for the interior girder to 2.04 for the exterior girder of the Slaughter Creek Bridge. For operating level, the rating factors increase to 2.44 and 3.40 for the two girders respectively. Note that the checks for the stress

in the prestress strands are easily satisfied, indicating the low level of stress in the strands at the HS-20 loading relative to the stress at the flexural capacity of the member.

Table 6.3 Rating Factors Calculated Using the Load Factor Method

Symbol	Slaughter Creek Bridge		Nolanville Bridge		References - Equations - Comments
	Interior Girder	Exterior Girder	Interior Girder	Exterior Girder	
RF^{inv}	1.46	2.04	1.67	1.65	Eq. 6.1 - Inventory Level Rating (Strength)
RF^{oper}	2.44	3.40	2.78	2.76	Eq. 6.1 - Operating Level Rating (Strength)
$RF^{inv,ct}$	1.10	1.79	0.90	1.06	Eq. 6.3 - Concrete Tensile Stress
$RF^{inv,cc}$	4.03	7.51	3.92	3.46	Eq. 6.5 - Concrete Compressive Stress
$RF^{inv,cc}$	3.21	6.13	3.22	2.72	Eq. 6.4 - Concrete Compressive Stress
$RF^{inv,ps}$	5.06	13.6	8.63	8.78	Eq. 6.6 - Strands Tensile Stress
$RF^{oper,ps}$	9.75	22.4	13.2	13.2	Eq. 6.7 - Strands Tensile Stress

Table 6.4 HS-20 Rating for the Members Based on the Load Factor Method

Symbol	Slaughter Creek Bridge		Nolanville Bridge		References-Comments-Equations
	Interior Girder	Exterior Girder	Interior Girder	Exterior Girder	
RF^{inv}	29.2	40.8	33.3	33.1	Eq. 6.1 - Inventory Level Rating (Strength)
RF^{oper}	48.7	68.0	55.7	55.2	Eq. 6.1 - Operating Level Rating (Strength)
$RF^{inv,ct}$	21.9	35.9	17.9	21.2	Eq. 6.3 - Concrete Tensile Stress
$RF^{inv,cc}$	80.7	150	78.3	69.2	Eq. 6.5 - Concrete Compressive Stress
$RF^{inv,cc}$	64.2	123	64.5	54.4	Eq. 6.4 - Concrete Compressive Stress
$RF^{inv,ps}$	101	272	173	176	Eq. 6.6 - Strands Tensile Stress
$RF^{oper,ps}$	195	448	265	264	Eq. 6.7 - Strands Tensile Stress
DF_{max} used	0.73	0.73	0.86	0.86	

6.5 RATING USING INFORMATION FROM THE DIAGNOSTIC LOAD TESTS

The ratings were revised using the results from the diagnostic load tests. First, the rating was revised by calculating the live-load moments due to the HS-20 vehicle using an analytical model of the beams with rotational restraint at one end to represent observed conditions in the field (Chapter 5). Then, the strains measured during the tests were incorporated directly into the load rating procedure using the method outlined in Section 8.8.2.3 of the 1999 Manual [7].

6.5.1 Revised Rating by Adjusting the Live-Load Moments

During these calculations, the dead-load, live-load and dynamic amplification factors were not changed. All changes were in the live-load moments used in the rating equation (Eq. 6.1). The loading vehicles were run on line-girder models of the bridges with springs at the restrained ends. Appropriate values of the rotational restraints were estimated by comparing the maximum moment calculated from the measured strains with the maximum moment from the line-girder analysis. Details of this procedure are described in Chapter 5. A line-girder analysis was then conducted using the restrained models of the bridges and the HS-20 rating vehicle. The resulting maximum moments and those obtained from models with simply-supported ends are presented in Table 6.5. The rotational restraint observed during the load tests reduced the maximum live-load moment due to the HS-20 vehicle between 25 and 35 percent.

Table 6.5 Summary of Maximum Line-Girder Moments for the HS-20 Rating Vehicle, k-ft

Rating Vehicle	Slaughter Creek Bridge		Nolanville Bridge	
	Simply-supported ends	Rotational Restraint at one end	Simply-supported ends	Rotational Restraint at one end
HS20	1500	1130	1530	1010

The values of the distribution factors were also examined in these calculations to represent the worst cases from the load tests. For the Slaughter Creek Bridge, distribution factors of 0.78 and 0.58 were used for the exterior and interior girders, respectively. These represented critical values determined during the runs with two trucks on the span simultaneously. Measured values were multiplied by a factor of two to be consistent with the AASHTO Design Specifications [2].

For the Nolanville Bridge, the maximum distribution factor that was calculated based on a single-truck run was equal to 0.40, and it was the same for the exterior and interior girders. There were only single-truck runs during this load test and it was felt that the maximum distribution factors were not obtained. Therefore, it was decided to add the value of 0.15 measured at the interior girder during Run 33 (Table 5.19) to the value of 0.40 that was measured during Run 30 in order to reflect a run involving the combination of two trucks. The resulting value of 0.55 was very close to that obtained for the exterior girder by adding the value of 0.14 measured during Run 31 to the 0.40 that was measured during Run 33. Also, the ratio of 0.55 to 0.40 is approximately equal to the ratio of 0.86 and 0.68, which are the design distribution factors given by Eq. 5.15a and 5.15b based on the AASHTO Specifications [2].

The results of the revised set of calculations are presented in Table 6.6. As expected, the lower live-load moments have increased the rating factors.

Table 6.6 Results of the Revised Load Rating Using Live-Load Moments Based on Diagnostic Load Tests

Symbol	Slaughter Creek Bridge		Nolanville Bridge		References - Equations - Comments
	Interior Girder	Exterior Girder	Interior Girder	Exterior Girder	
RF^{inv}	2.43	2.52	3.98	3.95	Eq. 6.1 - Inventory Level Rating (Strength)
RF^{oper}	4.06	4.21	6.65	6.60	Eq. 6.1 - Operating Level Rating (Strength)
$RF^{inv,ct}$	1.83	2.22	2.14	2.53	Eq. 6.3 - Concrete Tensile Stress
$RF^{inv,cc}$	6.72	9.30	9.36	8.27	Eq. 6.5 - Concrete Compressive Stress
$RF^{inv,cc}$	5.34	7.59	7.71	6.50	Eq. 6.4 - Concrete Compressive Stress
$RF^{inv,ps}$	8.43	16.9	20.6	21.0	Eq. 6.6 - Strands Tensile Stress
$RF^{oper,ps}$	16.2	27.7	31.6	31.6	Eq. 6.7 - Strands Tensile Stress
DF_{max} used	0.58	0.78	0.55	0.55	
Ratio of Revised to Initial Rating	1.67	1.24	2.39	2.39	

Table 6.6 also lists the ratios of the rating factors obtained from the initial load rating with those that resulted from the moments based on the diagnostic load tests. The rating factors are increased by 24% and 67% for the exterior and interior girders of the Slaughter Creek Bridge, respectively, and by 139% in the case of the Nolanville Bridge. The differences are based on the new distribution factors and reduced total moment in the bridge, due to the observed rotational restraint. Other researchers have hesitated to use the rotational restraint observed during diagnostic load tests for load rating, because they have little confidence that the restraint will be present at higher levels of live load [5]. However, the rotational restraint in the Nolanville Bridge was nearly the same for the standard dump truck and the HETS vehicle, while the induced strains were three times

larger when the HETS was on the bridge. Based on this experience, the rotational restraint has been included in the rating procedures for these bridges.

6.5.2 Revised Rating by the Method Outlined in the 1999 Manual [7]

The second method used to revise the load rating is outlined in Chapter 8 of the 1999 Pre-Final Draft Manual for Condition Evaluation and Load and Resistance Factor Rating of Highway Bridges [7]. The results of the diagnostic load test are used to define an adjustment factor, K. This factor represents the difference between the expected and measured strains. The revised rating factors are increased or decreased using Eq. 6.8 and the calculated value of the K factor.

$$RF_T = RF_C \times K \tag{6.8}$$

where

RF_T = Rating factor based on the load-test results

RF_C = Rating factor based on the initial rating calculations

K = Adjustment for the rating

The Adjustment Factor (K) is given by Eq. 6.9.

$$K = 1 + K_a K_b \tag{6.9}$$

where

K_a = Factor that considers the section modulus that resists the applied load and relates the measured to calculated strains

K_b = Factor that accounts for the understanding of the load test results when compared with those calculated using standard design provisions

Equation 6.10 gives the expression used to determine the factor K_a:

$$K_a = \frac{\varepsilon_C}{\varepsilon_T} - 1 \tag{6.10}$$

where

ε_T = Maximum member strain measured during the load test

ε_C = Calculated strain from a line-girder analysis on a simply-supported beam with the test vehicle at the position on the bridge that produced ε_T

For the case where the live-load effect is a bending moment, the expression for the calculated strain is given by Eq. 6.11.

$$\varepsilon_C = \frac{L_T}{(SF)E} \tag{6.11}$$

where

SF = Appropriate section modulus for the member

E = Member modulus of elasticity

L_T = Maximum calculated live-load moment in the member induced by the test vehicle at the location where ε_T was measured

The fraction of the total moment in the bridge that is resisted by a single member is equal to half the total moment on the bridge, reflecting one line of wheels directly over the girder, plus a fraction of the remaining moment reflecting the effect of the second line of wheels. The fraction is based on the definition of the distribution factor in the 1996 Standard Specifications [2] and the 1993 Manual [8]. This is given by Eq. 6.12. Impact is not included in the expression.

$$L_T = (0.5M_T)(1+\frac{DF_{\max}}{S}) = (0.5M_T)(1+\frac{1}{5.5}) \qquad (6.12)$$

where

M_T = Maximum total live-load moment induced by the test vehicle on the bridge calculated from a line-girder analysis on a simply-supported beam

$DF_{\max}$ = Maximum moment distribution factor for a member calculated based on the AASHTO Specifications [2]

S = Transverse spacing of the girders, ft

The factor K_b is determined based on Table 6.7, which is identical to Table 8.8.25.3-1 of the 1999 Manual [7]. This factor depends on the size of the loading vehicle and the confidence that the engineer has on the results obtained from the test.

Table 6.7 Table to Determine K_b

Can member behavior be extrapolated to 1.33W?		Magnitude of Test load			K_b
Yes	No	T/W<0.4	0.4<T/W<0.7	T/W>0.7	
x		x			0
x			x		0.8
x				x	1
	x	x			0
	x		x		0
	x			x	0.5

Referring to Table 6.7, the parameter T is equal to the moment L_T, given by Eq. 6.12. The parameter W represents the maximum live-load moment in a member, including impact, due to the HS-20 rating vehicle, and is given by Eq. 6.13.

$$W = (DF_{\max})L_R(1+I) \tag{6.13}$$

where

W = Live-load moment, including impact, induced by the rating vehicle on a member

L_R = Total live-load moment induced by the rating vehicle on the bridge ignoring impact

I = Dynamic amplification (impact) factor

This method can be used to revise the initial rating factors based on the results of the diagnostic load tests that were conducted on the two prestressed concrete bridges. The calculations are performed based on the procedures

included in the 1993 Manual for Bridge Rating through Load Testing [8]. Table 6.8 presents the notation used for the various parameters involved in the calculations. Table 6.9 presents the sequence of calculations necessary to obtain the adjustment factors in each case, based on the maximum strains induced by the standard test vehicles in the load tests. The values of K_a, K_b and K for each section are also included in the table.

Table 6.8 Notation Used for Revised Rating Based on the 1999 Manual Method [7]

Parameter	Symbol	Units
Maximum measured strain	ε_T	-
Modulus of elasticity	E	ksi
Section modulus	SF	in^3
Maximum calculated moment from test vehicle on bridge	M_T	k-ft
Maximum calculated member moment from test vehicle (no impact)	$T=L_T$	k-ft
Calculated strain = $L_T/E(SF)$	ε_C	-
Transverse spacing of girders	S	ft
Distribution Factor	DF_{max}	-
Ratio of member moment to total bridge moment	M_T/L_T	-
Live-load moment from HS-20 ignoring impact	L_R	k-ft
Dynamic amplification (impact) factor	I	-
Live-load moment from HS-20 including impact	W	k-ft
Ratio of maximum calculated member moment due to test vehicle to maximum calculated member moment due to HS-20 vehicle	$^T/_W$	-
K_b-Table 6.8	K_b	-
$K_a=(\varepsilon_c/\varepsilon_T)-1$	K_a	-
$K=1+K_aK_b$	K	-

The value of 1.0 for the parameter K_b is used in the case of the HETS, because the ratio $^T/_W$ was equal to 1.33. Note that the values of K_b for the Slaughter Creek Bridge during Test Series 2 and for the Nolanville Bridge were taken to be 0.8. A strict interpretation of Table 6.7 would yield values of zero.

The two testing vehicles used during Test Series 1 were nominally identical to these dump trucks, yet the values of $^{T}/_{W}$ were slightly higher. These modest differences were not considered to be sufficient to warrant such a dramatic difference in the parameter K_b.

Table 6.9 Calculations of the K-Factors for Each Girder

		Slaughter Creek Bridge						Nolanville Bridge			
		Interior Girder	Exterior Girder	Interior Girder	Exterior Girder	Interior Girder	Exterior Girder	Interior Girder	Exterior Girder	Interior Girder	Exterior Girder
Symbol	Units	Test Vehicle D1		Test Vehicle D2		Test Vehicle D3		Test Vehicle D4		Test Vehicle HETS	
ε_T	-	32	43	33	43	32	43	32	33	99	102
E	ksi	4595	5467	4595	5467	4595	5467	5002	5002	5002	5002
SF	in^3	16886	19514	16886	19514	16886	19514	17984	17114	17984	17114
M_T	k-ft	906	906	946	946	890	890	1076	1076	3630	3630
$T=L_T$	k-ft	535	535	559	559	526	526	636	636	2145	2145
ε_C	-	83	60	86	63	81	59	85	89	286	301
S	ft	8	8	8	8	8	8	9.5	9.5	9.5	9.5
DF_{max}	-	0.73	0.73	0.73	0.73	0.73	0.73	0.86	0.86	0.86	0.86
M_T/L_T	-	0.59	0.59	0.59	0.59	0.59	0.59	0.59	0.59	0.59	0.59
L_R	k-ft	1498	1498	1498	1498	1498	1498	1534	1534	1534	1534
I	-	0.22	0.22	0.22	0.22	0.22	0.22	0.22	0.22	0.22	0.22
W	k-ft	1333	1333	1333	1333	1333	1333	1618	1618	1618	1618
$^{T}/_{W}$	-	0.40	0.40	0.42	0.42	0.39	0.39	0.39	0.39	1.33	1.33
K_b	-	0.8	0.8	0.8	0.8	0.8	0.8	0.8	0.8	1.0	1.0
K_a	-	1.60	0.42	1.62	0.46	1.57	0.39	1.68	1.72	1.89	1.95
K	-	2.28	1.33	2.30	1.36	2.26	1.31	2.35	2.37	2.89	2.95

The maximum measured strains for each girder are given in Table 6.9, along with the maximum strains calculated using Eq. 6.11. The last row has the resulting K factors, which are not sensitive to the actual dump truck used in the different Test Series. The average calculated value of K for each girder is summarized in Table 6.10. Note that in the case of the Nolanville Bridge, the values of K that were calculated for the overweight HETS vehicle are higher than

those corresponding to the standard vehicle. The resulting value of the K-factor for the HETS reduces to 2.55 when the parameter K_b is set equal to 0.8 instead of 1.0 as shown in Table 6.9.

Table 6.10 Calculated Values of K for the Four Girders

Slaughter Creek Bridge		Nolanville Bridge			
Test Vehicles D1, D2, D3		Test Vehicle D4		Test Vehicle HETS	
Interior Girder	Exterior Girder	Interior Girder	Exterior Girder	Interior Girder	Exterior Girder
2.28	1.34	2.35	2.37	2.89	2.95

Table 6.11 lists the calculated values of the rating factors. The corresponding increases in the initial rating factors are different for the two methods of adjusting the initial rating factors of Table 6.5. These differences are discussed next.

Table 6.11 Results of the Revised Rating Based on the 1999 Manual Method

Symbol	Slaughter Creek Bridge		Nolanville Bridge		References - Equations - Comments
	Interior Girder	Exterior Girder	Interior Girder	Exterior Girder	
RF^{inv}	3.33	2.72	3.91	3.93	Eq. 6.1 - Inventory Level Rating (Strength)
RF^{oper}	5.55	4.55	6.53	6.56	Eq. 6.1 - Operating Level Rating (Strength)
$RF^{inv,ct}$	2.50	2.40	2.10	2.52	Eq. 6.3 - Concrete Tensile Stress
$RF^{inv,cc}$	9.20	10.04	9.20	8.22	Eq. 6.5 - Concrete Compressive Stress
$RF^{inv,cc}$	7.31	8.19	7.57	6.45	Eq. 6.4 - Concrete Compressive Stress
$RF^{inv,ps}$	11.5	18.2	20.3	20.8	Eq. 6.6 - Strands Tensile Stress
$RF^{oper,ps}$	22.2	29.9	31.1	31.4	Eq. 6.7 - Strands Tensile Stress
DF_{max} used	0.73	0.73	0.86	0.86	
M_T/L_T	0.59	0.59	0.59	0.59	
K-standard vehicle	2.28	1.34	2.35	2.37	
K-HETS	-	-	2.89	2.95	

6.5.3 Discussion of the Initial and Revised Load Rating Results

This section compares the results from the two revised ratings and discusses the differences between the two approaches and the initial rating procedure. As indicated in Tables 6.6 and 6.11, the load ratings linked to the diagnostic tests were larger than the initial values. It is not surprising that the two approaches give different results, because they are based on different philosophies.

The first method of revised rating only involves changes in the live-load moment of the rating equation (Eq. 6.1). The ratio of initial to revised rating factors is expressed in Eq. 6.14. The terms relating to flexural capacity and dead-load moments cancel, leaving an expression related to live-load moments and distribution factors. The second term expresses the increase in the rating factor, and may be expressed as a function of the measured and calculated moments in the member, as given by Eq. 6.15 and 6.16.

$$\frac{RF_T}{RF_C} = \frac{\dfrac{C - A_1 D}{A_2 (DF_T)(LR_T)(1+I)}}{\dfrac{C - A_1 D}{A_2 (DF_C)(LR_C)(1+I)}} = \frac{(DF_C)(L_{RC})}{(DF_T)(L_{RT})} = 1 + \frac{(DF_C)(L_{RC}) - (DF_T)(L_{RT})}{(DF_T)(L_{RT})} \tag{6.14}$$

$$\frac{(DF_C)(L_{RC}) - (DF_T)(L_{RT})}{(DF_T)(L_{RT})} = \frac{M_{design} - M_{measured}}{M_{measured}} \tag{6.15}$$

$$\frac{RF_T}{RF_C} = 1 + \frac{M_{design} - M_{measured}}{M_{measured}} \tag{6.16}$$

where

RF_T = Revised rating factor calculated based on the results of the diagnostic load test

RF_C = Initial rating factor calculated using AASHTO procedures [3]

DF_T = Maximum fraction of total moment distributed to a single member based on results of the diagnostic load test

DF_C = Distribution factor per AASHTO procedures [2]

L_{RT} = Maximum total moment on the bridge due to HS-20 vehicle, calculated using line-girder analysis assuming rotational springs at the ends of the span

L_{RC} = Maximum total moment on the bridge due to HS-20 vehicle, calculated using line-girder analysis assuming simply-supported ends

M_{design} = Calculated maximum moment in member due to HS-20 vehicle, based on AASHTO distribution factors and simply-supported end conditions

$M_{measured}$ = Calculated maximum moment in member due to HS-20 vehicle, based on measured distribution factors and restrained end conditions

Using a similar approach, the results of the second method are related to the values of the constants K_a and K_b from Eq. 6.9. The ratio of initial to revised rating factors can be expressed as shown in Eq. 6.17. The product of K_a and K_b reflects the increase in the rating factor as a function of the measured and

calculated moments in the individual girders (Eq. 6.18). For elastic members, the strains may be related to the moments in the members through the section modulus and the elastic modulus.

$$\frac{RF_T}{RF_C} = 1 + K_a K_b \tag{6.17}$$

$$K_b K_a = 0.8\left(\frac{\varepsilon_C}{\varepsilon_T} - 1\right) = 0.8\left(\frac{\varepsilon_C - \varepsilon_T}{\varepsilon_T}\right)\left(\frac{E(SF)}{E(SF)}\right) = 0.8\left(\frac{M_C - M_T}{M_T}\right) \tag{6.18}$$

$$\frac{RF_T}{RF_C} = 1 + 0.8\left(\frac{M_C - M_T}{M_T}\right) = 1 + 0.8\left(\frac{M_{design} - M_{measured}}{M_{measured}}\right) \tag{6.19}$$

where

K_b= 0.8 (Table 6.7)

M_C= Maximum calculated moment in the girder due to the test vehicle, simply-supported boundary conditions and distribution factors specified in the AASHTO specifications [2]

M_T= Maximum moment in girder during the diagnostic load test

The general forms of Eq. 6.16 and Eq. 6.19 are nearly identical. The first method uses the HS-20 vehicle to determine the maximum moments while the second method is based on the moments induced by the test vehicle. The second method also uses a factor of 0.8 to modify the amplification term, because the maximum moment induced by the standard vehicle during the diagnostic load test did not exceed 70% of the design moment. This factor is set equal to 1.0 for the case of the overweight test vehicle (HETS) used in Test Series 3. It is important

to note that the boundary conditions used to calculate M_{design} and M_C differ from those inferred during the diagnostic load tests.

6.6 SUMMARY

The results of the rating calculations for the interior and exterior girders of the two bridges based on the Load Factor method were presented in this section. The initial calculations were followed by two different methods that used information obtained for the two bridges from the diagnostic load tests. Both bridges exceed the current design limits based on the HS-20 vehicle. From the BRINSAP database, the rating for both bridges is HS-20 for inventory and HS27 for operating level ratings [9]. These ratings correspond to the highest values given in the database for bridges in the state of Texas.

Table 6.12 summarizes the results obtained for inventory and operating levels based on the strength calculations (Eq. 6.1) and for inventory level based on concrete tensile stresses. In all cases, the revised ratings based on the diagnostic load tests are considerably larger than the initial values.

Table 6.12 Summary of HS-ratings for the Slaughter Creek and Nolanville Prestressed Concrete Bridges – Load Factor Method

Rating Level	Method	Slaughter Creek Bridge		Nolanville Bridge	
		Interior Girder	Exterior Girder	Interior Girder	Exterior Girder
Inventory (Strength)	Initial Rating	29.2	40.8	33.3	33.1
	Moments from Diagnostic Load Tests	48.6	50.5	79.7	79.1
	1999 Manual	66.5	54.5	78.3	78.6
Operating (Strength)	Initial Rating	48.7	68.0	55.7	55.2
	Moments from Diagnostic Load Tests	81.1	84.3	133	132
	1999 Manual	111	90.9	131	131
Inventory (Allowable Stresses)	Initial Rating	21.9	35.9	17.9	21.2
	Moments from Diagnostic Load Tests	36.5	44.4	42.8	50.7
	1999 Manual	50.0	47.9	42.1	50.3

Chapter 7. CONCLUSIONS AND RECOMMENDATIONS

This chapter is divided into four sections. The first provides a set of recommendations for future diagnostic load tests and the second summarizes the key findings from the load tests discussed in this thesis. The conclusions of this investigation are summarized in Section 7.3 and topics for future research are listed in Section 7.4.

7.1 RECOMMENDATIONS FOR LOAD TESTS

The field tests described in this thesis demonstrate that valuable information can be obtained from diagnostic load tests. However, care must be taken during the planning process in order to obtain the appropriate information. The following recommendations are based on the experiences obtained from testing the Slaughter Creek and Nolanville Prestressed Concrete Bridges.

Once a bridge has been identified for testing, a careful examination of the structural plans and an investigation of the condition of the bridge must take place. Structural characteristics, such as openings or cracks in the roadway at the ends of the spans, should be noted and documented with photographs. The degree of cracking, if any, in the cast-in-place concrete slab or precast concrete girders should be examined. The presence of secondary structural elements, such as diaphragms and traffic rails, must be documented and the expected participation of these members in bending should be assessed. Any gaps in the

rails that would suggest a lower contribution to the effective bending stiffness of the structure should be noted.

The types of instrumentation and the locations of the instruments should be determined based on the measurements that the researchers want to obtain. The test plan must consider the limitations of the data acquisition system in determining the number of instruments that can be used simultaneously during a particular test run. Also, the researchers must be able to access the different instrument locations, and accessibility issues must be addressed during the planning stage in order to avoid problems during the instrumentation and testing phases.

For a prestressed concrete girder bridge, the cross-sections of the precast girders are the most important locations to measure the bending strains. The induced strains from the loading vehicles should be estimated. Careful troubleshooting of the data-acquisition system before and during the test can ensure that the gages function properly and that the readings are close to the expected values.

Initial calculations should also establish the expected range of neutral axis depths in the girders based on noncomposite and composite sections. At least two strain gages should be attached to the surface of the concrete on the precast girders to infer the neutral axis depths from the measured strains and calculate the live-load moments. A third gage close to the slab-girder interface would provide more information about the assumed linear distribution of the strains in the sections and the location of the neutral axis depths. The use of nondestructive

methods to determine the in-situ compressive strength and the modulus of elasticity of the concrete materials would be useful in subsequent analyses of the measured data. These measurements would lead to higher levels of confidence in the calculated live-load moments.

For the type of prestressed concrete girder bridges investigated in this thesis, the maximum moment is expected to occur at mid-span. Additional instrumentation should be placed at other locations along the span so that the end moments based on the measured data can be investigated. If the approach described in Chapter 5 is used, then a careful selection of the instrumented sections based on the dimensions of the test vehicles and expected end restraint will permit the maximum end moments to be determined. Also, if multiple sections are instrumented close to mid-span, then the end moments can be examined by considering different combinations of moments that would help verify the results.

Using reliable rotation or vertical deflection measurement devices during the load tests has the potential to provide useful information in addition to the strain readings. This information can be used to define the effective stiffness of the members and the distribution of load among them.

The truck paths in each case should be determined based on a number of criteria. Paths along the central part of the bridge and adjacent to the traffic rails should be planned in order to induce maximum load effects in interior and exterior girders respectively. The maximum load effects must be examined both

by setting a line of wheels directly over a single girder and by centering the test vehicle over a girder.

Additionally, the selection of the paths should allow the investigation of symmetry in the response of the bridge. In cases were symmetry is established, more gages can be located at alternate locations for subsequent tests. Finally, a diagnostic load test is more complete when two trucks are run simultaneously along the span. This permits the evaluation of the maximum distribution factor for the girders with both vehicles present, and it also allows the assessment of superposition in the response.

7.2 Summary of Measured and Calculated Response

Standard ten-cubic yard dump trucks of similar dimensions and axle configurations were used for the tests and an overweight Heavy Equipment Transportation System (HETS) was also used during the Test Series 3 at the Nolanville Bridge. The reproducibility of the data was verified by running two passes along each transverse path for every test vehicle. The measured strains were found to be repeatable in terms of their signs and magnitudes at each longitudinal location. The readings did not indicate any strain reversals during the runs. Peak strains were recorded when the rear axles were directly over the strain gages.

The maximum strain recorded at the extreme tension fiber of the precast girders at the Slaughter Creek Bridge was approximately 44 microstrain when a single, 10-yd^3 dump truck was driven across the bridge. This reading was

recorded while the front tire of the vehicle was located 1'-9" from the face of the parapet rail. The maximum strain value recorded at the Nolanville Bridge was 33 microstrain for a truck path 6 ft from the face of the traffic rail. The corresponding value that was induced by the HETS vehicle was 106 microstrain.

The possibility that the beams were cracked was examined. The neutral axis depths inferred from the measured strain data were found to be close to the values calculated based on composite, gross cross-section properties. Also, calculations were initially performed to establish the level of additional live-load stresses and strains necessary to cause cracking of the concrete at the extreme tension fiber of the girders. The minimum values were 183 microstrain for the Slaughter Creek Bridge and 152 microstrain for the Nolanville Bridge. It was concluded that the beams were uncracked after 7 and 21 years in service for the Slaughter Creek and Nolanville Bridges, respectively.

The neutral axis depths also indicated that the parapet rails at the Slaughter Creek Bridge contributed to the bending stiffness of the exterior beams. These parapet rails had been designed as non-structural elements, and were cut at three locations along the span. In spite of these discontinuities, the precast concrete parapets did contribute to the flexural stiffness of the exterior girders. The neutral axis depths measured at the Nolanville Bridge were approximately 15% deeper than what had been calculated using gross cross-section properties for the composite section. This suggested the possibility of cracking in the cast-in-place slab and indicated that the traffic rail was not participating significantly in bending.

The symmetry in the response of the Slaughter Creek Bridge was verified by placing the two truck paths adjacent to the parapet rails and the two paths at the interior of the bridge symmetric to each other with respect to the centerline. The measured data at the girders adjacent to the loads indicated symmetry in the response of the structure. Also, superposition in the measured response of the Slaughter Creek Bridge was verified with two similar ten-cubic yard dump trucks traveling side by side along the span. The moments measured by these runs were within 5% of the combined effects of two single runs of the vehicles.

Similar maximum distribution factors were calculated based on the measured moments at the Nolanville Bridge with both the overweight HETS vehicle and the standard dump truck. As expected, the maximum strains measured in this case were higher than the strains corresponding to the lighter vehicle.

The strain readings obtained from gages attached to the diaphragms at the Nolanville Bridge indicated that the diaphragms resist out-of-plane motions of the precast girders. Maximum strains in the diaphragms when the dump truck was driven across the bridge ranged between –7 and 10 microstrain. The corresponding values for the HETS ranged between –18 and 38 microstrain.

The presence of diaphragms resulted in a more uniform distribution of load among the girders. A maximum of 43% of the total moment across the section of the bridge was resisted by a single girder during the test at the Nolanville Bridge. This percentage was the same for interior and exterior sections and was observed during runs of both the standard and the overweight

vehicle as well. In contrast, the maximum bending moment in an exterior girder was approximately 60% of the total moment for the Slaughter Creek Bridge. The exterior girders attracted more load due to higher stiffness from two sources: (a) the higher compressive strength of the concrete in the girders and (b) the contribution of the parapet rail to the bending stiffness of the girder.

Although the maximum moments were calculated based on gross cross-section properties and composite sections, the results from the diagnostic load tests indicated a significantly lower total moment across the width of the bridges than was determined from statics. The measured strains yielded moments ranging between 65 and 80% of the maximum expected moment computed based on a two-dimensional line-girder analysis assuming the ends of the girders to be simply-supported.

Investigation of the measured moments at the instrumented sections suggested that appreciable moments developed at the interior and abutment ends of the Slaughter Creek and Nolanville Bridges respectively. Restraint was provided by the continuous slab at the Slaughter Creek Bridge and by the framing of the slab and end-diaphragms at the abutment end of the Nolanville Bridge. These end moments ranged from 35% of the maximum moment at mid-span in the case of the Slaughter Creek Bridge to 85% for the Nolanville Bridge.

The maximum total moments measured during the tests were compared with the results of a line-girder analysis assuming a fixed end for each girder. The calculated maximum moments were 10 to 70% lower than the measured moments. The line-girder models were modified by using rotational springs with

stiffness proportional to EI/L at one end of the girders. The values of the constants of proportionality that yielded results in the range of 95±5% of the calculated values were 1.8 for the Slaughter Creek Bridge and 2.25 for the Nolanville Bridge. The fixed-end case corresponded to a constant of 3 for each of the two cases.

Both bridges were found to rate favorably for the HS-20 vehicle for rating based on the strength of the girders, and for both inventory and operating rating levels. The results of these calculations ranged between HS-29 for the interior section at the Slaughter Creek Bridge to HS-55 at the exterior section of the Nolanville Bridge. Finally, the rating for the interior section at the Slaughter Creek Bridge was HS-22 based on allowable tensile stresses in the concrete. However, the corresponding rating for the interior section at the Nolanville Bridge was only HS-18.

7.3 CONCLUSIONS

Results of diagnostic load tests provided detailed information about the behavior of the prestressed concrete bridges tested. The tests were relatively easy to set up, each requiring two to three days to prepare and install the instrumentation. Evaluation of the data was the most time-consuming phase, but much of this can be automated to increase the efficiency of future tests.

The neutral axis depths that were inferred from the measured strain data matched well with the neutral axis depths calculated using gross cross-section properties for the composite section. The maximum live-load strains induced in

each section during the tests were lower than the calculated live-load strains that would cause cracking at the extreme tension fiber of the concrete. In the case of the Slaughter Creek Bridge, the strains from a combination of two trucks on the bridge were equal to the combined effects of the corresponding runs with a single truck, thus verifying superposition. The response of the Nolanville Bridge due to the HETS overweight vehicle was similar to that measured by the standard truck, although the induced strains were nearly three times higher. Based on these findings, it was concluded that the behavior of the bridges during the tests was elastic and the beams were uncracked.

The measured strains indicated the participation of nonstructural elements in the response of the bridges. In the case of the exterior girder at the Slaughter Creek Bridge, the neutral axis depths inferred from the measured strains suggested that the parapet rails contributed to the bending stiffness of the exterior girders although they were designed as non-structural elements. In the case of the Nolanville Bridge, the deep neutral axes indicated that the traffic rails did not participate in bending. The strains recorded at the diaphragms showed that these members provided restraint against out-of-plane motions of the girders and facilitated the distribution of moments among the members.

The maximum total moments at the mid-span sections were significantly lower than the moment determined from statics for simply-supported spans, even if gross cross-section properties were used in the moment calculations. The measured results ranged between 65 and 80% of the total static moment calculated based on a two-dimensional line-girder analysis. Appreciable end

moments were indicated by the measured moments. These were found to range approximately between 20 and 35% for the Slaughter Creek Bridge and 55 to 85% for the Nolanville Bridge.

A maximum of 60% of the total moment across the bridge was resisted by the exterior girder in the case of the Slaughter Creek Bridge, and a maximum of 40% was resisted by the interior girder. The higher concrete compressive strength of the exterior girder and the participation of the parapet rail in bending resulted in higher loads to be attracted by the exterior girder relative to the interior girder. The 15° skew was not found to influence the measured response of the Slaughter Creek Bridge. A small difference in the location of the peak strains in the beams was observed because the gages were located at the mid-spans of the individual girders. This difference was only 1-2 ft based on the given angle of skew and transverse spacing of the girders.

In the case of the Nolanville Bridge, the maximum percentage of total moment resisted by a single member was approximately equal to 40% for both the interior and the exterior girders. The moments were more uniformly distributed among the girders than in the Slaughter Creek Bridge. This occurred partly because the stiffness of the interior girders was approximately equal to that of the exterior girders, and partly because of the diaphragms present.

The two bridges are rated in the BRINSAP database at the maximum ratings of HS-20 for inventory level rating and HS-27 for operating level rating. Using the Load Factor method based on strength, the ratings for the two bridges were calculated to be HS-29 and HS-33 for inventory level and HS-48 and HS-55

for operating level rating of the Slaughter Creek and Nolanville Bridges respectively. Based on allowable stresses, the ratings for inventory level were HS-22 for the Slaughter Creek Bridge and HS-18 for the Nolanville Bridge.

The revised rating based on two methods was calculated for each bridge. Although the methods have different philosophies, they both increase the initial rating calculations. The benefit that is calculated based on the first method ranges from 24 to 67% for the Slaughter Creek Bridge, and 139% for the Nolanville Bridge. The second method gives benefits ranging from 34 to 128% for the Slaughter Creek Bridge and approximately 135% for the Nolanville Bridge when the standard 10-yd^3 vehicle is considered and 190% when the HETS vehicle is considered.

It is concluded that important information about the response of prestressed concrete bridges can be obtained through diagnostic load testing. The responses of the two bridges investigated in this thesis indicate some important aspects of the response of prestressed concrete bridges. These include the validity of elastic response and gross cross-section properties in the moment calculations, the participation of nonstructural elements in the response, the level of total measured moment relative to the total static moment, the distribution of the moments among the girders and the load rating of the bridge.

7.4 FUTURE RESEARCH

Some issues that should be addressed in future research involving load testing of prestressed concrete bridges include the following:

1. Maximum moment distribution factors are calculated either by setting a line of wheels over a single girder or by centering the vehicle over the girder. Care should be taken during the planning stages of future tests to ensure that both transverse locations of the vehicles relative to the girders are investigated.
2. End restraint was observed from the response of each bridge during the diagnostic load tests. The approach suggested in Chapter 5 for estimating end moments based on the measured data can be improved by carefully selecting three sections close to mid-span and combining the results of the three pairs in examining the end moments.
3. More accurate methods for examining deflections in the field should be employed to provide additional information to the strain readings.
4. A three-dimensional model of the bridge would represent the actual structure more accurately than a two-dimensional beam. The use of three-dimensional finite element programs to model and examine the response of these bridges can provide greater flexibility in investigating the various parameters affecting the response of the bridge. These include the degree of end restraint, the degree of composite action, the material properties, the effects of the traffic rails and the effects of the diaphragms.

Appendix A. REPRESENTATIVE STRAIN HISTORIES MEASURED DURING THE LOAD TESTS

This Appendix presents representative plots of the measured strain histories from the three diagnostic load tests conducted at the Slaughter Creek and Nolanville Prestressed Concrete Bridges. Table A.1 lists the figures included in this appendix.

Table A.1 List of Figures in Appendix A

Location of Instrumented Section	Gage Location on the Cross-Section	Test Series 1	Test Series 2	Test Series 3	
		Standard Vehicle	Standard Vehicle	HETS Vehicle	Standard Vehicle
Mid-Span	Girder	A.1-A.8	A.17-A.20	A.25-A.27	A.34-A.36
	Parapet	A.9-A.16	A.21-A.24	-	-
	Top	-	-	A.28-A.30	A.37-A.39
	Diaphragm	-	-	A.31-A.33	A.40-A.42
2/3-Span	Girder	A.43-A.50	A.59-A.62	-	-
	Parapet	A.51-A.58	A.63-A.66	-	-
3/4-Span	Girder	-	-	A.67-A.69	A.70-A.72
5/6-Span	Girder	A.73-A.80	A.89-A.92	-	-
	Parapet	A.81-A.88	A.93-A.96	-	-

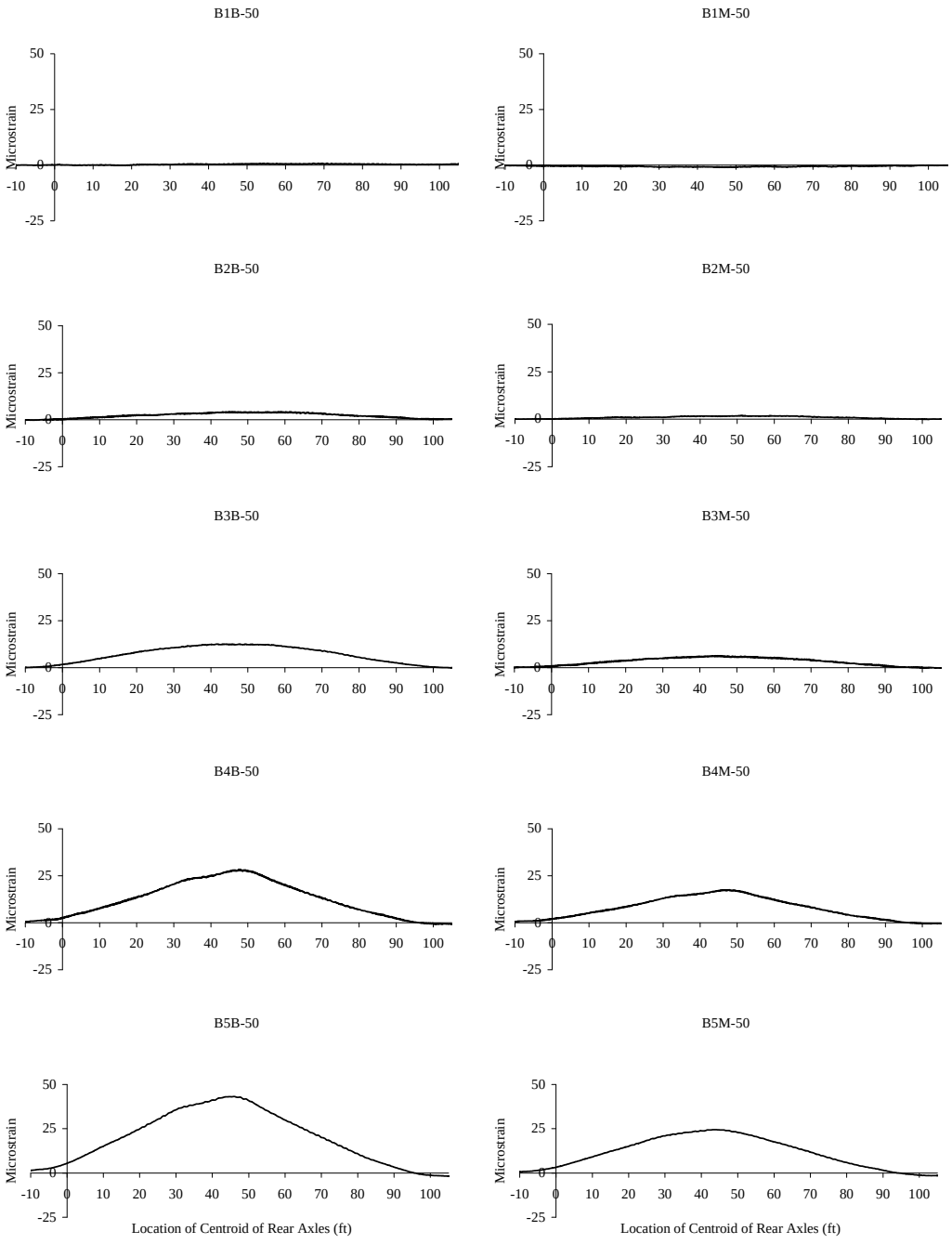

Figure A.1 Strains for the Mid-Span Girder Gages, Test Series 1, Run 1

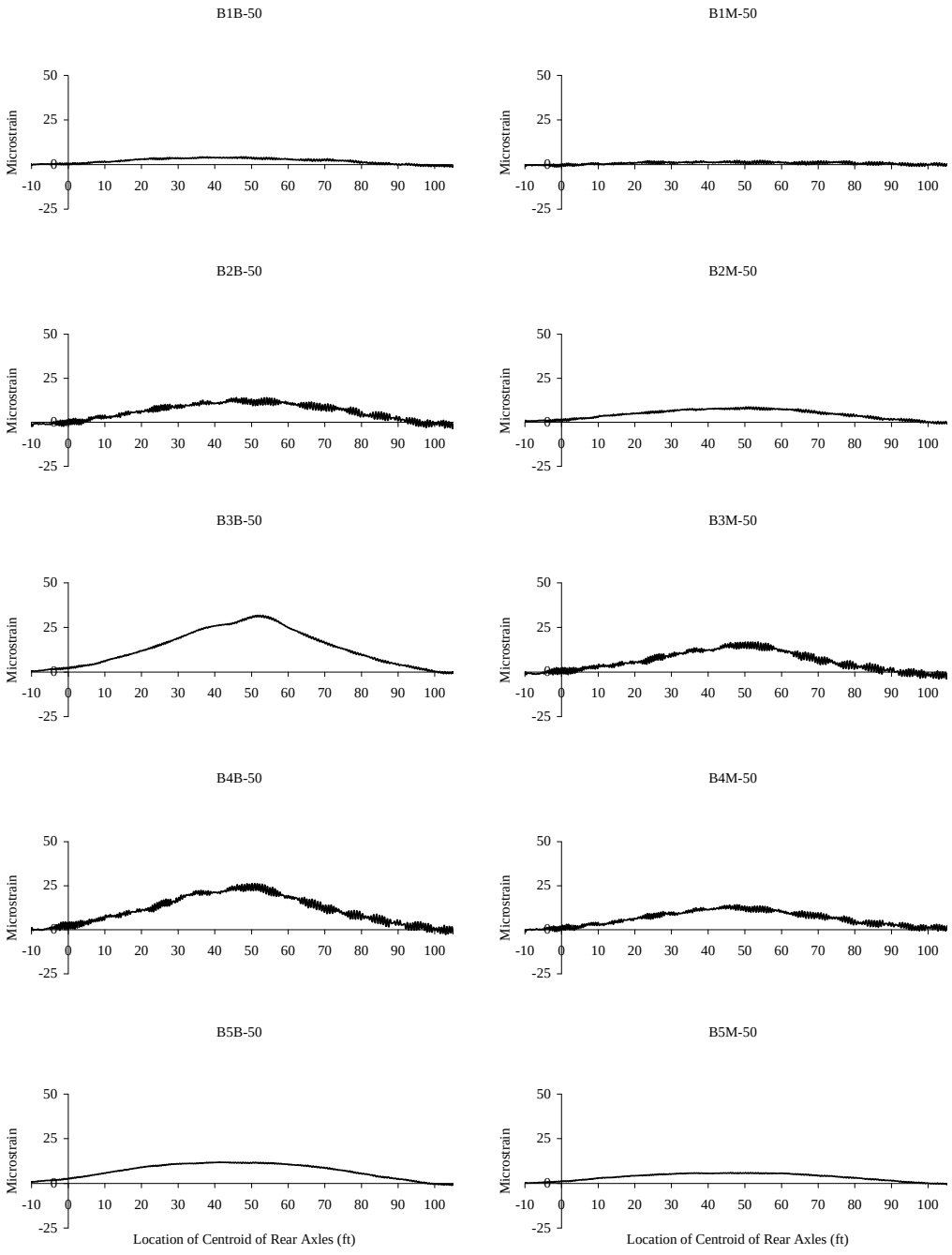

Figure A.2 Strains for the Mid-Span Girder Gages, Test Series 1, Run 4

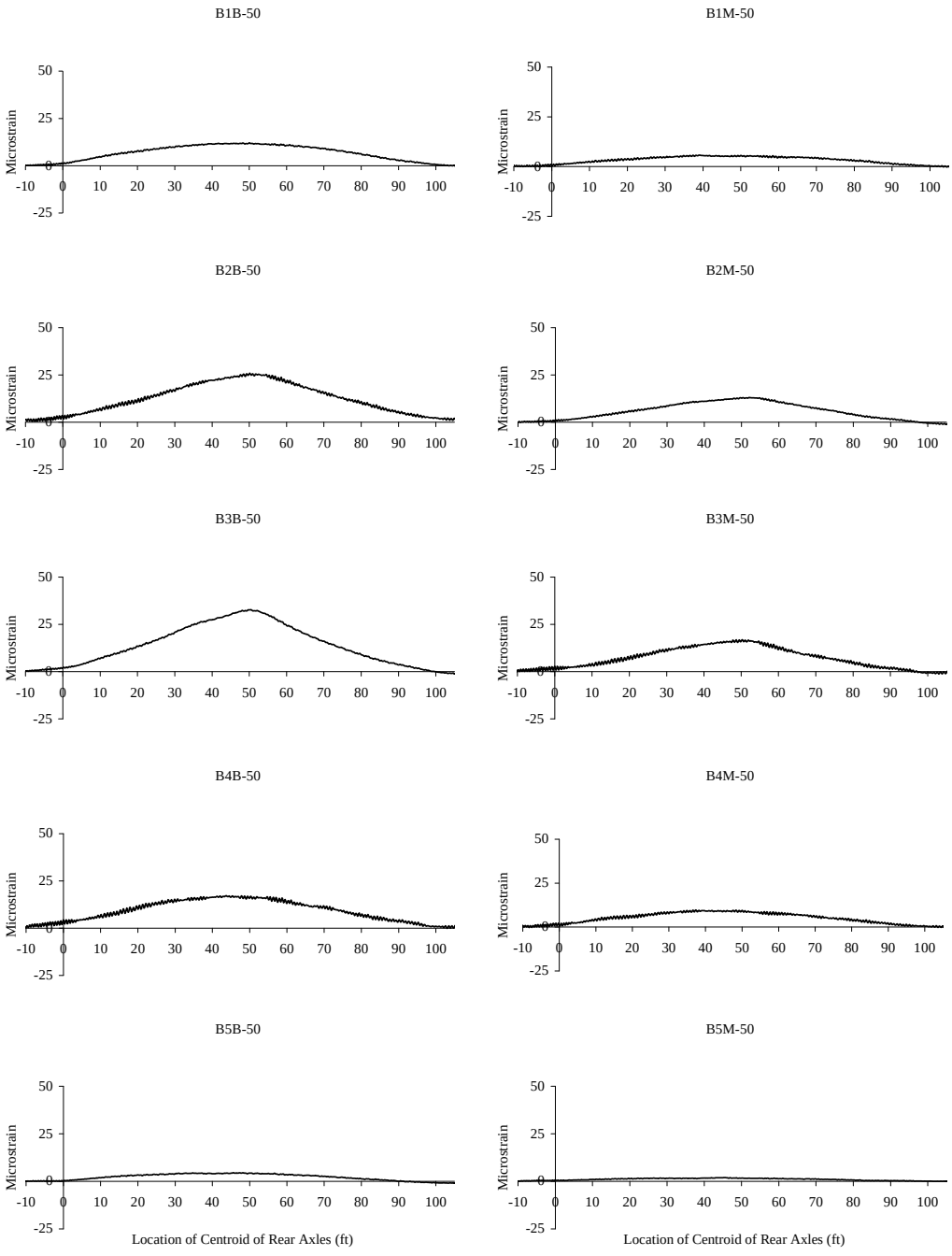

Figure A.3 Strains for the Mid-Span Girder Gages, Test Series 1, Run 6

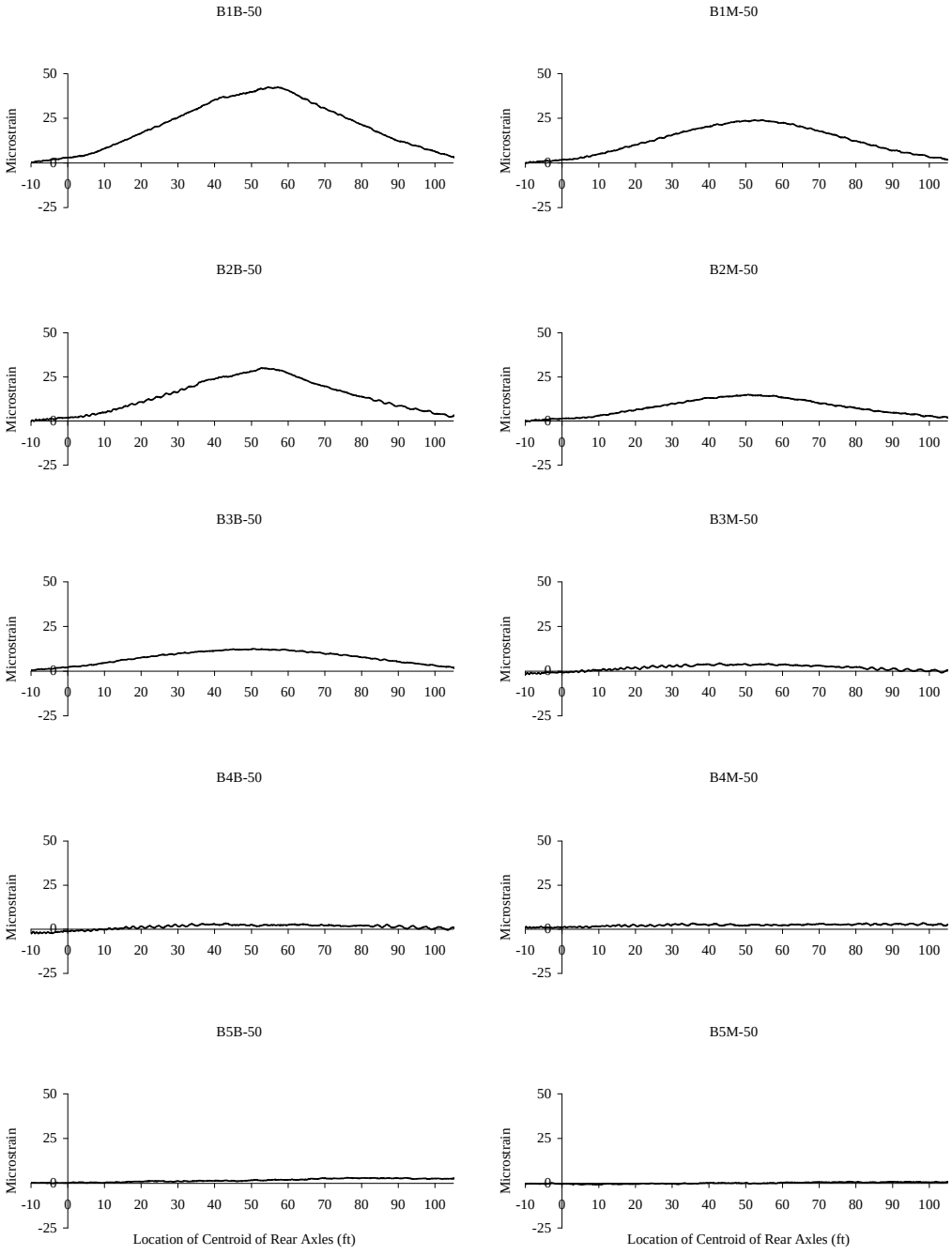

Figure A.4 Strains for the Mid-Span Girder Gages, Test Series 1, Run 7

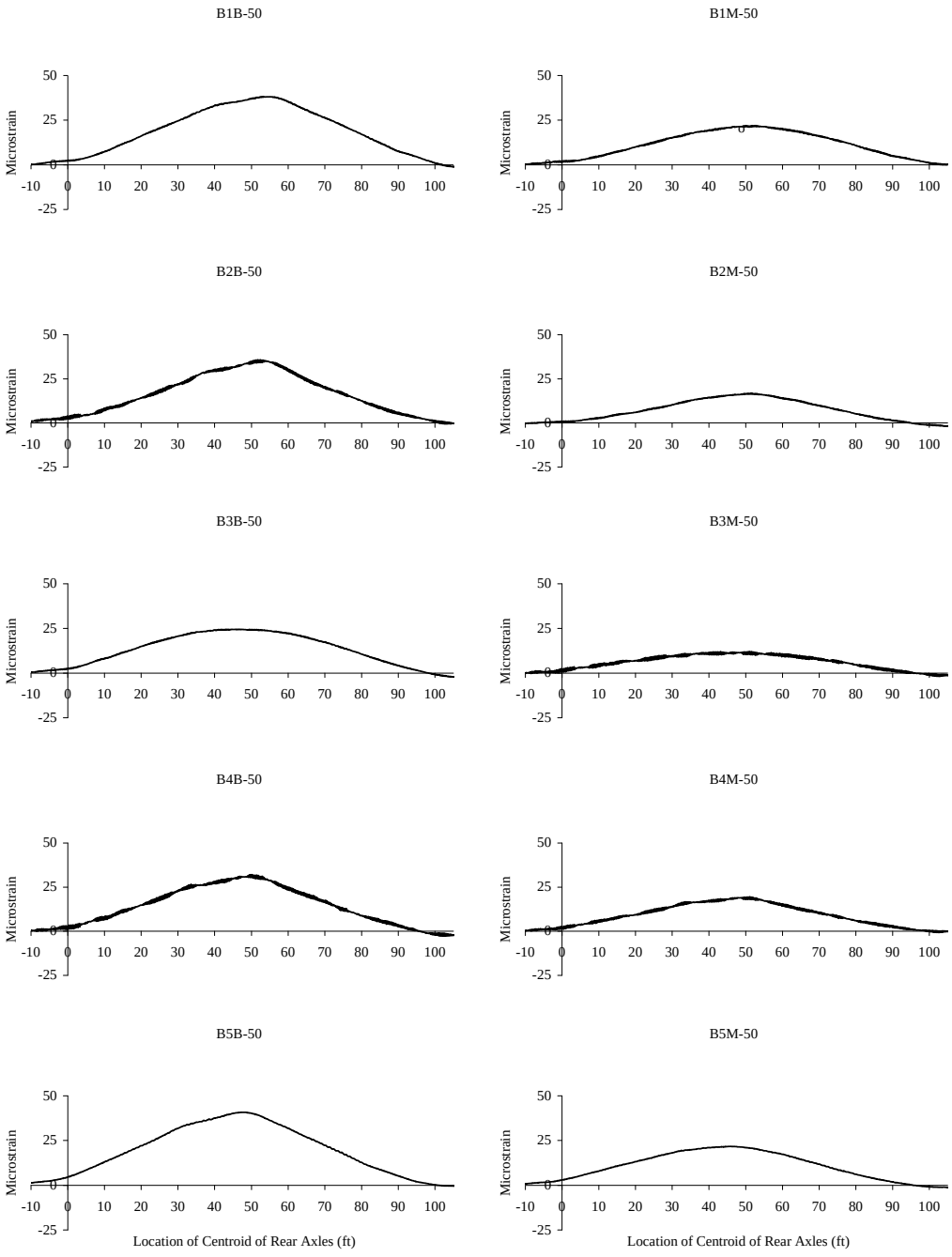

Figure A.5 Strains for the Mid-Span Girder Gages, Test Series 1, Run 9

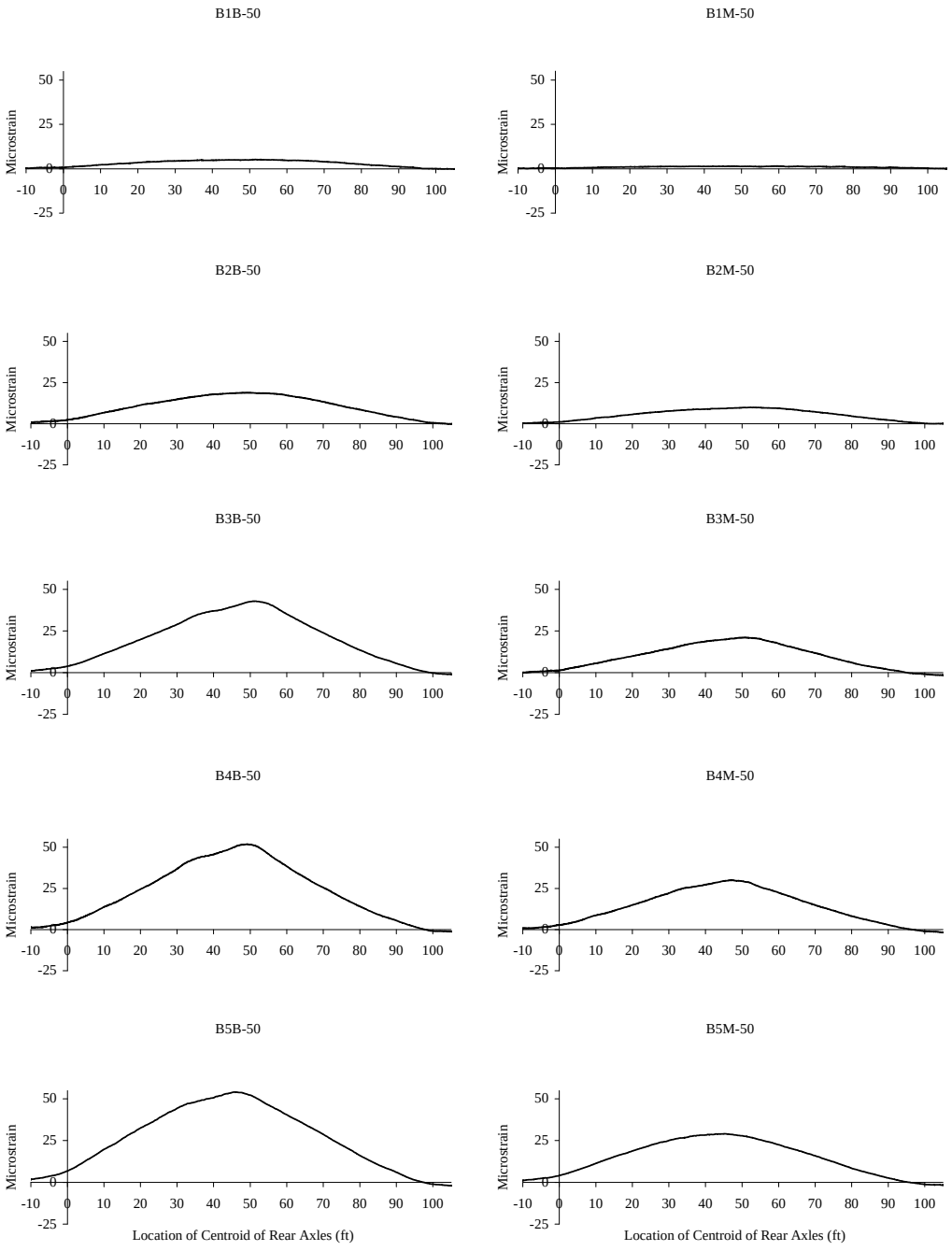

Figure A.6 Strains for the Mid-Span Girder Gages, Test Series 1, Run 11

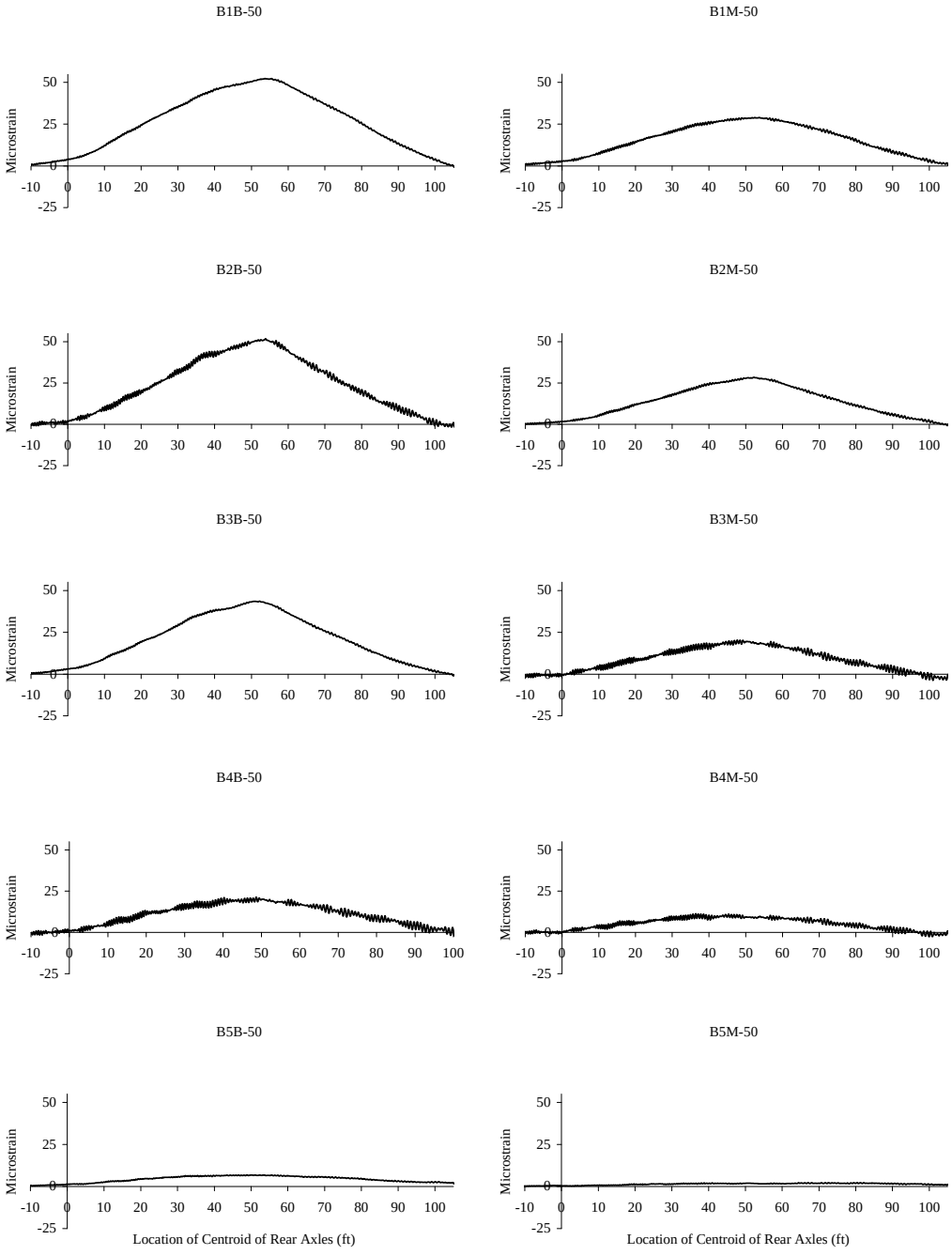

Figure A.7 Strains for the Mid-Span Girder Gages, Test Series 1, Run 13

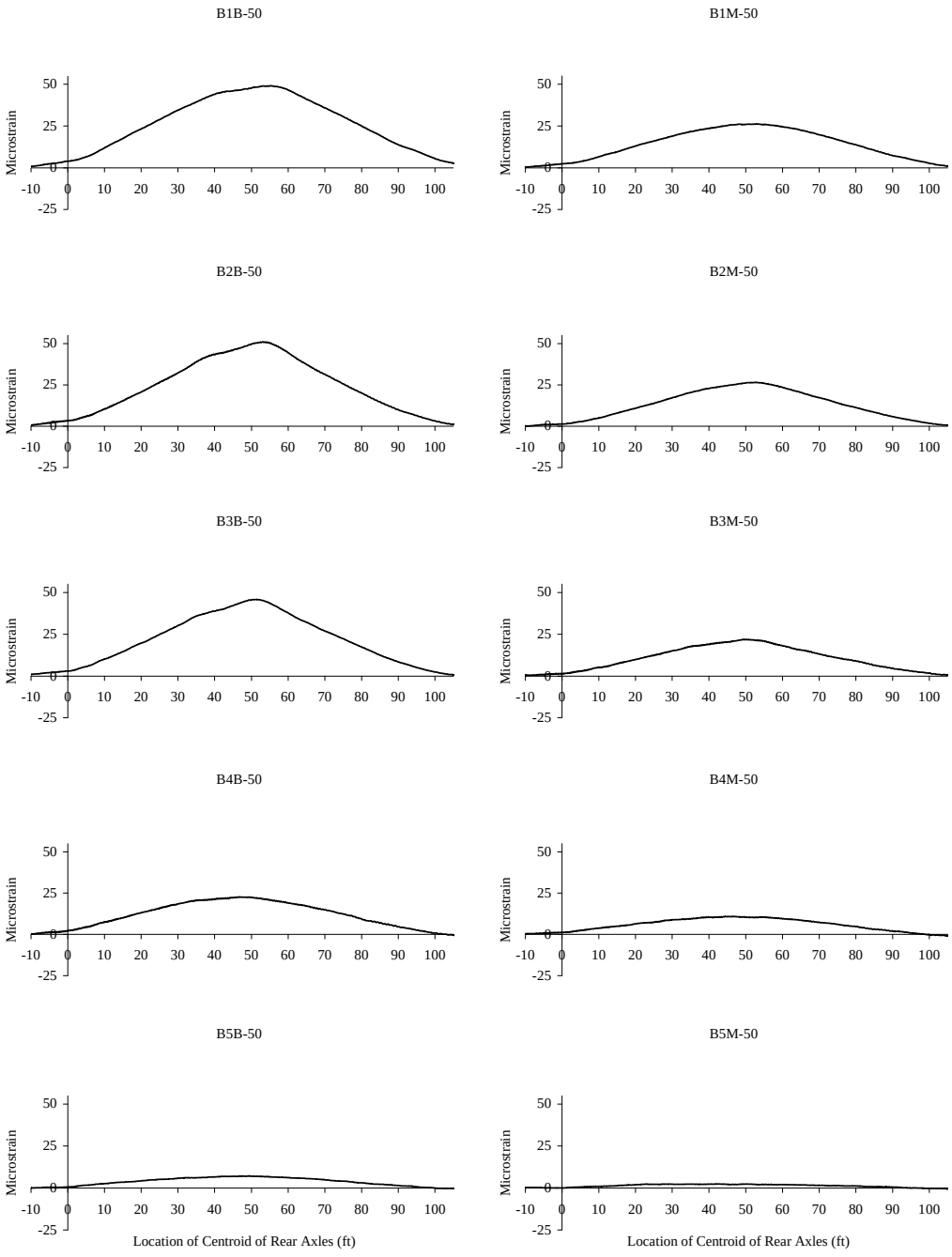

Figure A.8 Strains for the Mid-Span Girder Gages, Test Series 1, Run 14

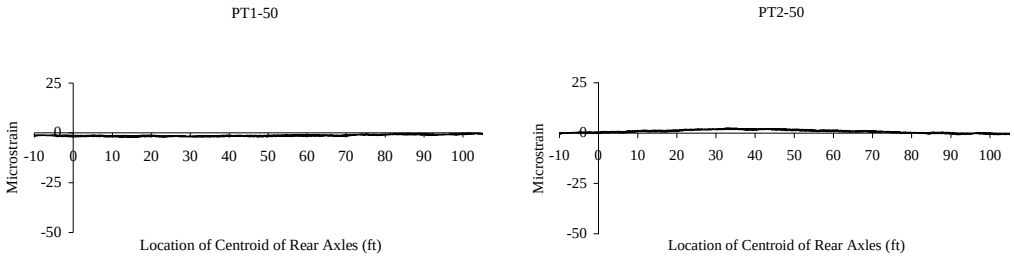

Figure A.9 Strains for the Mid-Span Parapet Gages, Test Series 1, Run 1

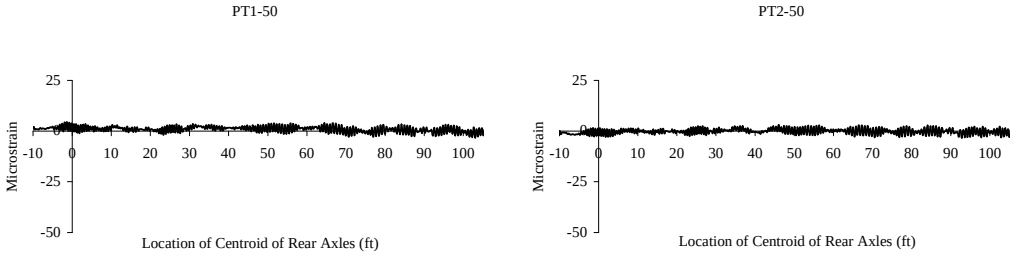

Figure A.10 Strains for the Mid-Span Parapet Gages, Test Series 1, Run 4

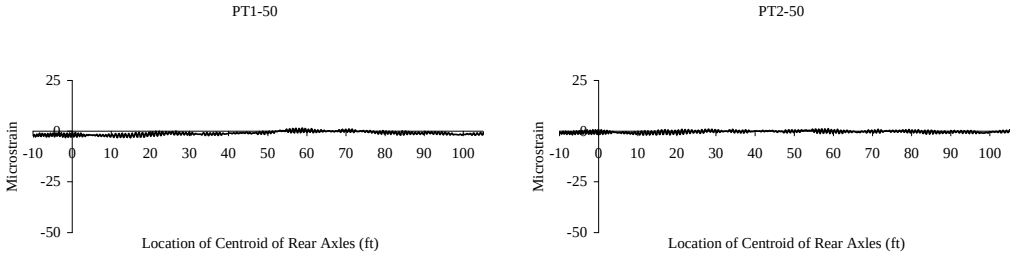

Figure A.11 Strains for the Mid-Span Parapet Gages, Test Series 1, Run 6

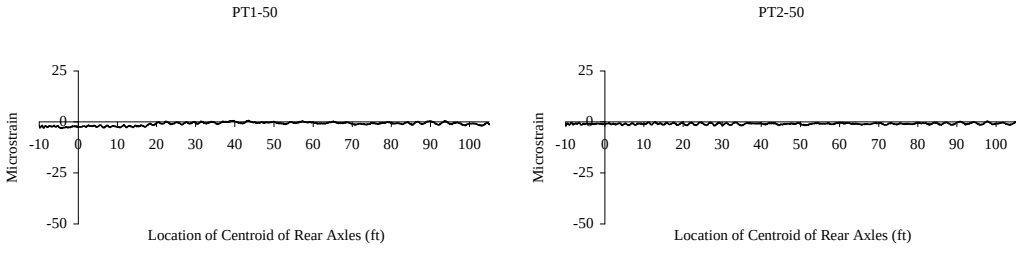

Figure A.12 Strains for the Mid-Span Parapet Gages, Test Series 1, Run 7

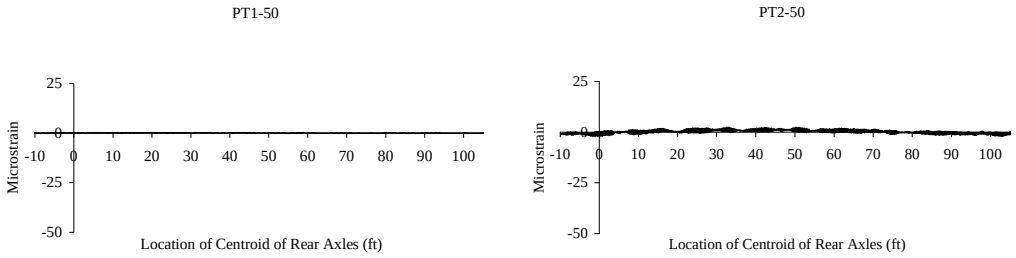

Figure A.13 Strains for the Mid-Span Parapet Gages, Test Series 1, Run 9

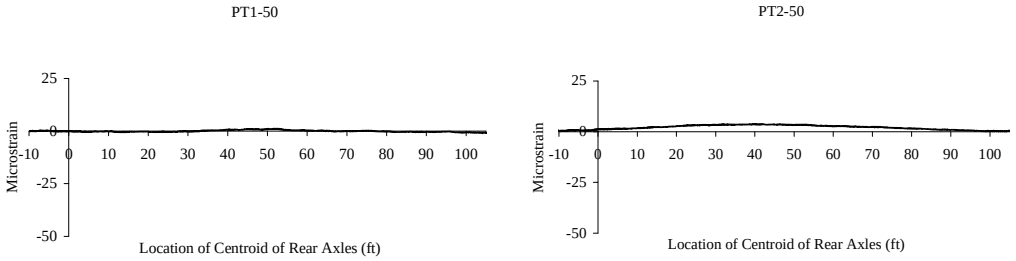

Figure A.14 Strains for the Mid-Span Parapet Gages, Test Series 1, Run 11

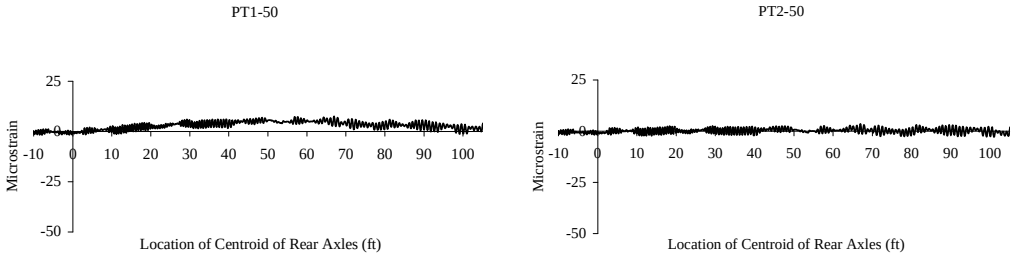

Figure A.15 Strains for the Mid-Span Parapet Gages, Test Series 1, Run 13

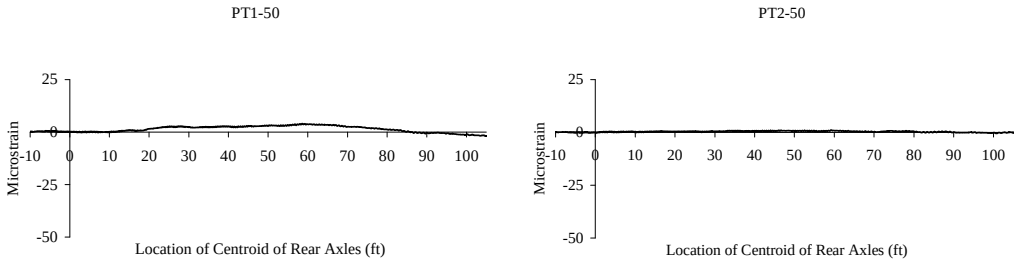

Figure A.16 Strains for the Mid-Span Parapet Gages, Test Series 1, Run 14

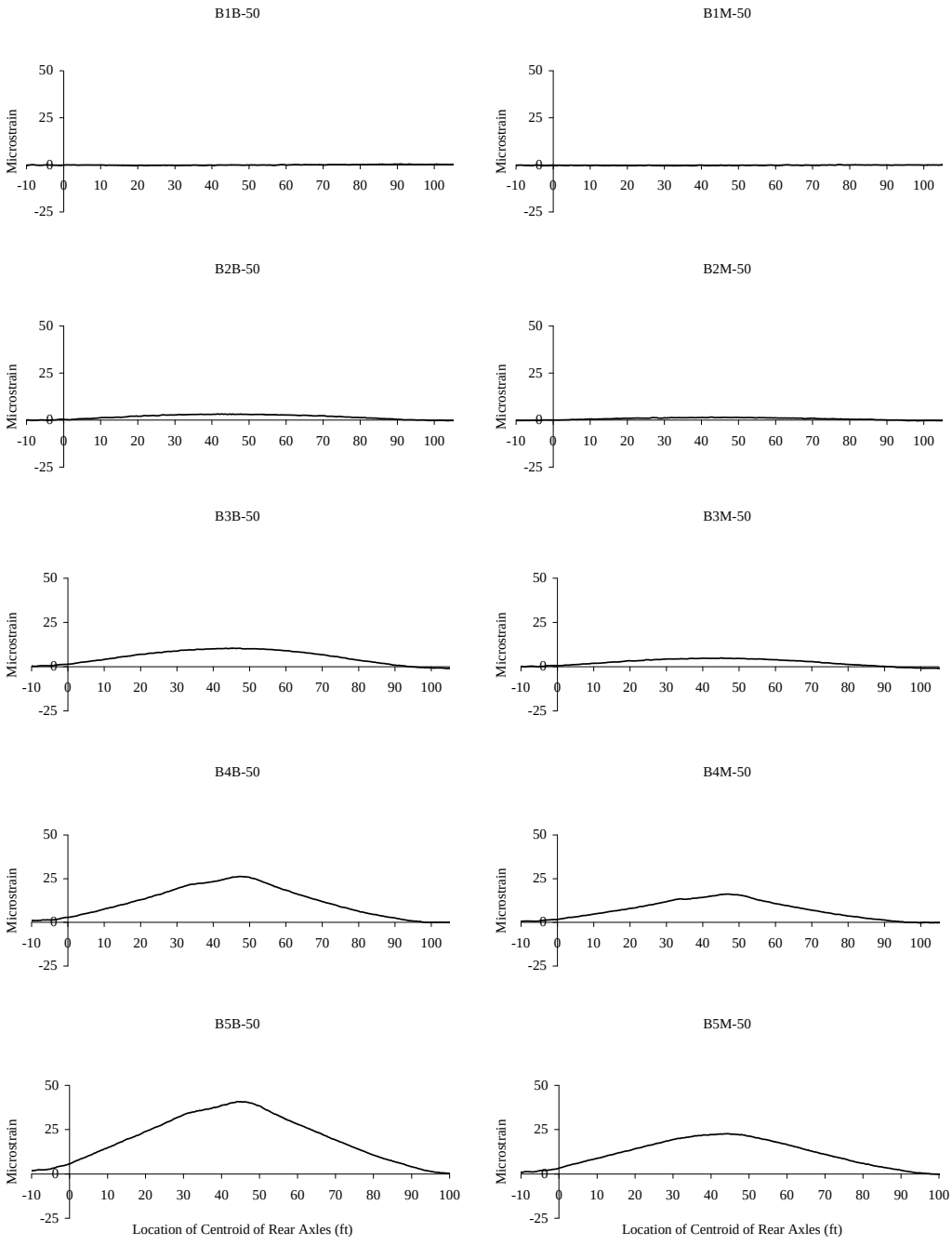

Figure A.17 Strains for the Mid-Span Girder Gages, Test Series 2, Run 15

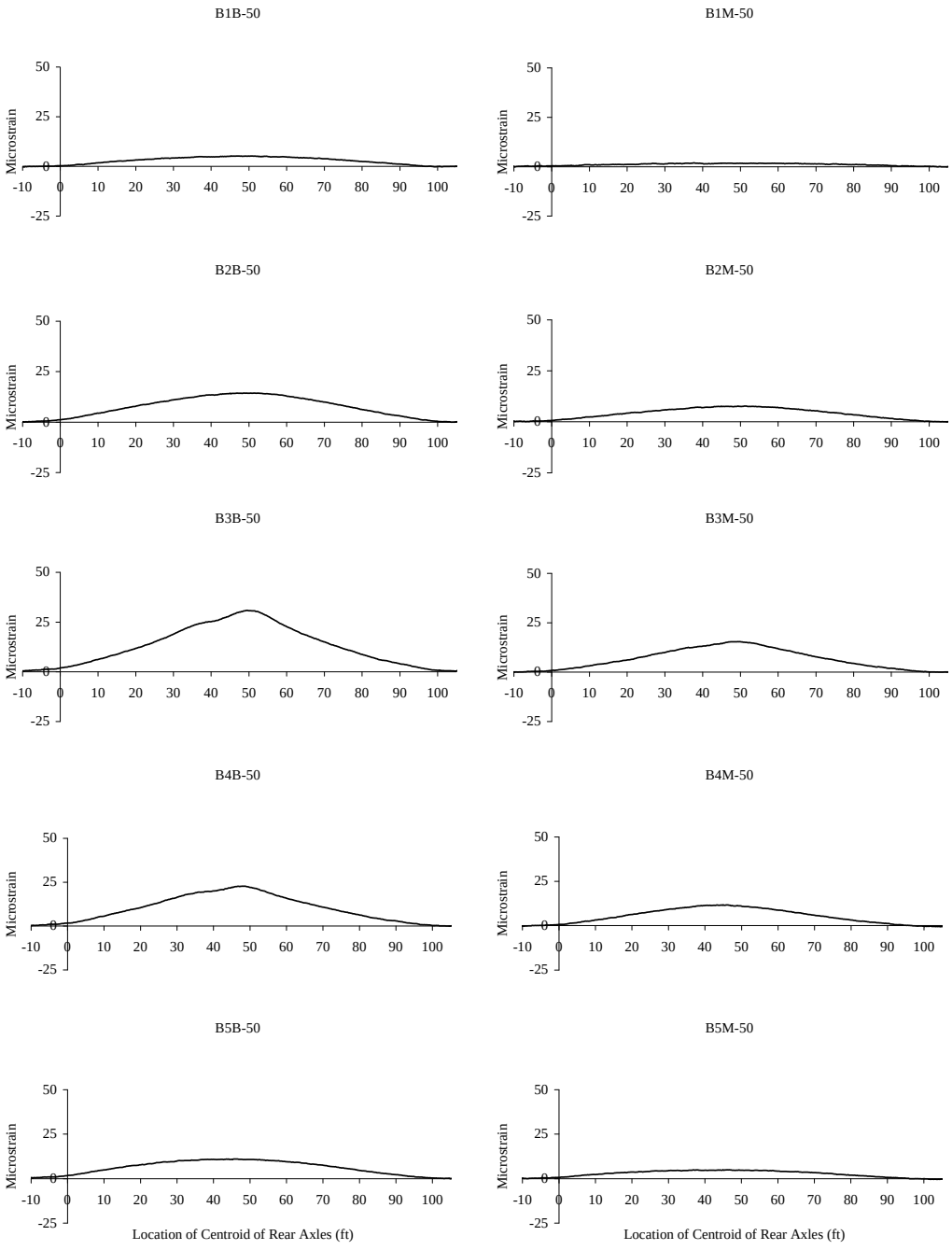

Figure A.18 Strains for the Mid-Span Girder Gages, Test Series 2, Run 17

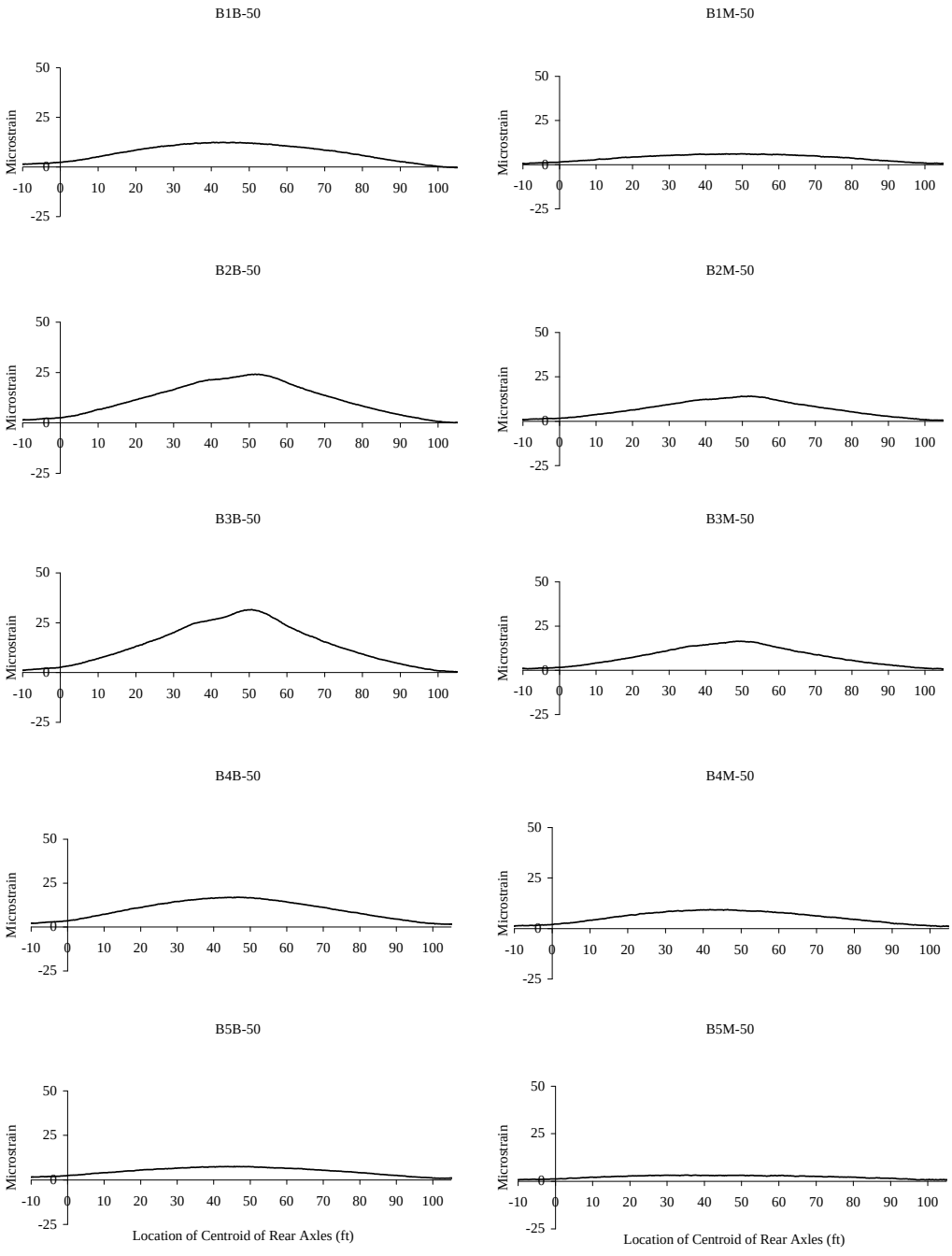

Figure A.19 Strains for the Mid-Span Girder Gages, Test Series 2, Run 19

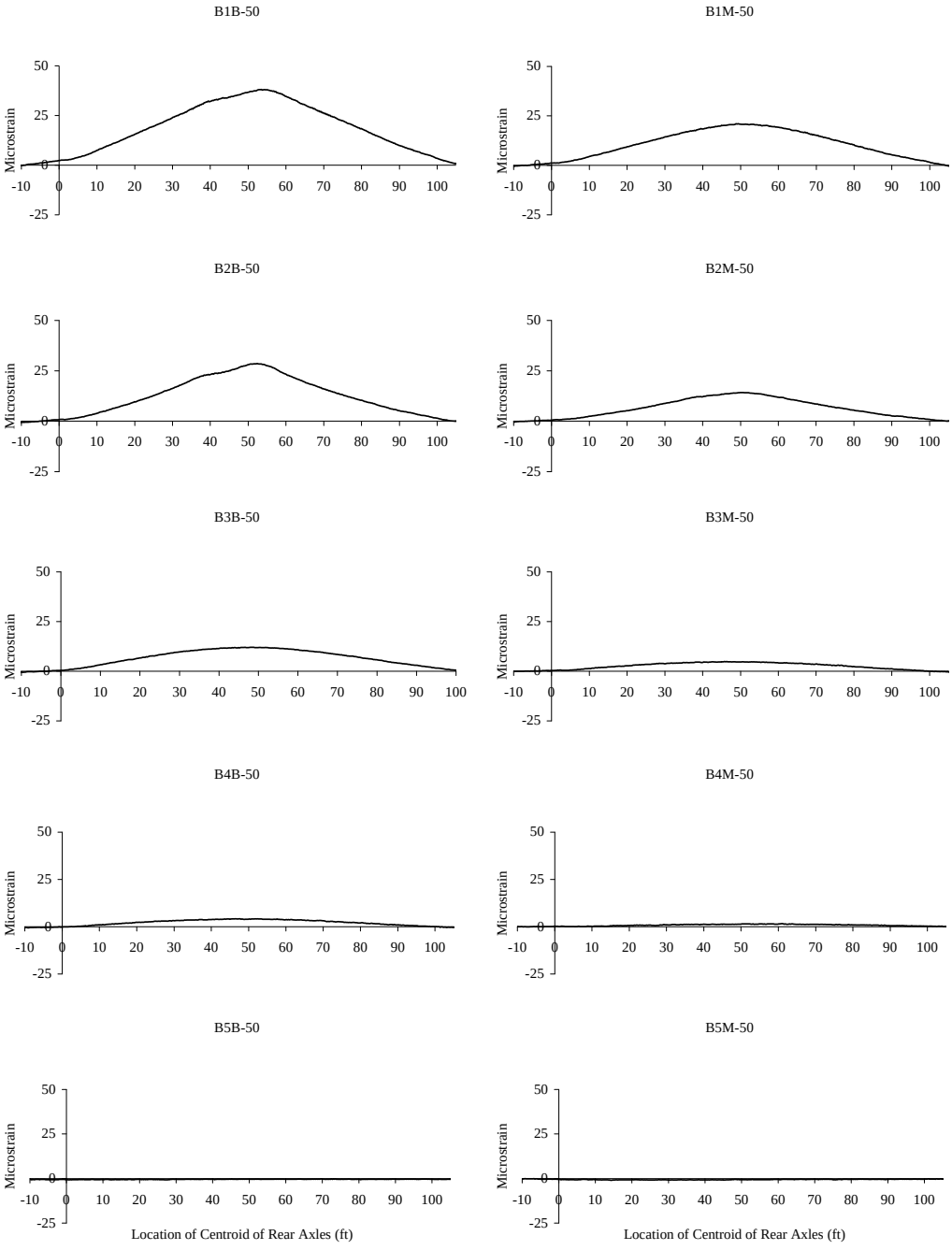

Figure A.20 Strains for the Mid-Span Girder Gages, Test Series 2, Run 21

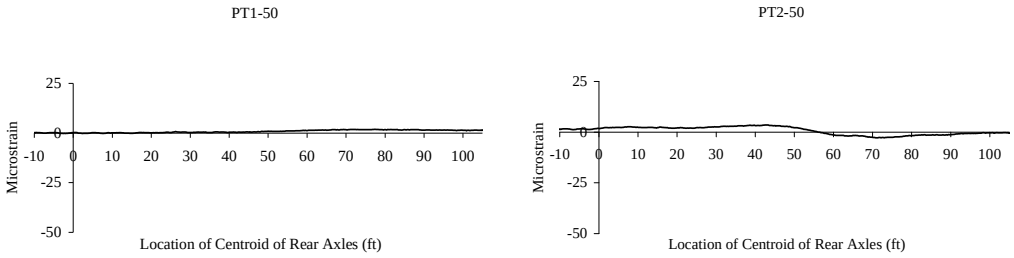

Figure A.21 Strains for the Mid-Span Parapet Gages, Test Series 2, Run 15

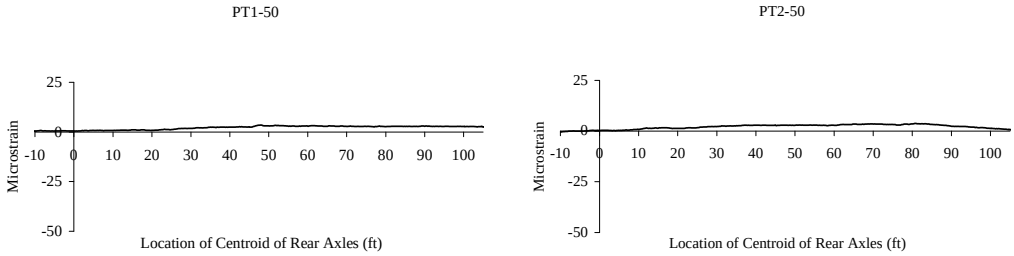

Figure A.22 Strains for the Mid-Span Parapet Gages, Test Series 2, Run 17

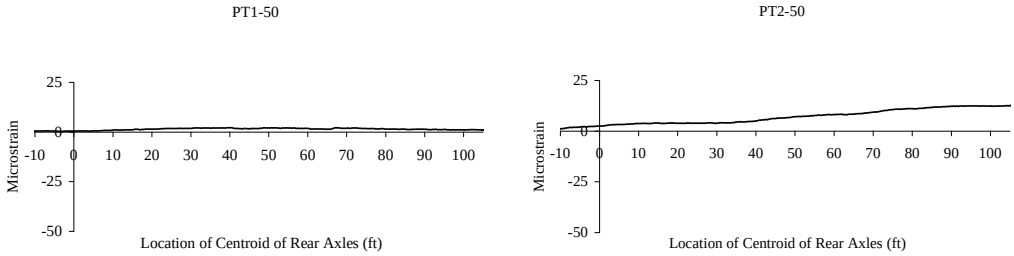

Figure A.23 Strains for the Mid-Span Parapet Gages, Test Series 2, Run 19

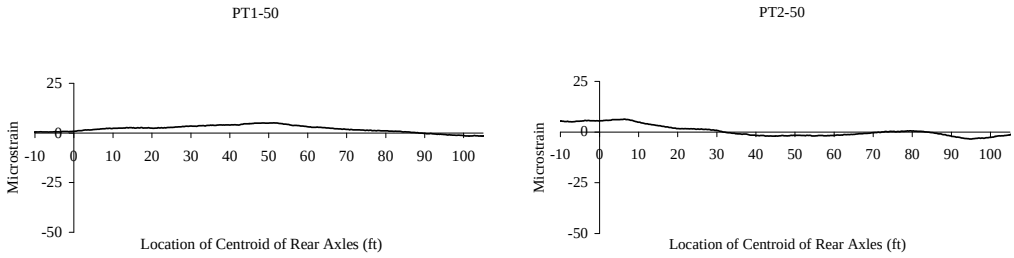

Figure A.24 Strains for the Mid-Span Parapet Gages, Test Series 2, Run 21

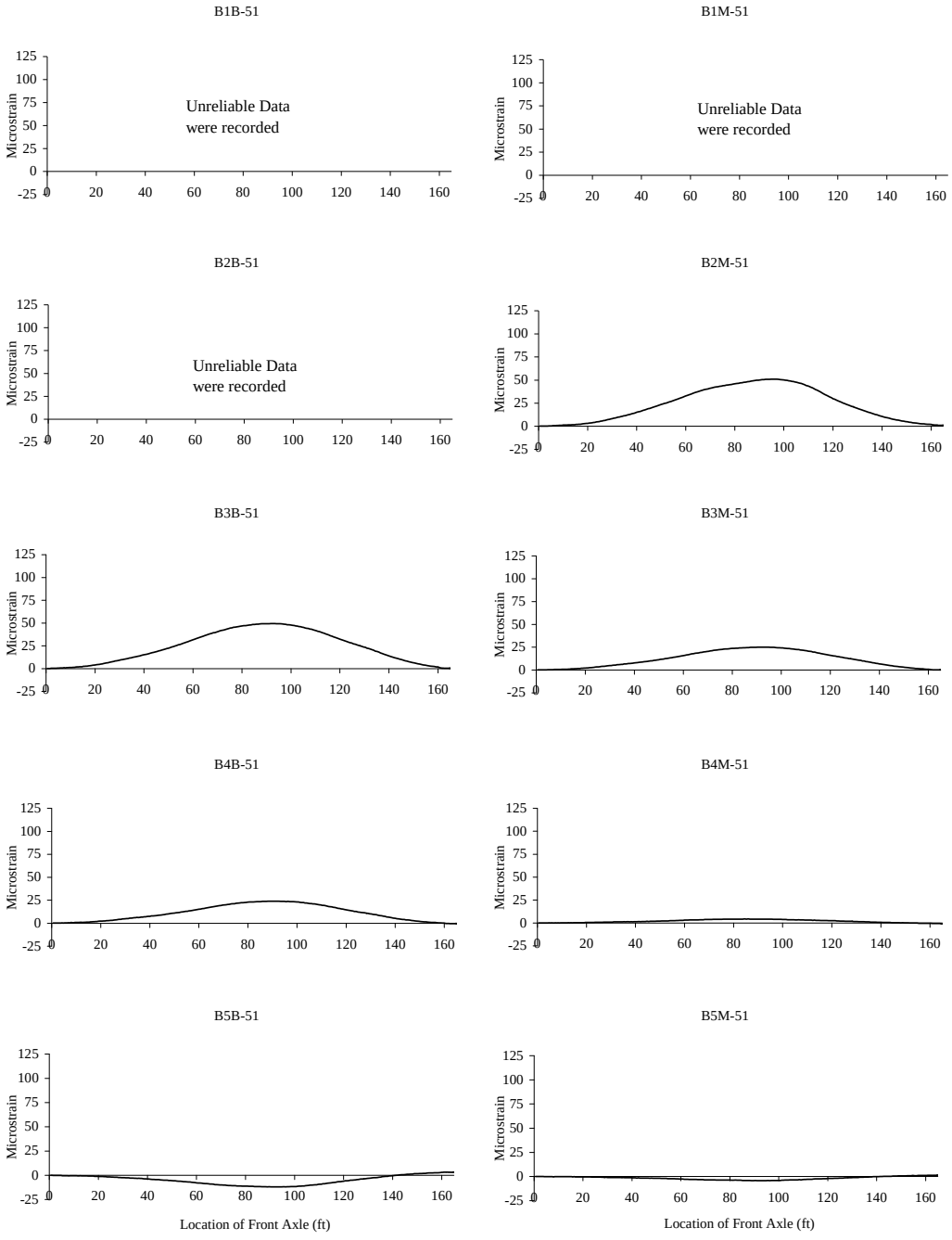

Figure A.25 Strains for the Mid-Span Girder Gages, Test Series 3, Run 23

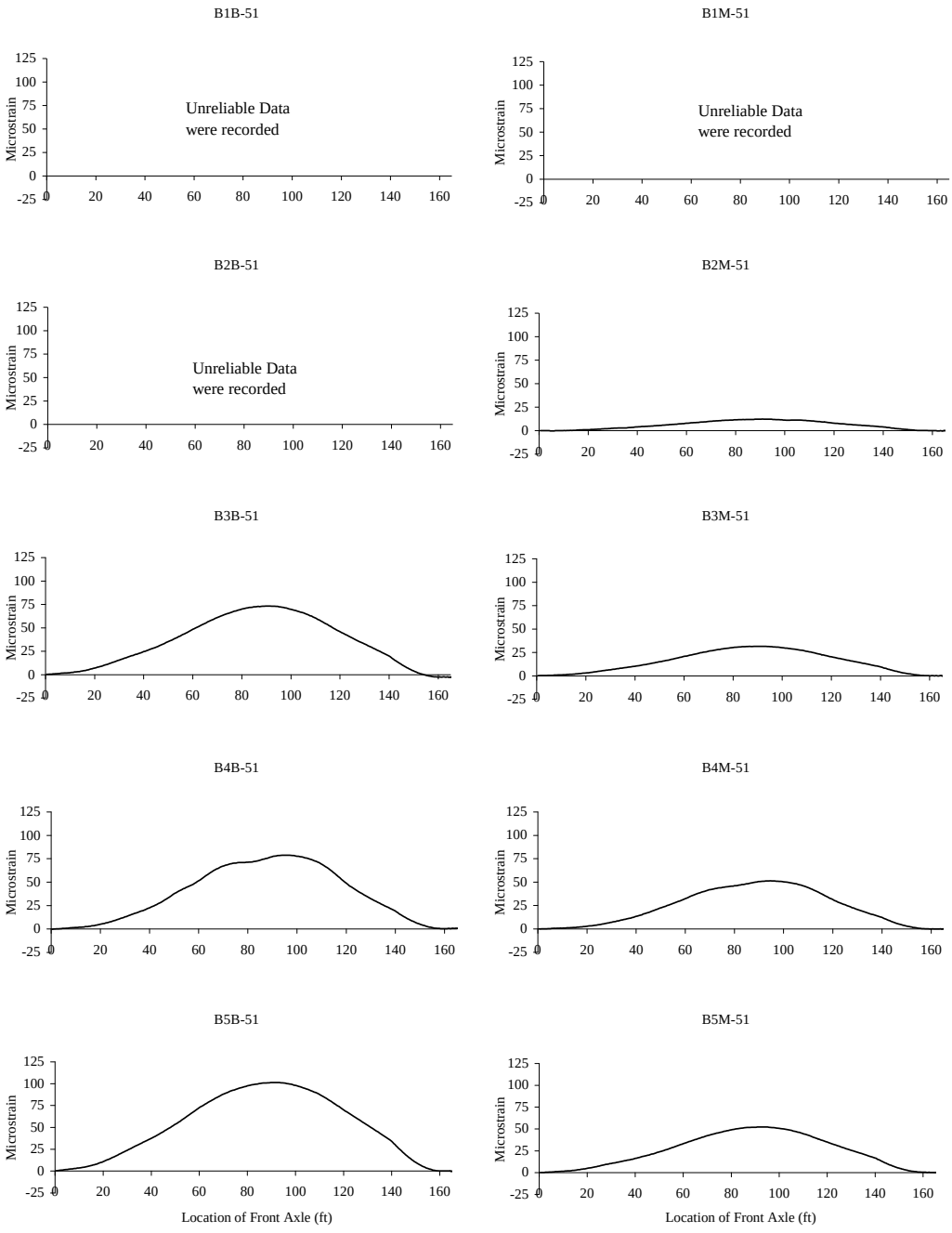

Figure A.26 Strains for the Mid-Span Girder Gages, Test Series 3, Run 24

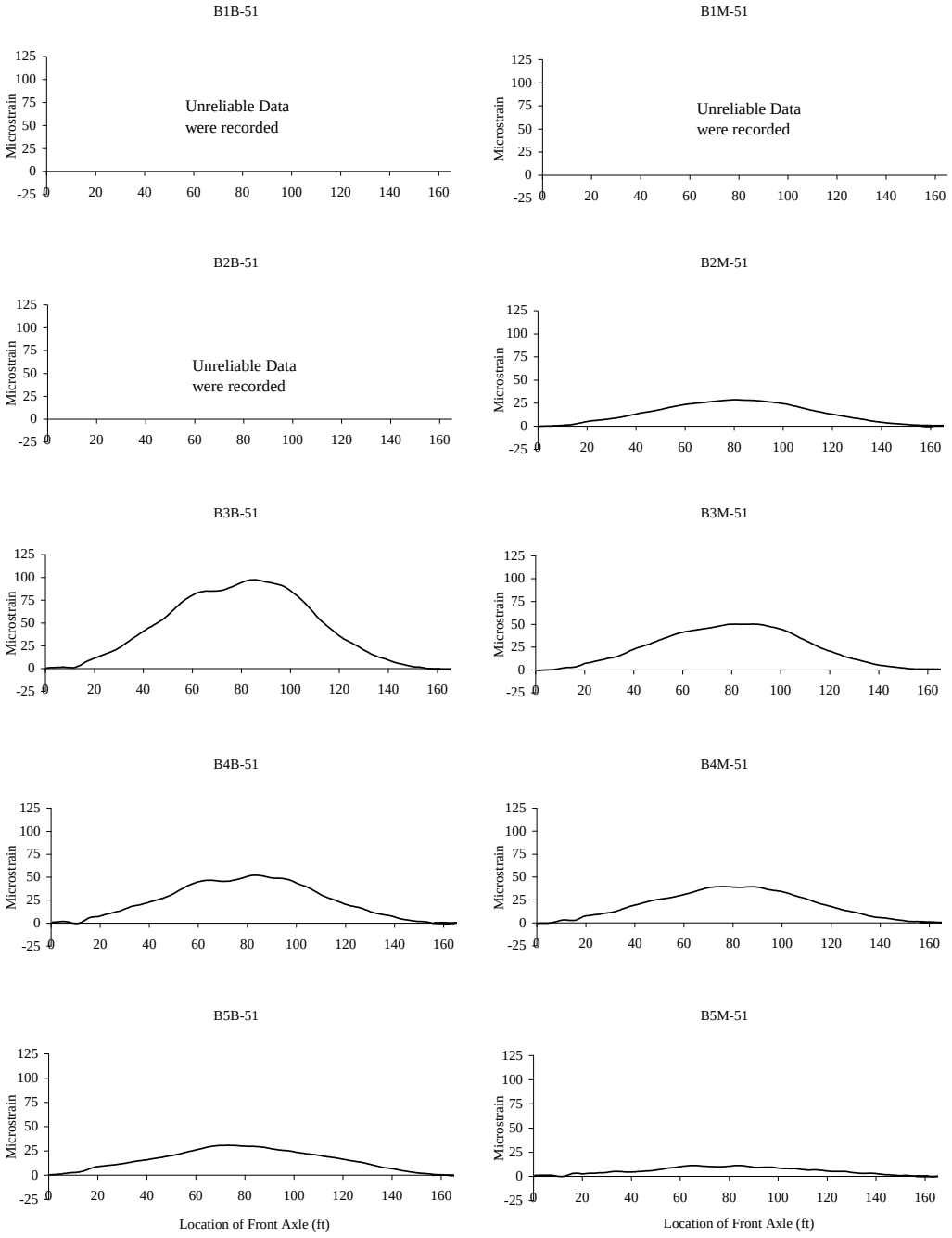

Figure A.27 Strains for the Mid-Span Girder Gages, Test Series 3, Run 25

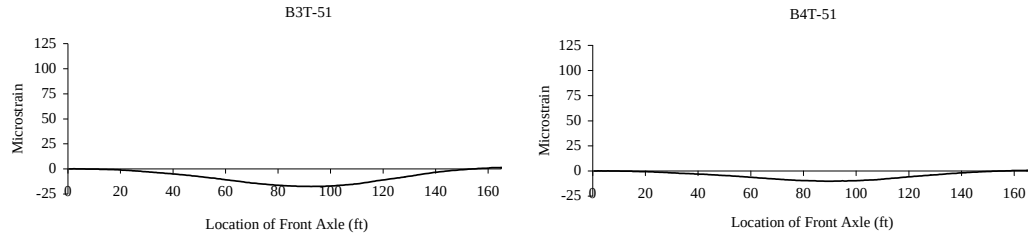

Figure A.28 Strains for the Mid-Span Top Gages, Test Series 3, Run 23

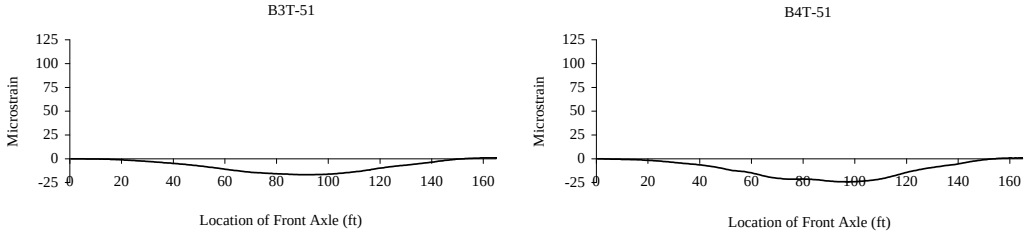

Figure A.29 Strains for the Mid-Span Top Gages, Test Series 3, Run 24

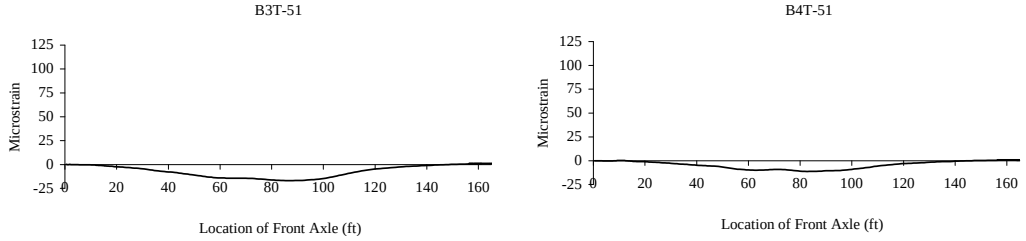

Figure A.30 Strains for the Mid-Span Top Gages, Test Series 3, Run 25

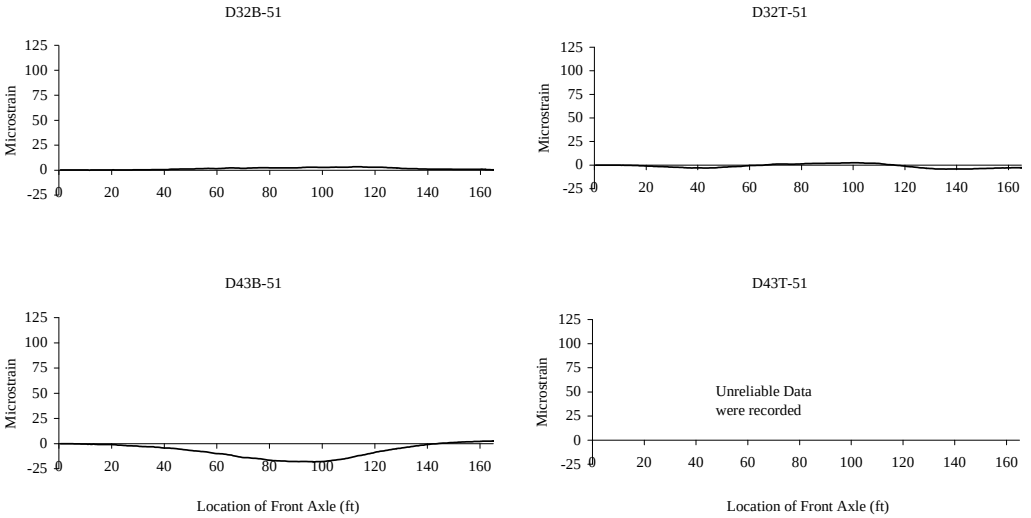

Figure A.31 Strains for Mid-Span Diaphragm Gages, Test Series 3, Run 23

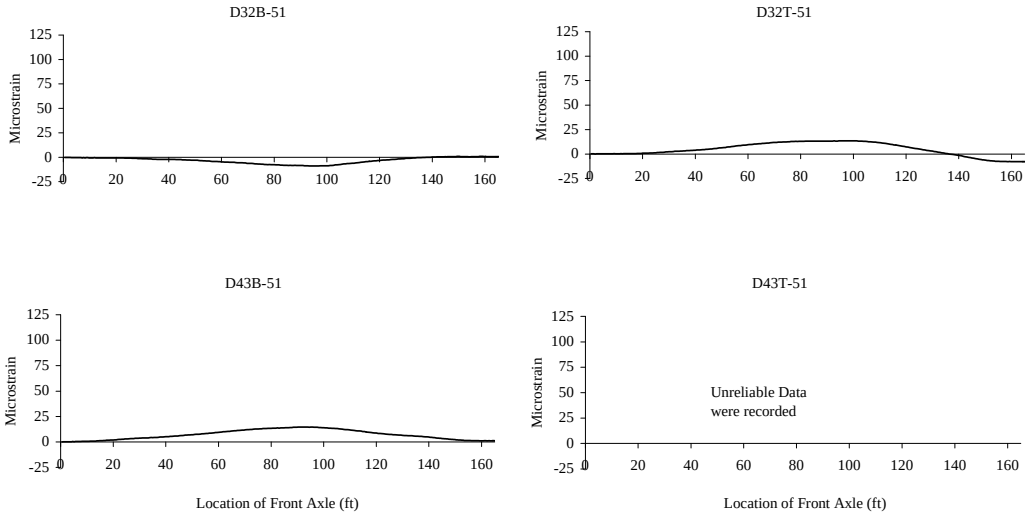

Figure A.32 Strains for Mid-Span Diaphragm Gages, Test Series 3, Run 24

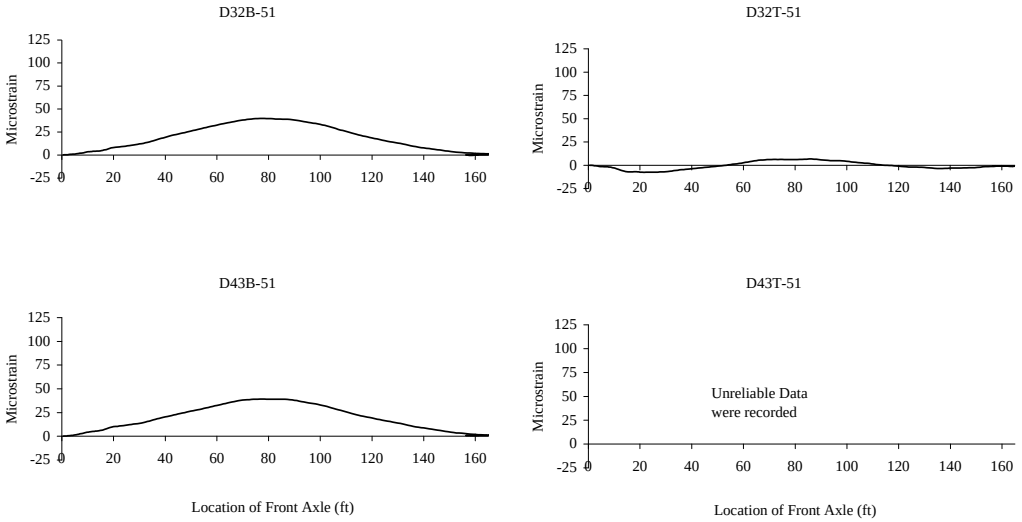

Figure A.33 Strains for Mid-Span Diaphragm Gages, Test Series 3, Run 25

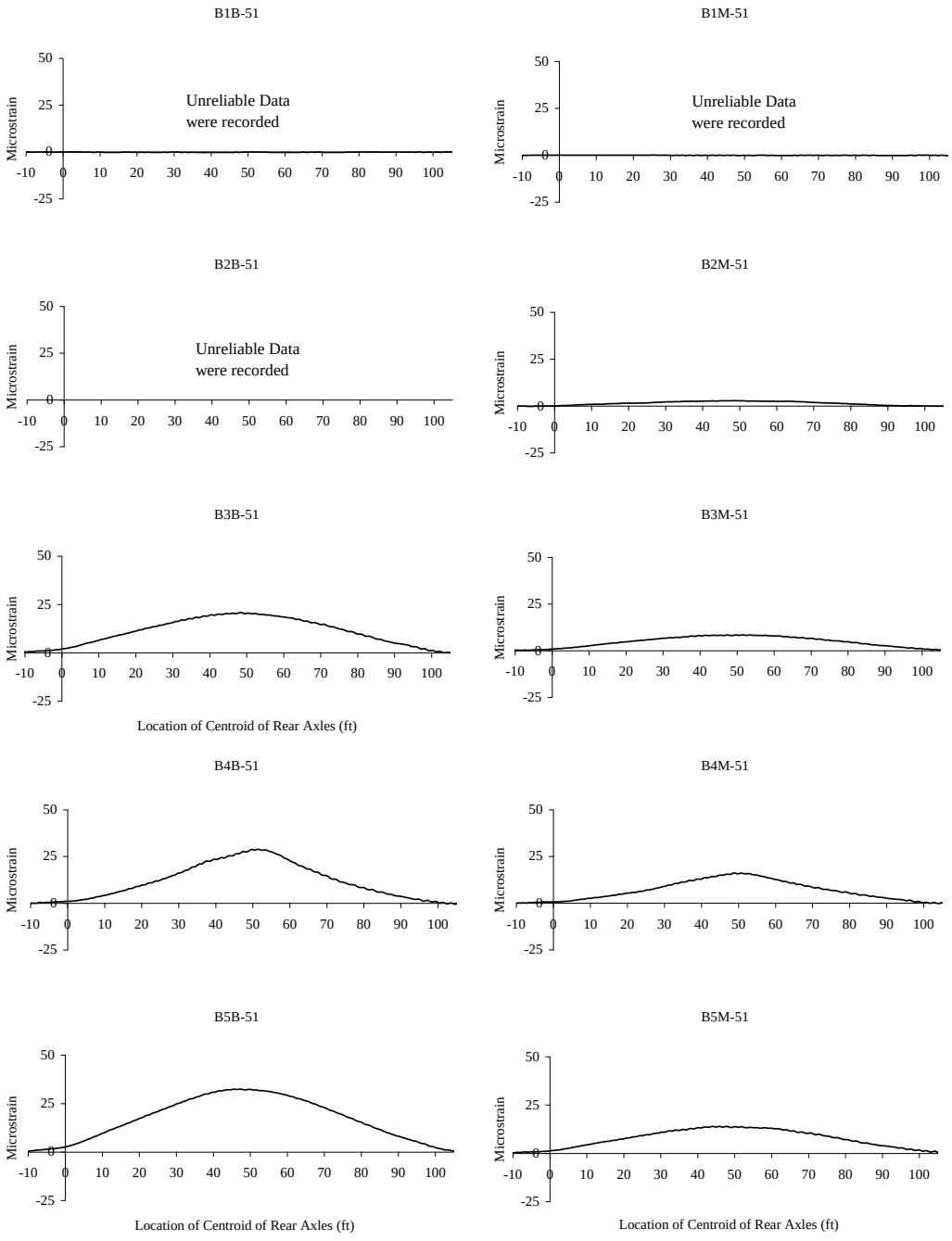

Figure A.34 Strains for the Mid-Span Girder Gages, Test Series 3, Run 28

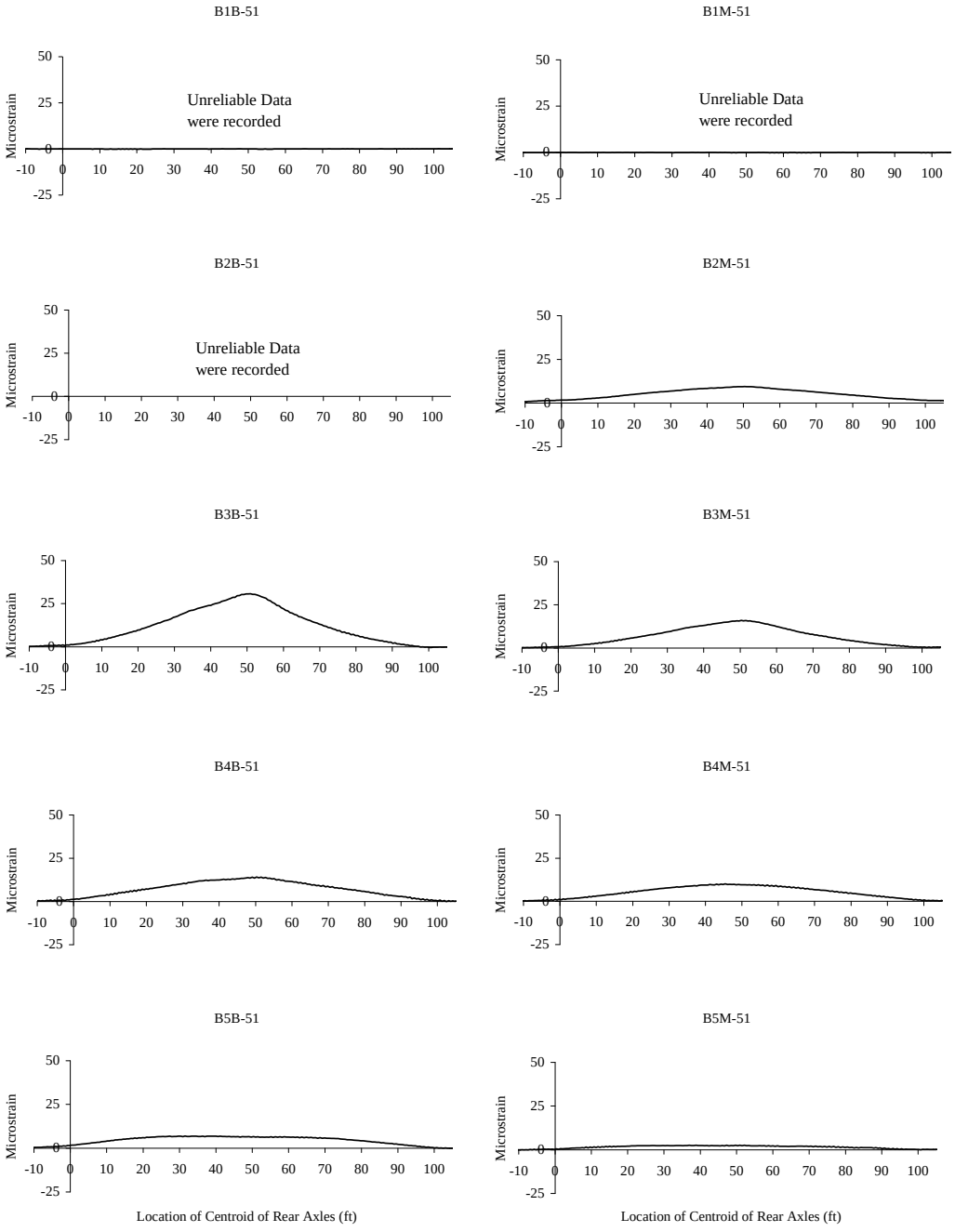

Figure A.35 Strains for the Mid-Span Girder Gages, Test Series 3, Run 30

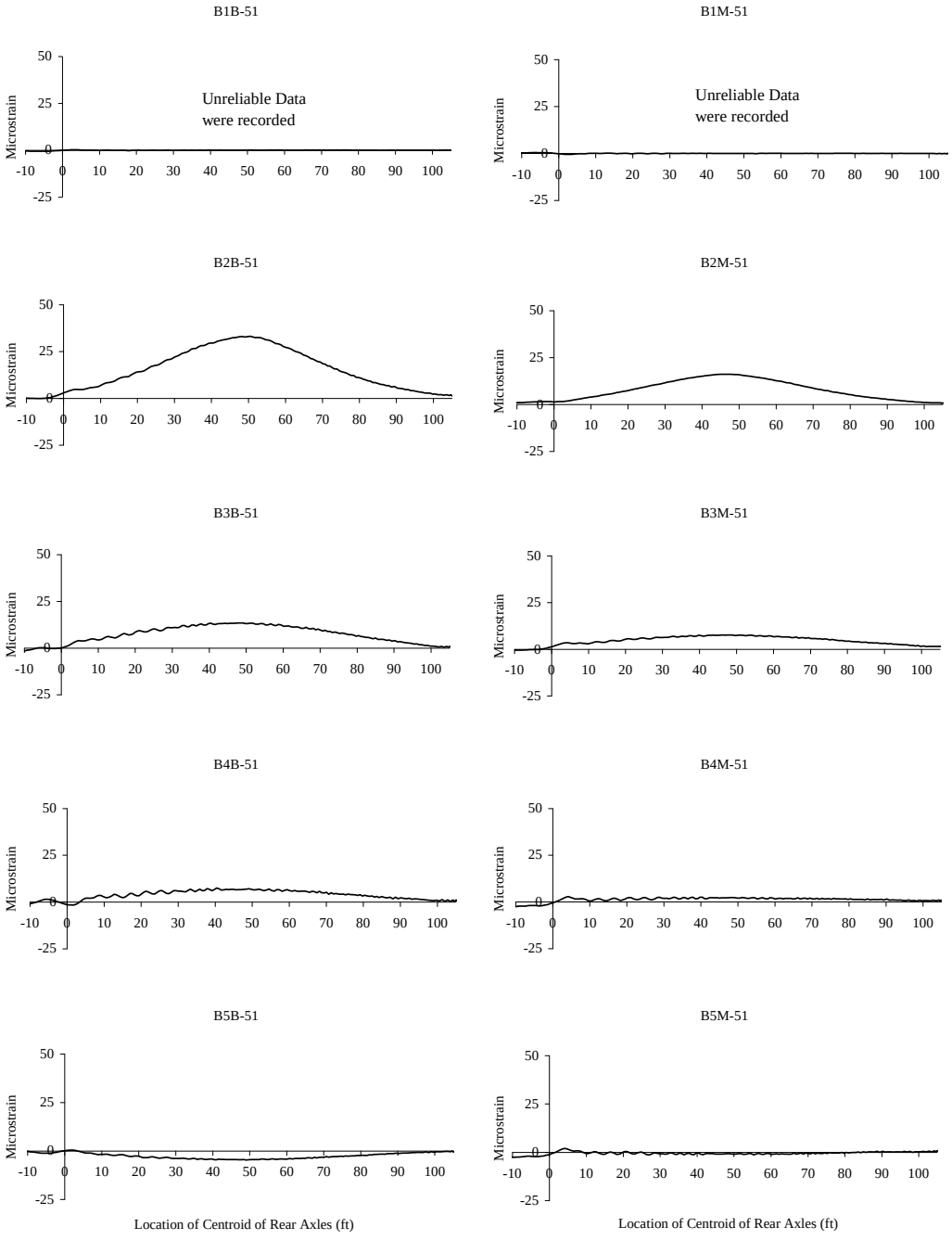

Figure A.36 Strains for the Mid-Span Girder Gages, Test Series 3, Run 32

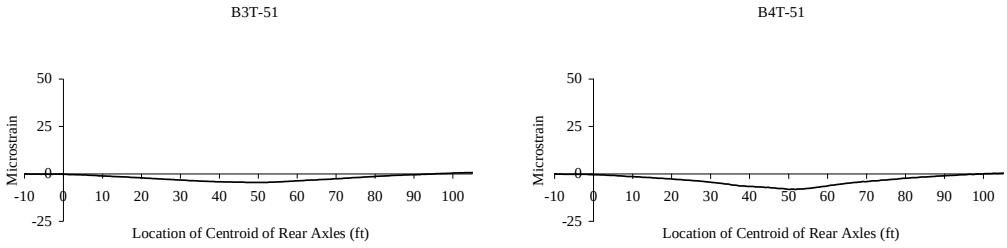

Figure A.37 Strains for the Mid-Span Top Gages, Test Series 3, Run 28

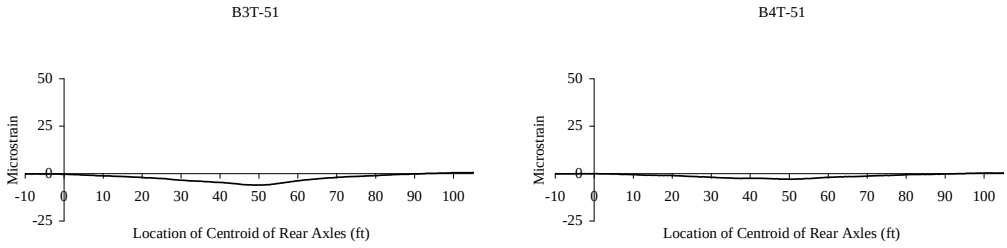

Figure A.38 Strains for the Mid-Span Top Gages, Test Series 3, Run 30

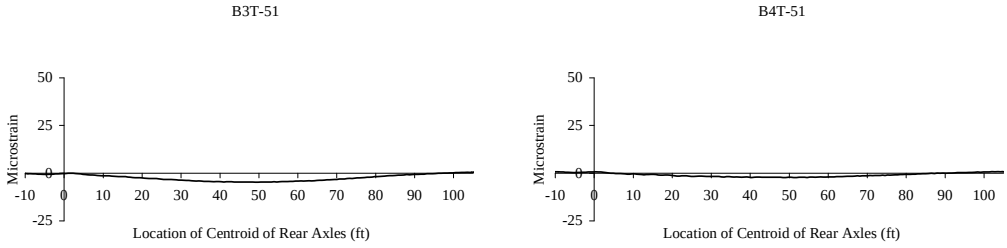

Figure A.39 Strains for the Mid-Span Top Gages, Test Series 3, Run 32

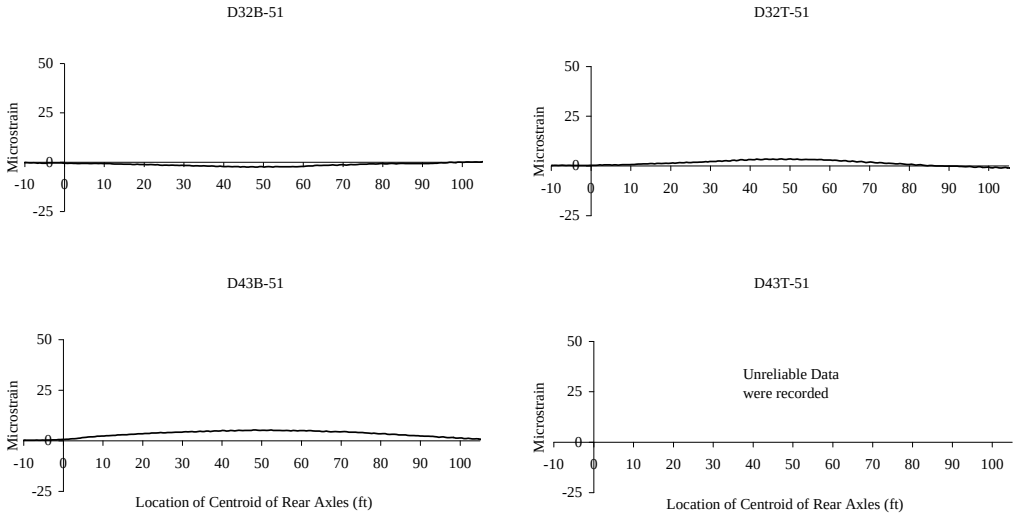

Figure A.40 Strains for Mid-Span Diaphragm Gages, Test Series 3, Run 28

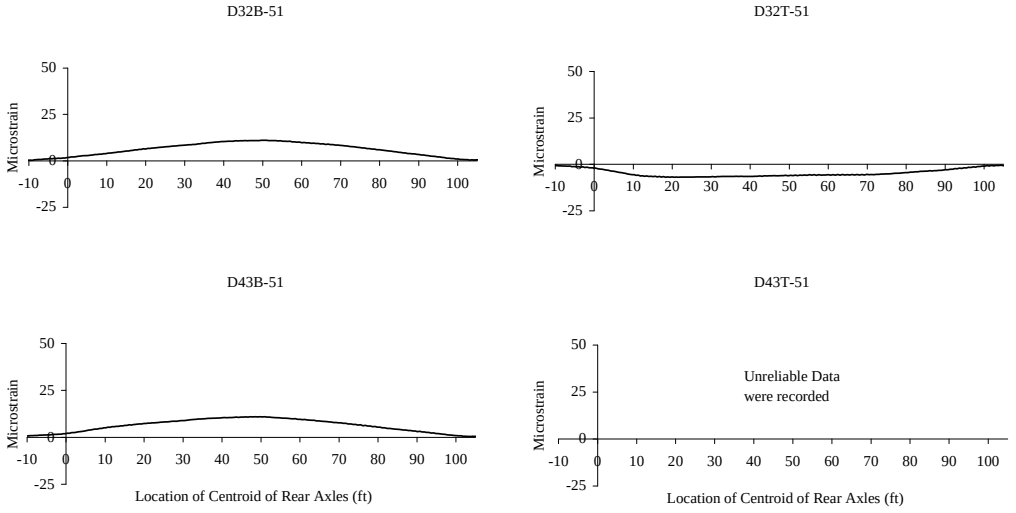

Figure A.41 Strains for Mid-Span Diaphragm Gages, Test Series 3, Run 30

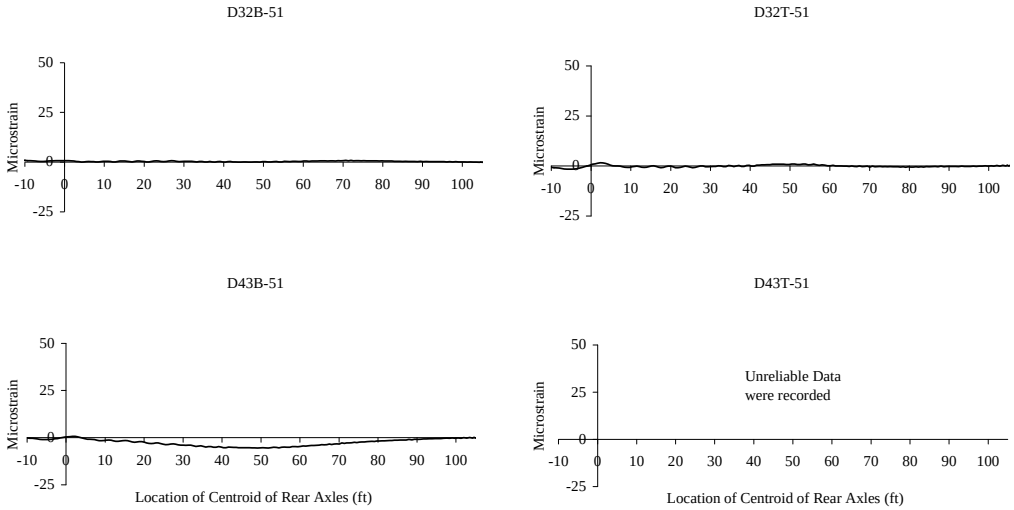

Figure A.42 Strains for Mid-Span Diaphragm Gages, Test Series 3, Run 32

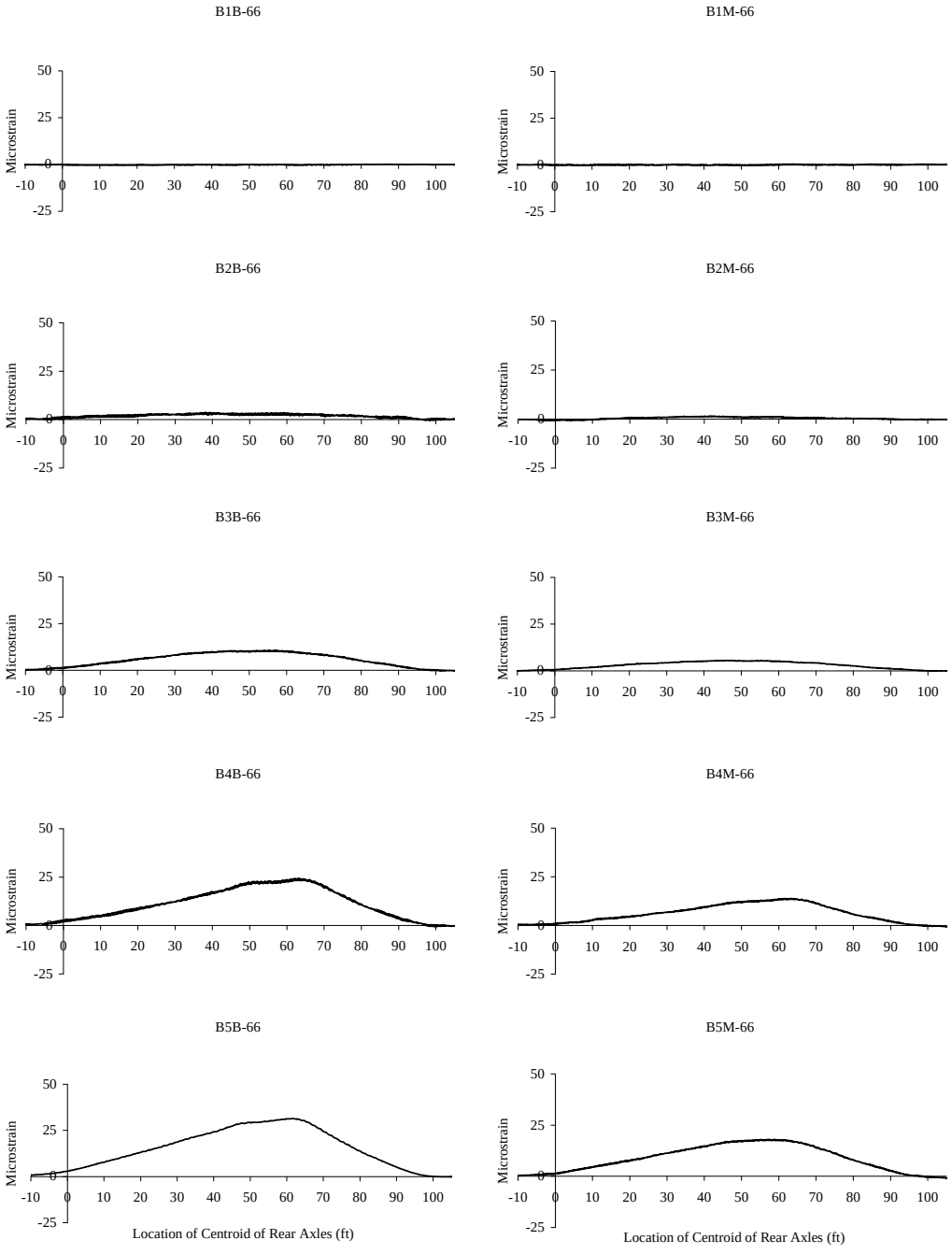

Figure A.43 Strains for the 66.7-ft. Girder Gages, Test Series 1, Run 1

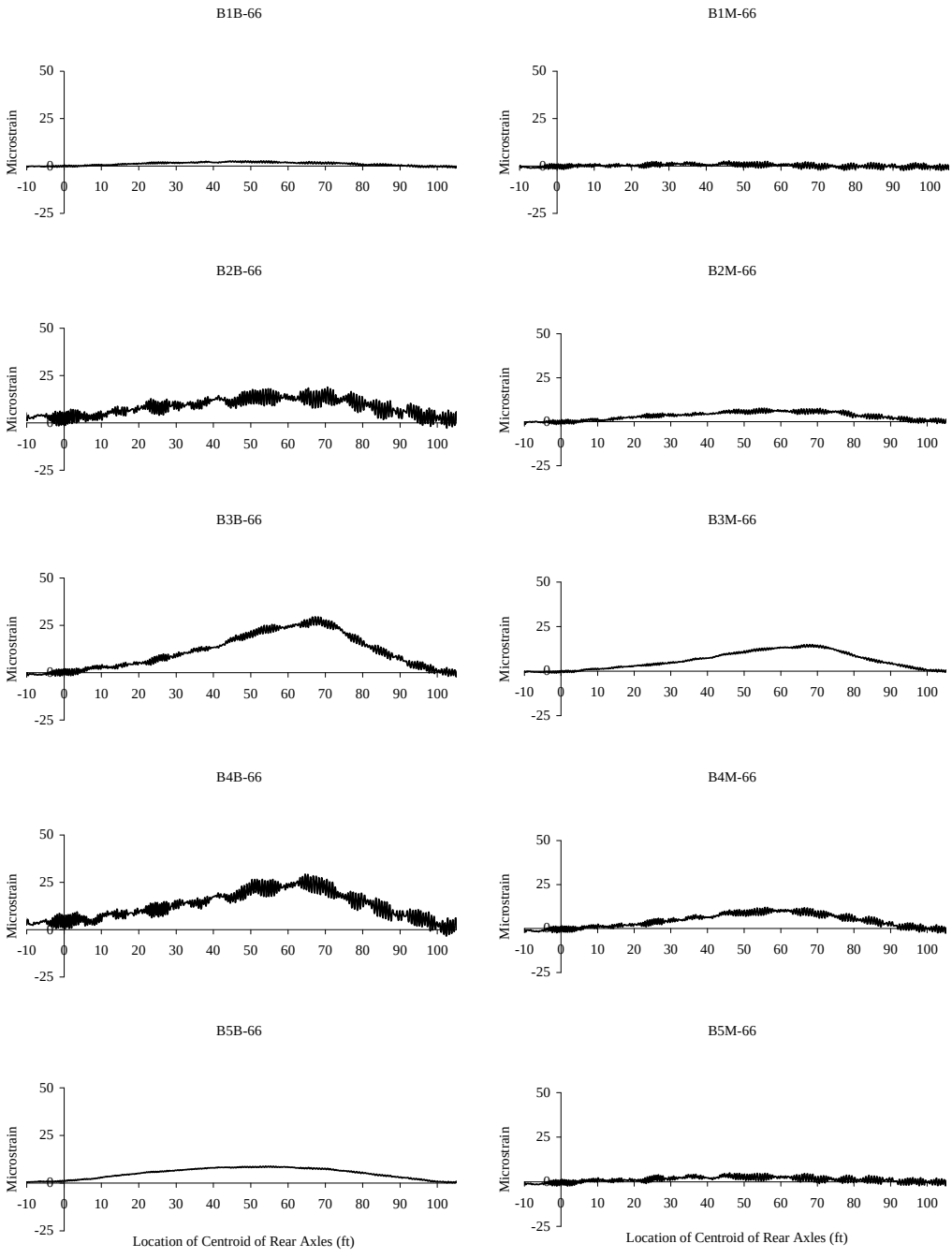

Figure A.44 Strains for the 66.7-ft. Girder Gages, Test Series 1, Run 4

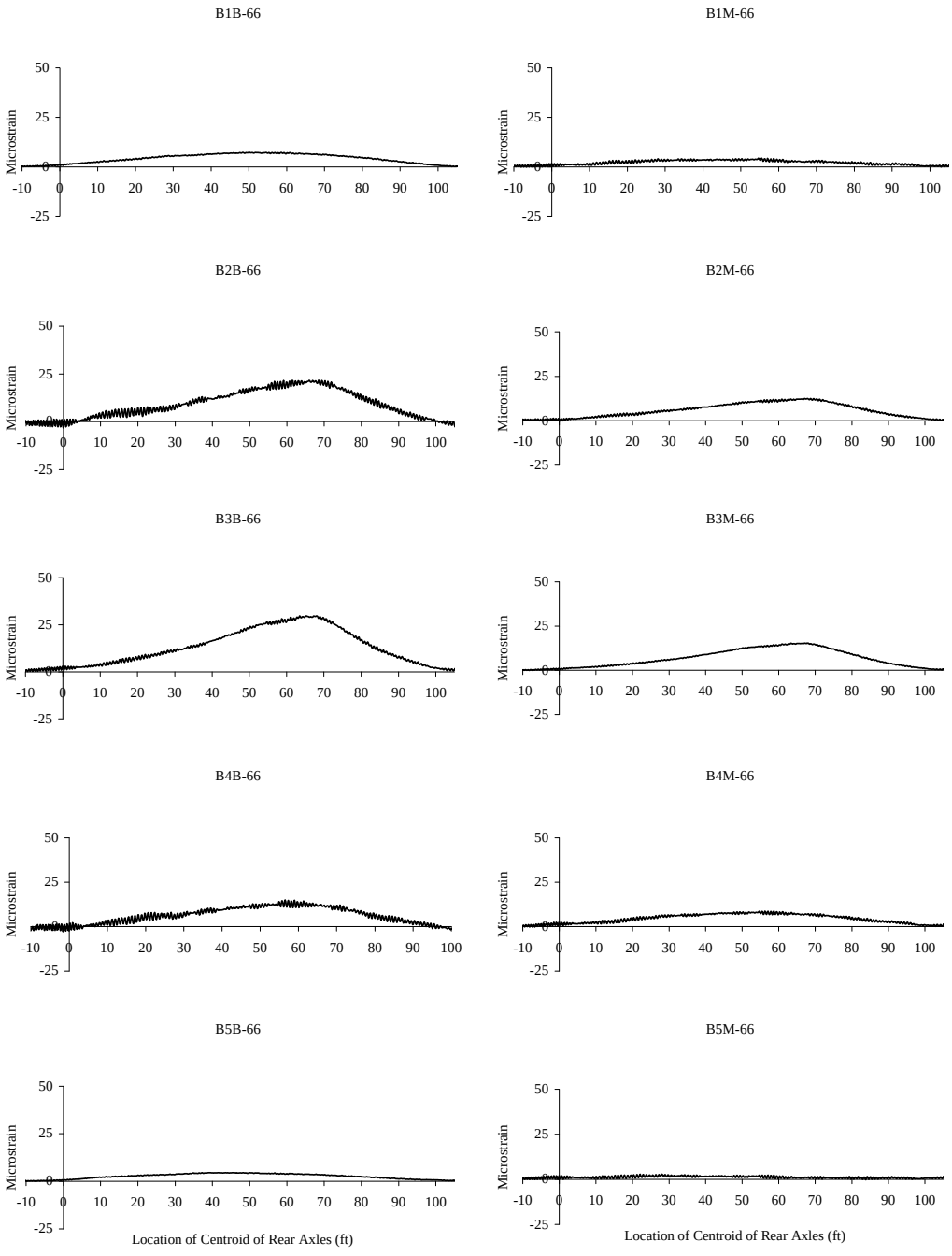

Figure A.45 Strains for the 66.7-ft. Girder Gages, Test Series 1, Run 6

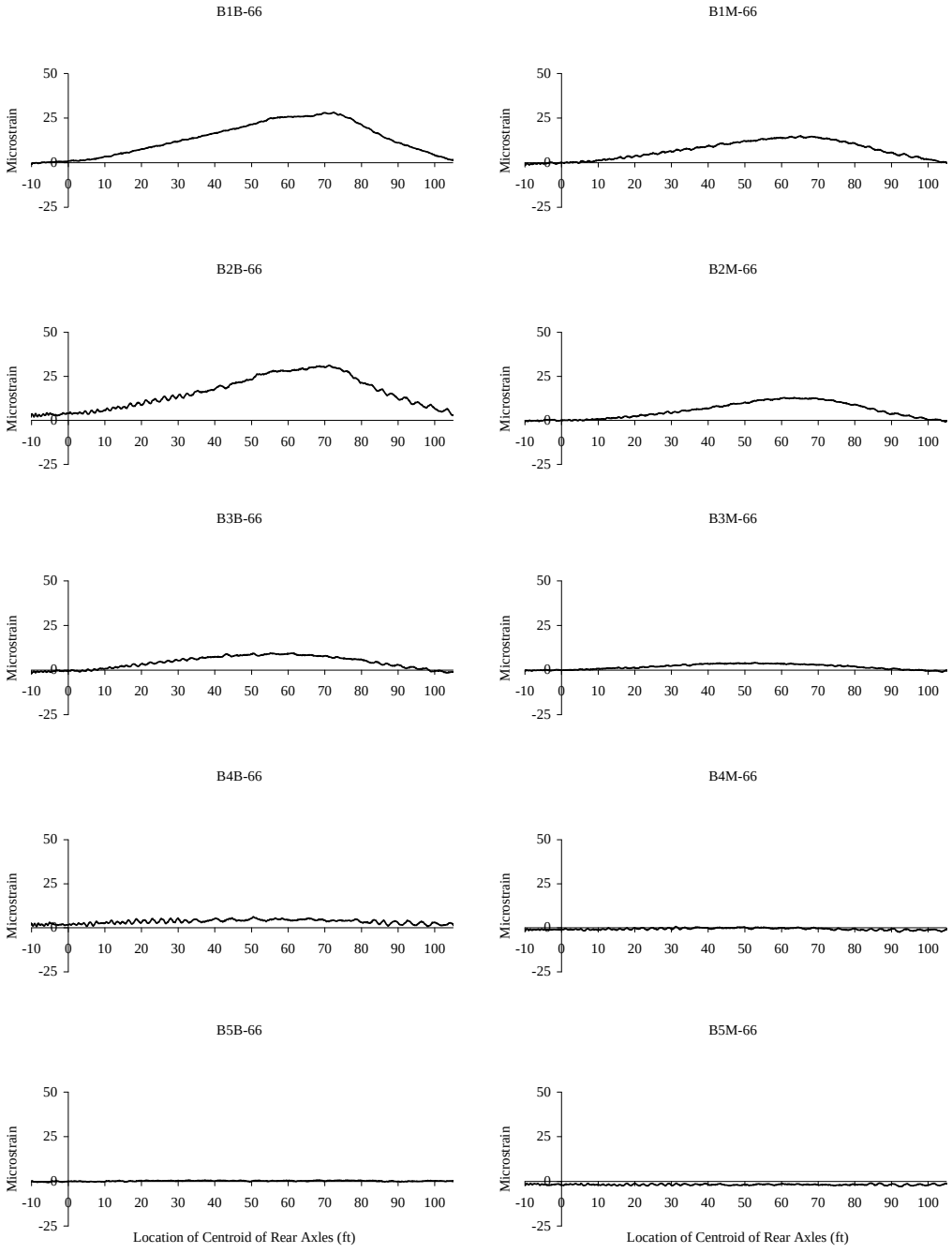

Figure A.46 Strains for the 66.7-ft. Girder Gages, Test Series 1, Run 7

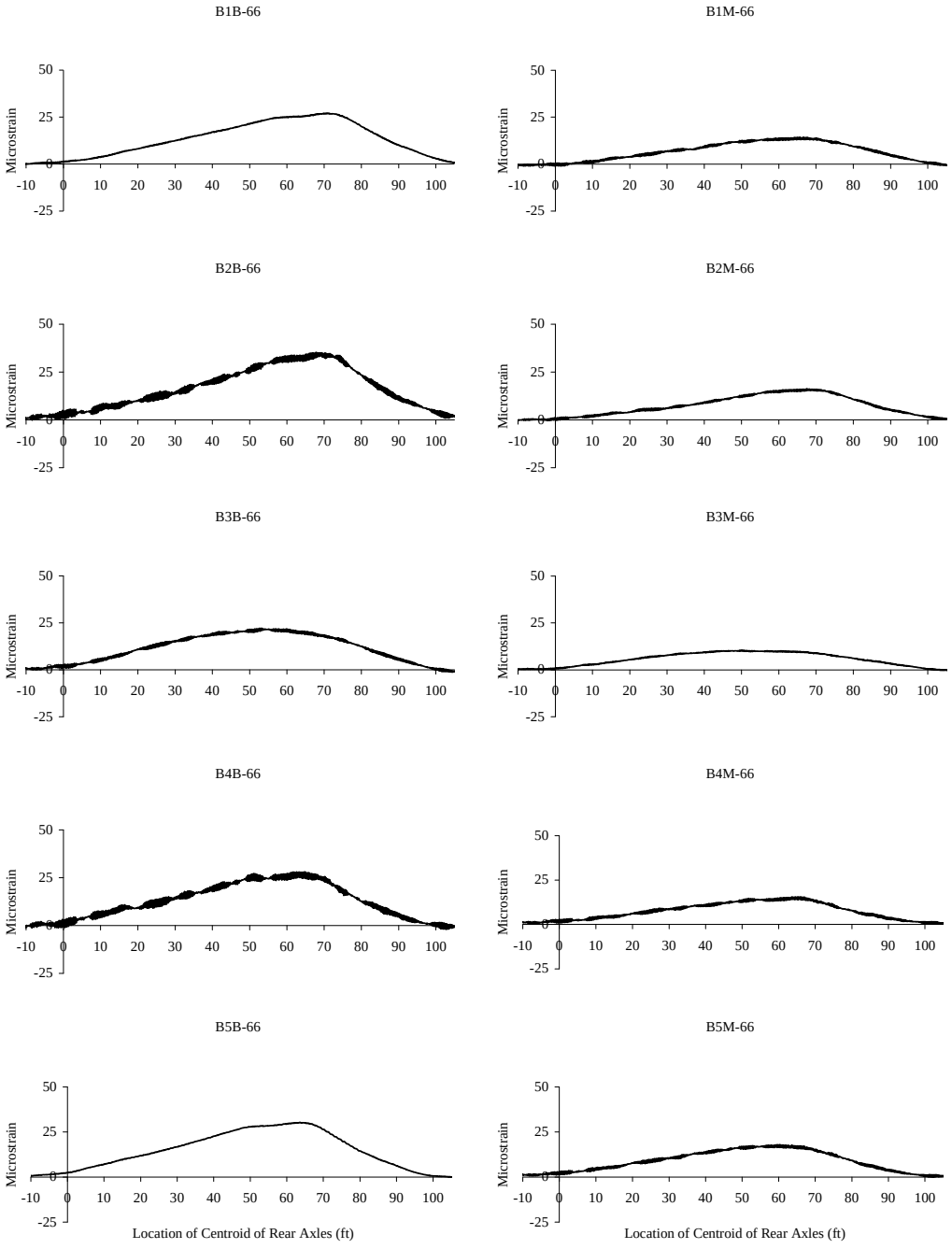

Figure A.47 Strains for the 66.7-ft. Girder Gages, Test Series 1, Run 9

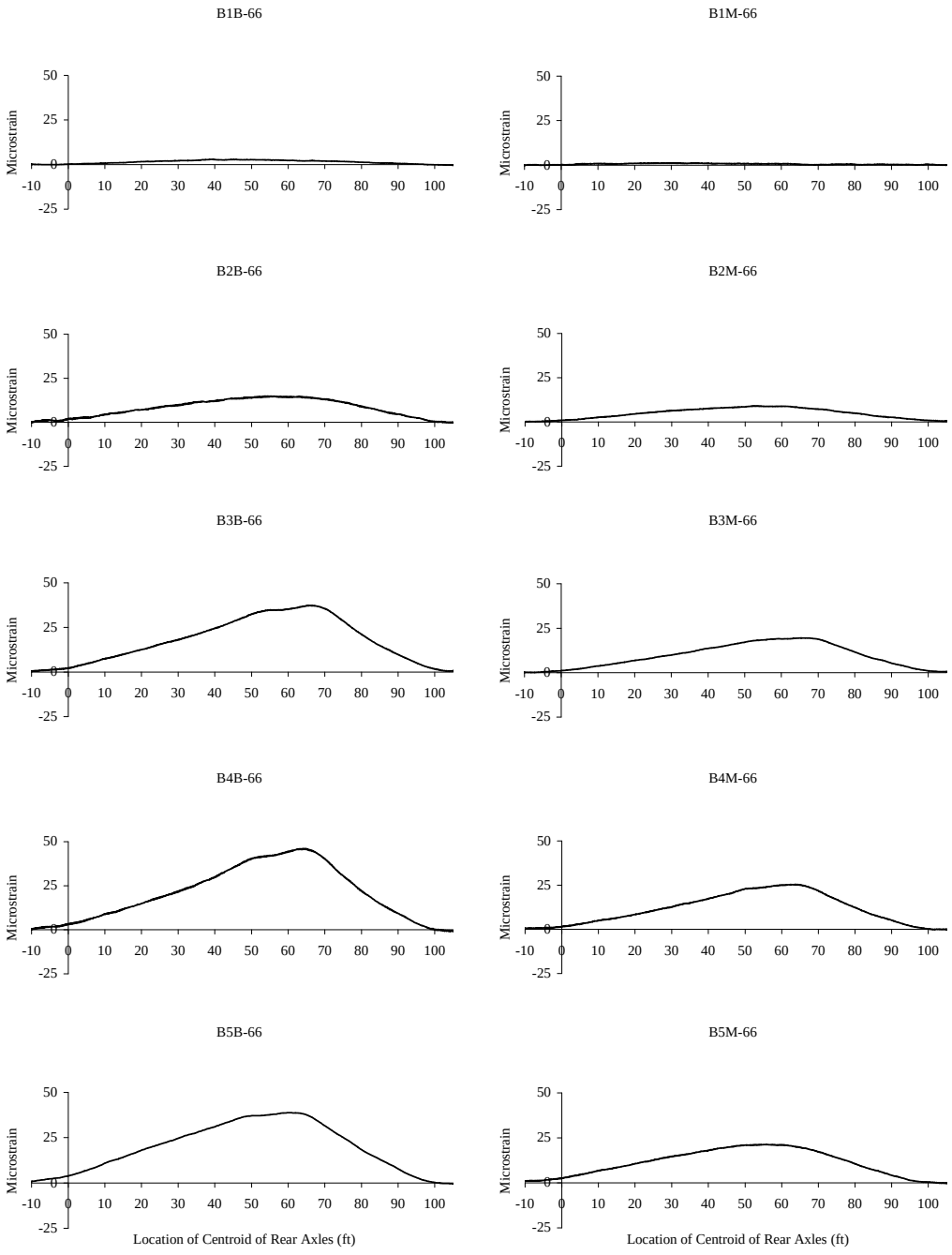

Figure A.48 Strains for the 66.7-ft. Girder Gages, Test Series 1, Run 11

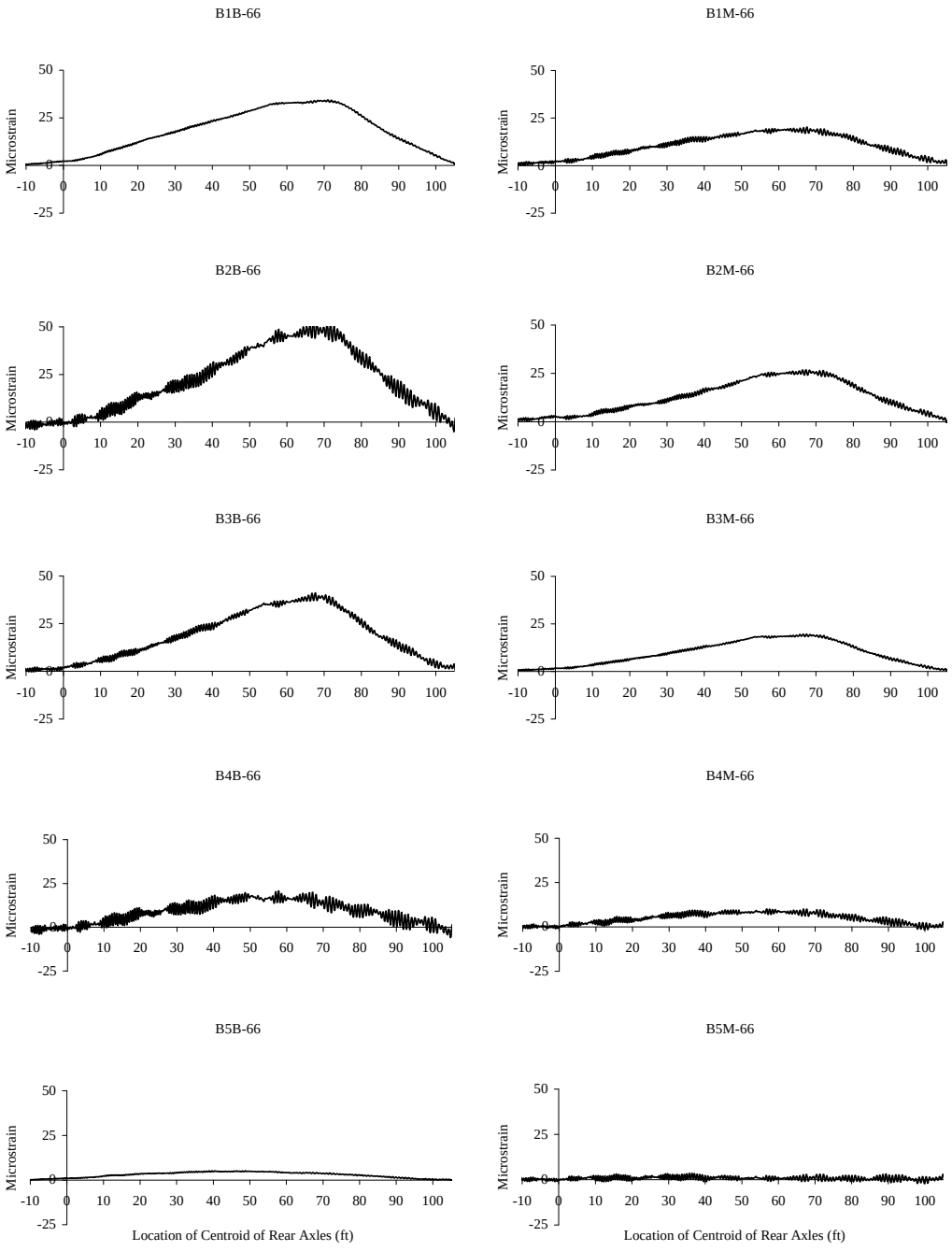

Figure A.49 Strains for the 66.7-ft. Girder Gages, Test Series 1, Run 13

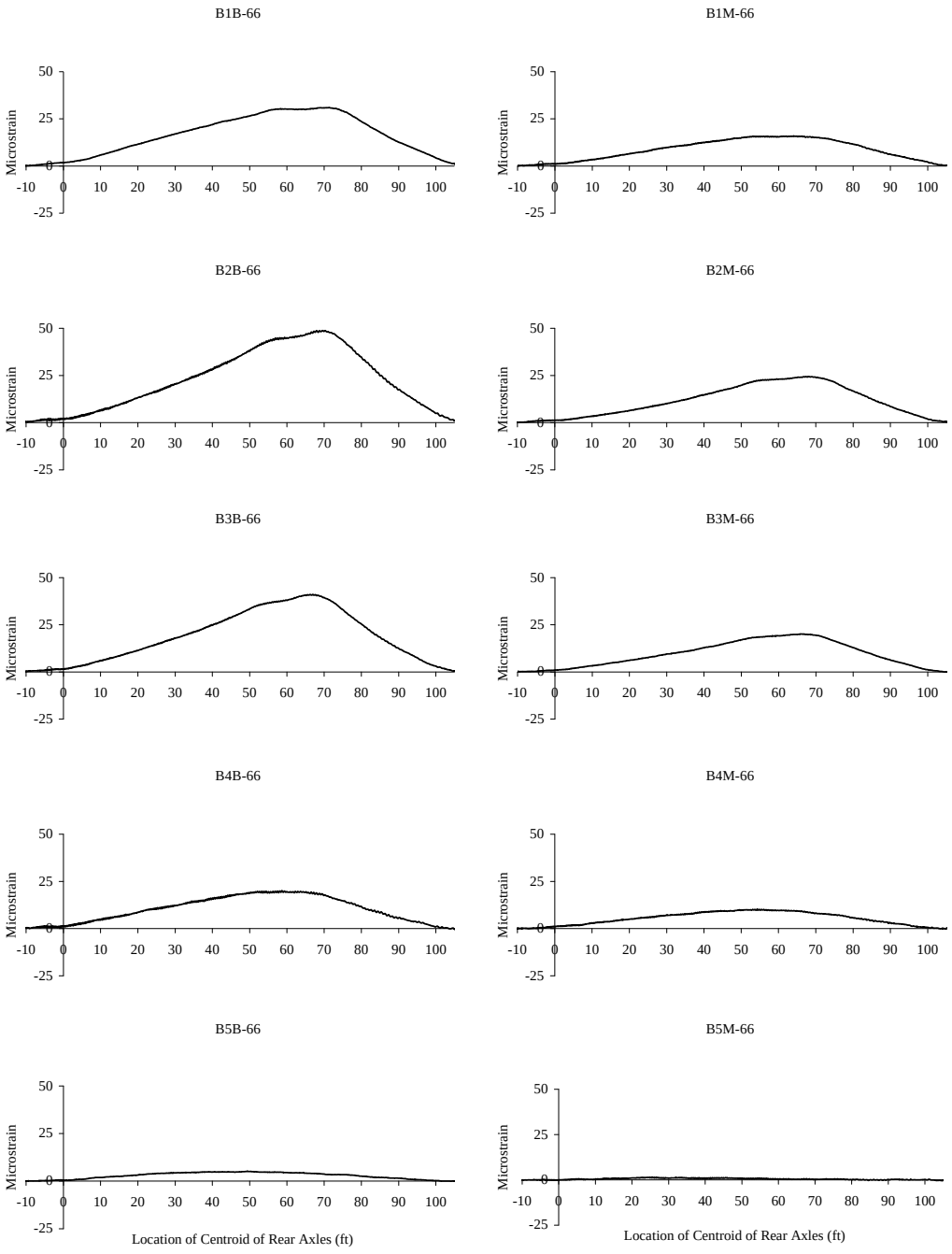

Figure A.50 Strains for the 66.7-ft. Girder Gages, Test Series 1, Run 14

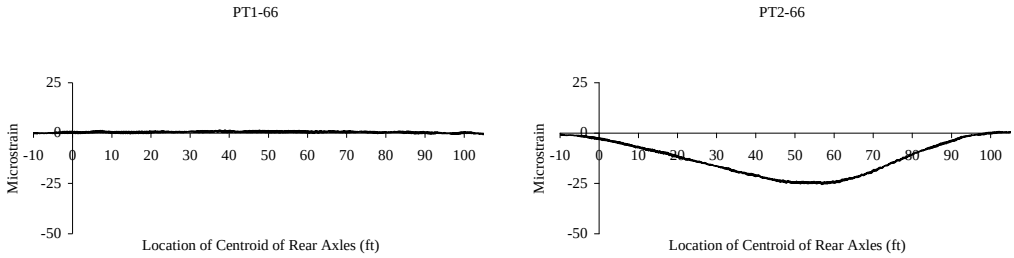

Figure A.51 Strains for the 66.7-ft. Parapet Gages, Test Series 1, Run 1

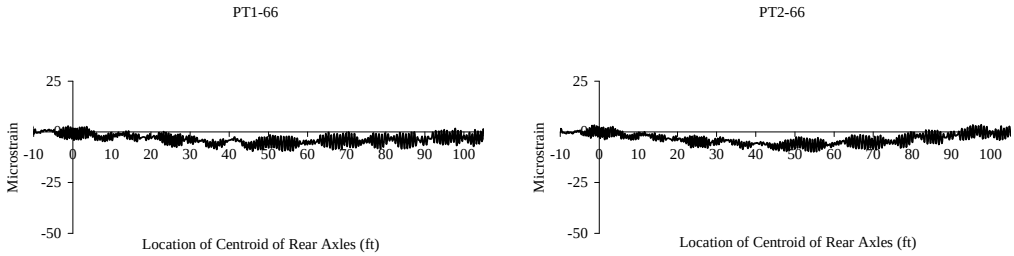

Figure A.52 Strains for the 66.7-ft. Parapet Gages, Test Series 1, Run 4

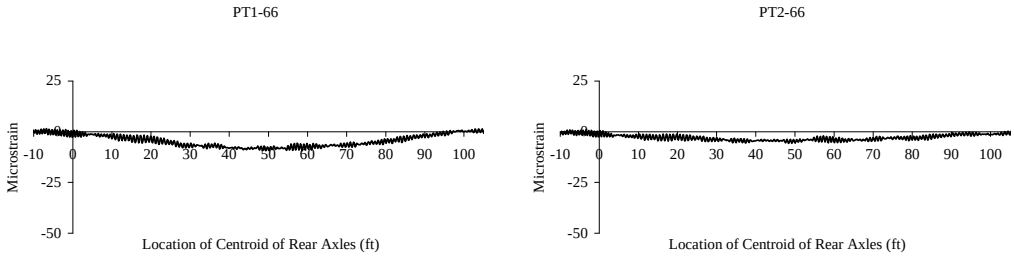

Figure A.53 Strains for the 66.7-ft. Parapet Gages, Test Series 1, Run 6

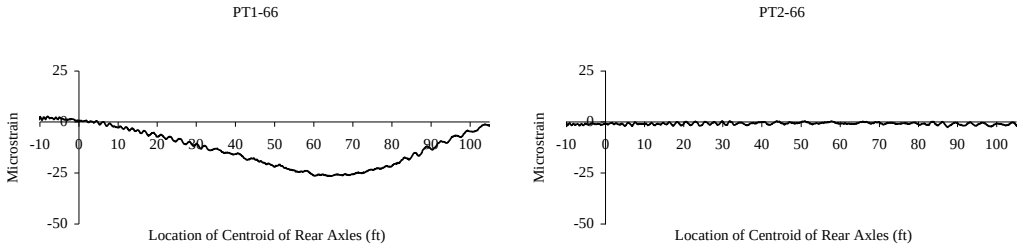

Figure A.54 Strains for the 66.7-ft. Parapet Gages, Test Series 1, Run 7

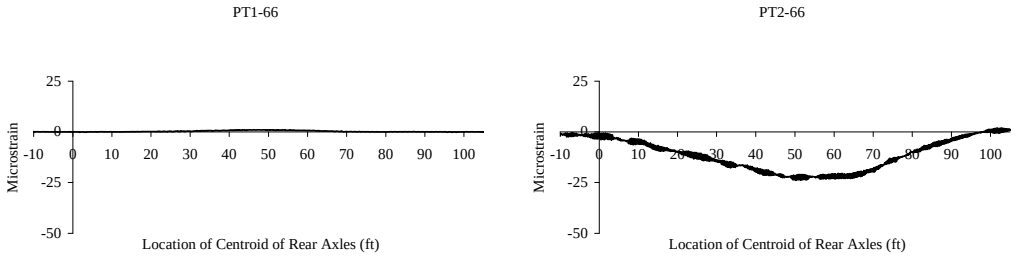

Figure A.55 Strains for the 66.7-ft. Parapet Gages, Test Series 1, Run 9

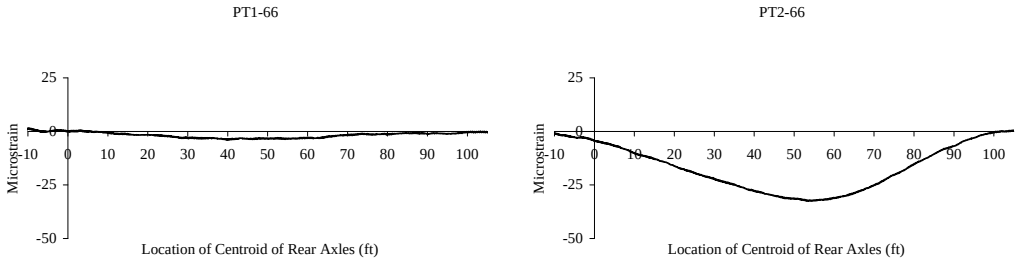

Figure A.56 Strains for the 66.7-ft. Parapet Gages, Test Series 1, Run 11

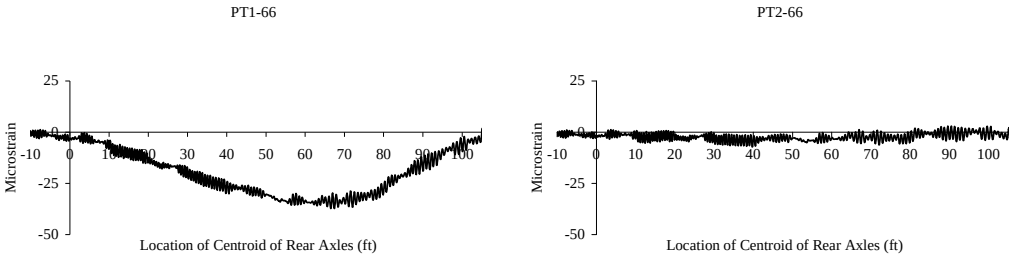

Figure A.57 Strains for the 66.7-ft. Parapet Gages, Test Series 1, Run 13

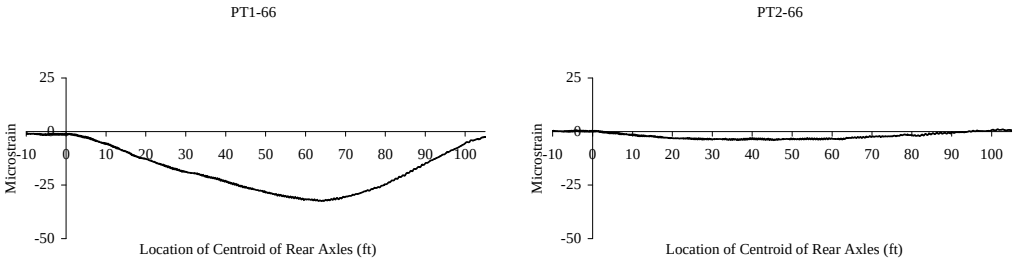

Figure A.58 Strains for the 66.7-ft. Parapet Gages, Test Series 1, Run 14

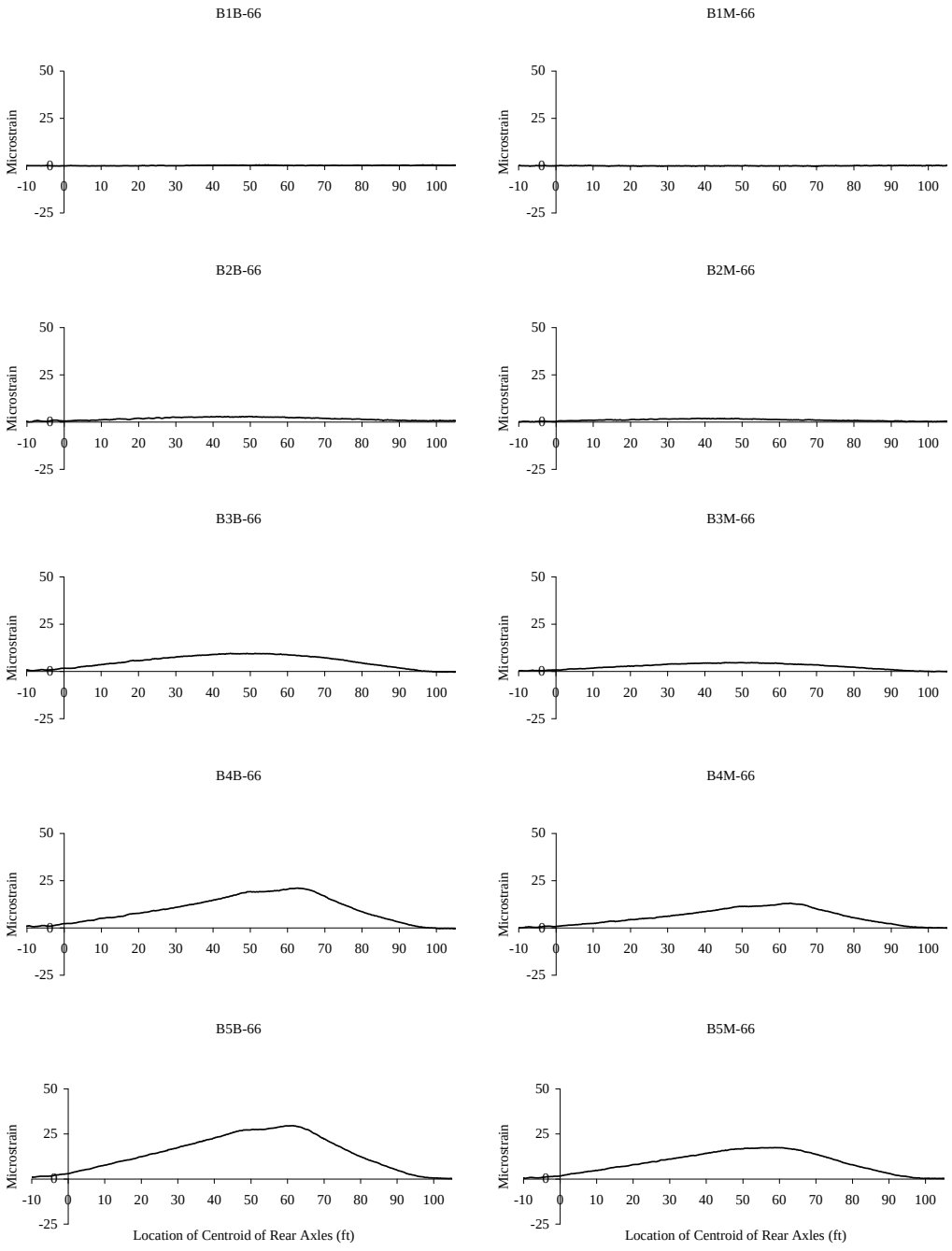

Figure A.59 Strains for the 66.7-ft. Girder Gages, Test Series 2, Run 15

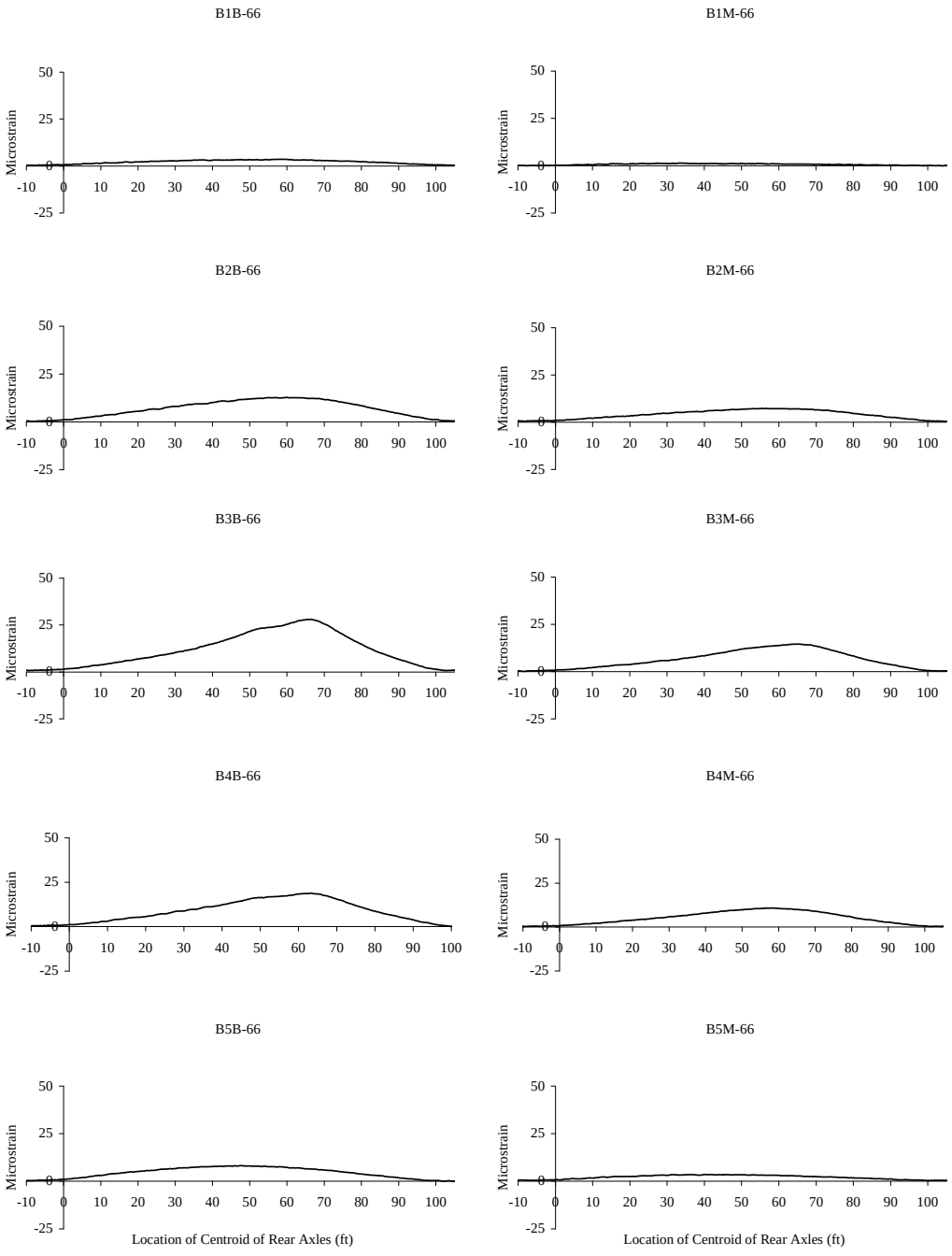

Figure A.60 Strains for the 66.7-ft. Girder Gages, Test Series 2, Run 17

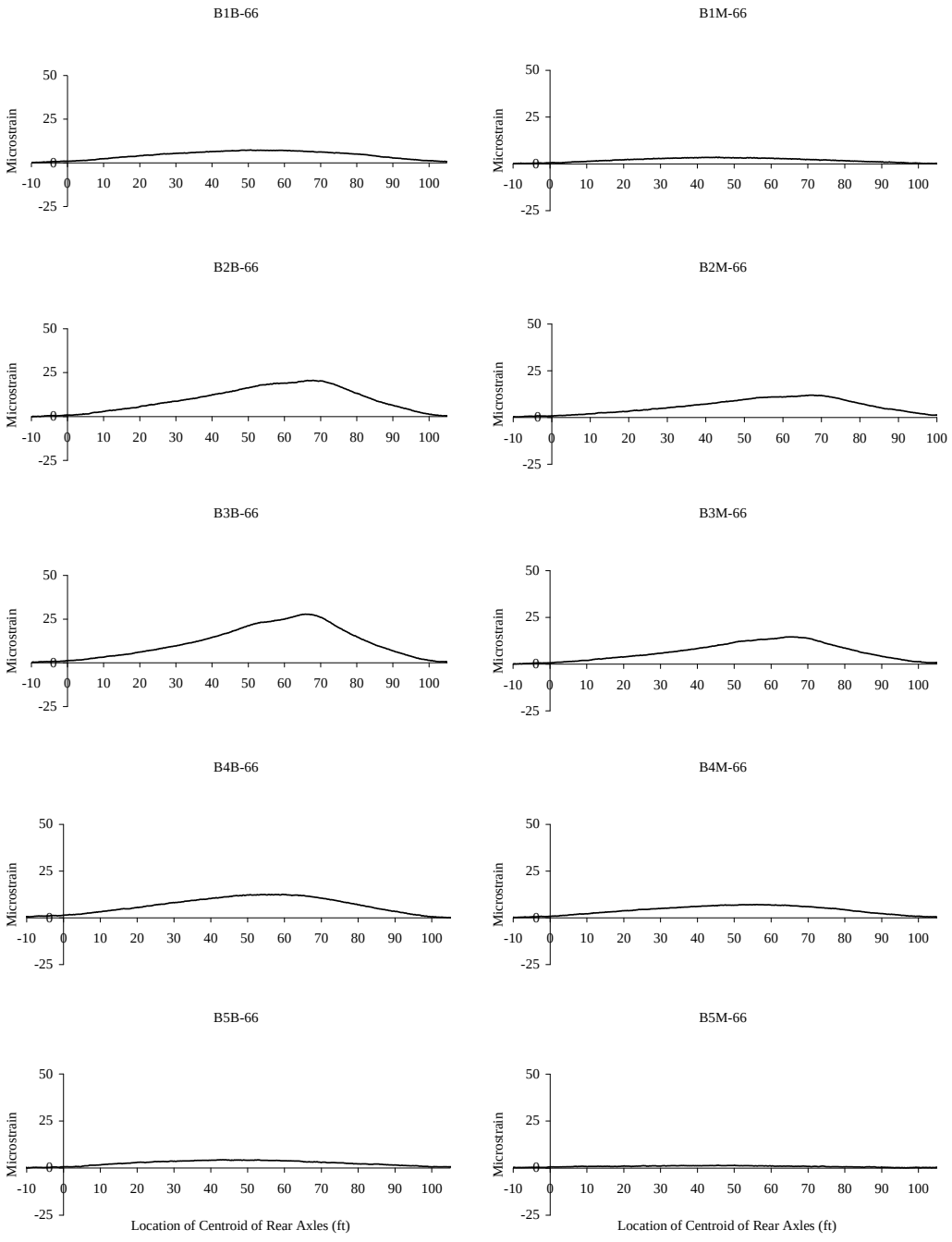

Figure A.61 Strains for the 66.7-ft. Girder Gages, Test Series 2, Run 19

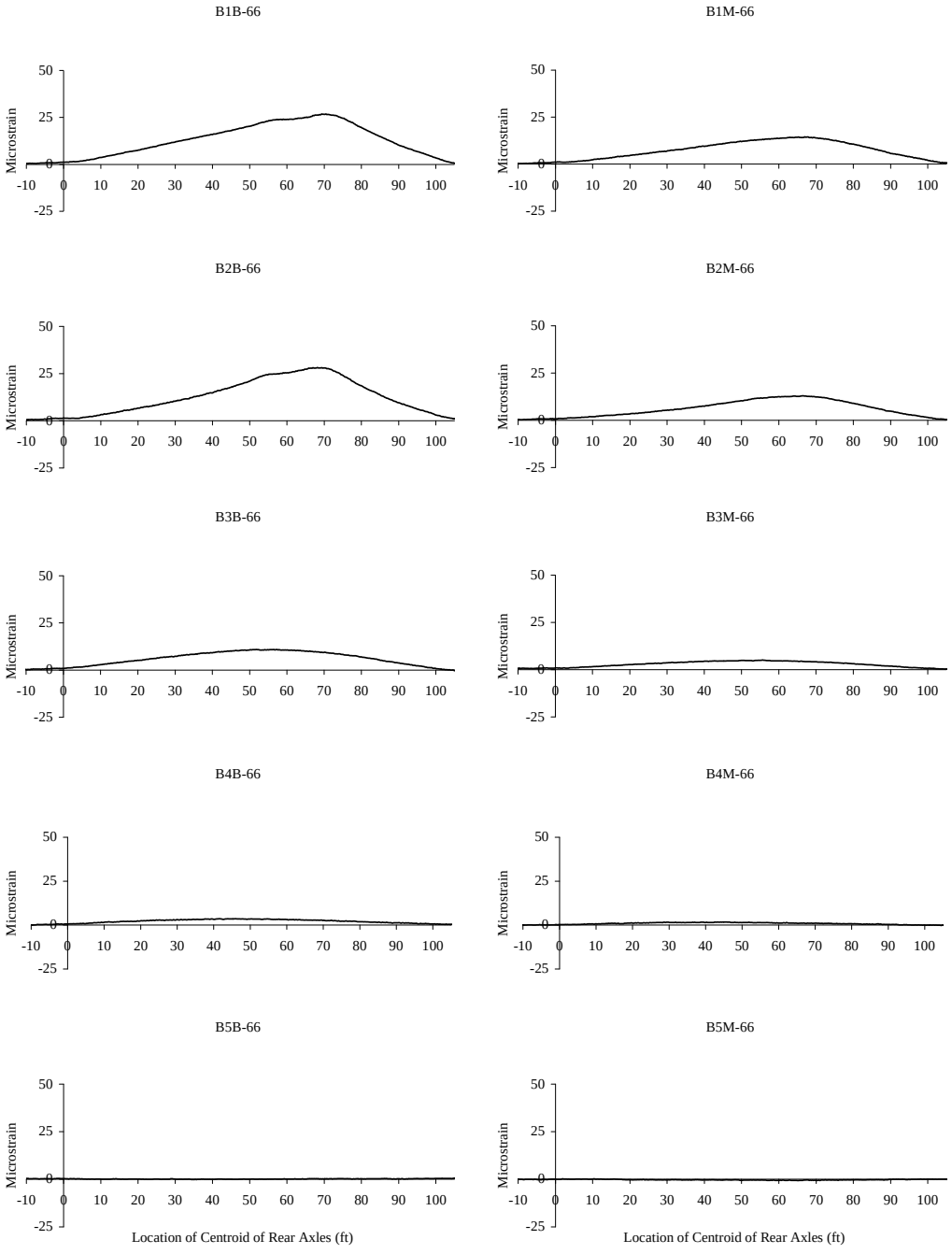

Figure A.62 Strains for the 66.7-ft. Girder Gages, Test Series 2, Run 21

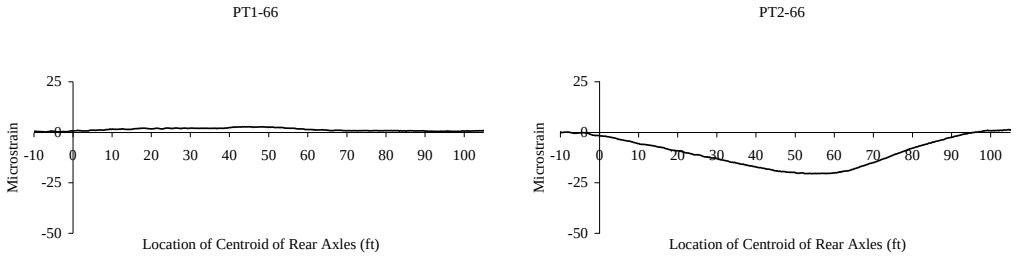

Figure A.63 Strains for the 66.7-ft. Parapet Gages, Test Series 2, Run 15

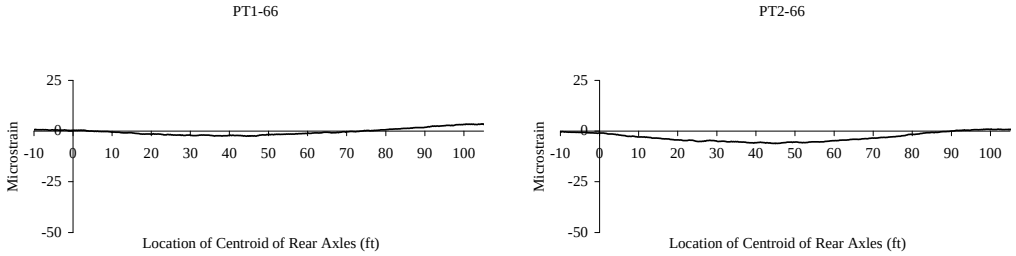

Figure A.64 Strains for the 66.7-ft. Parapet Gages, Test Series 2, Run 17

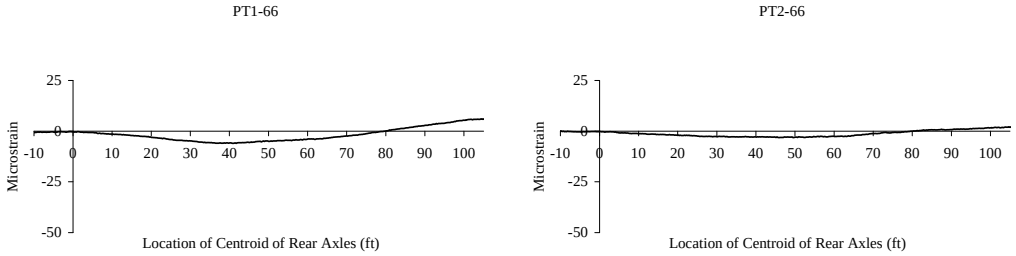

Figure A.65 Strains for the 66.7-ft. Parapet Gages, Test Series 2, Run 19

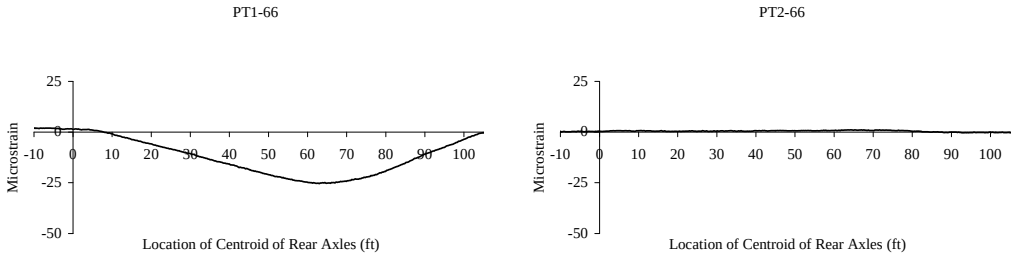

Figure A.66 Strains for the 66.7-ft. Parapet Gages, Test Series 2, Run 21

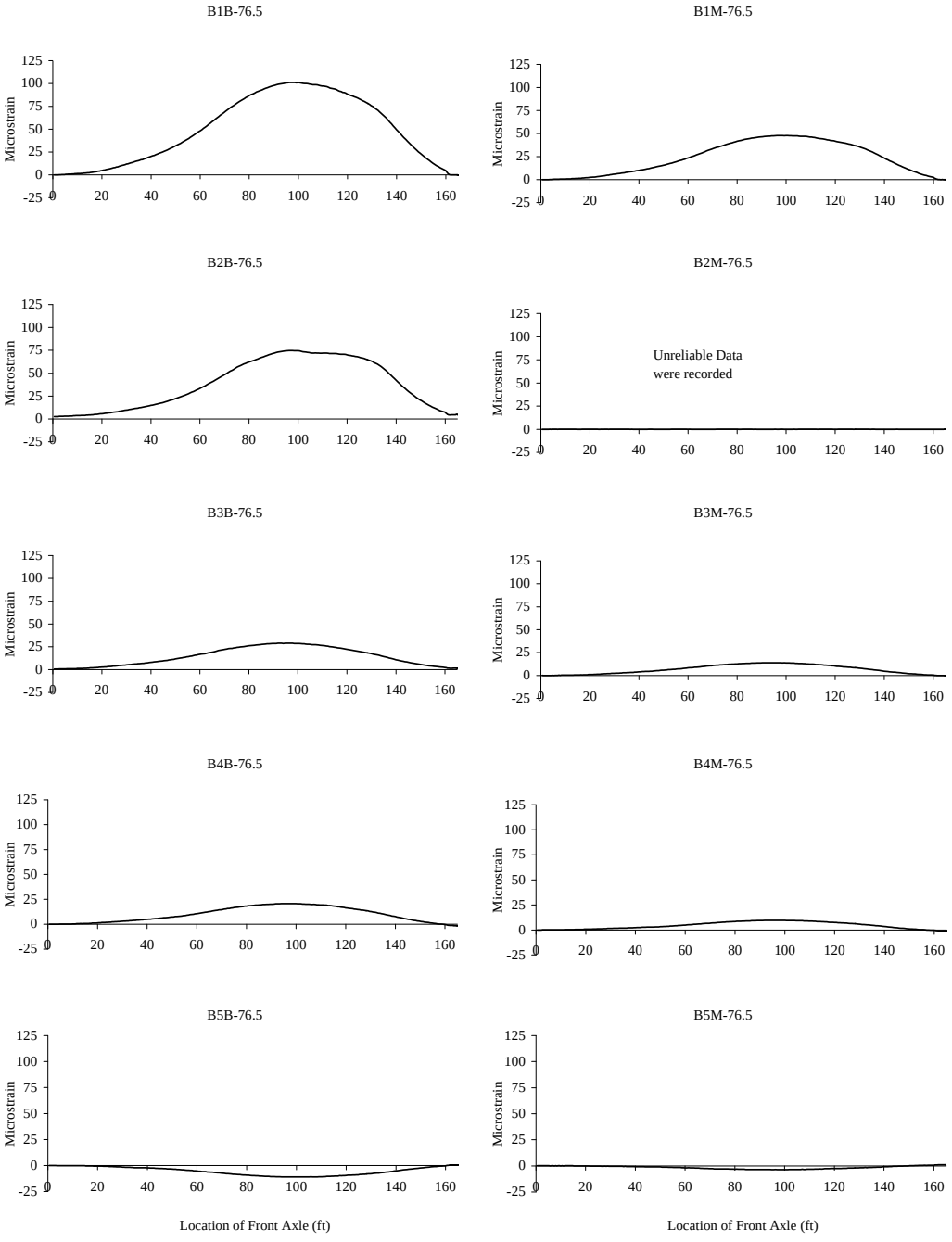

Figure A.67 Strains for the 76.5-ft. Girder Gages, Test Series 3, Run 23

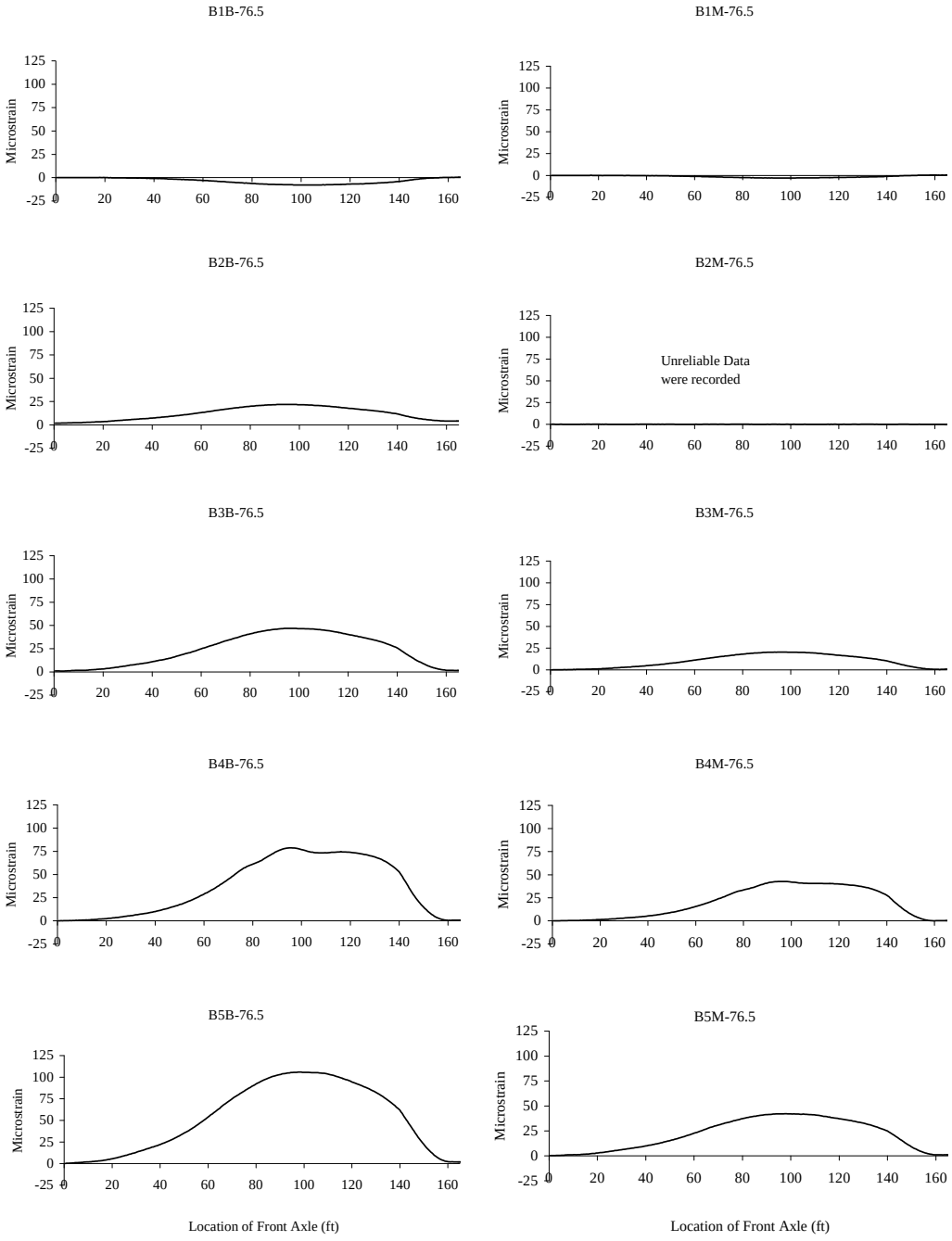

Figure A.68 Strains for the 76.5-ft. Girder Gages, Test Series 3, Run 24

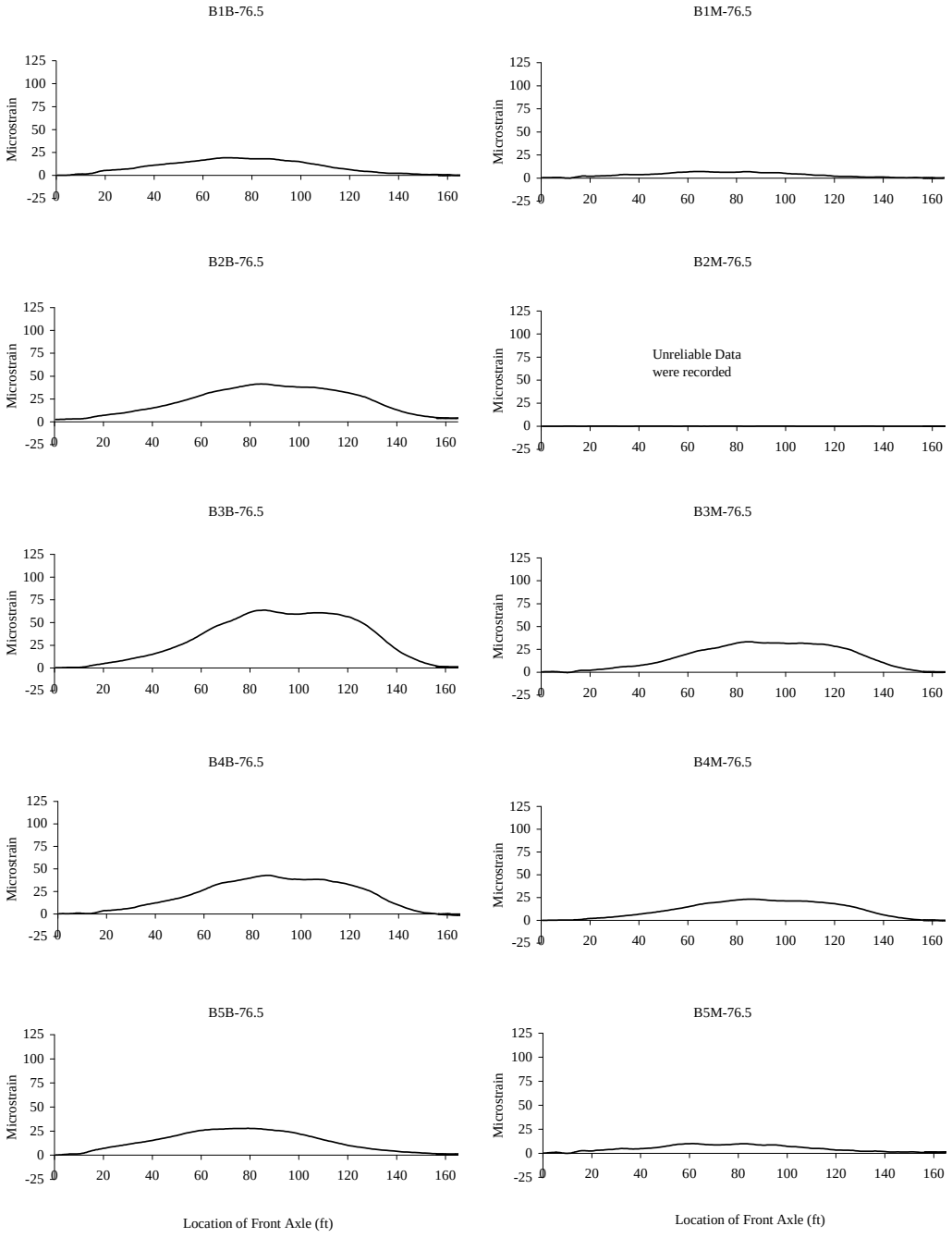

Figure A.69 Strains for the 76.5-ft. Girder Gages, Test Series 3, Run 25

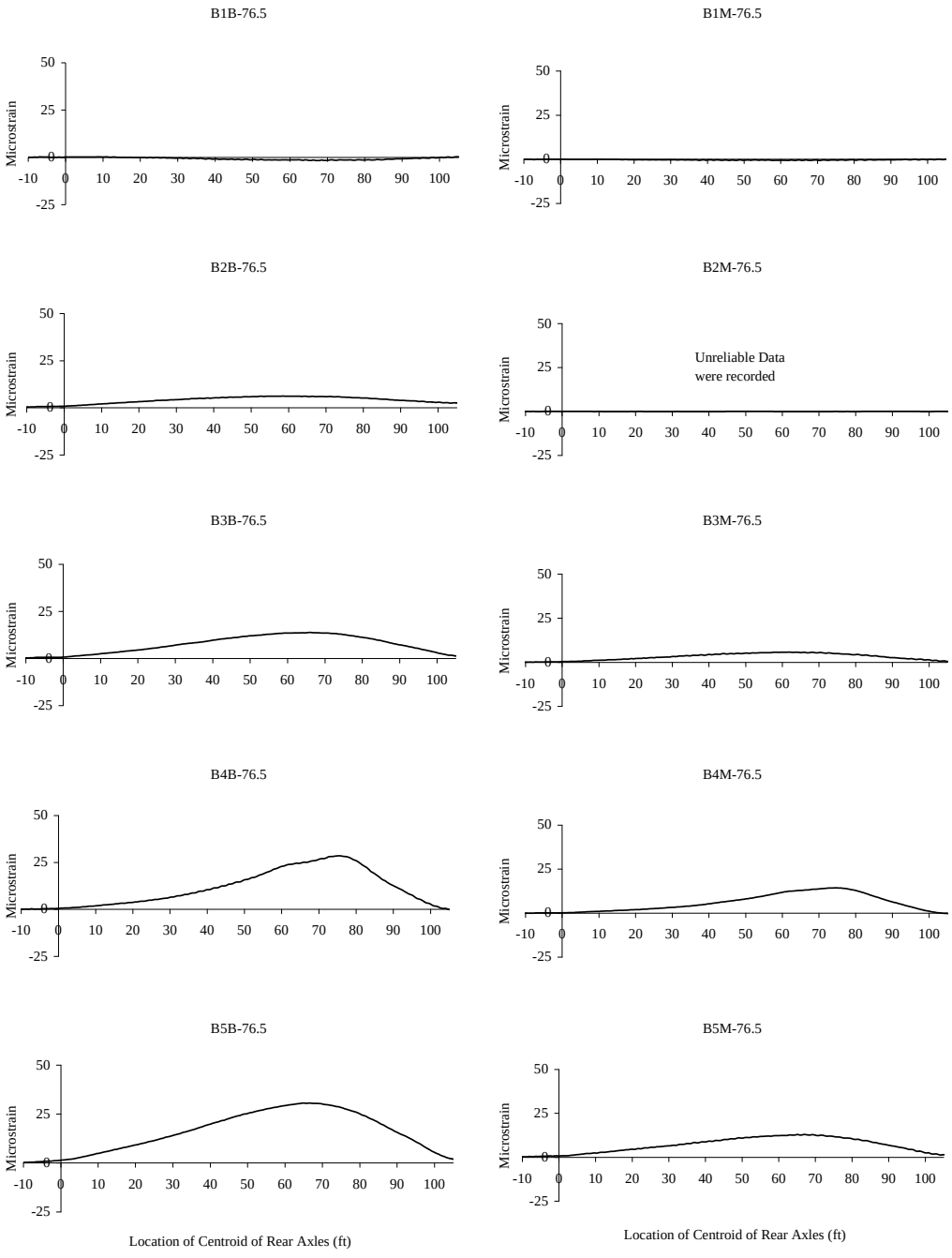

Figure A.70 Strains for the 76.5-ft. Girder Gages, Test Series 3, Run 28

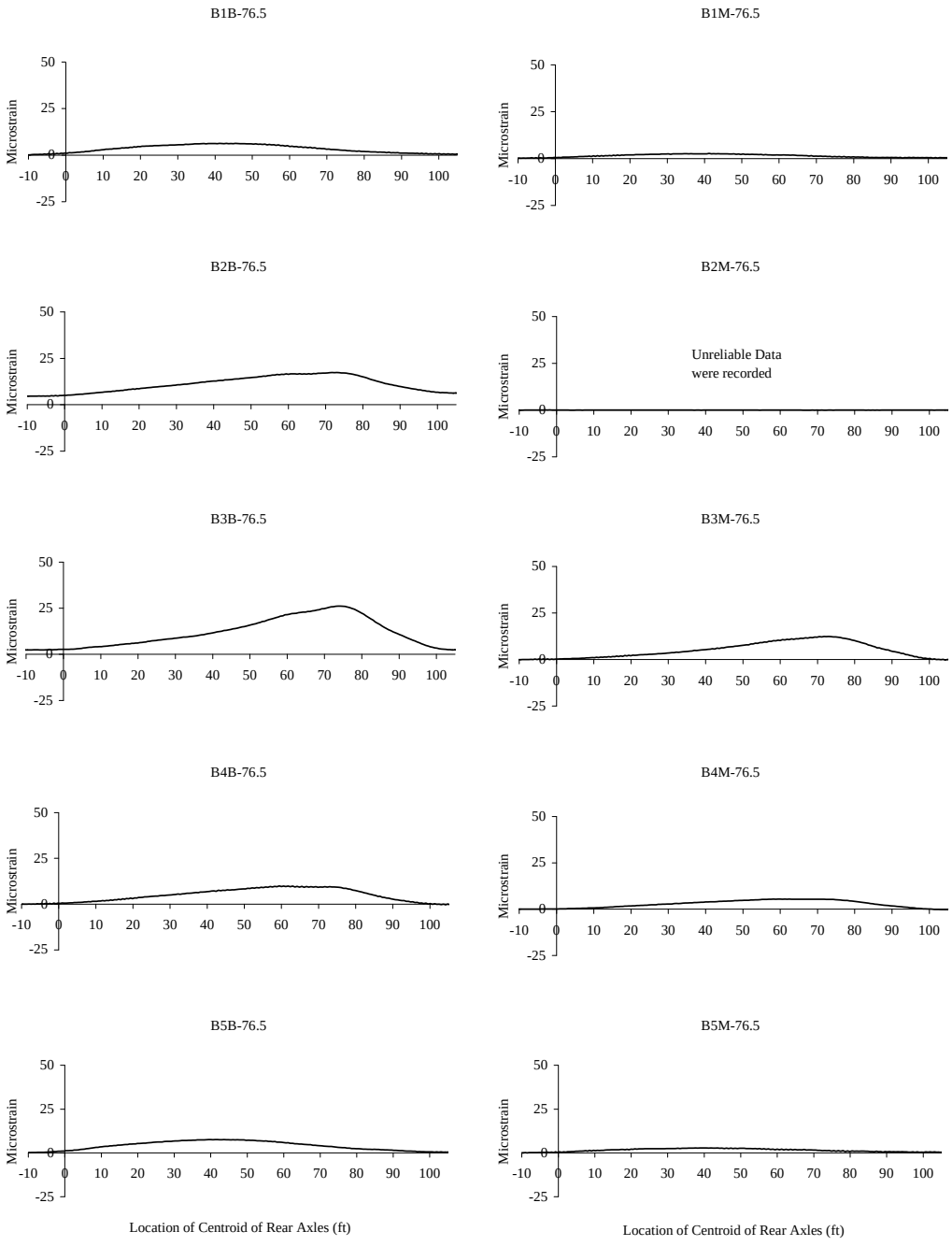

Figure A.71 Strains for the 76.5-ft. Girder Gages, Test Series 3, Run 30

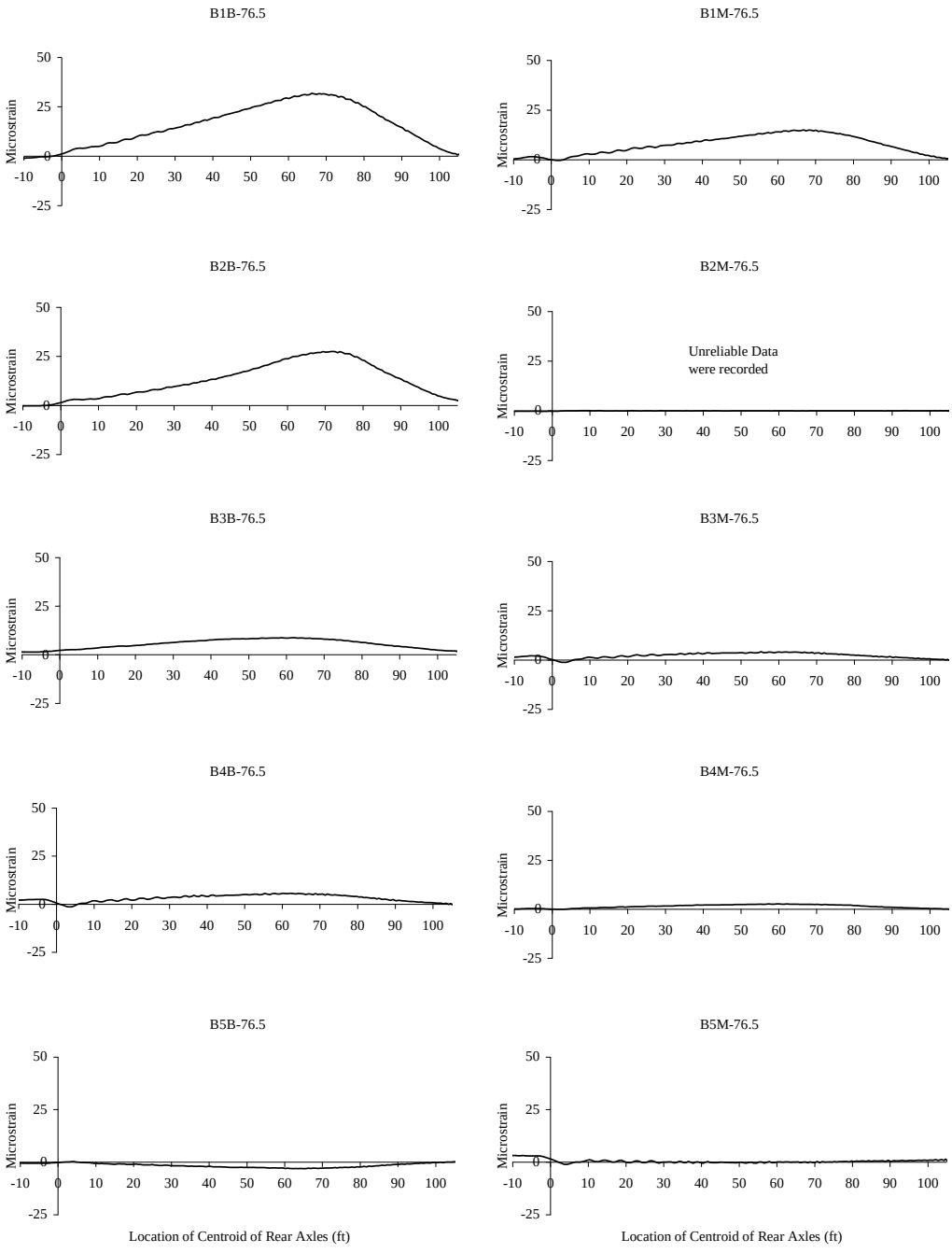

Figure A.72 Strains for the 76.5-ft. Girder Gages, Test Series 3, Run 32

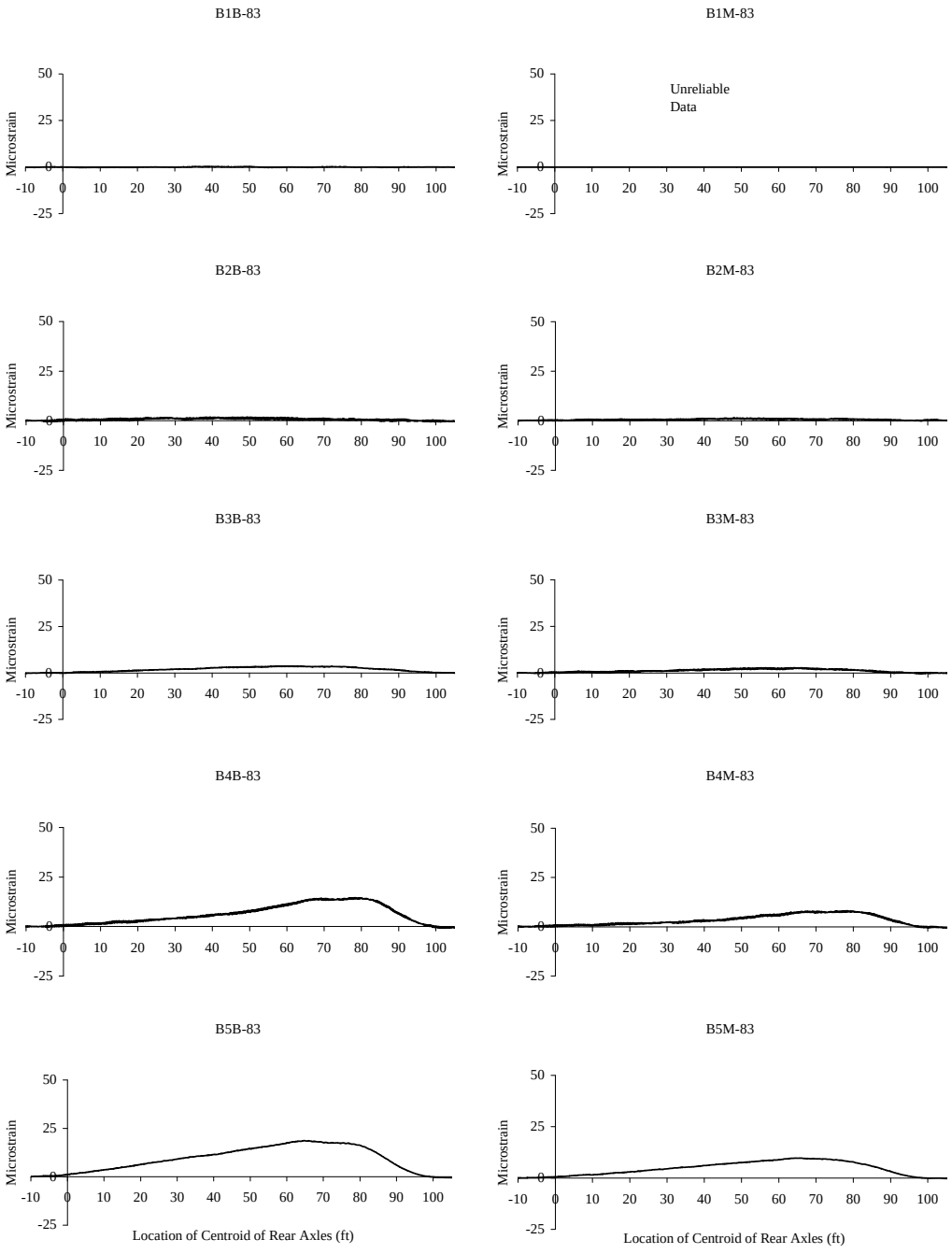

Figure A.73 Strains for the 83.3-ft. Girder Gages, Test Series 1, Run 1

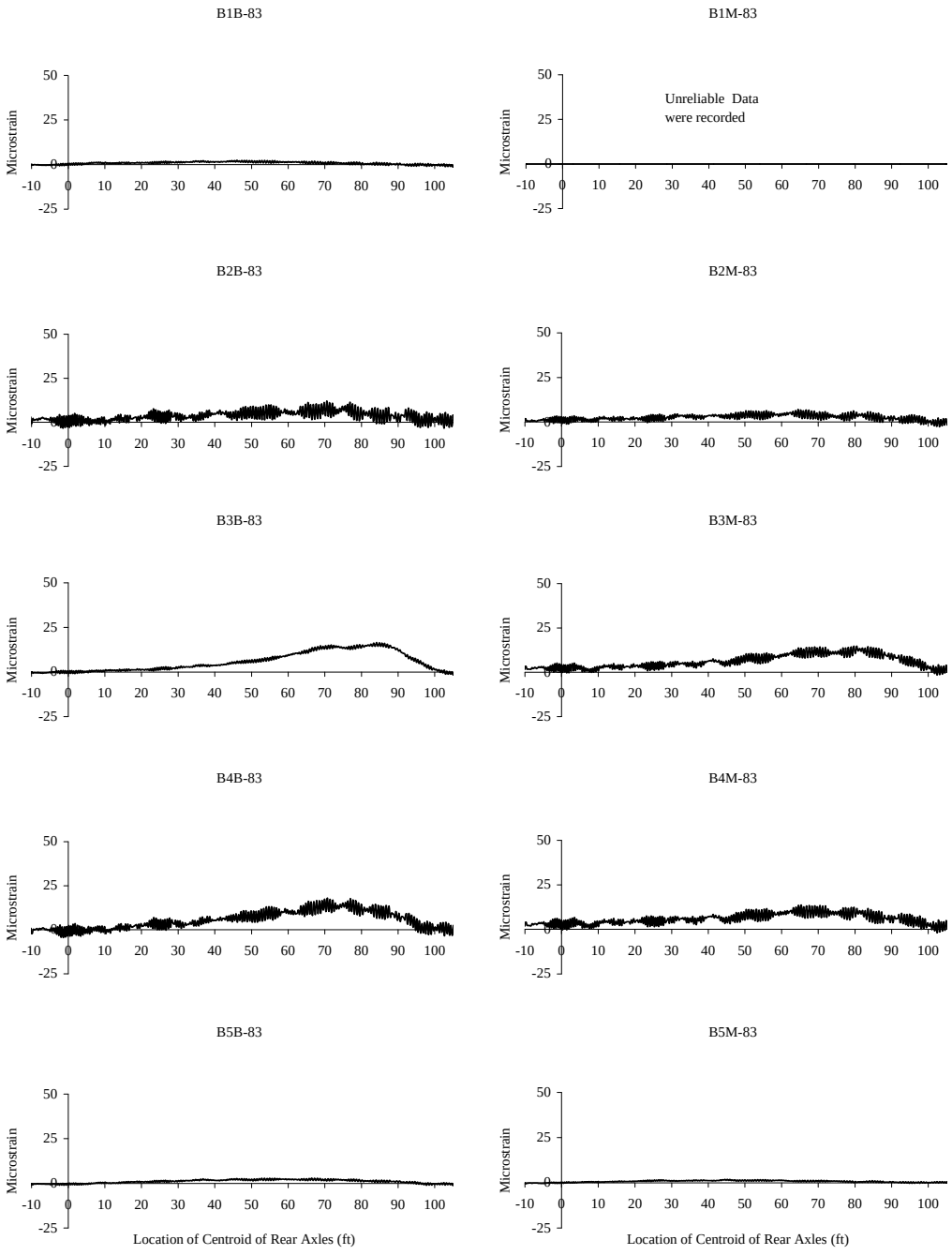

Figure A.74 Strains for the 83.3-ft. Girder Gages, Test Series 1, Run 4

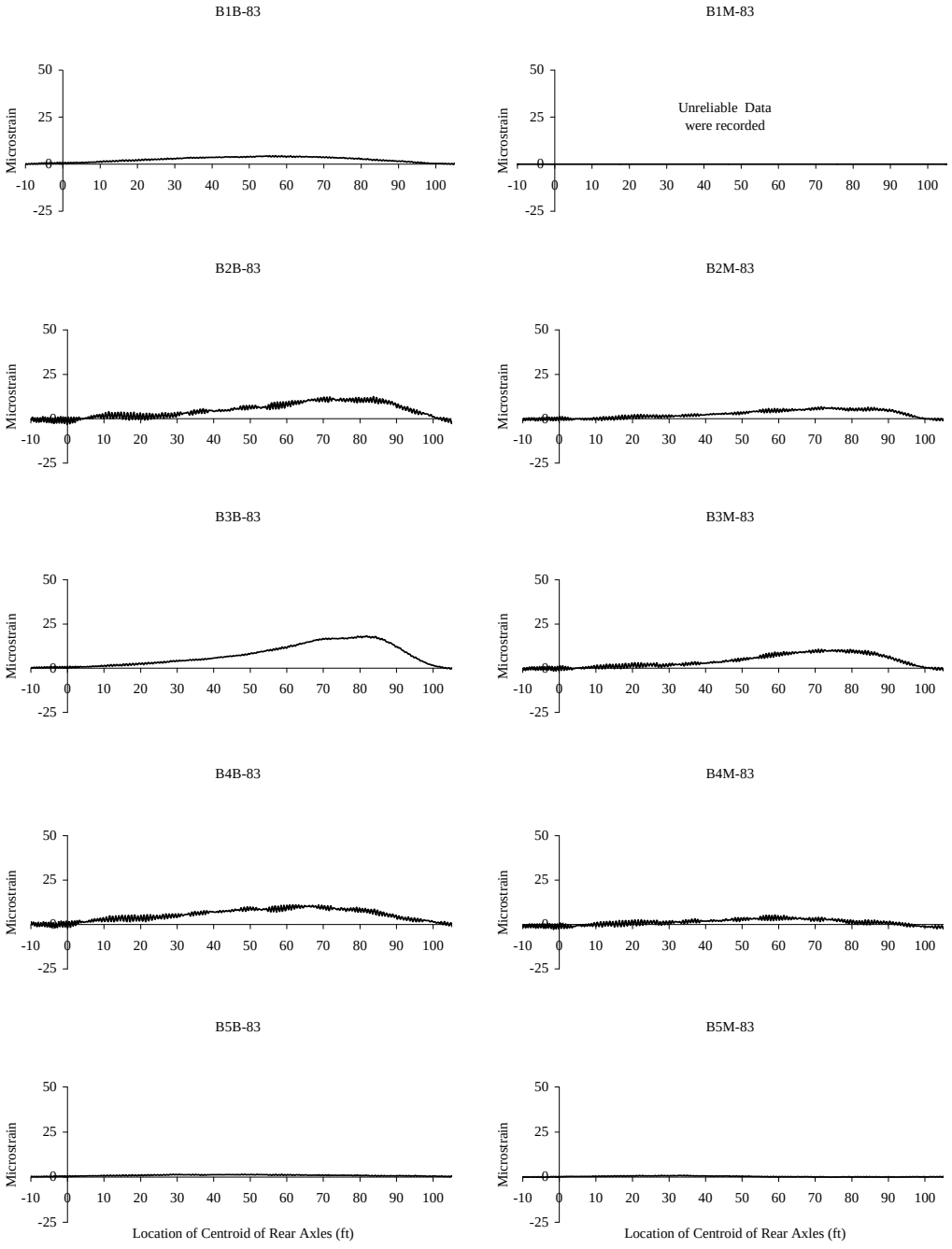

Figure A.75 Strains for the 83.3-ft. Girder Gages, Test Series 1, Run 6

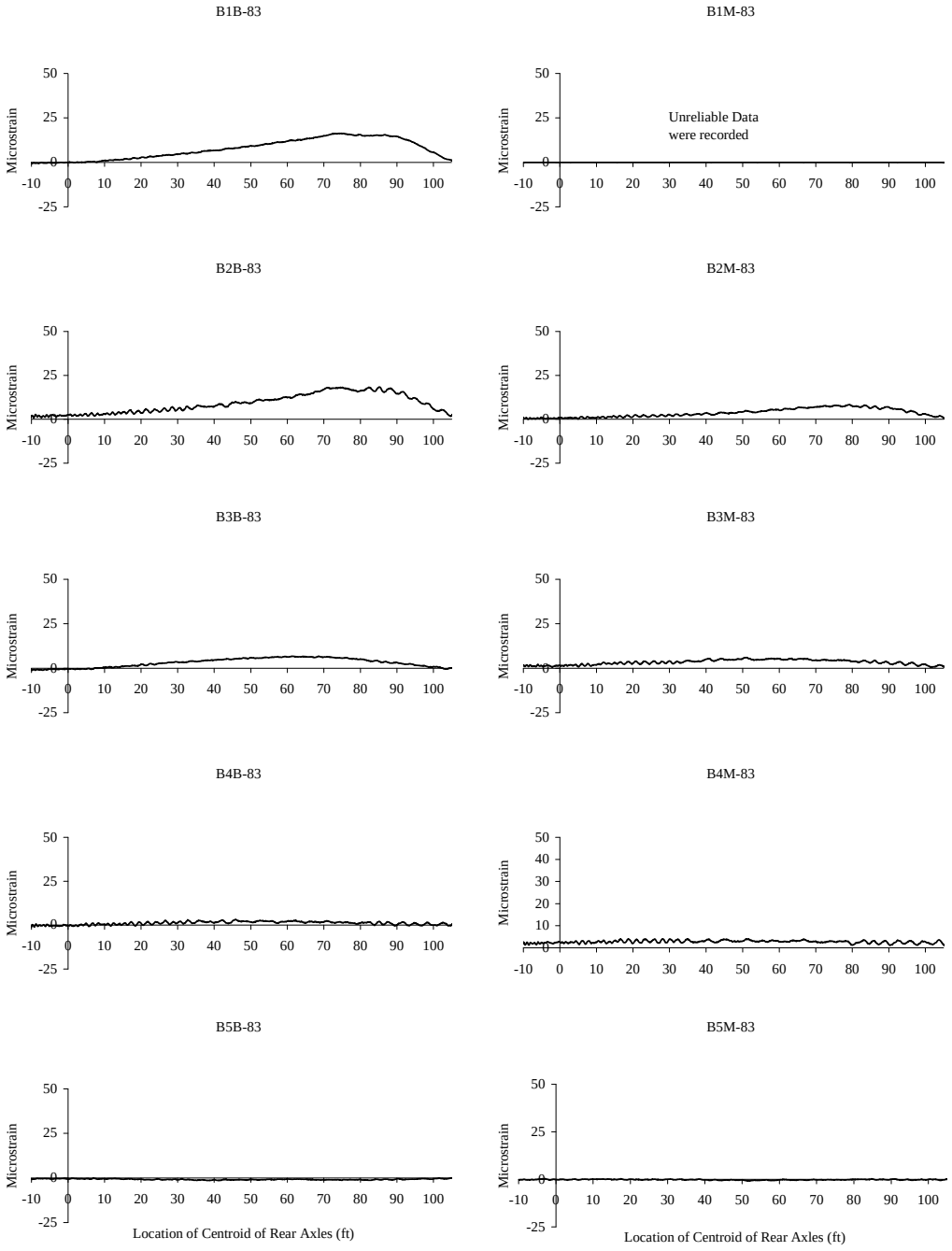

Figure A.76 Strains for the 83.3-ft. Girder Gages, Test Series 1, Run 7

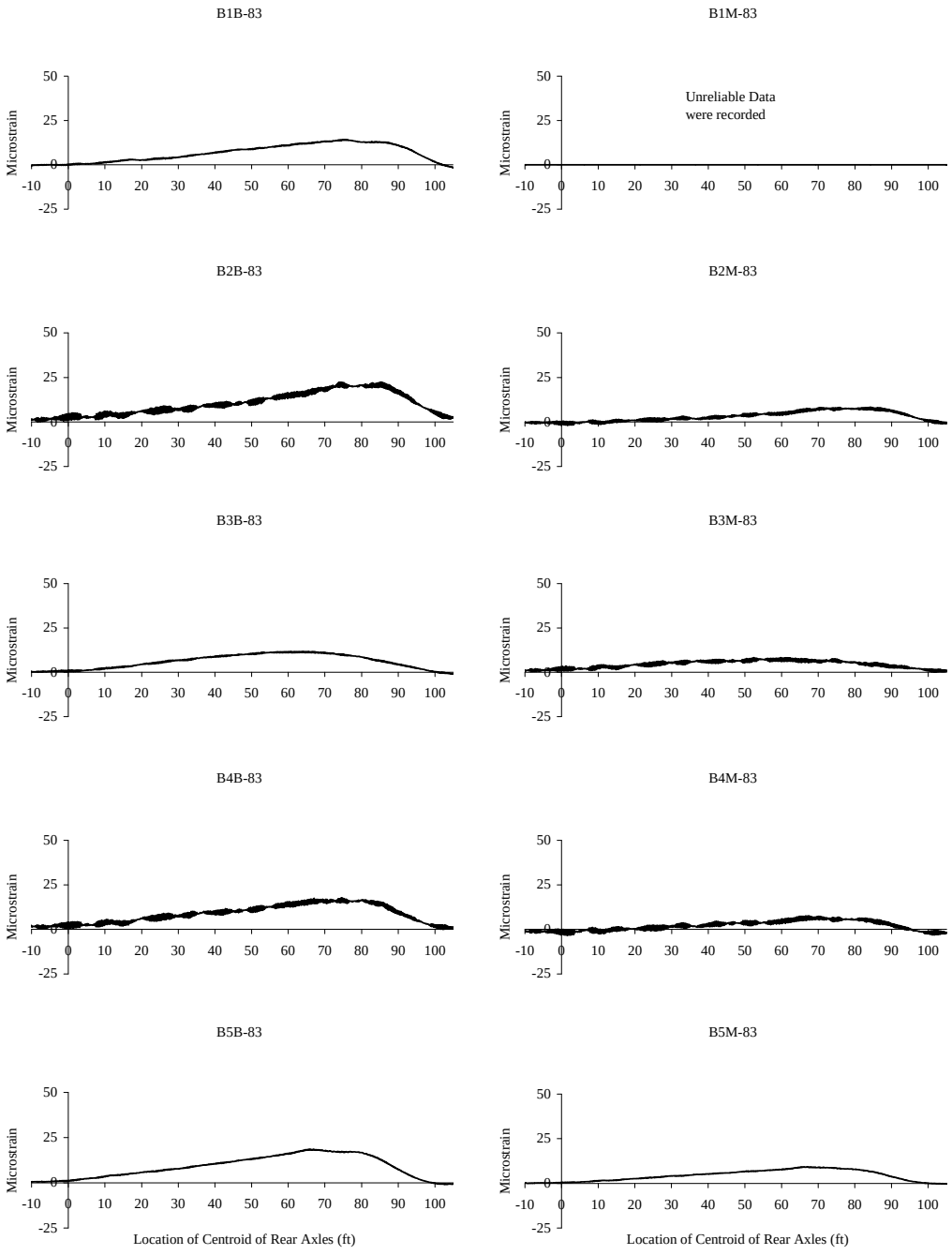

Figure A.77 Strains for the 83.3-ft. Girder Gages, Test Series 1, Run 9

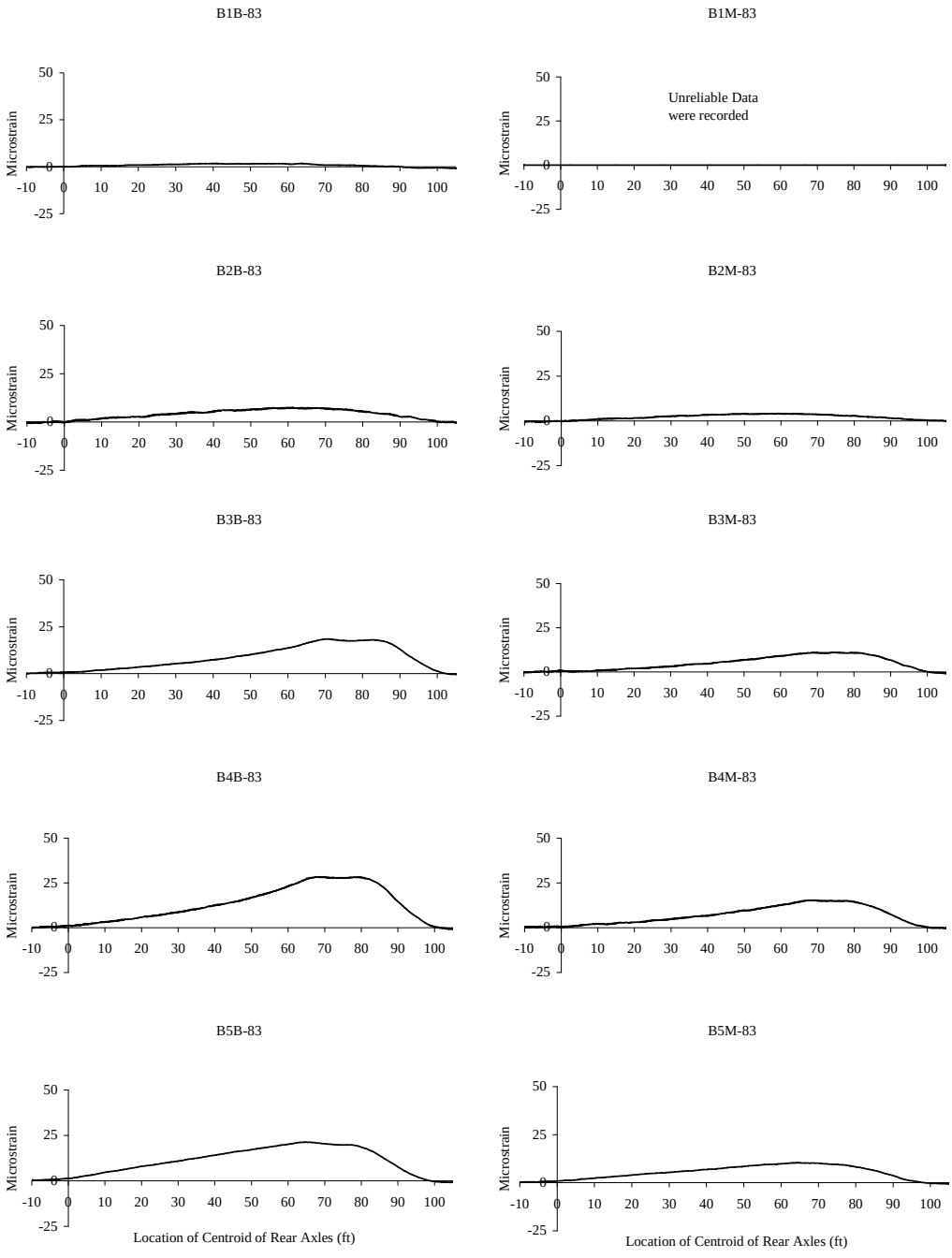

Figure A.78 Strains for the 83.3-ft. Girder Gages, Test Series 1, Run 11

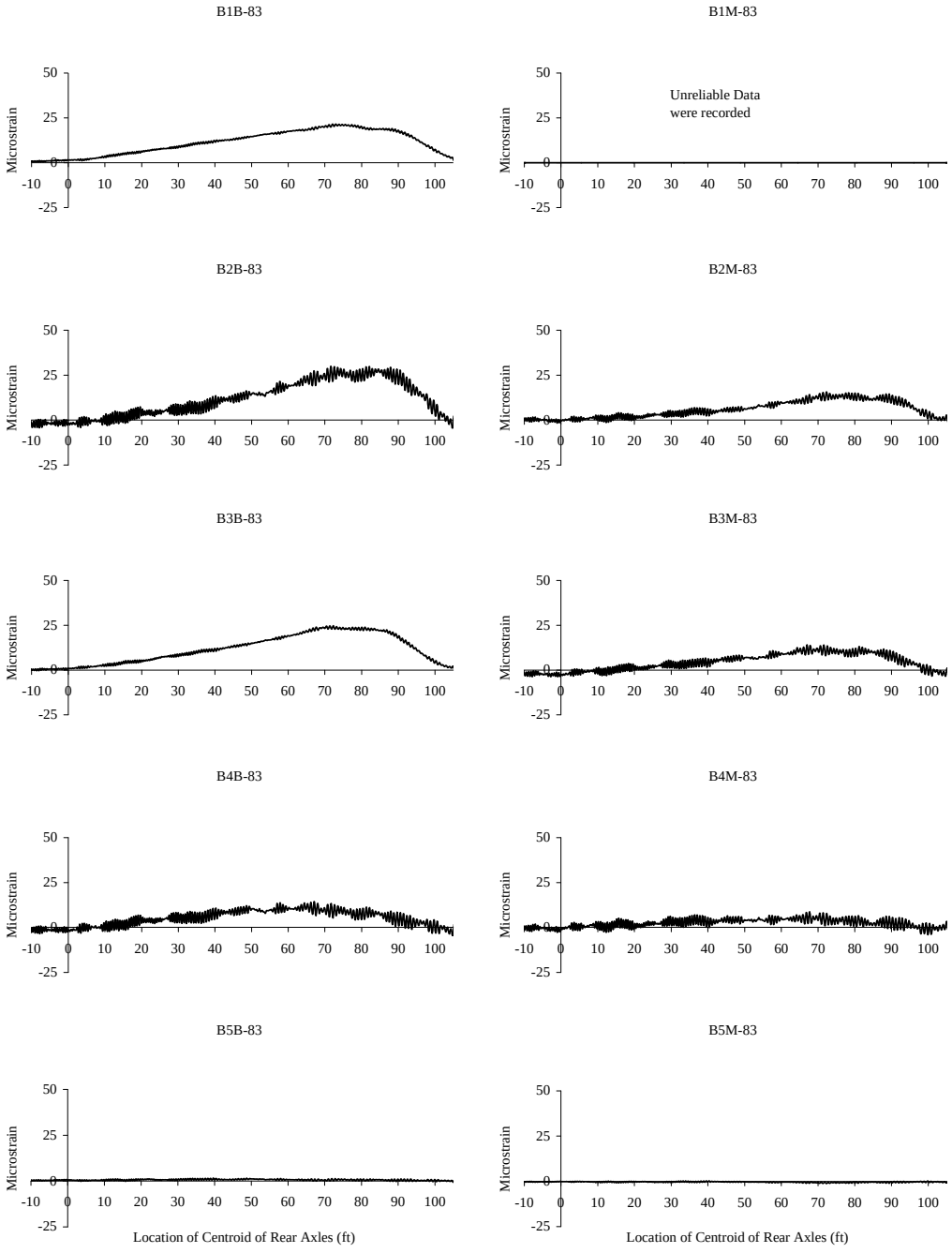

Figure A.79 Strains for the 83.3-ft. Girder Gages, Test Series 1, Run 13

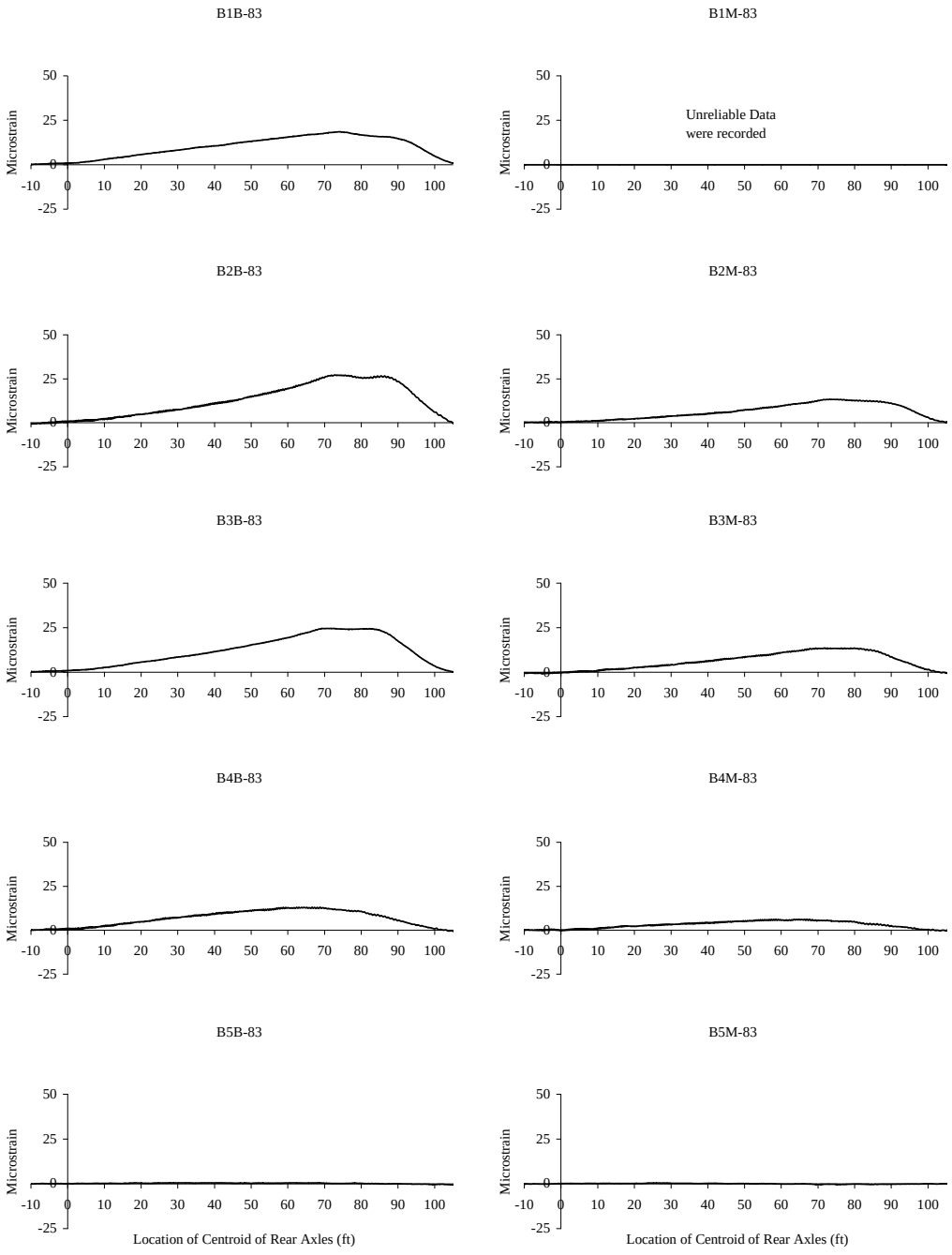

Figure A.80 Strains for the 83.3-ft. Girder Gages, Test Series 1, Run 14

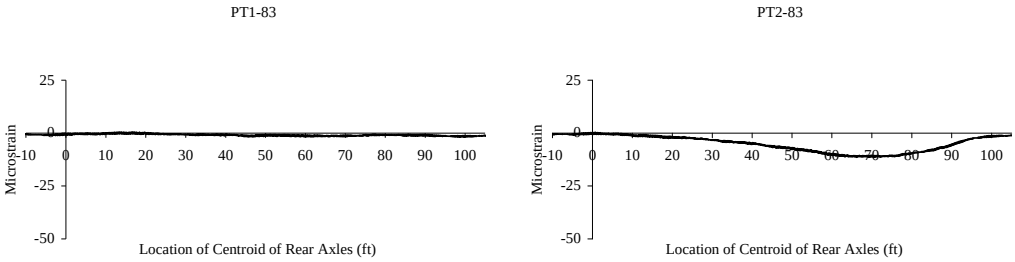

Figure A.81 Strains for the 83.3-ft. Parapet Gages, Test Series 1, Run 1

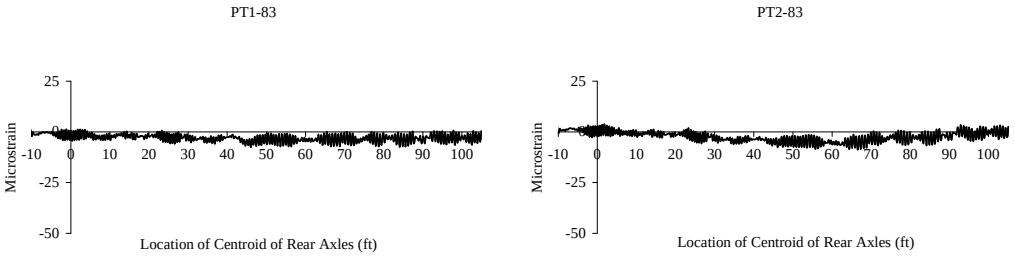

Figure A.82 Strains for the 83.3-ft. Parapet Gages, Test Series 1, Run 4

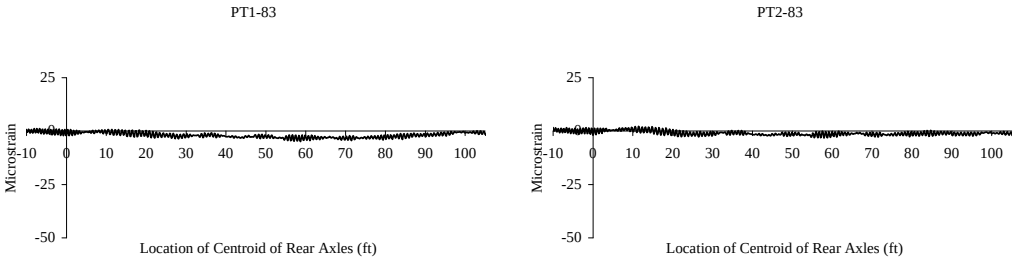

Figure A.83 Strains for the 83.3-ft. Parapet Gages, Test Series 1, Run 6

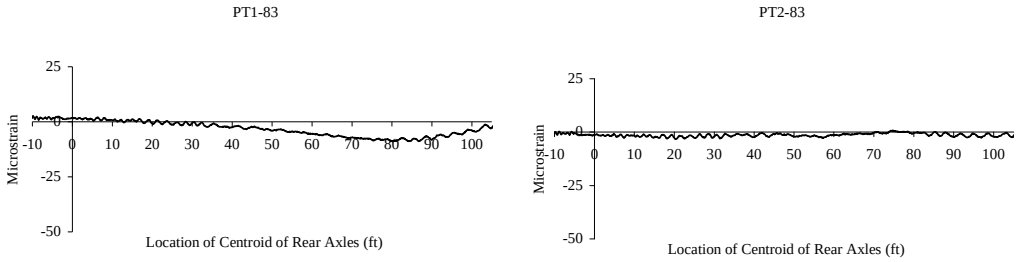

Figure A.84 Strains for the 83.3-ft. Parapet Gages, Test Series 1, Run 7

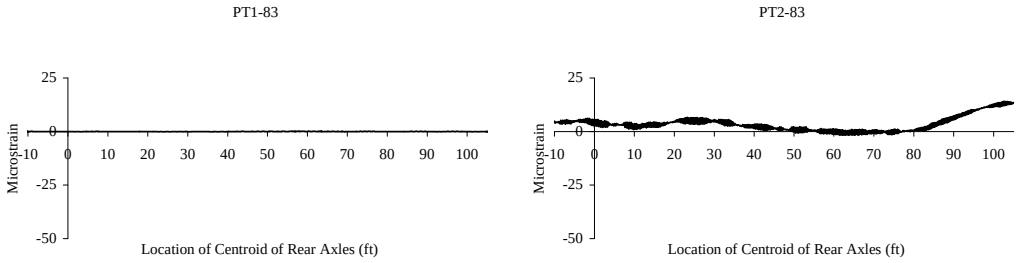

Figure A.85 Strains for the 83.3-ft. Parapet Gages, Test Series 1, Run 9

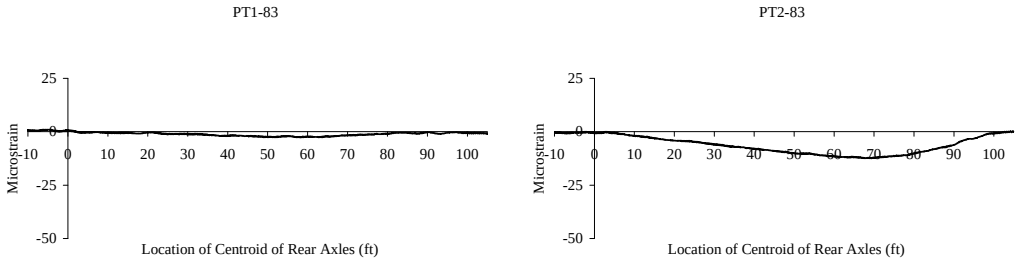

Figure A.86 Strains for the 83.3-ft. Parapet Gages, Test Series 1, Run 11

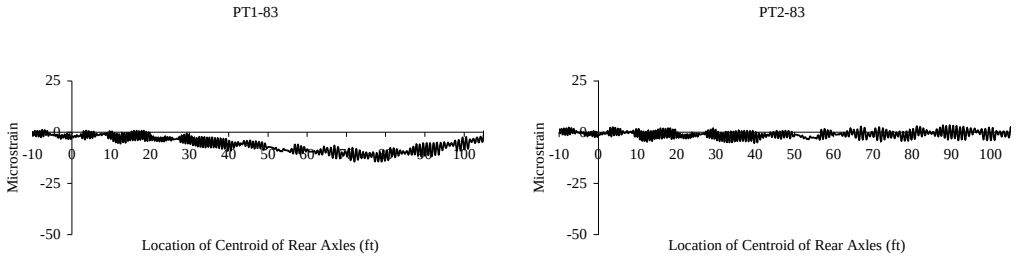

Figure A.87 Strains for the 83.3-ft. Parapet Gages, Test Series 1, Run 13

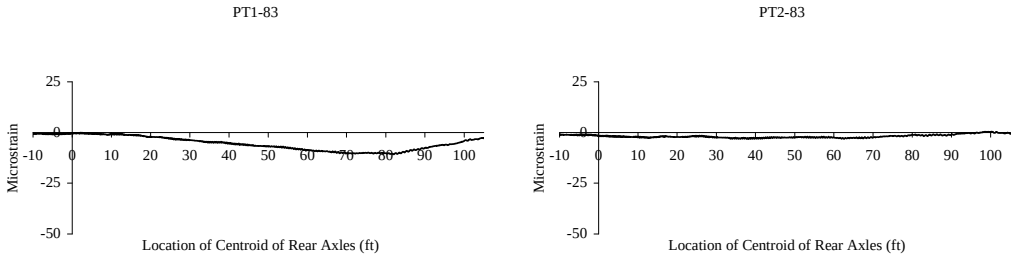

Figure A.88 Strains for the 83.3-ft. Parapet Gages, Test Series 1, Run 14

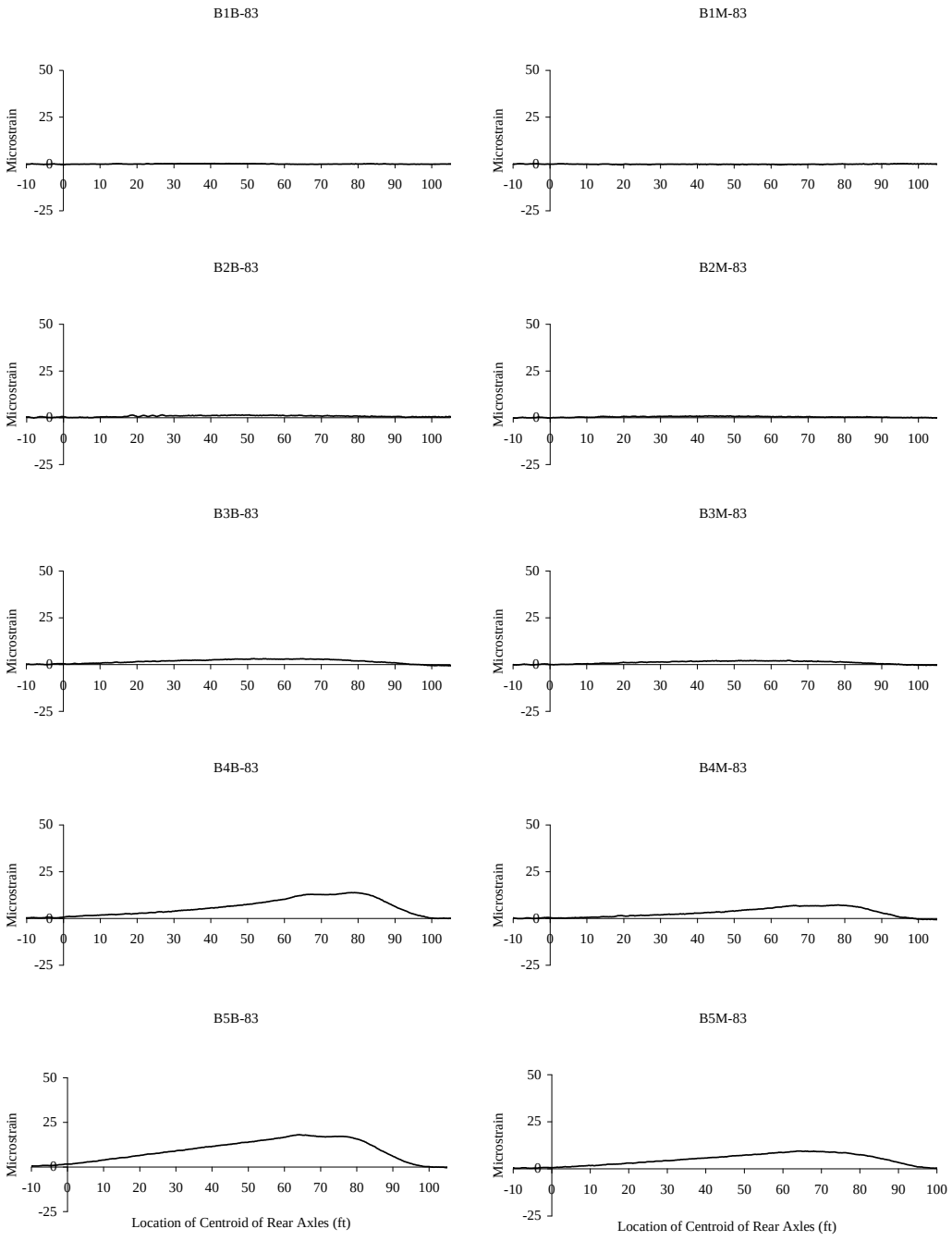

Figure A.89 Strains for the 83.3-ft. Girder Gages, Test Series 2, Run 15

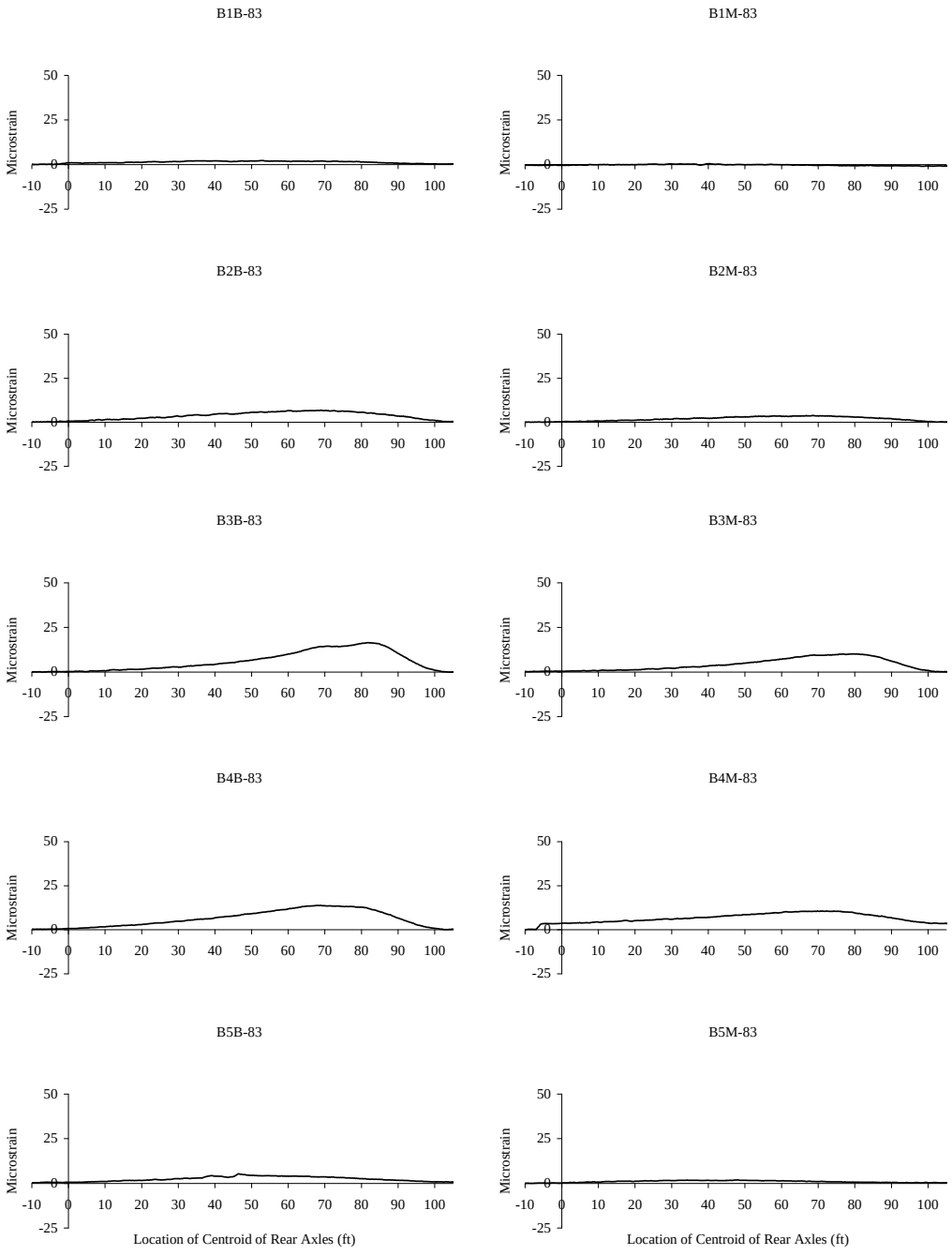

Figure A.90 Strains for the 83.3-ft. Girder Gages, Test Series 2, Run 17

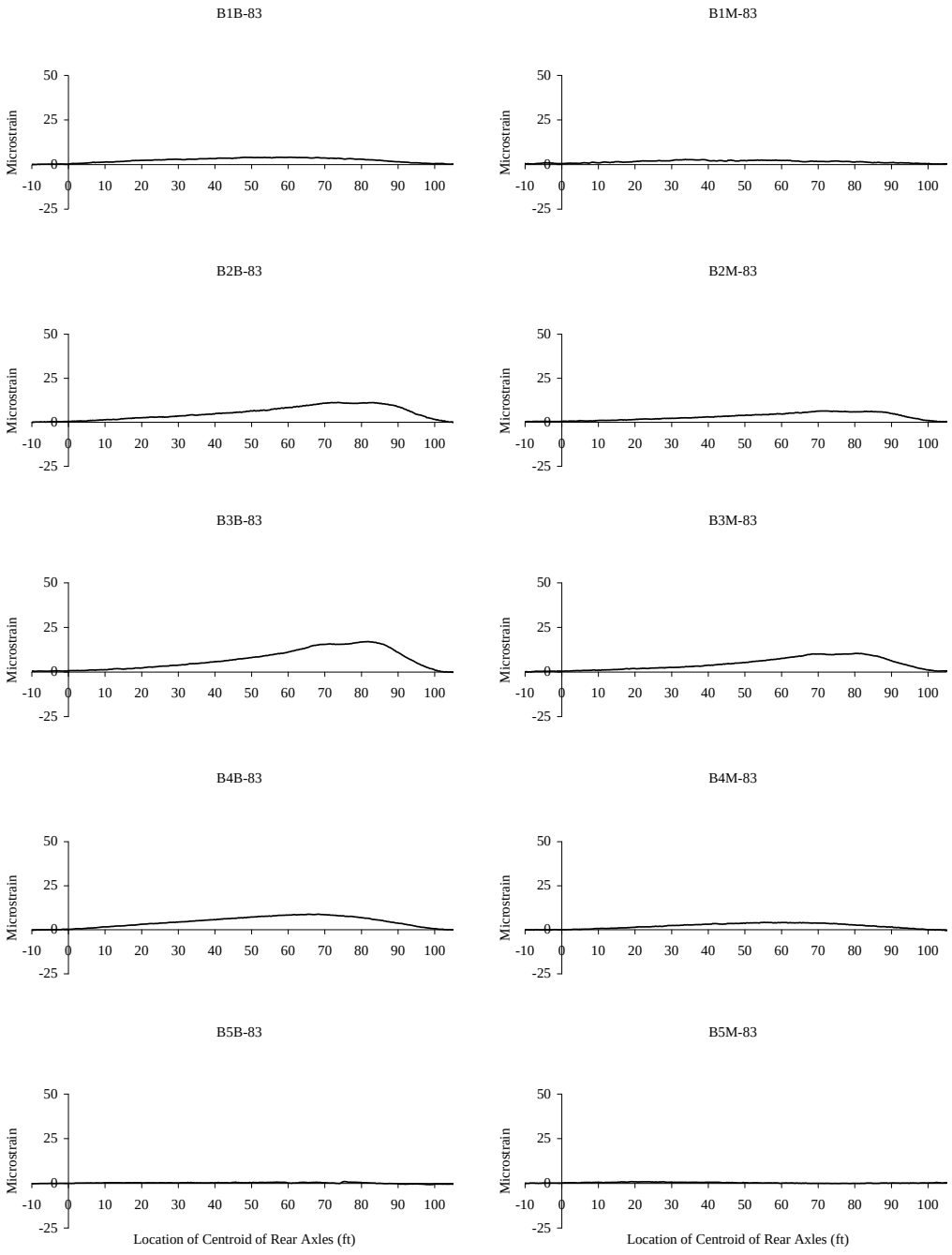

Figure A.91 Strains for the 83.3-ft. Girder Gages, Test Series 2, Run 19

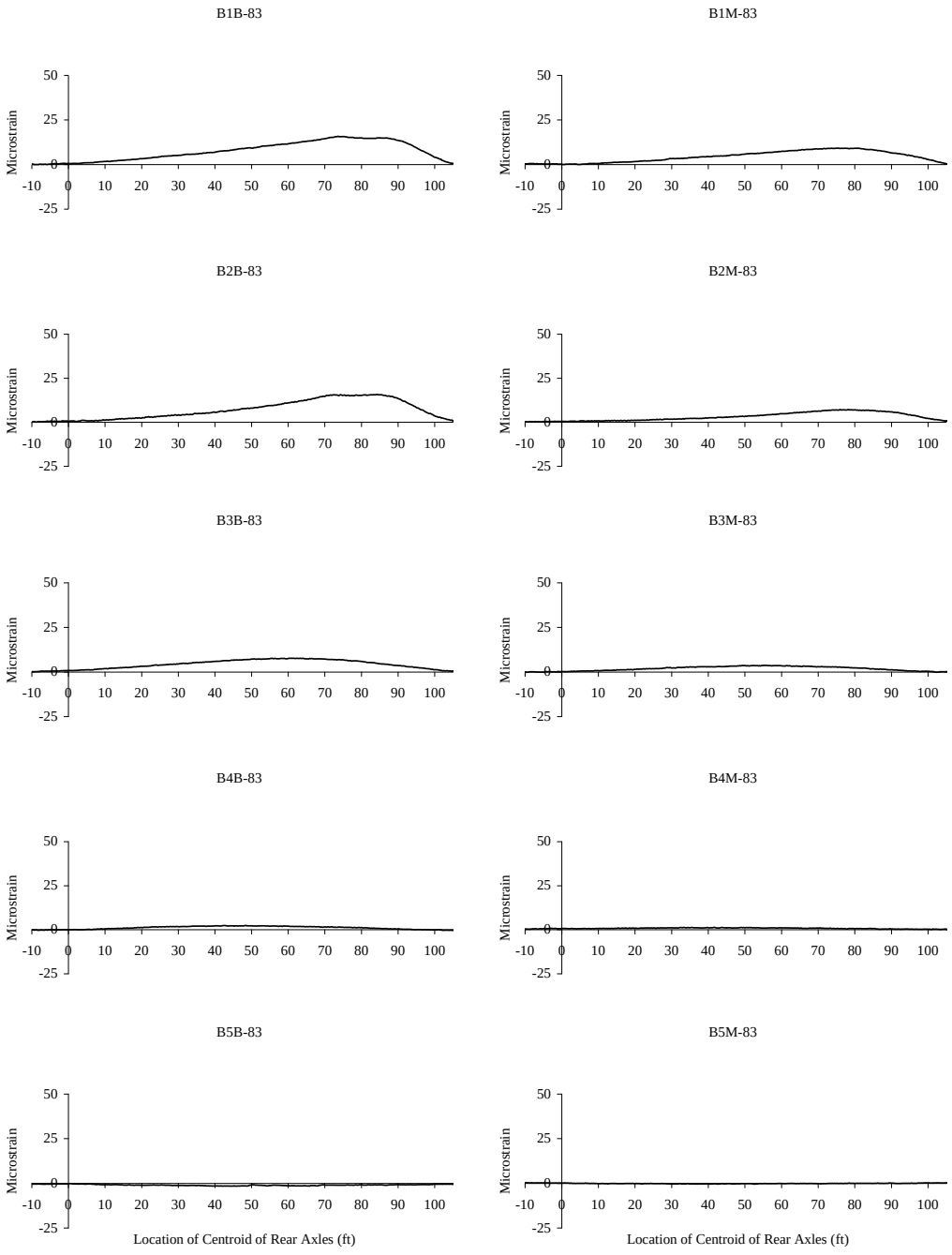

Figure A.92 Strains for the 83.3-ft. Girder Gages, Test Series 2, Run 21

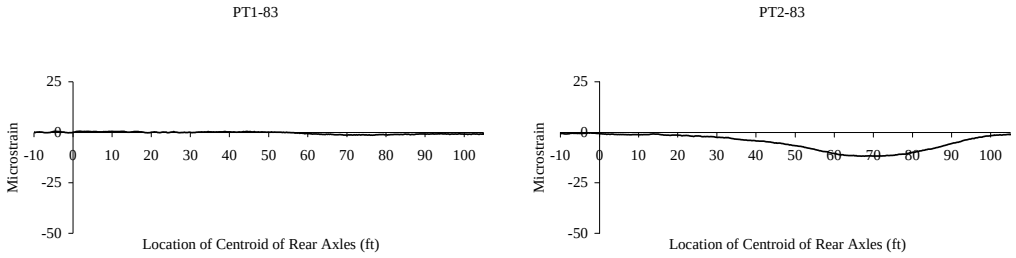

Figure A.93 Strains for the 83.3-ft. Parapet Gages, Test Series 2, Run 15

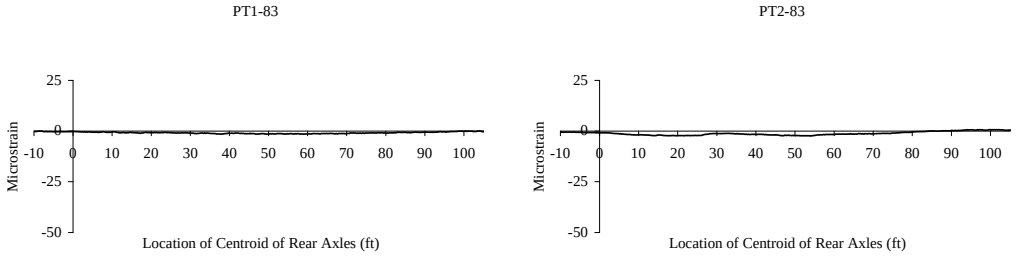

Figure A.94 Strains for the 83.3-ft. Parapet Gages, Test Series 2, Run 17

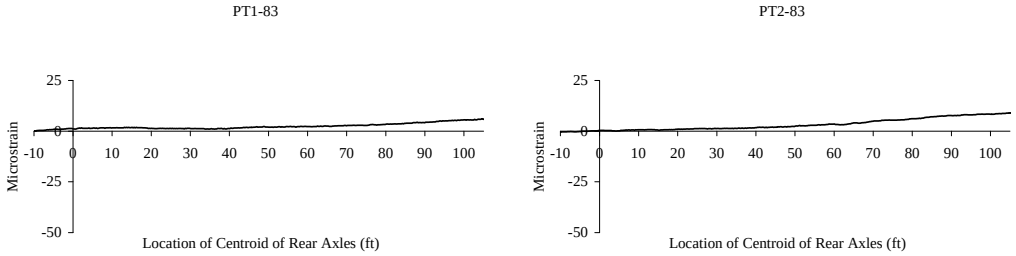

Figure A.95 Strains for the 83.3-ft. Parapet Gages, Test Series 2, Run 19

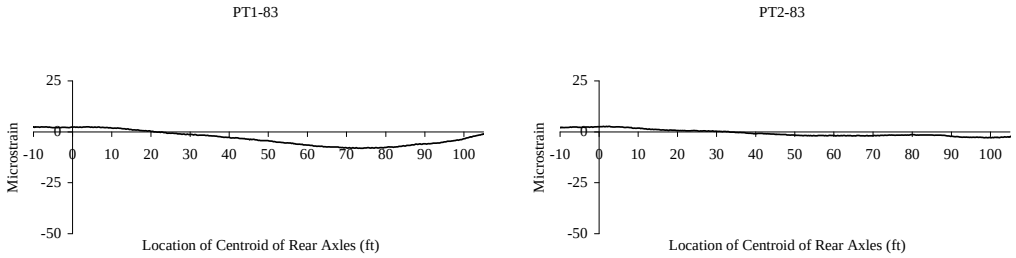

Figure A.96 Strains for the 83.3-ft. Parapet Gages, Test Series 2, Run 21

Appendix B. CALCULATIONS OF THE NEUTRAL AXIS DEPTHS

A set of spreadsheets was developed to calculate the neutral axis depths at mid-span for the interior and exterior girders at both bridges. Four representative spreadsheets are presented in Tables B.1 through B.4. The notation used is consistent with that given in Appendices C and D.

The symbol $y_{N/A}$ in Tables B.1 through B.4 refers to the distance from the composite neutral axis to the bottom fiber of the girder. This distance is calculated based on gross cross-section properties according to Eq. B.1.

$$y_{N/A} = \frac{\sum A_i y_i}{\sum A_i} = \frac{\sum A_i y_i}{A} \tag{B.1}$$

where

$y_{N/A}$= Distance from composite neutral axis to bottom fiber of the girder

A_i= Area of each part of the cross-section that resists bending (precast girder, slab and panels, parapet and strands)

y_i= Distance from centroid of each part of the cross-section to bottom fiber of the girder

A= Area of the composite section

Table B.1 Calculation of the Neutral Axis Depth for the Interior Composite Section at the Slaughter Creek Bridge

E_{sl}=	3908	psi	f'_{csl}=	4700	psi	b_4=	8	ft		
E_r=	4595	psi	f'_{cr}=	6500	psi	t_{sl}=	3	in.		
E_g=	4595	psi	f'_{cg}=	6500	psi	n=	6.20			
E_{ps}=	28500	psi				t_l=	0.5	in.		
A_{ps}=	5.508	in^2	N_{st}=	36		h=	62	in.		
E_{pnl}=	4595	psi	f'_{cpnl}=	6500	psi	t_{pnl}=	4.5	in.		

	$A_i(in^2)$	y_i(in)	$A_iy_i(in^3)$						
Precast Beam*	789	24.75	19528				A_{effsl}=	245	in^2
Slab	432	56.25	24300	b_{effsl}=	82	in.	A_{effpnl}=	432	in^2
Precast Panels	245	60	14694						
Steel	28.7	4	115	b_{effpnl}=	96	in.			
	-	-	-						
Strip	10	54.25	543	e=	20.75	in.			

*Type IV-9 member	Calculated	y_{NA}=	39.3	in.	62-$y_{N/A}$=	22.7	in

Table B.2 Calculation of the Neutral Axis Depth for the Exterior Composite Section at the Slaughter Creek Bridge

E_{sl}=	3908	psi	f'_{csl}=	4700	psi	b_4=	7	ft		
E_r=	3605	psi	f'_{cr}=	4000	psi	t_{sl}=	3	in.		
E_g=	5467	psi	f'_{cg}=	9200	psi	n=	5.21			
E_{ps}=	28500	psi				t_l=	0.5	in.		
A_{ps}=	8.874	in^2	N_{st}=	58		h=	62	in.		
E_{pnl}=	4595	psi	f'_{cpnl}=	6500	psi	t_{pnl}=	4.5	in.		

	$A_i(in^2)$	y_i(in)	$A_iy_i(in^3)$	C_r=	13.8	in.	A_{effsl}=	180	in^2
Precast Beam*	789	24.75	19528	b_{effsl}=	60	in.			
Slab	180	60	10807				A_{effpnl}=	318	in^2
Precast Panels	318	56.25	17872	b_{effpnl}=	71	in.			
Steel	37.4	14.34	536				$A_{effrail}$=	207	in^2
Parapet	206.6	75.3	15555.8	e=	10.41	in.	A_r=	313	in^2
Strip	10	54.25	543						

*Type IV-12 member	Calculated	y_{NA}=	42.1	in.	62-$y_{N/A}$=	19.9	in.

Table B.3 Calculation of the Neutral Axis Depth for the Interior Composite Section at the Nolanville Bridge

E_{sl}=	3908	psi	f'_{csl}=	4700	psi	b_4=	9.5	ft
						t_{sl}=	8.25	in.
E_g=	5002	psi	f'_{cg}=	7700	psi	n=	5.70	
E_{ps}=	28500	psi				t_l=	0.5	in.
A_{ps}=	7.344	in^2	N_{st}=	48		h=	62.75	in.

	$A_i(in^2)$	$y_i(in)$	$A_iy_i(in^3)$						
Precast Beam	789	24.75	19528						
Slab	735	58.13	42710	b_{effsl}=	89	in.	$A_{effslab}$=	735	in^2
-	-	-	-						
Steel	34.5	5.05	174						
Parapet	-	-	-	e=	19.7	in.			
Strip	10	54.5	545						
		Calculated		y_{NA}=	40.1	in.	62.75-$y_{N/A}$=	22.6	in.

Table B.4 Calculation of the Neutral Axis Depth for the Exterior Composite Section at the Nolanville Bridge

E_{sl}=	3420	ksi	f'_{csl}=	3600	psi	b_4=	7.58	ft
						t_{sl}=	8.25	in.
E_g=	5002	ksi	f'_{cg}=	7700	psi	n=	5.70	
E_{ps}=	28500	ksi				t_l=	0.5	in.
A_{ps}=	7.344	in^2	N_{st}=	48		h=	62.75	in.

	$A_i(in^2)$	$y_i(in)$	$A_iy_i(in^3)$						
Precast Beam	789	24.75	19528	b_{effsl}=	62.2	in.	$A_{effslab}$=	513	in^2
Slab	513	58.13	29825						
-	-	-	-						
Steel	34.5	5.05	174	e=	19.7	in.			
Parapet	-	-	-						
Strip	10	54.5	545						
		Calculated		y_{NA}=	37.2	in	62.75-$y_{N/A}$=	25.6	in.

Appendix C. LOAD RATING CALCULATIONS - INPUT INFORMATION, DEAD LOADS, FLEXURAL CAPACITY AND DUCTILITY CALCULATIONS FOR THE SECTIONS

This appendix summarizes the calculation of various parameters used in the load rating calculations. The characteristics of the bridge, the dead load calculations, the determination of flexural capacity and the ductility checks for the four sections of the bridge are discussed. In each case, the values obtained for every step of the calculations are listed sequentially in the form of tables. The load rating calculations are presented in Appendix D.

C.1 NOTATION USED IN THE CALCULATIONS

The general spreadsheet that was developed to perform the load rating calculations for the prestressed concrete sections involves a number of parameters that need to be determined as part of the sequence of calculations leading to the terms of the general rating equation. The tables presented in this section define the variables and list the symbols that are used to express each parameter. Tables C.1 and C.2 define the parameters that are related to the characteristics of the bridges and the section and material properties for the prestressed concrete members. Table C.3 lists the parameters that are used in the dead load calculations. Table C.4 presents the notation used for the variables involved in the calculations of capacity and Table C.5 lists the values of the variables used to check the ductility of the sections. These symbols are throughout Appendices C and D, as well as Chapter 6.

Table C.1 Notation Used in the Calculations – Bridge Characteristics, Section and Material Properties

Category	Parameter	Symbol	Units
Bridge characteristics	Span Length (centerline-to-centerline of bearings)	L	ft
	Number of Rails	N_r	-
	Number of Girders	N_g	-
	Girder Spacing	S	ft
	Number of Interior Girders	N_i	-
	Number of Diaphragms	N_d	-
	Overhang	d_e	in.
	Relative Humidity	RH	%
Unit weights	Concrete Unit Weight (Girders)	γ_c	lb/ft^3
	Concrete Unit Weight (Rails)	γ_{rail}	lb/ft^3
Girder (noncomposite)	Area	A	in^2
	Moment of Inertia	I	in^4
	Distance from cg girder to bottom fiber	y_b	in.
	Distance from cg girder to top fiber	y_t	in.
	Width of top flange	b_{top}	in.
	Web thickness	t_w	in.
	28-day Concrete compressive strength	f'_{cg}	psi
	Modulus of elasticity for the girder	E_g	ksi
	Concrete compressive strength at transfer	f'_{cig}	psi
	Modulus of elasticity for the girder at transfer	E_{ig}	ksi
Slab	Slab thickness	t_{sl}	in.
	28-day Concrete compressive strength	f'_{csl}	psi
	Modulus of elasticity for the slab	E_{sl}	ksi
Precast panels	Panel thickness	t_{pnl}	in.
	28-day Concrete compressive strength	f'_{cpnl}	psi
	Modulus of elasticity for the panels	E_{pnl}	ksi
	Distance from cg girder to cg slab-panels	e_g	in.
20-in. Concrete layer	Layer thickness (assumed)	t_l	in.
	28-day Concrete compressive strength	f'_{clayer}	psi
	Modulus of elasticity for the 20-in. layer	E_l	ksi

Table C.2 Notation Used in the Calculations – Bridge Characteristics, Section and Material Properties - continued

Category	Parameter	Symbol	Units
Traffic rail	Area of rail	A_r	in^2
Diaphragms	Thickness of the diaphragms	t_d	in.
	Depth of the diaphragms	h_d	in.
	Assumed area of diaphragms included girder's web	A_{dw}	in^2
1/2"-low-relaxation strands	Factor for strand type	k or γ*	-
	Number of strands	N_{st}	-
	Area per strand	A_s	in^2
	Area of strands	A_{ps}	in^2
	Ultimate stress in the strands	$f'_s=f_{pu}$	ksi
	Ratio of initial stress in the strands to ultimate	f_{pi}/f_{pu}	%
	Initial stress in the strands	f_{pi}	ksi
	Modulus of elasticity for the strands	E_{ps}	ksi
	Eccentricity at mid-span	e	in.
Composite section	Total depth	h	in.
	Composite neutral axis	$C'_{n/a}$	in.
	Moment of inertia for composite section	$I'_{n/a}$	in^4

Table C.3 Notation Used in the Dead-Load Calculations

Category	Parameter	Symbol	Units
Effective width (int./ext.)	$L_{eff}/4$ for int. , $L_{eff}/8$ for ext.	b_1	in.
	$12t_{slab}+t_{web\ for\ int.}$, $6t_{slab}+t_{web\ for\ ext.}$	b_2	in.
	$12t_{sl}+0.5*b_{top}$ for int. , $6t_{sl}+0.25*b_{top}$ for ext.	b_3	in.
	Actual slab width	b_4	in.
	Overhang	d_e	in.
	Effective width (minimum of four quantities)	b_{eff}	in.
Dead Loads	Self-weight	w_{self}	k/ft
	Diaphragms	w_d	k/ft
	Slab-panels	w_{s-p}	k/ft
	Dead Load on the noncomposite section	DC_1	k/ft
	Moment due to DC_1	$M^{**}_{d/nc}=M_{DC1}$	k-ft
	Dead load stress at bottom of noncomposite section	$f_{DC1\text{-bottom fiber}}$	ksi
	Dead load stress at top of noncomposite section	$f_{DC1\text{-top fiber-compr.}}$	ksi
	Dead Load on the composite section	DC_2	k/ft
	Distribution to interior and exterior	f	-
	Dead Load on the composite section	M_{DC2}	k-ft
	Dead load stress at bottom of composite section	$f_{DC2\text{-bottom fiber}}$	ksi
	Dead load stress at top of composite section	$f_{DC2\text{-top fiber-compr.}}$	ksi
	Total dead load stress on the member	D	k-ft
$^{**}M_{d/nc}$ is used in [2]			

Table C.4 Notation Used in the Calculations of the Flexural Capacity

Category	Parameter	Symbol	Units
Nominal Capacity	Distance from cg strands to top fiber	$d=d_p$	in.
	Ratio of stress block depth to neutral axis depth (depends on f'_{cslab})	β_1	-
	Ratio of prestressing steel	p*	-
	Average stress in prestressing steel at ultimate	$f^*_{su}=f_{ps}$	ksi
	Depth of stress block	a	in.
	Nominal Flexural Capacity	$C=M_n$	k-ft

Table C.5 Notation Used in the Calculations to Check Ductility

Category	Parameter	Symbol	Units
Ductility Checks	Reinforcement Index	$A_{ps}f_{ps}/ (bd_pf'_c)$	-
	Upper limit to the reinforcement index	$0.36\beta_1$	-
	Modulus of rupture for the concrete	f_r	psi
	Losses in the prestress due to shrinkage	SH	ksi
	Moment due to self-weight only	M_{self}	k-ft
	Initial prestress force	F_i	kips
	Concrete stress at cg strands after transfer	f_{cir}	ksi
	Losses in the prestress due to elastic shortening	ES	ksi
	Concrete stress at cg strands from dead loads (no self-weight)	$f_{cds\text{-}cg\_strands}$	ksi
	Losses in the prestress due to creep	CR_c**=CR	ksi
	Losses in the prestress due to relaxation	CR_s**=RE	ksi
	Total losses in the prestress	Δf_s**=TL	ksi
	Effective prestress	$f_{eff}=f_{pi}$-TL	ksi
	Effective prestress force	F_{eff}	kips
	Compressive stress from effective prestress at bottom fiber	f_{pe}	ksi
	Composite section modulus	S_c	in^3
	Section Modulus for the precast girder	S_b	in^3
	Cracking moment	M_{cr}	k-ft
	Strength capacity reduction factor	ϕ	-
	Design capacity	ϕM_n	k-ft
	Ratio of design moment capacity to cracking moment	$\phi M_n/ M_{cr}$	-

** Notation used in [2]

C.2 BRIDGE CHARACTERISTICS, SECTION AND MATERIAL PROPERTIES

The information about the bridge characteristics, and the section and material properties form the input data for the spreadsheet that performs the load rating calculations. Tables C.6 and C.7 list the input values of the parameters for the four sections based on the notation that was explained in Section C.1. The equations and references used in each step are also included in the tables.

Table C.6 Input for Bridge Characteristics, Section and Material Properties

Symbol	Units	Slaughter Creek Bridge		Nolanville Bridge		References - Equations - Comments
		Interior Section	Exterior Section	Interior Section	Exterior Section	
L	ft	98.8	98.8	100.8	100.8	Centerline-to-centerline
N_r	-	2	2	2	2	
N_g	-	5	5	5	5	
S	ft	8	8	9.5	9.5	
N_i	-	3	3	3	3	
N_d	-	0	0	5	5	
d_e	in.	0	26	0	24	
RH	%	70	70	70	70	Fig.9.16.2.1.1 [2] - Texas
γ_c	lb/ft^3	150	150	150	150	
γ_{rail}	lb/ft^3	200	200	200	200	
A	in^2	789	789	789	789	
I	in^4	260740	260740	260740	260740	
y_b	in.	24.75	24.75	24.75	24.75	
y_t	in.	29.25	29.25	29.25	29.25	
b_{top}	in.	20	20	20	20	
t_w	in.	8	8	8	8	
f'_{cg}	psi	6500	9200	7700	7700	
E_g	ksi	4595	5467	5002	5002	8.7.1 [2]
f'_{cig}	psi	4310	6300	5350	5350	
E_{ig}	ksi	3980	4812	4434	4434	9.16.2.1.2 [2] $E=33(\gamma_c)^{1.5}(f'_c)^{0.5}$
t_{sl}	in.	3	3	8.25	8.25	
f'_{csl}	psi	4700	4700	4700	3600	
E_{sl}	ksi	3908	3908	3908	3420	8.7.1 [2] $E=57(f'_c)^{0.5}$
t_{pnl}	in.	4.5	4.5	0	0	
f'_{cpnl}	psi	6500	6500	0	0	
E_{pnl}	ksi	4595	4595	0	0	8.7.1 [2] $E=57(f'_c)^{0.5}$
e_g	in.	33.500	33.500	33.875	33.875	$e_g=y_t+t_l+0.5(t_{sl}+t_{pnl})$
t_l	in.	0.5	0.5	0.5	0.5	
f'_{clayer}	psi	4700	4700	4700	4700	
E_l	ksi	3908	3908	3908	3908	8.7.1 [2] $E=57(f'_c)^{0.5}$

Table C.7 Input Values for the Bridge Characteristics, Section and Material Properties - continued

Symbol	Units	Slaughter Creek Bridge		Nolanville Bridge	
		Interior Section	Exterior Section	Interior Section	Exterior Section
A_r	in^2	313	313	180	180
t_d	in.	0	0	6	6
h_d	in.	0	0	35	35
A_{dw}	in^2	0	0	350	350
k or γ*	-	0.28	0.28	0.28	0.28
N_{st}	-	36	58	48	48
A_s	in^2	0.153	0.153	0.153	0.153
A_{ps}	in^2	5.508	8.874	7.344	7.344
$f'_s=f_{pu}$	ksi	270	270	270	270
f_{pi}/f_{pu}	%	75	75	70	70
f_{pi}	ksi	202.5	202.5	189	189
E_{ps}	ksi	28000	28000	28000	28000
e	in.	20.75	10.41	19.67	19.67
h	in.	62.00	62.00	62.75	62.75
$C'_{n/a}$	in.	22.7	19.9	22.6	25.6
$I'_{n/a}$	in^4	664184	821193	721943	636346

The modulus of elasticity given in Table C.6 for the exterior section at the Nolanville Bridge is lower than that corresponding to the interior section. The lower value reflects the possibility that the slab is cracked, as indicated by the relatively deep neutral axis depths measured at the exterior girder.

C.3 DEAD-LOAD CALCULATIONS (D)

This section discusses the dead-load calculations and presents the results for each of the four members. Table C.8 lists the values for each quantity that are obtained using the equations given in the last column of the table. The total dead-load moment acting on each girder is listed in the last row of the table.

The first step in the calculations is to establish the width of slab that acts compositely with the interior precast girder. This is shown in the first section of Table C.8 where the lengths b_1 through b_4 are defined as shown in Table C.3. The effective widths for the interior and exterior sections are related to the minimum value of these four lengths (b_1 through b_4) in each case. This is expressed by the equations shown in the last column of the table.

Table C.8 Effective Width and Dead-Load Calculations for the Four Girders

Symbol	Units	aughter Creek Brid		Nolanville Bridge		References - Equations - Comments
		Interior Section	Exterior Section	Interior Section	Exterior Section	
b_1	in.	296.4	148.2	302.4	151.2	8.10.1 [2]
b_2	in.	98	53	107	57.5	
b_3	in.	100	50	109	54.5	
b_4	in.	96	84	114	91	Spacing for int. , half spacing+half b_{top}+d_e for ext.
d_e	in.	0	26	0	24	$b_{effext}=\min(b_1,b_2,b_3,b_4)+0.5S$
b_{eff}	in.	96	68	107	70	$b_{effint}=\min(b_1,b_2,b_3,b_4)$
w_{self}	k/ft	0.82	0.82	0.82	0.82	3.4.1-1,2 [2] $w=\gamma A$
w_d	k/ft	0.000	0.000	0.049	0.039	$w_{d,int}=\gamma t_d(b_4h_d-0.5A_{wd})(N_d/L)$
w_{s-p}	k/ft	0.75	0.66	0.98	0.78	$w_{d,=ext}=0.5\gamma t_d(b_4h_d-0.5A_{wd})(N_d/L)$
DC_1	k/ft	1.57	1.48	1.85	1.64	$DC_1=w_{self}+w_d+w_{s-p}$
$M^{**}_{d/nc}=M_{DC1}$	k-ft	1918	1804	2351	2086	$M_{DC1}=w_{DC1}L^2/8$
$f_{DC1\text{-bottom fiber}}$	ksi	2.18	2.05	2.68	2.38	$f_{DC1\text{-bottom}}=12M_{DC1}y_b/I$
$f_{DC1\text{-top fiber-compr.}}$	ksi	2.58	2.43	3.16	2.81	$f_{DC1\text{-top}}=12M_{DC1}y_t/I$
DC_2	k/ft	0.43	0.43	0.25	0.25	$w=\gamma_r A_r$
f	-	0.06	0.12	0.04	0.07	f=1/7 (int.) and 2/7 (ext.)
M_{DC2}	k-ft	76	152	45	91	$M_{DC2}=w_{DC2}L^2/8$
$f_{DC2\text{-bottom fiber}}$	ksi	0.05	0.09	0.03	0.06	$f_{DC2\text{-bottom}}=12M_{DC2}(h-C'_{n/a})/I'_{n/a}$
$f_{DC2\text{-top fiber-compr.}}$	ksi	0.03	0.04	0.02	0.04	$f_{DC2\text{-top}}=12M_{DC2}C'_{n/a}/I'_{n/a}$
D	k-ft	1994	1955	2396	2177	$D=M_{DC1}+M_{DC2}$

The next step is to determine the dead-load moments at the mid-span section. These moments are subtracted from the flexural capacity of the member, as directed by the rating equation. The calculation of the weight equivalents for the various components is followed by the calculation of the moments. Table C.3 differentiates between the moments acting on the noncomposite precast,

prestressed concrete girder (DC_1), and the moments acting on the composite section (DC_2) assuming unshored construction for all calculations. The separation of the total moment into two terms will be used in the calculations of the prestress losses in the following section. The noncomposite moment consists of the self-weight of the Type IV girder, the diaphragms, the concrete slab and the precast panels that act on the girder cross section. The composite term includes the loads from the traffic rails. In all cases, the moment M_{DC1} is significantly higher than the corresponding moment M_{DC2}.

C.4 FLEXURAL CAPACITY CALCULATIONS (C)

This section discusses the main steps in the calculations of the flexural capacity of the prestressed concrete sections. The provisions in Section 9.1.2 of the Standard Specifications [2] are used. The variable a in Table C.9 refers to the depth of the rectangular stress block used in the analysis. The value of d_p represents the distance from the centroid of the strands to the extreme compressive fiber. The equations used to calculate these parameters and the values obtained for each section are listed in the table.

Table C.9 Calculations of the Flexural Capacity of the Four Girders

Symbol	Units	Slaughter Creek Bridge		Nolanville Bridge		References - Equations - Comments
		Interior Section	Exterior Section	Interior Section	Exterior Section	
$d=d_p$	in.	58.0	47.7	57.7	57.7	$d=d_p=h-(y_b-e)$ (d is used in [2])
β_1	-	0.82	0.82	0.82	0.85	8.16.2.7 [2]
p*	-	0.0010	0.0022	0.0011	0.0014	$p^*=A_{ps}/(b_4 d_p)$
$f^*_{su}=f_{ps}$	ksi	264.8	258.3	264.1	260.7	9.17.4 [2] $f_{ps}=f_{pu}[1-(\gamma^*/\beta_1)(p^* f_{pu}/f'_{cslab})]$
a	in.	3.8	6.8	4.3	6.9	9.17.2 [2] $a=(A_{ps}f_{ps}/0.85b_4 f'_{cslab}) < (t_{sl}+t_{pnl})$
$C=M_n$	k-ft	6813	8437	8970	8641	9.17.2 [2] $M_n=A_{ps}f_{ps}d_p(1-0.6p^* f_{ps}/f'_{cslab})$ (f^*_{su} is used in [2])

The stress in the strands at the flexural capacity of the girder (f_{ps}) must be calculated to compute the nominal flexural strength of the section. Equation C.1 is taken from Section 9.17.4.1 of the Standard Specifications [2] and it was used for this calculation.

$$f_{ps} = f_{pu}[1 - \frac{\gamma^*}{\beta_1}(\rho^* \frac{f_{pu}}{f'_c})] \quad \text{(C.1)}$$

where

f_{ps} = Average stress in the strands when the flexural capacity of the composite section is achieved, ksi

f_{pu} = Ultimate stress in the strands = 270 ksi

γ^* = Factor for type of strands = 0.28 for low-relaxation strands

β_1 = Ratio of the stress block depth to the neutral axis depth, depends on f'_c of the slab in this case (8.16.2.7 [2])

$\rho^* = \frac{A_{ps}}{bd_p}$ =Reinforcement ratio for the strands

A_{ps} = Area of prestressing steel, in^2

b = Width of flange, in.

d_p = Distance from strands to top compressive fiber, in.

The nominal moment capacity is calculated based on the expression shown by Eq. C.2 with each term defined in Table C.4. The expression is based on Section 9.17.2 of the Standard Specifications.

$$M_n = A_{ps} f_{ps} d_p (1 - \frac{0.6 p^* f_{ps}}{f'_c}) \quad \text{(C.2)}$$

C.5 DUCTILITY CHECKS AND PRESTRESS LOSSES

Additional requirements involve checking the maximum and minimum amounts of prestressing steel. The first requirement ensures that the steel yields before the flexural capacity of the section is achieved and that the steel is used efficiently in the cross section. The second requirement forces the cracking moment to be less than the flexural capacity of the section to ensure that cracking would occur before the member fails. Table C.10 summarizes the calculations needed to check these two requirements for the four sections.

Equation C.3, taken from Section 9.18.1 of the Standard Specifications [2], checks the maximum reinforcement index. The index for each of the four sections is much smaller than the value of the right hand side of the inequality, thus satisfying the first requirement.

$$\frac{A_{ps}f_{ps}}{bd_p f'_c} < 0.36\beta_1 \qquad \text{(C.3)}$$

The requirement for minimum amount of reinforcement is satisfied by Section 9.18.2.1 of the Standard Specifications [2] that presents the equation used for calculating the cracking moment. The modulus of rupture is given in Section 9.15.2.3. Equations C.4 and C.5 show the expressions for the cracking moment and cracking modulus respectively.

$$M_{cr} = (f_r + f_{pe})S_c - M_{d/nc}\left(\frac{S_c}{S_b} - 1\right) \qquad \text{(C.4)}$$

$$f_r = 7.5\sqrt{f'_c} \qquad \text{(C.5)}$$

where

M_{cr} = Cracking moment, lb-in.

f_r = Modulus of rupture, psi

f'_c = Concrete compressive strength, psi

f_{pe} = Effective prestress after losses, psi

S_c = Section modulus of composite section, in^3

$M_{d/nc}$ = Non-composite dead load moment, lb-in.

Table C.10 Calculations to Check the Ductility of the Four Girders

Symbol	Units	Slaughter Creek Bridge		Nolanville Bridge		References - Equations - Comments
		Interior Section	Exterior Section	Interior Section	Exterior Section	
$A_{ps}f_{ps}/(bd_pf'_c)$	-	0.04	0.08	0.04	0.06	
$0.36\beta_1$	-	0.30	0.30	0.30	0.31	9.18.1 [2]
f_r	psi	605	719	658	658	9.15.2.3 [2] $f'_r=7.5(f'_c)^{0.5}$
SH	ksi	6.5	6.5	6.5	6.5	Eq. 9-4 / 9.16.2.1.1 [2] SH=17-0.15(RH)
M_{self}	k-ft	1003	1003	1044	1044	$M_{self}=w_{self}L^2/8$
F_i	kips	1115	1797	1388	1388	$F_i=A_{ps}f_{pi}$
f_{cir}	ksi	2.30	2.54	2.87	2.87	$f_{cir}=F_i/A+F_ie^2/I-12M_{self}e/I$
ES	ksi	16.2	14.8	18.1	18.1	Eq. 9-6 / 9.16.2.1.2 [2] $ES=E_{ps}f_{cir}/E_{ci}$
$f_{cds\text{-}cg\_strands}$	ksi	0.92	0.45	1.21	1.00	$f_{cds}=12(M_{DC1}-M_{self})e/I+12M_{DC2}(h-C'_{n/a}-y_b+e)/I'_{n/a}$
CR_c**=CR	ksi	21.12	27.41	26.02	27.50	Eq. 9-9 / 9.16.2.1.3 [2] $CR=12f_{cir}-7f_{cds}$
CR_s**=RE	ksi	2.00	1.82	1.56	1.49	Eq. 9-10 / 9.16.2.1.4 [2] RE=5-0.1(ES)-0.05(SH+CR)
Δf_s**=TL	ksi	45.8	50.5	52.2	53.6	Eq. 9-3 / 9.16.2.1 [2] Δf_s=TL=SH+ES+CR_c+CR_s
$f_{eff}=f_{pi}$-TL	ksi	156.7	152.0	136.8	135.4	
F_{eff}	kips	863	1349	1004	994	(def.) $F_{eff}=A_{ps}(f_{pi}-TL)$
f_{pe}	ksi	2.79	3.04	3.15	3.12	(def.) $f_{pe}=F_{eff}/A+(F_{eff}e)y_b/I$
S_c	in^3	16886	19514	17984	17114	$S_c=(I'_{n/a})/(h-C'_{n/a})$
S_b	in^3	10535	10535	10535	10535	$S_b=I/y_b$
M_{cr}	k-ft	3627	4579	4043	4080	9.18.2.1 [2] $M_{cr}=((0.001f_r+f_{pe})S_c-12M_{d/nc}(S_c/S_b-1))/12$
ϕ	-	1	1	1	1	9.14 [2]
ϕM_n	k-ft	6813	8437	8970	8641	
$\phi M_n/M_{cr}$	-	1.88	1.84	2.22	2.12	9.18.2.1 [2] $\phi M_n/M_{cr}$ >1.2

The effective prestress force for the prestressed concrete sections needs to be calculated next. The calculation involves an estimate of the losses of

prestress, which is done according to Section 9.16 [2] of the Standard Specifications. Equation C.6 expresses the total losses in the prestress.

$$TL = SH + ES + CR + RE \tag{C.6}$$

where

$SH =$ Losses due to shrinkage of the concrete, ksi

$ES =$ Losses due to elastic shortening of the concrete, ksi

$CR =$ Losses due to creep of the concrete, ksi

$RE =$ Losses due to relaxation of the strands, ksi

Equation C.7 is used to estimate the losses due to the shrinkage of the concrete.

$$SH = 17 - 0.15RH \tag{C.7}$$

where

$RH =$ Relative Humidity, %

Equation C.8 is used to estimate the losses due to the elastic shortening of the concrete. The term f_{cir}, expressed by Eq. C.9a, involves calculating the initial prestress force, F_i. This force is calculated using Eq. C.9b based on an initial prestress of 70% or 75% of the ultimate stress in the strands (270 ksi) for the Nolanville and Slaughter Creek Bridges respectively.

$$ES = f_{cir}\frac{E_{ps}}{E_{ci}} \tag{C.8}$$

where

$$f_{cir} = \frac{F_i}{A} + \frac{F_i e^2}{I} - \frac{12 M_{self} e}{I} \quad \text{(C.9a)}$$

$$F_i = A_{ps} f_{pi} \quad \text{(C.9b)}$$

f_{cir} = Average concrete stress at level of strands at transfer, ksi

E_{ps} = Modulus of elasticity of the prestressing strands, ksi

E_{ci} = Modulus of elasticity of the concrete, ksi

F_i = Initial force in the strands, kips

f_{pi} = Initial stress in the strands (70 or 75% of f_{pu}=270 ksi)

A_{ps} = Total area of prestressing steel, in^2

A = Area of girder, in^2

I = Moment of inertia of girder, in^4

e = Eccentricity of the strands at the mid-span section, in.

$M_{self\ \max} = \frac{w_{self} L^2}{8}$ =Moment due to the self-weight of the beam, k-ft

w_{self} = Beam self-weight, k/ft

Losses from creep are represented by the third term, and they are calculated using Eq. C.10.

$$CR = 12\, f_{cir} - 7\, f_{cds} \quad \text{(C.10)}$$

where

f_{cds} = Average concrete stress at the level of the strands under full dead load, ksi

The dead load stress f_{cds} is calculated using Eq. C.11, with the moment terms as defined earlier.

$$f_{cds} = \frac{12(M_{DC1} - M_{self})e}{I} + \frac{12M_{DC2}(h - C'_{n/a} - y_b + e)}{I'_{n/a}} \qquad \text{(C.11)}$$

The final term in the expression of total losses represents the losses due to the relaxation of the strands. This is calculated based on Eq. C.12 for low-relaxation strands. The terms in the equation represent the other three forms of prestress losses.

$$RE = 5 - 0.1ES - 0.05(SH + RE) \qquad \text{(C.12)}$$

The total losses were estimated by adding the four terms. These losses ranged from a minimum of approximately 46 ksi in the case of the interior section at the Slaughter Creek Bridge to a maximum of approximately 54.3 ksi in the case of the exterior section at the Nolanville Bridge.

The effective prestress after losses is calculated by subtracting the total losses from the initial prestress (f_{pi}). The reduced prestress force (F_{eff}) is calculated using Eq. C.13.

$$F_{eff} = A_{ps}(f_{pi} - TL) \qquad \text{(C.13)}$$

The cracking moment is calculated based on the properties of the composite and noncomposite sections using Eq. C.4. Section 9.18.2.1 is used to check the ductility of the member by verifying that the capacity is greater than the cracking moment by at least 20%. This requirement was satisfied for all the sections.

Appendix D. LIVE LOADS AND LOAD FACTOR RATING CALCULATIONS

This appendix summarizes the calculations of parameters related to the live-load moments and the load rating calculations. The main expressions used in the calculations are also described in this appendix. The values obtained for the variables in each case are presented sequentially in the form of tables.

D.1 NOTATION USED IN THE CALCULATIONS

The tables presented in this section define the variables and list the symbols that are used to express each parameter that is used in determining the live-load moments and the rating factors. The definitions shown in Appendix C apply in this Appendix as well. Table D.1 defines the parameters that are used for the calculations of the live load moments. Table D.2 presents the notation used for the calculations of the rating factors based on the Load Factor method. Table D.3 and D.4 also include the equations used to determine each parameter that is defined in Tables D.1 and D.2 respectively.

Table D.1 Notation Used in the Calculations of the Live-Load Moments

Category	Parameter	Symbol	Units
Live-loads	Dynamic load allowance (impact factor)	I	-
	Maximum total live-load moment - HS-20 vehicle	M_T	k-ft
	Maximum moment amplified by the impact factor	M_T*(1+I)	k-ft
	Distribution factor (single lane)	DF(*) one lane	-
	Distribution factor (one traffic lane)	DF(*) two lanes	-
	Maximum calculated distribution factor	DF_{max}	-
Load rating based on the Load Factor method	Dead load factor - inventory and operating	A_1-inv, oper	-
	Live load factor - operating	A_2-inv	-
	Live load factor - inventory	A_2-oper	-
	Unfactored dead load moment on composite section	D	k-ft
	Unfactored live load moment on composite section	L	k-ft
	Unfactored live load moment including impact	L(1+I)	k-ft

Table D.2 Notation Used in the Calculations of the Rating Factors

Category	Parameter	Symbol	Units
Load rating based on the Load Factor method	Allowable tensile strength for the concrete (f'c-psi)	$(0.001)6(f'_c)^{0.5}$	ksi
	Allowable service-load compressive stresses	$0.6f'_c$	ksi
	Unfactored dead-load stress at bottom fiber	f_{db}	ksi
	Unfactored compressive stress due to prestress after losses	f_{pb}	ksi
	Unfactored live load stress with impact at tension fiber	f_{lb}	ksi
	Prestressing steel yield stress	f_y	ksi
	Unfactored dead-load stress at strands	f^*_d	ksi
	Unfactored stress due to prestress after losses - at strands	f^*_p	ksi
	Unfactored live load stress with impact at strands	f^*_l	ksi
	Unfactored dead-load stress at top girder fiber	f_{dt}	ksi
	Unfactored compressive stress due to prestress after losses	f_{pt}	ksi
	Unfactored live-load stress at top girder fiber with impact	f_{lt}	ksi
	Rating factor - inventory - Flexural and shear strength	RF^{inv}	-
	Rating factor - operating level - Flexural and shear strength	RF^{oper}	-
	Rating factor - inventory level rating - Concrete tensile stress	$RF^{inv,ct}$	-
	Rating factor - inventory - Concrete compressive stress	$RF^{inv,cc}$	-
	Rating factor - inventory - Concrete compressive stress	$RF^{inv,cc}$	-
	Rating factor - inventory - Prestressing steel tensile stress	$RF^{inv,ps}$	-
	Rating factor - operating level - Prestressing steel tensile stress	$RF^{oper,ps}$	-

D.2 CALCULATIONS OF LIVE-LOAD MOMENTS AND DISTRIBUTION FACTORS

This section discusses the maximum live-load moment that is expected to occur in each member with the AASHTO rating vehicle set along the span. A discussion of the distribution factors that express the maximum fraction of the load that is carried by a single member, the dynamic amplification factors and the live load factors is also presented in this section. The results of the calculations are listed sequentially in Table D.3 at the end of this section.

The general expression for the live load moment that must be resisted by a member is given by Eq. D.1.

$$M_{Live-load} = A_2 DF_{\max} M_T (1+I) \qquad \text{(D.1)}$$

where

$M_{live-load}$ = Live-load moment demand on a member used in the load-rating equation (Denominator in Eq. 6.1)

M_T = Maximum live-load moment demand in the bridge

$DF_{\max}$ = Maximum distribution factor for the moment

I = Dynamic allowance factor

A_2 = Live-load factor

2.17 for inventory level (Load Factor rating, 6.5.3-[3])

1.30 for operating level (Load Factor rating, 6.5.3-[3])

The expression includes load factors that are multiplied by the live load moments. As it was explained in Section 6.2, these factors provide a margin of safety to account for the uncertainties in the expected loads and their

combinations. The values of A_2 used in the Load Factor method are 2.17 for inventory level rating and 1.3 for operating level rating.

The dynamic load allowance factor allows for an increase in the live load due to dynamic, vibratory and impact effects. For example, the presence of rough surfaces with bumps on the roadway would amplify the static moment induced by a passing vehicle. Equation D.2 is taken from Section 3.8.2.2 of the Standard Specifications [2].

$$IM = \frac{50}{L + 125} \tag{D.2}$$

where

$IM =$ Dynamic load allowance factor

$L =$ Span length taken from centerline-to-centerline of the bearings, ft

The moment demand is found by considering the maximum moment that is induced by the AASHTO rating vehicle described in Section 3.7.6 of the 1996 Specifications. The loading is called HS-20 loading and it represents a tractor truck with semi-trailer as shown in Fig. D.1. The axle loads are 8 kips, 32 kips and 32 kips moving from the front to the rear axles of the vehicle. The distance between the second and third axle is varied to obtain the worst loading condition. For the simply-supported girders in this case, the rear axle spacing used was equal to the minimum of 14 ft. The maximum moment is obtained using statics on a simply-supported beam. This information is included as an input parameter in Table D.3.

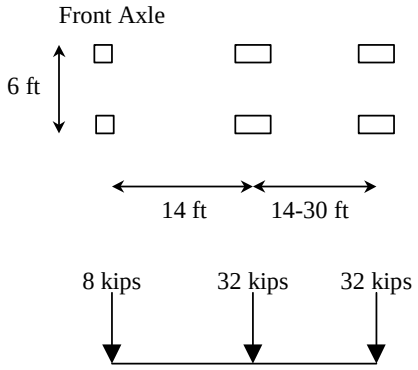

Figure D.1 Plan View and Axle Loads for the AASHTO HS-20 Rating Vehicle

The final term in the expression for the live-load demand on the member is the distribution factor for the moment. This factor represents the fraction of the total moment on the bridge that is expected to act on a single member. A discussion of these factors is presented in Section 5.4. Eq. D.3 shows the expression that was used to calculate the maximum distribution factors using the equations taken from Table 3.23.1 of the Standard Specifications [2] with two traffic lanes on the bridge. Note that this distribution factor defines the percentage of the load effect due to one line of wheels. The result is divided by 2 in order to reflect the fraction of the total moment induced by the vehicle.

Equation D.3 gives the expression for the Nolanville Bridge and Eq. D.4 gives the expression corresponding to the Slaughter Creek Bridge.

$$DF_{\max} = \frac{S}{5.5} = \frac{9.5}{5.5} = 1.72 \Rightarrow DF_{\max - used} = \frac{1.72}{2} = 0.86 \qquad \text{(D.3)}$$

$$DF_{\max} = \frac{S}{5.5} = \frac{8}{5.5} = 1.45 \Rightarrow DF_{\max - used} = \frac{1.45}{2} = 0.73 \qquad \text{(D.4)}$$

where

S= Spacing of the girders in feet

Table D.3 summarizes the results of the calculations of the live load moment and distribution factors for each girder.

Table D.3 Calculations of the Live-load Moments and Distribution Factors

Symbol	Units	Slaughter Creek Bridge		Nolanville Bridge		References - Equations - Comments
		Interior Girder	Exterior Girder	Interior Girder	Exterior Girder	
I	-	0.22	0.22	0.22	0.22	3.8.2 [2] I=50/(L+125)
M_T	k-ft	1498	1498	1534	1534	
M_T*(1+I)	k-ft	1833	1833	1874	1874	
DF(*) one lane	-	0.57	0.57	0.68	0.68	DF_{max}=0.5(S/7)
DF(*) two lanes	-	0.73	0.73	0.86	0.86	DF_{max}=0.5(S/5.5)
DF_{max}	-	0.73	0.73	0.86	0.86	
A_1-inv, oper	-	1.3	1.3	1.3	1.3	6.5.3 [9]
A_2-inv	-	2.17	2.17	2.17	2.17	6.5.3 [9]
A_2-oper	-	1.3	1.3	1.3	1.3	6.5.3 [9]
D	k-ft	1994	1955	2396	2177	$D=M_{DC1}+M_{DC2}$
L	k-ft	1089	1089	1325	1325	$L=DF_{max}(M_T)$

D.3 CALCULATIONS OF THE RATING FACTORS (LOAD FACTOR METHOD)

The expressions that are presented in Section 6.6.3.3 of the 1996 Interim Provisions of the 1994 Manual for Condition Evaluation of Bridges [3] are used to perform the load-rating calculations. The expressions are listed in Table D.4. Two of the equations are related to strength requirements and they are identical to the general rating equation discussed in Chapter 6 and given by Eq. 6.1. The other equations use stresses to perform the checks for concrete tension at the extreme tension fiber, concrete compression at the precompressed zone, and prestressing steel tension to ensure that the service-load stress in the strands is at

a level lower than their yield stress. These additional equations and the resulting rating factors are presented in the table. The results are discussed in Chapter 6. Note that any revised rating calculations were performed using the same spreadsheet and notation described in this appendix and Appendix C.

Table D.4 Rating Factor Calculations Using the Load Factor Method

Symbol	Units	Slaughter Creek Bridge		Nolanville Bridge		References - Equations - Comments
		Interior Section	Exterior Section	Interior Section	Exterior Section	
$(0.001)6(f'_c)^{0.5}$	ksi	0.48	0.58	0.53	0.53	6.6.3.3 [3] , 9.15.2.2 [2]
$0.6f'_c$	ksi	3.90	5.52	4.62	4.62	
f_{db}	ksi	2.24	2.15	2.71	2.44	6.5.1 [3] $f_{db}=12M_{DC1}y_b/I+12M_{DC2}(h-C'_{n/a})/I'_{n/a}$
f_{pb}	ksi	2.79	3.04	3.15	3.12	$f_p=f_{pe}=(F_{eff}/A)+(F_{eff})(e)y_b/I$
f_{lb}	ksi	0.95	0.82	1.08	1.13	$f_l=12L(1+I)(h-C'_{n/a})/I'_{n/a}$
f_y	ksi	243	243	243	243	9.1.2 [2] Low relaxation $f^*_y=0.9f_{pu}$
f^*_d	ksi	11.45	4.74	12.06	10.88	$f_d^*=(E_{ps}/E_g)(12M_{DC1}e/I+12M_{DC2}(h-C'_{n/a}-y_b+e)/I'_{n/a})$
f^*_p	ksi	156.7	152.0	136.8	135.4	$f_p^*=f_{pi}$-TL
f^*_l	ksi	5.18	2.77	5.28	5.48	$f_l^*=(E_{ps}/E_g)12L(1+I)((h-C'_{n/a}-y_b+e)/I'_{n/a})$
f_{dt}	ksi	2.61	2.47	3.18	2.85	$f_{dt}=12M_{DC1}y_t/I+12M_{DC2(}C'_{n/a}-t_{sl}-t_{pnl}-t_l)/I'_{n/a}$
f_{pt}	ksi	-0.92	0.13	-0.94	-0.93	$f_{pt}=(F_{eff}/A)-(F_{eff})(e)y_t/I$ - Negative sign implies tension
f_{lt}	ksi	0.55	0.39	0.61	0.78	$f_{lt}=12L(1+I)(C'_{n/a}-t_{sl}-t_{pnl}-t_l)/I'_{n/a}$
RF^{inv}	-	1.46	2.04	1.67	1.65	Eq. 6.1 - Inventory Level Rating (Strength)
RF^{oper}	-	2.44	3.40	2.78	2.76	Eq. 6.1 - Operating Level Rating (Strength)
$RF^{inv,ct}$	-	1.10	1.79	0.90	1.06	Eq. 6.3 - Concrete Tensile Stress
$RF^{inv,cc}$	-	4.03	7.51	3.92	3.46	Eq. 6.5 - Concrete Compressive Stress
$RF^{inv,cc}$	-	3.21	6.13	3.22	2.72	Eq. 6.4 - Concrete Compressive Stress
$RF^{inv,ps}$	-	5.06	13.6	8.6	8.8	Eq. 6.6 - Strands Tensile Stress
$RF^{oper,ps}$	-	9.75	22.4	13.2	13.2	Eq. 6.7 - Strands Tensile Stress